UNIVERSITÁ DEGLI STUDI DI NAPOLI
FEDERICO II
Scuola Politecnica e Delle Scienze Di Base
Department of Industrial Engineering

Doctoral Thesis in Industrial Engineering

Model-Based Systems Engineering for Multidisciplinary Optimization of Advanced Aircraft Rear-End

Supervisor:
Prof. Pierluigi Della Vecchia
Prof. Fabrizio Nicolosi

Coordinator:
Prof. Michele Grassi

Author:
Massimo Mandorino
DR995125

March 11, 2024

Declaration of Authorship

I, Massimo Mandorino, declare that this thesis, titled "Model-Based Systems Engineering for Multidisciplinary Optimization of Advanced Aircraft Rear-End" and the work presented in it are my own. I confirm that:

- This work was done wholly or mainly while in candidature for research degree at this University.
- Where any part of this thesis has previously been submitted for a degree or any other qualification at this University or any other institution, this has been clearly stated.
- Where I have consulted the published work of others, this is always clearly attributed.
- Where I have quoted from the work of others, the source is always given. With the exception of such quotations, this thesis is entirely my own work.
- I have acknowledged all main source of help.
- Where the thesis is based on work conducted in collaboration with others, I have made clear exactly what was done collectively and have delineated my individual contributions.

Date: 11th March 2024
Sign:

Abstract

The aviation industry is currently encountering unprecedented challenges, including the critical need to achieve climate neutrality and meet the growing demand for improved performance. The Flightpath 2050 initiative, led by the Advisory Council for Aeronautical Research in Europe, sets out ambitious objectives for reducing emissions and cutting costs in air travel. In this rapidly evolving landscape, aircraft manufacturers must transition to innovative aeronautical concepts. In pursuit of the ambition to minimize the environmental impact of the aviation industry, the EU Commission, in collaboration with industry partners, launched the Clean Sky 2 program. This program explores innovative concepts aimed at improving aircraft fuel efficiency and reducing air and noise emissions in comparison to current state-of-the-art solutions. Within the scope of this program, which emphasizes the exploration of advanced engines and aircraft configurations, the development of the Advanced Rear End demonstrator is currently in progress. This prototype combines a comprehensive array of interconnected aircraft rear-end and empennage components, taking advantage of the introduction of innovative configurations and technologies. Researchers have indeed recognized the potential benefits of these components in reducing weight and improving production rates for next-generation medium-sized passenger aircraft.

The introduction of these novel and disruptive technologies significantly increases the complexity of aeronautical systems, requiring a larger number of designers and generating vast amounts of data and information. Several disciplines and aspects beyond conventional design must be considered to address the complexity of such a system. This factor can lead to a situation in which any change can have significant implications for the entire process. Early aircraft design encounters challenges in exploring a high-dimensional design space, assessing innovative concepts, and handling continuous variations in requirements.

In response to these challenges, there is a growing interest in Model-Based Systems Engineering, which is considered a crucial step in addressing the complexity and challenges in early aircraft development. It offers benefits such as enhanced consistency, transparency, and collaboration across diverse disciplines. In addition, the aerospace industry has widely recognized the potential of Multidisciplinary Design and Optimization, which offers a novel approach to addressing challenges such as disruptive configuration design by seamlessly integrating and optimizing multiple disciplines or subsystems. The efficiency and effectiveness of aircraft conceptual design can be improved by using a synergistic approach that involves the seamless integration of Model-Based Systems Engineering and Multidisciplinary Design Analysis and Optimization methods. Their integration offers a synergistic solution for efficiently addressing the complexity of conceptual design, combining the benefits of both methodologies.

Based on these observations, the work described in this thesis addresses the following research question:

How can model-based systems engineering methodologies be effectively utilized to develop multidisciplinary analysis and optimization workflows for designing an innovative rear-end for large passenger commercial jet aircraft?

To facilitate the development of new solutions, such as innovative rear-end fuselage and tailplane configurations, including a forward-swept tailplane equipped with leading-edge extension and integrated into a bottle-neck-shaped fuselage, aircraft designers should have access to a specialized environment. The development of these complex systems involves multidisciplinary processes, imposing requirements on system components, technologies, and interactions. The interconnected data encompasses diverse aspects of product development. A dedicated environment should facilitate easy and prompt execution of optimizations and trade-off studies across all necessary disciplines, even at conceptual and preliminary design stages. Furthermore, the system must gather all relevant information that impacts the final solution within a model-based framework and automatically generate a structure based on this data. This approach would offer aircraft designers the ability to trace all data that influences the steps in the system development process from the early design stages. Furthermore, it would provide a flexible framework capable of adapting to specific requirements and illustrating the impact of each individual model component.

However, the existing literature lacks evidence of studies utilizing the integrated application of MBSE and MDAO methodologies for designing unconventional aircraft configurations. Specifically, there is an absence of this kind of analysis focusing on forward-swept horizontal tailplanes. Furthermore, the assessment of this innovative technology in aeronautics fails to encompass various disciplines, such as aerodynamics, structure, and ice formation, as well as considerations related to aeronautical design, regulation, and certification.

The primary goal of this thesis is to develop a framework with these features to support the design of advanced rear-end configurations. The proposed methodology facilitates the development of the rear-end of a large passenger commercial jet aircraft, incorporating features such as a negative-sweep horizontal tail, a leading-edge extension, and a bottleneck-shaped fuselage. The proposed solutions are obtained through a Multidisciplinary Design and Optimization approach which is emerged from analyses conducted using Model-Based Systems Engineering technologies. This analysis outlines all stakeholder needs and translates them into requirements that serve as the foundation for modeling the system under examination. Multiple

workflows are subsequently created to develop the system, leading to a solution designed to meet all identified requirements. The entire process is capable of encompassing various aspects that extend beyond design considerations, integrating disciplines at a high level of fidelity, such as aeroelasticity and in-flight ice formation. The framework's adaptability to the selected requirements and its flexibility in addressing various types of optimization problems are demonstrated through the generation of four different optimization problems. Optimizations are conducted with reference to geometric macro-parameters, taking into account multiple flight conditions. The proposed framework efficiently employs modeling techniques to enhance agility in defining complex systems, integrating various automated processes to streamline development. Key benefits include improved coherence among data, enhanced traceability through a model-based approach, and comprehensive stakeholder needs addressing. Time and efficiency in development are optimized through a shift to model-based approaches, with seamless integration of Systems Engineering activities. Significant time savings are achieved in problem formulation and resolution, aided by surrogate models and advanced optimization algorithms.

The results suggest innovative tailplane configurations that offer improved aerodynamics, reduced weight, and flexible characteristics. The study reveals a 4% reduction in tail area and a mass decrease of up to 16%, while maintaining comparable drag capabilities. Additionally, there is noted enhancement in lift and aeroelastic performance. The utilization of a forward-swept tailplane with a leading-edge extension device shows potential for reducing horizontal empennage dimensions. Multi-objective optimization results provide designers with various optimal solutions tailored to specific requirements. Evaluation at the aircraft level suggests a potential 2% reduction in block fuel compared to the Airbus A320-neo, with a design range of 3200 nautical miles and 180 passengers. These configurations take into account stability constraints and critical ice accretion conditions. The developed framework enabled the illustration of the impact of specific requirements on the final solutions. Furthermore, the impact of the optimized tail arrangement at the aircraft level is illustrated. From an industrial standpoint, this study illustrates how an automated framework can expedite complex multidisciplinary optimization processes, accelerating formulation, integration, and execution phases. This improvement has the potential to reduce time to market and costs associated with developing a new aircraft configuration.

Contents

List of Figures

List of Tables

Nomenclature

Acronyms and abbreviations

Acronym	Description
AAO	All At Once
AC	Aerodynamic Center
ACARE	Advisory Council for Aeronautical Research in Europe
AD	Automatic Differentiation
ADF	AGILE Development Framework
ADSG	Architecture Design Space Graph
AOA	Angle Of Attack
API	Application Programming Interface
APPS	Asynchronous Parallel Pattern Search
AR	Aspect Ratio
ARE	Advanced Rear End
BC	Boundary Condition
BH	Body Horizontal
BRF	Body Reference Frame
CA	Collaborative Architecture
CAD	Computer Aided Design
CAS	Calibrated AirSpeed
CFD	Computational Fluid Dynamics
CG	Center of Gravity
COBYLA	Constrained Optimization BY Linear approximations
CPACS	Common Parametric Aircraft Configuration Schema
CSV	Comma Separated Values
CT	Component Tool
DACE	Design and Analysis of Computer Experiment
DLM	Doublet Lattice Method
DOE	Design Of Experiments
DSM	Design Structure Matrix
DSO	Data Schema Operation
DSV	De Saint Venant
EAS	Equivalent AirSpeed
FD	Finite Differences
FEA	Finite Element Analysis
FEM	Finite Element Model
FFD	Free Form Deformation
FL	Flight Level
FSHTP	Forward Swept Horizontal Tailplane
GUI	Graphical User Interface
HHB	Hicks Henne Bump
HS	High Speed
HTP	Horizontal Tail Plane

IADP	Innovative Aircraft Demonstrator Platforms
IDF	Individual Discipline Feasible
IWT	Icing Wind Tunnel
INCOSE	International Council on Systems Engineering
KA	Knowledge Architecture
KPI	Key Performance Indicator
LA	Logical Architecture
LE	Leading Edge
LEX	Leading Edge eXtension
LFL	Landing Field Length
LHS	Latin hypercube sampling
LPA	Large Passenger Aircraft
LS	Low Speed
LWC	Liquid Water Content
MALE UAV	Medium Altitude Long Endurance Unmanned Aerial Vehicle
MBSA	Model-Based Safety Assessment
MBSE	Model-Based Systems Engineering
MDAO	Multidisciplinary Design Analysis and Optimization
MDF	Multi Discipline Feasible
MDO	Multidisciplinary Design and Optimization
MOEA	Multi Objective Evolutionary Algorithm
MOGA	Multi Objective Genetic Algorithm
MRO	Maintenance Repair and Overhaul
MTOM	Maximum Take Off Mass
MVD	Mean Volumetric Diameter
NLF	Natural Laminar Flow
OA	Operational Analysis
OCCT	OpenCASCADE Technology
OCE	Operational Collaborative Environment
OEM	Original Equipment Manufacturer
OES	Operational Entities Scenario
OOP	Object Oriented Programming
PA	Physical Architecture
PDE	Partial Differential Equation
PIDO	Process Integration and Design Optimization
QOI	Quantity of Interest
RANS	Reynolds Averaged Navier Stokes
RBF	Radial Basis Function
RCE	Remote Component Environment
RSM	Response Surface Model
RVF	Requirement Verification Framework
SA	System Analysis
SAND	Simultaneous Analysis and Design
SE	Systems Engineering
SST	Shear Stress Transport

SysML	Systems Modeling Language
TAS	True AirSpeed
TLARS	Top Level Aircraft Requirements
TOFL	Takeoff Field Length
TP	Tail Plane
TR	Taper Ratio
TRL	Technology Readiness Level
VLM	Vortex Lattice Method
WP	Work Package
XDSM	eXtended Design Structure Matrix
XML	eXtensible Markup Language

Symbols

Symbol	**Units**	**Description**
α	$deg.$	Angle of attack
α_b	dimensionless	Spar contribution coefficient
β_i	dimensionless	Optimization weight
γ	dimensionless	Design variables of interest
Γ	$deg.$	Dihedral angle
$\Delta CL_{Max,ICE}$	dimensionless	Maximum lift coefficient penalty introduced in the case of icing effects
ϵ	$deg.$	Downwash
η	dimensionless	Dynamic pressure ratio
η_{flex}	dimensionless	Tail elastic efficiency parameter
Θ	$deg.$	Rotation around the beam axis
λ	dimensionless	Taper ratio
Λ_{EA}	$deg.$	Sweep angle of the elastic axis
λ_i	dimensionless	Approximation coefficient for RBF
Λ_{LE}	$deg.$	Sweep at leading edge
ν	dimensionless	Poisson modulus
ρ	Kg/m^2	Air density
ρ_{mat}	Kg/m^2	Material density
σ	dimensionless	Local Shape Parameter
σ_y	$N/m^2 \cdot m^2$	Stress distribution
τ_y	$N/m^2 \cdot m^2$	Shear stress distribution
ϕ	dimensionless	Radial Basis Function
A_{box}	m^2	Wing Box Area
A_{cap}	m^2	Spar cap area
A_{skin}	m^2	Skin area
A_{web}	m^2	Spar web area

b	m	Span
b_{cap}	m	Spar cap span
c	m	Chord
c_{box}	m	Wing Box length
CD	dimensionless	Drag Coefficient
C_f	dimensionless	Generic aerodynamic coefficient
c_i	dimensionless	Approximation coefficient for RBF
CL	dimensionless	Lift Coefficient
C_{L_α}	$1/deg.$	Derivative of lift coefficient with respect to alpha
$C_{L_{\alpha,Flex.}}$	$1/deg.$	Flexible derivative of lift coefficient with respect to alpha
$CL_{max,neg}$	dimensionless	Maximum negative lift coefficient
$CL_{max,neg,Flex.}$	dimensionless	Maximum flexible negative lift coefficient
C_{L_0}	dimensionless	Lift Coefficient in zero lift condition
C_M	dimensionless	Moment Coefficient
C_{mac}	m	Wing mean aerodynamic chord
C_{M_α}	$1/deg.$	Derivative of moment coefficient with respect to alpha
$C_{M_{\alpha,Flex.}}$	$1/deg.$	Flexible derivative of moment coefficient with respect to alpha
C_{M_0}	dimensionless	Moment Coefficient in zero lift condition
CO_2	dimensionless	Carbon dioxide
c_r	m	Root chord
C_s	dimensionless	Generic structural coefficient
c_t	m	Tip chord
$\mathbf{d_s}$	m	Distance between structural line nodes and deformation nodes
$\bar{e}$	m	General lever arm
g	m/s^2	Gravitational acceleration
G	N/m^2	Shear modulus
$\mathbf{g^{IDF}}$	dimensionless	Consistency constraint
h	dimensionless	Horizontal tailplane
h_i	m	Height of the i spar
h_m	m	Average height
I	Kg/m^2	Moment of Inertia
In	dimensionless	Input
J	dimensionless	Optimization function
J_i	m^4	Torsional constant
l_d	N	Lift distribution
l_h	m	Distance between WF and HTP aerodynamic centers
M	Kg	Mass
M_b	$N \cdot m$	Bending moment
M_t	$N \cdot m$	Torsional moment

n	dimensionless	Load Factor
NO_x	dimensionless	Nitrogen oxides
N_{rib}	dimensionless	Number of ribs
N_s	dimensionless	Number of samples
Out	dimensionless	Output
$\mathbf{p}$	dimensionless	Wing geometry macro parameters
r	m	Distance
S_f	N	Shear force
S_H	m^2	Horizontal tail plane surface
S_M	dimensionless	Safety Margin
S_{Ref}	m^2	Reference surface
S_W	m^2	Main Wing surface
s_y	N/m^2	Yielding stress
t	m	Spar thickness
$\mathbf{t}$	dimensionless	Wing structural proprieties
T	N	Thrust
t/c	dimensionless	Thickness to Chord ratio
t_{cap}	m	Spar cap thickness
t_d	$N \cdot m$	Aerodynamic pitching torque
t_{rib}	m	Rib thickness
t_{skin}	m	Skin thickness
$\mathbf{u}$	dimensionless	Structural displacements
$\mathbf{u}*$	dimensionless	Surrogate structural displacements
$\mathbf{u}^{(\mathbf{rot})}$	$deg.$	Axial rotations of nodes on the structural line
$\mathbf{u}^{(\mathbf{tr})}$	m	Vertical translations of nodes on the structural line
V	m/s	Speed
V_D	m/s	Diving Speed
V_{rib}	m^2	Rib volume
w	m/s	Downwash velocity
W	N	Weight
w_{cap}	N	Spar cap weight
W_i	dimensionless	Optimization Weight
w_{web}	N	Spar web weight
w_{skin}	N	Skin weight
WF	dimensionless	Wing Fuselage
W_{MTO}	Kg	Maximum take-off weight
X_{apex}	m	Leading edge X coordinate
$\mathbf{x_f}$	dimensionless	Points of the surface mesh
$\mathbf{x_s}$	m	Location of the surrounding wingbox nodes on structural line

1 Introduction

Contents

1.1 Research Context and Motivation

The aviation industry is poised to face new challenges in the coming decades, including meeting the growing demand for enhanced performance and striving for climate neutrality. Despite the progress made in reducing the environmental impact of aviation over the last 40 years, the impact continues to grow due to the expanding air traffic. According to the IATA Technology Roadmap [1], the number of flights in Europe is projected to increase by 1.5 times in 2035 compared to 2012, based on a conservative scenario. This growth will be even more substantial outside of Europe, with an estimated global traffic increase of 4.3% annually over the next 20 years. Targeted and timely action is essential to achieve a more environmentally friendly air transport system. As illustrated in Figure 1.1, innovative technologies play a crucial role in achieving carbon-neutral growth. These challenges are compelling aeronautical industries and research centers to explore new and innovative concepts characterized by disruptive technologies.

Consequently, the introduction of radically innovative technologies has significantly increased the complexity of aeronautical systems, involving a greater number of designers and generating vast amounts of data and information. The development of innovative complex systems involves highly multidisciplinary processes with requirements and constraints on the system itself, its individual components and integrated technologies, as well as interactions with the external environment and other involved systems. Furthermore, the aeronautical industry must integrate all individuals, expertise, and technologies involved in collaborative, international,

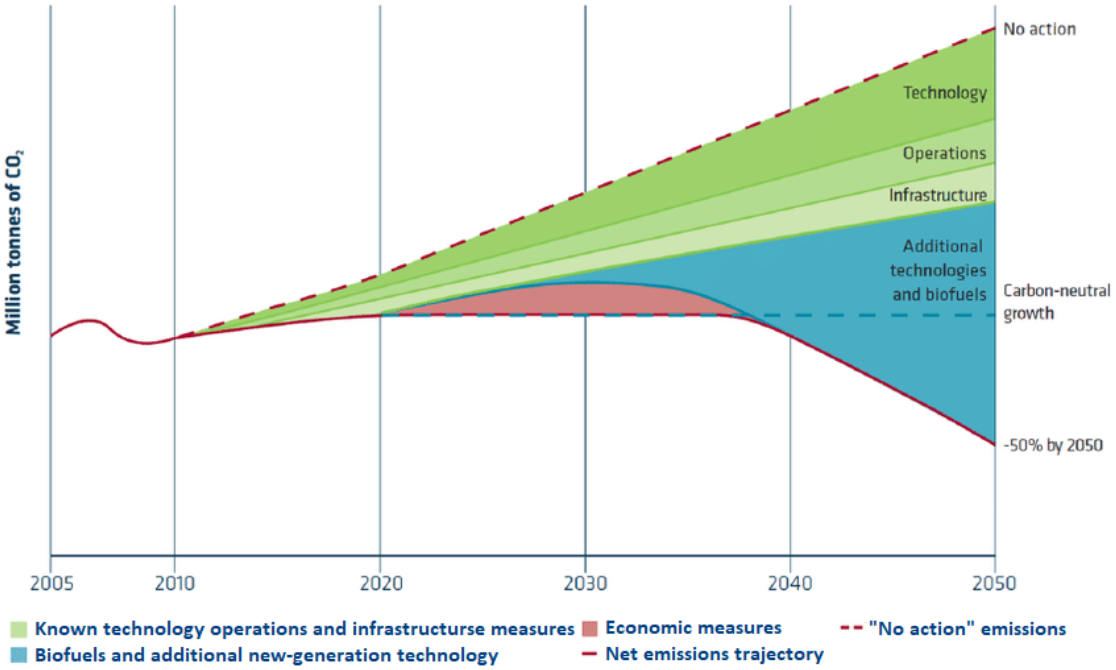

Figure 1.1: Schematic CO_2 emissions reduction roadmap. Adapted from [1].

and cross-organizational processes, to establish smooth operations across diverse disciplines and throughout the entire product life cycle. All these factors can contribute to a comprehensive dataset that covers various aspects of the product under development, such as requirements, specifications, descriptions, and interfaces of different systems, components, and aircraft parts. Any alteration to specific elements within this interconnected data can have extensive implications for the entire system [2]. The challenges in the early stages of aircraft development involve exploring a high-dimensional design space, evaluating multiple concepts, and managing numerous variations in requirements. A significant portion of program costs is committed during these initial phases, and the inadequate integration in the aeronautical supply chain presents obstacles to efficient and cost-effective development processes [3, 4]. In response to these critical aspects, there is a growing interest in novel development paradigms and the adoption of Model-Based Systems Engineering (MBSE), which offers benefits such as managing complexity, ensuring consistency, and improving communication among the involved actors [5,6]. This transition addresses the need for efficient requirement management, where models serve as a single source of truth, enhancing consistency, transparency, and enabling reuse in different projects [7]. The current trend involves managing requirements using dedicated software packages, emphasizing the direct inclusion of

requirements in the design process to achieve optimal system designs that comply with specified requirements [8, 9].

Traditionally, reliability and safety analysis in aircraft development has been conducted using a document-based approach, which involves creating extensive tables and reports [10]. However, this conventional approach faces challenges, particularly in light of the increasing complexity of modern aircraft systems. The conventional document-based methodology is hindered by issues such as insufficient traceability, lack of clarity, and the potential for errors due to the extensive dispersion of information. Consequently, there is a shift towards adopting MBSE to enhance design activities and foster improved communication within development teams [11]. Numerous companies, especially in the aerospace sector, are shifting towards model-based approaches, expecting an increasing role for MBSE in Systems Engineering in the coming decades [12]. In contrast to document-based methods, which are prone to challenges in managing information and an increased risk of human errors, a model-based approach offers advantages such as streamlining development, improving design quality, and enhancing team communication [13, 14]. MBSE is recognized as a crucial technology for developing innovative systems across various industries, including aerospace, automotive, and defense. Interest in MBSE is driven by potential advantages such as enhanced traceability, improved communication, automated validation and verification activities, and data reuse in subsequent projects [15]. The International Council on Systems Engineering (INCOSE) is a key proponent of the transition from document-based to model-based approaches [16]. According to INCOSE, models can support activities traditionally performed through document-based approaches, such as system requirements development, function identification, system architecture determination, and validation/verification tasks [17]. The adoption of MBSE is expected to play an increasingly significant role in Systems Engineering [18], offering advantages such as enhanced collaboration, a centralized source of truth, improved complexity management, and increased traceability [11,12]. MBSE extends beyond design and verification tasks to support activities such as developing system requirements, identifying system functions, and determining system architectures [7, 19]. In practice, models effectively support, improve, and accelerate all activities of a Systems Engineering Product Development process, including the definition of customer needs, identification of system functionalities, collection of requirements, generation of alternative system architectures, and verification and validation tasks [20]. MBSE, by offering a centralized source of information throughout system development, can enhance coherence, reduce ambiguity, and facilitate collaboration in the design of systems [21].

The efficiency and effectiveness of aircraft conceptual design can be improved by using a synergistic approach that involves the seamless integration of MBSE and Multidisciplinary Design Analysis and Optimization (MDAO) methods. In the conceptual design phase, where requirements, system architecture, and aircraft feasibility are conceptualized, MBSE proves valuable [22]. However, to fully address system complexity, there is a crucial need for the integration of MBSE with MDAO techniques [23]. The collaboration between these two domains can elevate the preliminary design phase to a higher level, enabling the designer to consider all stakeholders and domains that influence the solution during the definition phase. This ensures data traceability and facilitates verifying the consistency and consequences of any modifications made to the entered information. The MDAO technologies serve as a crucial cornerstone in modern engineering. Multidisciplinary Design and Optimization (MDO) offers a novel approach to tackling complex design challenges by seamlessly integrating and optimizing multiple subsystems and disciplines. The driving philosophy behind MDO is based on the recognition that the performance of a complex system is determined not only by individual components but also by the interactions between them. As a result, MDO takes a comprehensive approach to managing these interdependencies holistically. It utilizes advanced computational tools to improve design quality while also reducing the time and cost associated with the design process. The aerospace industry has widely recognized the potential of MDO, with a growing appreciation for its numerous benefits.

Nevertheless, to fully unlock the potential of MDO, an efficient and agile implementation is necessary for generating an MDAO framework. Early explorations into MDO, as observed in [24, 25], laid the groundwork for understanding how different MDO approaches could be implemented. The formulation and implementation of the MDO problem itself are crucial and are referred to as the MDO architecture. This architectural framework can be categorized into two main approaches: monolithic and distributed. Monolithic architectures are well-suited for tightly coupled systems in which individual disciplines have a strong interdependence. This architecture ensures good computational efficiency, as long as the system's size and complexity are manageable. In monolithic architectures, each discipline is modeled using specialized tools, which can vary from empirical curve fitting to physics-based simulations. The MDO problem is then approached as a unified optimization challenge that integrates design objectives and constraints across multiple disciplines and design variables. This approach directly addresses the interdependencies of design variables and analysis results from various disciplines, leading to more precise and physically consistent designs. On the other hand, distributed architectures break down the optimization problem into smaller, independently solvable subproblems

through the use of multiple optimizers. These subproblems are then integrated to achieve an optimal design. While this approach reduces the problem size, it introduces challenges related to maintaining consistency between disciplines, ensuring convergence, and selecting an appropriate coordination strategy [26]. Within the realm of monolithic architecture, various techniques have emerged to orchestrate the interaction between aerodynamic, structural solvers, as well as optimization tools, in distinct ways. Indeed, MDAO approaches offer the possibility to exploit both the interaction of system and discipline components. A comprehensive review of these methods is available in [26], encompassing approaches such as "All-at-Once" (AAO), Simultaneous Analysis and Design (SAND), Individual Discipline Feasible (IDF), and Multi-Discipline Feasible (MDF).

In the field of aviation, the utilization of MDAO architectures and methodologies extends beyond theoretical exploration of innovative technologies, leading to tangible and revolutionary aircraft configurations that have a significant impact. The application of MDO not only facilitates the de-risking of groundbreaking technologies but also serves as a catalyst for the development of disruptive solutions that redefine the boundaries of traditional design. The systematic exploration of the design space, made possible by MDO, enhances understanding of complex products and empowers engineers to surpass the boundaries of conventional thinking. The effectiveness of MDO is particularly evident in its capability to integrate and optimize physics-based simulations across multiple domains without the need for reducing the level of fidelity. This allows for maintaining an appropriate level of fidelity. This approach is essential for developing innovative and disruptive solutions that address the dynamic challenges of the constantly evolving aviation industry [27]. As the aviation industry continues to undergo transformation, MDO techniques are positioned to play a crucial role in guiding this paradigm shift [28,29]. Notably, these techniques provide a unique opportunity for the development of innovative aircraft designs by revealing interdependencies and design factors that might otherwise be overlooked [30]. Novel design configurations can significantly impact the achievement of ambitious goals to reduce fuel consumption, emissions, and noise, as detailed in the 2019 Advisory Council for Aeronautical Research in Europe (ACARE) Flightpath 2050 initiative [31]. In pursuit of the ambition to minimize the environmental impact of the aviation industry, the EU Commission, in collaboration with industry partners, launched the Clean Sky 2 program [1]. This program explores innovative concepts aimed at developing cleaner air transport technologies to improve aircraft fuel efficiency and reduce CO_2 NO_x and noise

[1]Clean Sky 2 Programme Overview and Structure: `https://www.clean-aviation.eu/clean-sky-2/programme-overview-and-structure` [retrieved March 11, 2024]

emissions compared to current state-of-the-art solutions. Every new technology undergoes rigorous testing and validation to meet strict performance and safety requirements. Demonstrators [2] serve as experimental platforms for manufacturers to test and validate new technologies. Within the Clean Sky 2 framework and as a component of Platform 1, which is dedicated to researching advanced engines and aircraft configurations, the Advanced Rear End (ARE) demonstrator is currently in development for the entirety of Clean Sky 2 program projects.

The ARE demonstrator integrates a comprehensive combination of interconnected aircraft rear-end and empennage elements, using advanced materials and innovative manufacturing techniques to decrease weight and enhance production rates for medium-sized passenger aircraft of the future. A significant deviation from the traditional tail planes in the ARE project is the forward-pointing horizontal stabilizers. Two primary reasons support this design choice. Firstly, there is a direct performance-driven advantage: positioning the horizontal tail forward enhances Natural Laminar Flow (NLF) on the tail, thereby reducing fuel consumption. Secondly, by reducing the sweep angle of the tail, it is possible to shorten the rear end since the sections of the fuselage in which the horizontal tailplane is inserted are located further behind compared to a conventional configuration. This layout can lead to weight savings in the fuselage. A shorter rear end allows for extending the passenger cabin, occupying more of the overall aircraft length. This design modification has the potential to accommodate additional seat rows, which could increase revenue for airlines and reduce fuel consumption per passenger. Despite the traditional rearward sweep observed in horizontal tailplanes throughout aviation history, advancements in aeroelastic technology development, as emphasized by [32], highlight the growing importance of forward-swept horizontal tailplanes and wings. This innovative approach is being explored for its potential to revolutionize aircraft performance, stability, control, and maneuverability. In fact, the aviation industry has embarked on an exciting journey to unlock the benefits of these unconventional configurations. These efforts are driven by a pursuit of achieving improvements in both aerodynamics and environmental effects. The adoption of forward sweep in aircraft design is primarily motivated by its promising aerodynamic benefits. These benefits include reduced drag divergence, improved stall characteristics, and enhanced lift-to-drag ratios.

[2] Clean Sky's Demonstrators: `https://www.clean-aviation.eu/clean-skys-demonstrators` [retrieved March 11, 2024]

1.2 State of the Art

The utilization of MBSE in industrial contexts, particularly within the aeronautical industry, is increasingly prevalent in the integration of MBSE into the development processes of complex systems. The aeronautical sector is experiencing a growing momentum in the adoption of MBSE [33], with ongoing research exploring its effective utilization [34, 35]. Concurrently, the industry is exploring a Model-Based Safety Assessment (MBSA) approach [36–40], particularly relevant for aircraft certification processes that adhere to standards such as SAE ARP4761 [41]. Safety assessment, closely tied to system architecture development, needs to be considered from the early design phases. Tepper [42], Maheshwari [35], and Jeyaraj [43] provide overviews of MBSE, shedding light on its diverse models and subprocesses. MBSE extends beyond aeronautics and finds applications in light rail systems [44], space system architectures [45, 46] and the semiconductor industry supply chains [47]. Within aircraft systems, Mathew et al. [48] demonstrates the role of MBSE in developing system architecture specifications. Liscouet-Hanke et al. apply MBSE to develop aircraft flight control systems [49], and Malone describes the use of MBSE in developing industrial aircraft system architecture in [50]. MBSE also makes a significant contribution to conceptual design stages [33, 43]. Efforts to link MBSE with MDAO have been a focal point of previous research. Cencetti et al. [51], Leserf et al. [52], and Beernaert and Etman [53] present various frameworks that connect these methodologies, although they acknowledge limitations in flexibility. Some studies focus on improving the early stages of Systems Engineering Product Development, particularly in requirement development. Génova et al. [54] propose desirable properties for textual requirements, emphasizing verifiability, completeness, consistency, understandability, ambiguity-free nature, and traceability. MBSE further facilitates the capture of certification regulations, as demonstrated by Bleu-Laine et al. [34], establishing associations with accepted means of compliance. Recognizing the benefits of a model-based approach, Joshi et al. advocate for utilizing modeling and simulation tools, such as Simulink [55] and SCADE [3], in Model-Based Safety Analysis [56, 57]. This process involves conducting safety analyses, establishing safety requirements, designing the system, and creating system models and fault models to support verification activities. Van Tooren and La Rocca emphasize the complementary roles of Systems Engineering and MDAO in supporting the product development process [58]. Systems Engineering encompasses a comprehensive engineering effort, while MDAO refines design solutions against

[3] Ansys SCADE Software home page: `https://www.ansys.com/products/embedded-software/ansys-scade-suite` [retrieved March 11, 2024]

quantitative requirements, positioning itself as a crucial tool within the expansive Systems Engineering framework [15]. Recent research efforts, as exemplified by Ciampa et al. [5], underscore the integration of MBSE practices and tools in the complex development processes of aeronautical products. This integration extends to the development of systems such as MDAO, with the aim of expediting deployment and operations, thereby accelerating overall complex system development [2]. The AGILE 4.0 [4] project showcases the progressive adoption of model-based approach within the aircraft development domain [59,60], establishing crucial linkages between aircraft development and MDAO frameworks [61,62]. The project introduces model-based approaches to system architecture definition, serving as a crucial connection between architecture definition and MDAO within the AGILE 4.0 toolchain [63,64]. Notable contributions include addressing key aspects such as certification, supply chain, and production layers within a distributed MDAO workflow [65–68].

MDAO frameworks are essential for addressing the complexity of aircraft architectures. Due to their high level of multidisciplinarity, these frameworks allow for early consideration of the mutual influence among various design disciplines. Neglecting these interdependencies can result in designs that fail to meet critical requirements or operate inefficiently [69]. This interplay becomes especially noticeable when considering aerodynamics and structural factors. Indeed, there are cases where aerodynamic optimization clashes with structural integrity. Conversely, a design optimized for structural considerations might exhibit poor aerodynamic performance, emphasizing the necessity of MDO in achieving a well-balanced aerostructural design.

As Martins et al. [26] note, the earliest works on MDO primarily focused on structural optimization, but later expanded to encompass a broader spectrum of disciplines. Aircraft wing design represented one of the earliest applications of MDO [70,71]. This field presents a complex challenge, as it involves the intricate interplay of aerodynamics, structural considerations, and control systems [72,73]. Since those pioneering days, MDO has made significant progress, expanding its application to encompass entire aircraft [74] and a diverse array of other engineering systems, including propellers [75] and rotorcraft [76] to wind turbines [77] and other related topics. In recent years, MDO has continued to thrive as an active area of research. New architectural approaches have been developed, and successful industrial applications have emerged [78]. Numerous projects sponsored by national and international research programs have aimed to advance MDO [79]. These initiatives have refined specific elements within MDO systems, including the development of more efficient optimization algorithms and strategies [80]. Moreover,

[4] AGILE 4.0 Project home page: `https://www.agile4.eu/` [retrieved March 11, 2024]

simulation solvers suitable for gradient-based optimizations have been created [81,82], and design and optimization integration environments have been established [83,84].

Historically, many MDO practices have used low- or medium-fidelity analysis tools for structural or aerodynamic analysis. However, these tools may not fully meet the evolving requirements of the aviation industry, especially in terms of environmental efficiency and operational safety. Advances in computing power and parallelization techniques have led to the increased use of high-fidelity analysis in aerostructural problems. Studies, such as [85, 86], propose MDF approaches that integrate Computational Fluid Dynamics (CFD) with Finite Element Analysis (FEA) solvers. These methods employ coupled adjoint techniques for sensitivity analysis, providing faster and more accurate gradient estimation compared to traditional Finite Differences (FD) methods. They also help reduce computational costs, which can become prohibitive for large-scale problems characterized by a high number of design variables, as mentioned in [87].

Lower-fidelity aerostructural optimization, which involves Euler CFD or quasi-three-dimensional aerodynamic analysis coupled with equivalent beam Finite Element Models (FEM) [88], has also been applied using MDF [89], IDF [90], and even SAND [91]. High-fidelity aerostructural optimization, accomplished by coupling 3D CFD with 3D FEA, has been achieved using the IDF technique [69, 92]. A comparable method has been investigated in a recent study by Patel et al. [93], that utilizes a coupled adjoint technique.

The use of low to medium-fidelity methods for addressing aerostructural issues offers several advantages in terms of cost-effectiveness, enabling the collection of extensive datasets for analysis. Nevertheless, it is important to recognize that low-fidelity data may have limitations in accurately predicting real-world behavior and may not encompass the full range of physical phenomena relevant to the investigated problem. The existing literature contains numerous examples of the development and deployment of reliable low-fidelity tools to address aerostructural challenges. Jasa et al. [94] introduced a coupled aerostructural software using low-fidelity methods to predict the aeroelastic performance of a wing. The software integrated a Vortex Lattice Method (VLM) and 1-D finite-element analysis to simulate the lifting surfaces. A more advanced method was proposed by Chauhan [95], in which the structure of the lifting surface was modeled as a wing box, including upper and lower skins and two spars. This approach was successfully used to optimize the aerostructural design of the Boeing 777 wing, showing a remarkable 10% concurrence with results obtained from high-fidelity tools, as confirmed by Brooks et al. [96]. Changchuan [97] proposed a lightweight method to address coupled aeroelastic problems characterized by significant nonlinearities. This approach

used a low-fidelity strategy to reduce computational costs. In his work, Drela [98] utilized various tools, such as a VLM code and an aircraft design framework with simplified analytical structural models, to develop an unconventional transport aircraft configuration.

However, relying solely on the direct implementation of low, medium, or even high-fidelity tools for aerodynamic and structural analyses is not the most effective approach to tackle aerostructural optimization problems. To expedite the execution of MDO, it is possible to approximate the aerodynamics and structural behavior of the specific problem by constructing response surfaces or using reduced order methods. By implementing Design of Experiments (DOE), these response surfaces can be generated by manipulating the key design variables that influence the problem under examination. Subsequently, these design variables are used in the optimization process. This methodology enables the creation of various optimization problems and greatly reduces the computational time needed for optimization, especially when the workflow analysis involves a high-fidelity CFD tool [99, 100].

To fully harness the potential of MDO, certain components and capabilities are essential. High-performance computing infrastructures are crucial, along with efficient optimization algorithms [83] and strategies [26]. Additionally, advanced simulation-based analyses covering all aspects of flight physics are indispensable [101]. Robust process management and integration frameworks are essential to ensure the seamless implementation of MDO principles [84]. In fact, contemporary system design often requires collaborative efforts across diverse fields of expertise. Coordinating specialized tools, collecting, distributing, and archiving intermediate data all pose substantial organizational challenges in the design workflow. Integration frameworks play a crucial role in streamlining these complexities. Prominent tools in this field include RCE [5] (Remote Component Environment) [102] and OpenMDAO [83], which emphasize optimization. Similar software solutions such as ModelCenter by Phoenix Integration [6] and Knime [7] or Optimus[8], an automation and optimization tool by Noesis Solutions offer user-friendly graphical interfaces. The AGILE [9] project implemented these and similar methodologies, along with additional technology enablers, to develop a dedicated MDO framework for aircraft design, known as the AGILE Development Framework (ADF) [103, 104]. The ADF proved capable of significantly expediting the setup of the distributed multidisciplinary

[5]RCE Software home page: `https://rcenvironment.de/` [retrieved March 11, 2024]
[6]Phoenix Integration home page: `https://www.phoenix-int.com/` [retrieved March 11, 2024]
[7]Knime software home page: `https://www.phoenix-int.com/` [retrieved March 11, 2024]
[8]Optimus software home page: `https://www.noesissolutions.com/our-products/optimus` [retrieved March 11, 2024]
[9]AGILE Project home page: `https://www.agile-project.eu/` [retrieved March 11, 2024]

system by enabling a rapid and fully automated design process formulation. One of the major benefits demonstrated during the project was the expansion of the design space, which allowed for the design of novel aircraft configurations and supported the de-risking of new technologies. This phenomenon is exemplified by the application of MDAO methods and approaches to significantly different and disruptive aircraft configurations, known as Novel Configurations. Examples include the design of the Blended Wing Body [105–107], Box Wing, Strut-Braced Wing [108, 109], advanced Turboprop [110–112], and a MALE UAV (Medium Altitude Long Endurance Unmanned Aerial Vehicle) [113, 114].

The implementation of new aircraft concepts and technologies is being explored in the Clean Sky 2 program as a means to achieve the goal of developing cleaner air transport technologies. The program is structured around seven technology themes, each of which includes a set of Demonstrators. Demonstrators are experimental tools that manufacturers use to test new technologies and validate concepts. The goal is to integrate, demonstrate, and validate the most promising technologies that can contribute to Clean Sky's high-level and program-specific objectives. Key Demonstrators include advanced geared engine configurations, the next-generation civil tiltrotor, hybrid laminar flow control on the tailplane, and ARE configurations. The ARE demonstrator [10] integrates conceptual design, structural and systems architectures, materials, technologies, and industrial processes associated with a disruptive rear fuselage and empennage configuration. The goal is to optimize these components for use in the next generation of commercial aircraft [115]. The project introduces a new aircraft design featuring a forward-swept tail to reduce fuel consumption and allow for a more compact rear end. Furthermore, enabling technologies are being researched to implement the aerodynamic concept and maximize its advantages. A European project aligned with the broader Clean Sky 2 program is represented by the IMPACT [11] project, whose primary objective revolves around the shape optimization of the Rear Fuselage and Empennage of Large Passenger Aircraft (LPA), including anti-icing technologies. The project aims to improve understanding and technology related to aircraft icing, contributing to advancements in both safety and efficiency for LPA. In this case, the ARE configuration includes a forward-swept tail. However, the current state of the art lacks analyses on negatively-swept horizontal planes, with the primary focus being on main wings with a negative sweep. Krone [116] explores the historical development of forward-swept wings,

[10] Advanced Rear End Demonstrator: `https://www.clean-aviation.eu/clean-sky-2/key-demonstrators/advanced-rear-end` [retrieved March 11, 2024]

[11] IMPACT Project home page: `https://www.impact-cleansky-project.eu/` [retrieved March 11, 2024]

tracing their origins back to the 1940s. The advantages and challenges of forward sweep are thoroughly examined, emphasizing the importance of dedicated flight demonstrators to reveal their full potential. Several studies have examined the divergence behavior of high-aspect-ratio, laminated composite swept wings [117–121]. The consensus from these studies indicates that aeroelastic tailoring is crucial for fully harnessing the benefits of positive sweep wings. Consequently, groundbreaking works such as [122] and [123] introduced aeroelastic tailoring as an essential part of the design process. They developed a comprehensive strategy that utilizes aerostructural wing optimization to enhance aerodynamics, structural strength, and fuel efficiency while effectively managing aeroelastic deformation. Forward-swept wings also present an exciting opportunity to integrate NLF technology with aeroelastic tailoring. Redeker et al. [124] highlighted this possibility, and subsequent studies have underscored its potential benefits, such as reducing fuel consumption and expanding high-speed capabilities [125]. Further investigations have examined modifications to the lift coefficient and the effective control of lateral dynamics [126]. Studies focused on transonic NLF transport aircraft with forward-swept wings have highlighted the benefits of forward sweep in achieving NLF at high cruise Mach numbers. This, in turn, leads to significant reductions in fuel consumption compared to conventional designs [127, 128].

The Clean Sky's Advanced Rear End project involves the development of anti-ice coatings for aircraft tails. These coatings are validated through wind tunnel testing to reduce tail size and achieve a NLF-compliant aerodynamic design. Additionally, the IMPACT project aims to conduct 3D ice accretion simulations that are applicable to non-straight leading-edge empennages, while considering the effects of passive anti-ice coatings and devices. The objective is to develop aerostructural optimization methods for ARE, taking into account the impact of ice. Ice accretion is a significant factor to consider when designing the tailplane. Certification authorities require demonstrations of aircraft stability and controllability in critical icing conditions. However, in the current state of the art, there is a noticeable lack of references that address ice formation analyses on positively swept wings. A comprehensive review [129] summarized experimental measurements of different ice accretions on fixed-wing aircraft, encompassing in-flight icing categories and highlighting deficiencies in the existing database. Research on inter-cycle ice shapes [130] revealed significant performance degradation, including reduced maximum lift and increased drag coefficients. Gile-Laflin and Papadakis conducted aerodynamic testing [131] that demonstrated a 30% decrease in maximum lift for a 48-inch chord NLF airfoil model. An historical analysis of airfoil and wing aerodynamics in icing [132] categorized ice accretions into roughness, horn ice, streamwise ice,

and spanwise-ridge ice. The study summarized the effects of Reynolds number and Mach number on iced-airfoil aerodynamics. Lee and Bragg's study on the impact of forward-facing quarter-round geometry on simulated ridge ice showed a significant reduction in the maximum lift coefficient [133]. Calay et al.'s study on spanwise-ridge ice [134] observed the most significant reductions in lift and drag at specific locations, with maximum lift reductions ranging from 10 to 20%. Kim et al. study [135] systematically investigated the effects of simulated ice shape geometry on a flapped airfoil, revealing a linear relationship between the reduction in maximum lift and the location of ice horn. In contrast, Hoerner and Borst's work [136] laid the groundwork for analyzing large ice accretions, outlining their effects on airfoil aerodynamics and highlighting important factors like nose radius and camber. In the analysis by Ingehnan-Sundberg et al. [137], various ice accretion shapes and sizes were tested, demonstrating significant reductions in maximum lift. The study particularly emphasized the nonlinear decrease in maximum lift coefficient with respect to size. Recent tests conducted by Lee et al. [138] emphasized the significance of chordwise position in simulating the accretion of supercooled large droplets, leading to alterations in stall characteristics and significant reductions in the maximum lift coefficient. In addition, [139] demonstrated that the location and height of ice horns, rather than the leading-edge radius, significantly influenced airfoil performance, affecting the maximum lift coefficient and static stability.

1.3 Thesis Objective and Outline

MDAO approaches, particularly when combined with MBSE, can play a crucial role in pushing the boundaries of conventional aircraft design, as explained in the current section. This offers the potential to develop innovative solutions that address the presented challenges of the aviation industry. In the current state of the art, the integration of MBSE with the MDAO framework has yielded promising results, introducing significant contributions to addressing key aspects such as certification, supply chain, and production layers in aircraft development, within a distributed MDAO workflow. However, there is no evidence in the existing literature of works that employ the seamless integration of MBSE and MDAO approaches aimed at designing non-conventional aircraft configurations, such as forward-swept horizontal tailplanes. For these configurations, there is a significant lack of practical design, resulting in a lower level of experience and fewer studies conducted in the area. Consequently, it becomes even more important in this field to have models that explicitly express the interactions among all stakeholders involved, the components of the system under analysis, and the disciplines. Such models

become more extensive and complex compared to those obtainable for traditional configurations. Therefore, the integration of MBSE and MDAO presents extra challenges, but at the same time, it can allow for overcoming them if properly integrated. Furthermore, the assessment of this innovative technology in aeronautics lacks consideration of diverse disciplines such as coupled aerodynamics and structure, or ice formation, as well as aspects related to aeronautical design, regulation, and certification fields, in the current state of the art.

The scenario outlined above underscores the motivations behind this research work:

How can model-based systems engineering methodologies be utilized to develop multidisciplinary analysis and optimization workflows for designing an innovative rear-end for large passenger commercial jet aircraft?

To fill the identified gap in the current state of the art, the research study utilized methodologies based on MBSE to develop and implement MDAO workflows. This approach facilitated the design of the rear end of a large passenger commercial jet aircraft, introducing innovative and disruptive solutions such as a negative-sweep horizontal tail, a Leading-Edge eXtension (LEX), and a bottle-neck-shaped fuselage. The final solution is derived from MDAO optimizations, achieved through multi-fidelity and multi-disciplinary frameworks emerged by system engineering analysis conducted using MBSE technologies. This analysis precisely defined all stakeholder needs and transformed them into requirements, which served as the basis for modeling the system to be analyzed. Indeed, the generated system is designed to possess all the necessary components capable of fulfilling the modeled functions introduced to represent the stakeholders' requirements. Several workflows were subsequently developed to design the system, leading to a solution aimed at meeting all identified requirements. The entire process is capable of considering various aspects of design, incorporating disciplines such as aeroelasticity and in-flight ice formation.

Specifically, this work is structured as follows:

- **Chapter 2** provides an overview of the European research projects that significantly influenced the author's work. The focus is on collaboratively developing and optimizing aircraft solutions through the adoption of MBSE and MDAO technologies. The chapter explores the structure of the projects, with an emphasis on the author's contributions. The primary goal of this chapter is to provide a comprehensive understanding of the approach, tools,

and methodologies used to address the entire aircraft design process by integrating MBSE within the MDAO framework. The insights gained from these projects have been crucial in shaping the author's research, allowing for the application of a multidisciplinary approach to an innovative and unconventional aircraft rear-end design.

- **Chapter 3** outlines the MBSE and MDAO technologies utilized to achieve the results presented in this study. The chapter explores the role of MBSE and MDAO paradigms in supporting the essential activities of a Systems Engineering Product Development process. MBSE technologies play a crucial role in designing complex products by taking into account stakeholders' needs, Top-Level Aircraft Requirements (TLARS), generative system scenarios, and the definition of system architecture. These technologies also provide methods for verifying requirements, making decisions, and validating. The process is guided by MBSE tools that streamline the development of an MDAO workflow capable of designing enabling systems and facilitating the verification of previously defined TLARS. The MDAO framework includes essential technologies for implementing a multidisciplinary collaborative workflow in a cross-organizational context. This chapter includes optimization and surrogate modeling tools, both of which are elaborated upon.
- **Chapter 4** outlines the methodologies used to develop design disciplines in MDAO workflows. The chapter introduces high, medium, and low-fidelity tools for analyzing the advanced rear end of the proposed solution, which includes components such as a forward-swept horizontal stabilizer, leading-edge extension, and bottleneck-shaped fuselage. These tools are classified into three groups. The first tool facilitates the computation of geometry parameters based on a tailplane sizing condition and generates a Computer-Aided Design (CAD) file with a CFD-compatible mesh. Additionally, a tool for morphing aerodynamic mesh based on macro design parameters is provided. Aerodynamic methodologies encompass VLM and CFD analysis to address challenges in diverse fluid domain conditions, as well as sensitivity analysis for aerodynamic gradients. A CFD-based methodology is used to analyze the impact of geometrical parameters on the aerodynamic performance of a horizontal stabilizer in icing conditions. Aerostructural methodologies yield deformation results under specific load conditions, as well as structural gradients associated with tailplane geometry and structural parameters.
- **Chapter 5** showcases the application of the described development process and methodologies on a large passenger jet aircraft to design an advanced rear-end concept. The innovative concept and the motivations behind its creation are

presented. Following this, the definition of stakeholders' needs, operational scenarios, system requirements, and architecture is outlined, guiding the generation of multiple MDAO workflows. Four distinct workflows generated through four test cases in the MBSE model are presented, along with results derived from their execution. The achieved results, along with the requirement verification process, allow for the visualization of improvements made through the implementation of the innovative solution compared to a conventional one. Additionally, the impact of minor modifications in the MBSE environment on the final solution is illustrated.

Finally, all primary research findings are discussed.

2

European Research Projects: Lesson Learnt

Contents

This chapter provides a comprehensive overview of the European projects that have significantly influenced the author's research. The focus is on the collaborative development and optimization of innovative aircraft solutions through the adoption of MBSE and MDAO technologies largely applied in the following chapters. Here, the main objectives and structure of the projects are explored, emphasizing the author's contributions. The aim is to provide insight into the approach, tools, and methodologies used to tackle complex challenges in the aeronautical industry. The experience gained from the IMPACT, AGILE, and AGILE4.0 projects has been foundational to the author's research. It facilitated the application of a multidisciplinary approach to an innovative and unconventional aircraft rear-end configuration. The integration of different software and methodologies within the AGILE and AGILE 4.0 framework, combined with the analysis of innovative rear-end configurations, was pivotal in shaping the author's research approach. They provided a strong foundation for addressing design, production and certification

requirements in the optimization process, representing an advancement beyond the State-of-The-Art.

2.1 The IMPACT Project

2.1.1 Project objective and motivation

The IMPACT project is an EU research initiative funded by the European Union's H2020 research and innovation program. The project was led and coordinated by the Austrian Institute of Technology. The main goal of this project is to optimize the shape of the Rear Fuselage and Empennage of LPA, including the integration of anti-icing technologies. This category encompasses modern narrow-body aircraft designed to accommodate an average of 150 seats, twin-aisle wide-body aircraft ranging from 200 to 300 seats, and twin-aisle wide-body large/very large aircraft with 300 to 400 seats or more. Within this framework, IMPACT focuses on a crucial aspect that significantly affects both the safety and efficiency of LPAs: the implementation of the ARE concept. The project is structured around four specific main objectives:

1. Unlocking the ability to perform fast and accurate 3D ice accretion simulations suitable for non-straight leading-edge empennages. This involves accounting for the effects of passive anti-ice coatings and devices.
2. Characterizing, integrating, and leveraging passive anti-ice coatings and devices for non-linear leading-edge empennage configurations, with the goal of achieving Technology Readiness Level (TRL) 5 by the end of the project.
3. Developing and applying innovative aerostructural optimization methods for ARE, considering the impact of passive anti-ice coatings and devices. The aim is to minimize drag and address structural and aeroelastic constraints.
4. Validating the accuracy of 3D icing accretion simulations and the performance of passive anti-ice coatings and devices through large-scale Icing Wind Tunnel (IWT) experimental tests.

The project is aligned with the broader Clean Sky 2 program and aims to improve understanding and technology related to aircraft icing, contributing to advancements in both safety and efficiency for large passenger aircraft. To achieve its goals, IMPACT leverages a consortium comprising nine European partners from Austria, Italy, and the UK, augmenting the value of EU funding through collaboration with a tenth partner from Canada. The outcomes of IMPACT are expected to make significant contributions to the goals of the CleanSky 2 Innovative Aircraft Demonstration Platform ARE. This involves a decrease in the ARE platform's

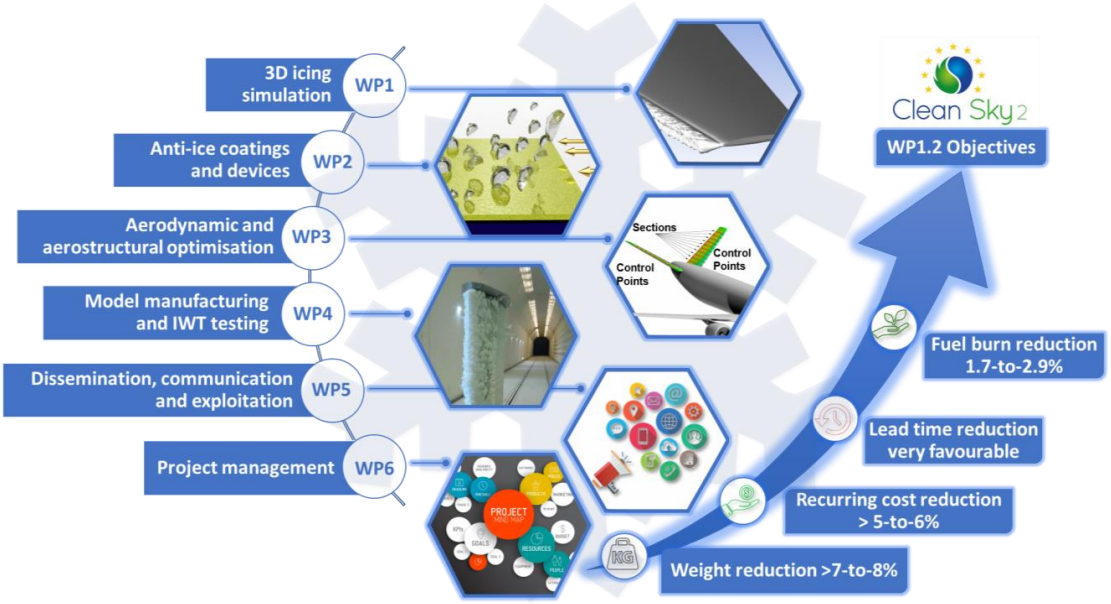

Figure 2.1: IMPACT Project Work Packages Structure and Main Objectives.

weight by 7-8%, recurring costs by 5-6%, LPA fuel consumption by 1.7-2.9%, and a positive effect on lead time reduction. IMPACT ultimately supports Airbus' progress with the ARE concept, enhancing the competitiveness of the European LPA industry and its value chain. Figure 2.1 presents a visual representation of the project, illustrating its structure, Work Packages (WPs), and primary objectives.

The IMPACT project aligns with all of the ARE objectives, aiming to achieve a 20% weight reduction, 20% recurring cost reduction, and 50% lead time reduction for the rear-end. The primary objective is to decrease fuel consumption by 1.5% at the aircraft level, in comparison to the best-in-class aircraft technology in the reference year 2014. Consequently, IMPACT supports the high-level objectives of reducing CO_2 and NO_x emissions in civil aviation, following the Flightpath 2050 roadmap [31] and aligning with the research activities of Innovative Aircraft Demonstrator Platforms (IADP) LPA Clean Sky 2 WP. To achieve its ambitious goals, IMPACT relies on a comprehensive range of skills and expertise from a consortium of 10 partners, led and coordinated by the Austrian Institute of Technology.

2.1.2 Lessons Learnt from IMPACT Project

The IMPACT project has provided the author with the opportunity to contribute to the design of an innovative rear-end configuration in a mixed research and industrial environment. The company's involvement in the project has been crucial, as feedback from the industry played a pivotal role in shaping the direction of

the work. These insights emphasize the importance of considering not only the objective functions involved in the optimizations but also the various constraints imposed by manufacturing and maintenance aspects. Additionally, certification requirements have been considered, with an emphasis on identifying the most crucial conditions for developing the final solution. All of these factors have been taken into consideration to develop a final solution that offers improved performance compared to conventional alternatives.

Throughout the project's development, the author adhered to a classical approach, employing human-driven analysis and optimization methodologies, considering results from low to high fidelity tools, and conducting wind tunnel tests. The author's research extended beyond the work explored in the IMPACT project, incorporating a unique design and optimization approach. The incorporation of this rear-end design into an MDAO environment represented a significant advancement. Automatic optimization processes have addressed various challenges by producing Pareto fronts and specific solutions, each with unique advantages and characteristics. Furthermore, the thorough understanding of the previously mentioned considerations was utilized by integrating the MDAO approach into a Systems Engineering Product Development process. This holistic approach takes into account the requirements of all stakeholders, leveraging insights gained from other European research projects.

2.1.3 Author Contribution to IMPACT Project

The author's primary contribution to the project involved designing the ARE concept within WP3. Numerous optimization analyses were conducted, ranging from low to high-fidelity examinations of aerodynamics and structure for an innovative ARE concept. The IMPACT project focused on designing a forward-swept horizontal tailplane, taking into account aerodynamic, stability, aerostructural, and icing effects. The development of such a disruptive solution follows a traditional approach, which includes human-driven analysis, optimization, and wind tunnel tests to create a solution that meets industrial, maintenance, and certification requirements.

Within the project context, the author of the thesis developed a methodology in collaboration with the University of Southampton. An architecture for IDF optimization workflow has been developed and tested to tackle an adjoint-driven high-fidelity aero-structural optimization problem using a monolithic approach. The methodology utilizes a high-fidelity commercial solver and enables the computation of gradients for adjoint optimization with respect to geometric or structural macro parameters, such as the tailplane sweep or the spar thickness. More details can be found in [92].

2.2 The AGILE Project

2.2.1 Project objective and motivation

AGILE (Aircraft 3rd Generation MDO for Innovative Collaboration of Heterogeneous Teams of Experts) [140] is an EU-funded project under the research framework Horizon 2020, coordinated by the DLR. Within AGILE, a team of 19 industry, research, and academic partners from Europe, Canada, and Russia collaborates to develop the next generation of aircraft MDO processes. These processes aim to achieve significant reductions in aircraft development costs and time to market, leading to more cost-effective and environmentally friendly aircraft solutions. The AGILE project primarily focuses on system design and optimization, specifically the MDO aspects of aircraft design [141]. The AGILE project introduced a new paradigm and advanced technologies for collaborative MDO processes across different organizations. This led to a significant reduction in setup time for MDO development systems [103].

The project aims to introduce and develop a new MDO aircraft framework that encourages a collaborative design approach, facilitates knowledge sharing among different teams of experts, and promotes innovative MDO approaches and applications. Implementing such a complex system requires making several assumptions about the methodology and technologies to be used for generating new systems. This set of assumptions and technologies is referred to as the 'AGILE Paradigm,' with its two enabling layers being the Collaborative Architecture (CA) and the Knowledge Architecture (KA), as depicted in Figure 2.2.

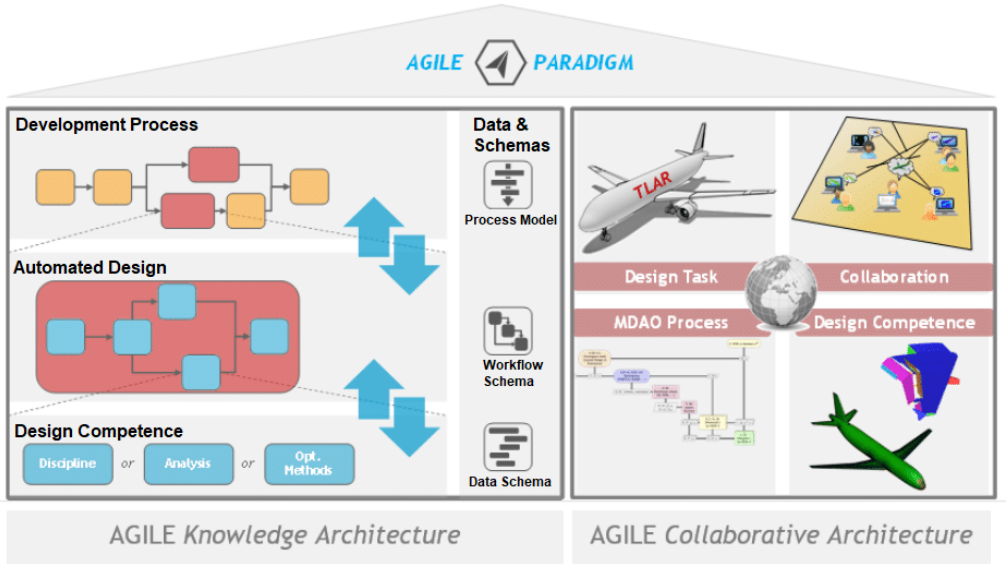

Figure 2.2: AGILE Paradigm Schema. Adapted from [142].

The CA focuses on developing technologies that enable distributed collaboration, involving the collaborative process among specialists within the existing framework. The KA-enabled technologies layer develops information technologies that support the management and formalization of knowledge within an MDO process. Both CA and KA are essential to support large, heterogeneous teams of experts in efficiently and effectively performing collaborative development within a specific timeframe.

The primary technical objectives of the AGILE project are [140]:

1. The development of advanced multidisciplinary optimization techniques and their integration aim to reduce the convergence time in aircraft optimization.
2. The development of processes and techniques for efficient collaboration among design teams across multiple sites.
3. The development of knowledge-enabled information technologies to support interdisciplinary design initiatives.
4. Develop and publish an Open MDO Test Suite, enabling other research activities to access project technologies and providing a reference database for future aircraft configurations research.

Achieving these objectives implies a significant improvement in the aircraft design and optimization process, leading to:

- A 20% reduction in the time required to converge the optimization of an aircraft configuration, attributed to AGILE optimization techniques.
- A 40% reduction in the time required to solve an MDO problem by a diverse team of specialists, attributed to the implementation of AGILE collaboration processes and AGILE optimization techniques.

Studies and MDO methods and approaches were applied to significantly different and disruptive aircraft configurations (Novel Configurations). The project aims to integrate more disciplines, higher fidelity, and certification constraints in the optimization process. It also aims to contribute to a European transport system that is resource-efficient, safe, climate- and environmentally-friendly.

2.2.2 Lessons Learnt from AGILE Project

The author gained the knowledge and capabilities to establish a multidisciplinary collaborative design analysis and optimization framework from scratch through the application of the AGILE project's developed methodologies. Through the work carried out in the AGILE project, the author gained insight into addressing the challenges presented by designing an innovative system in a multidisciplinary environment. The AGILE framework facilitates the seamless orchestration of complex workflows by managing multiple disciplines and systems for analysis within

the same environment. To integrate available tools and information into the described framework, preliminary setup work must be executed. All methodologies must be generated or modified to be compatible with a common collaborative environment. Additionally, input and output of each methodology must be managed through a common language. The author acquired the knowledge related to this type of operation during the AGILE project experience.

Furthermore, the author had the chance to make use of MDAO collaborative technologies provided by the project, gaining a deep understanding of their capabilities and limitations. This experience enabled the author to gain insights into the best ways to utilize these technologies for research activities. Having gained expertise in the technologies associated with the MDAO framework, the author decided to apply this approach to various contexts, as outlined in the following chapters.

2.2.3 Author Contribution to AGILE Project

The author contributed to the project by developing a high-fidelity aero-structural MDAO workflow within the AGILE collaborative multidisciplinary integration environment. This workflow can automatically generate a CFD mesh and perform high-fidelity aerodynamic computations, accounting for deformation effects. These flexible and robust automated workflows enable aero-structural analysis and optimization. Additionally, the approach enables adjoint-driven gradient-based shape optimization using reference Free Form Deformation (FFD) parameters. This work has been conducted on various aircraft systems, and additional details can be available in [143]. Furthermore, the author was involved in the testing phase of the MDAO technologies developed during the AGILE project.

2.3 The AGILE 4.0 Project

2.3.1 Project objective and motivation

AGILE 4.0: Towards cyber-physical collaborative aircraft development is an EU research project funded through the Horizon 2020 program and overseen by DLR from 2019 to 2023. This project involves a consortium of fifteen partners from various sectors, including industry, research organizations, and academia, distributed worldwide in Europe, Canada, and Brazil [144]. The main goal of the project is to achieve significant reductions in aircraft development costs and time-to-market. This is achieved by establishing an integrated cyber-physical aeronautical supply chain, which will promote innovation and improve the sustainability of aircraft products. Specifically, AGILE 4.0 is focused on the digital

transformation of critical components within the aeronautical supply chain, including design, production, certification, and maintenance. It builds upon the foundation established by the previous AGILE project [140], expanding its scope within the development process. Furthermore, AGILE 4.0 extends this development process by incorporating upstream activities that are inherent to a typical MBSE approach. This phase involves identifying stakeholders and their needs, defining technical requirements, and creating system architectures during the system design process. The original AGILE project had a narrow focus on designing and optimizing aircraft systems to meet specific design requirements and system architectures. This scope expanded during the subsequent EU-funded H2020 AGILE 4.0 project, incorporating additional phases of Systems Engineering into the system development cycle, alongside the customary design and optimization tasks. The expanded scope is visually represented in Figure 2.3, which illustrates the Systems Engineering Product Development process implemented in the AGILE 4.0 project [15]. The final two steps of this process (e.g. System Synthesis and System Design) align with the development activities explored in the AGILE project, which involve formulating and execution of MDAO processes for aeronautical product design and optimization. The remaining steps of the Systems Engineering Product Development process represent the extension introduced by AGILE 4.0.

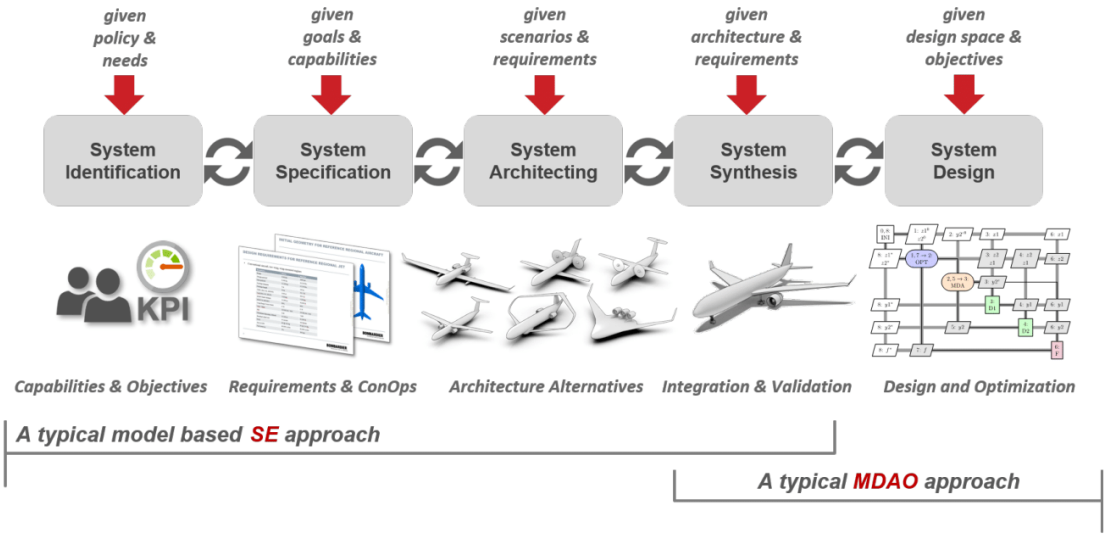

Figure 2.3: Systems Engineering Product Development process set up in AGILE 4.0 for the collaborative development of complex aeronautical systems. Adapted from [15].

The AGILE 4.0 research activity involves implementing design across multiple phases. These phases are intended to integrate a System Engineering approach into the development cycle, in addition to the standard design and optimization

activities. Figure 2.3 depicts these phases. The first three steps pertain to the MBSE approach. Indeed, the first phase involves modeling the scenario in which the activity is performed. The stakeholders' actions and interactions are defined here, specifying the steps required to realize the final product and its influence on the involved stakeholders. The second phase aims to define the needs and requirements of the stakeholders involved [2]. They can be modeled according to the MBSE approach, generating logical statements that make it easy to verify their fulfillment. The third phase involves modeling the system architecture [59]. A model of the systems under analysis is generated to describe how each system's components fulfill the requirements. Here, various solutions can be modeled, each generated through a decision-making process. The last two phases pertain to the MDAO process. The first part mainly focuses on defining the system to be analyzed. This step is carried out using the decision-making process described earlier. The second phase involves designing and optimizing the defined systems through the definition of a MDAO workflow which includes only the relevant disciplines. After completing these steps, methods for verifying requirements, decision-making modeling, and validation processes [7] can be carried out to select the optimal solution and confirm the satisfaction of the previously defined requirements. These operations are made possible thanks to the steps that characterize the MBSE approach. The main objective of the project is to demonstrate the capability of this innovative preliminary aircraft design methodology.

2.3.2 Lessons Learnt from AGILE 4.0 Project

The author utilized a Systems Engineering Product Development process, established within the framework of the AGILE 4.0 project, to develop and apply an innovative design approach to different configurations. Through this experience, the author gained an appreciation for the significance of system modeling in situations where multiple factors must be considered when designing a new configuration. The MBSE approach enables the schematization and traceability of elements that are crucial to consider during the preliminary design phase. Modeling scenarios and understanding the needs of all stakeholders involved in system design, followed by the creation of a system architecture, facilitates the development of a solution that arises from an optimization workflow and aligns with the requirements generated by these needs.

Furthermore, the author had the opportunity to employ MBSE modeling technologies provided by the project, gaining insight into their capabilities and limitations. In this way, the author gained insight into the most effective ways

to utilize these technologies for his research activities. Having gained expertise in the technologies related to MBSE modeling through the AGILE 4.0 project, the author decided to apply this paradigm to other contexts. This includes the design of an innovative configuration, as described in Section 2.1.

2.3.3 Author Contribution to AGILE 4.0 Project

The author's main contribution to the AGILE 4.0 project involves activities related to WP8, where the University of Naples Federico II held the position of WP leader. WP8 is dedicated to aircraft product upgrades and features two use cases. The first focuses on the design of aircraft airframe upgrades, while the second focuses on family concept design. Both use cases involve the same reference aircraft and establish design and optimization parameters for retrofitting and family concept tasks. The System Engineering Product Development process was utilized to validate the economic, environmental, and performance requirements linked to the retrofit of a 90-passenger regional jet aircraft. These requirements were defined based on the needs of stakeholders involved in the process. Various scenarios were considered, taking into account factors such as environmental restrictions, fluctuations in fuel prices, and the composition of the aircraft fleet to be retrofitted, as well as passenger comfort levels. The process began with defining architectures, which serve as the initial and final points of the design. A collaborative aircraft design workflow involving multiple disciplines was developed and implemented to analyze retrofit solutions. The introduced disciplinary competences were used to analyze and confirm the fulfillment of profitability, costs, performance, and emission requirements. For more in-depth information about the MBSE approach and the MDAO results can be found respectively in [65] and [145–147].

Furthermore, the author contributed to implementing workflows for the second use case in WP8 [148] and the use cases in WP7 [68].The WP7 addresses various aspects of aeronautical product certification. This includes defining system architecture for new on-board systems with different levels of electrification, conducting continuous airworthiness analysis, and integrating systems and airframe. Various tool methodologies were utilized to conduct mission analysis simulations, engine modeling, noise estimation, tail-plane design, and low-fidelity aerodynamic and stability computations for both WPs.

Lastly, the author was involved in testing the developed MBSE and MDAO technical solutions, as well as in utilizing optimization software, as presented in [149].

List of related publications

Journal papers

- P. Della Vecchia, **M. Mandorino**, V. Cusati and F. Nicolosi. Retrofitting Cost Modeling in Aircraft Design. *Aerospace MDPI*, Volume 9, No. 7, 349, 2022, 105667, ISSN 2226-4310, DOI: https://doi.org/10.3390/aerospace9070349.

  This paper proposes a methodology for assessing aircraft retrofitting costs at an industrial level and explains the related activities involved. The methodology is integrated into the AGILE 4.0 activity, considering variables and scenarios included in the project MDAO framework.

- (Under Review) S. Corcione, **M. Mandorino** and V. Cusati. Beyond Conventional: An Integrated Aerostructural Optimization Approach for Innovative Tailplane Configurations. *Aerospace Science and Technology*

  This paper presents a study focused on optimizing ARE configurations for transport jet aircraft, with the aim of improving fuel efficiency. The activity is carried out within the framework of the IMPACT project.

Conference papers

- **M. Mandorino**, P. Della Vecchia, F. Nicolosi, S. Corcione, V. Trifari, G. Cerino, M. Fioriti, C. Cabaleiro, T. Lefebvre, D. Charbonnier, Z. Wang and D.M.J. Peeters. Regional jet retrofitting design: from stakeholders' needs and system's requirements to MDAO workflow formulation. In *2022 ICAS 33rd Congress of international council of the aeronautical sciences*, 4-9 September 2022, Stockholm, Sweden. DOI: https://doi.org/10.5281/zenodo.7071016.

  This paper describes a process for verifying economic, environmental, and performance requirements associated with the retrofit of a 90-passenger regional jet aircraft. An comprehensive MBSE process is implemented within the framework of the AGILE 4.0 project.

- **M. Mandorino**, P. Della Vecchia, S. Corcione, F. Nicolosi, V. Trifari, G. Cerino, M. Fioriti, C. Cabaleiro, T. Lefebvre, D. Charbonnier, Z. Wang and D.M.J. Peeters. Multidisciplinary Design and Optimization of Regional Jet Retrofitting Activity. In *2022 AIAA Aviation and Aeronautics Forum and Exposition*, 27 June - 1 July 2022, Chicago, Illinois. DOI: https://doi.org/10.2514/6.2022-3933.

  In this paper, optimization of retrofitting activities on a 90-passenger regional jet aircraft is performed through a multidisciplinary collaborative aircraft design and optimization workflow. The entire

process is implemented within the framework of the AGILE 4.0 project.

- **M. Mandorino**, P. Della Vecchia, F. Nicolosi and G. Cerino. Regional jet retrofitting through multidisciplinary aircraft design. In *11th EASN Virtual International Conference Agenda*, 1-3 September 2021, virtual meeting. DOI: 10.1088/1757-899X/1226/1/012047.

  This paper applies multidisciplinary collaborative design to a retrofit of a 90-passenger regional jet aircraft, emphasizing its impact on costs and performance. The collaborative remote MDAO process is implemented within the framework of the AGILE 4.0 research project.

- C. Conti , **M. Mandorino**, A. Da Ronch and A. Elham. High-fidelity Aero-Structural Optimisation using Individual Discipline Feasible Strategy. In *2023 AIAA Aviation and Aeronautics Forum and Exposition*, 12-16 June 2023, San Diego, California. DOI: https://doi.org/10.2514/6.2023-3317.

  This paper presents adjoint-driven high-fidelity aero-structural optimization of a forward-swept tailplane using IDF architecture. The activity is conducted within the framework of the IMPACT project.

- M. Fioriti, C. Cabaleiro, T. Lefebvre, P. Della Vecchia, **M. Mandorino**, S. Liscouët-Hanke, A. Jeyaraj, G. Donelli, A. Jungo. Multidisciplinary design of a more electric regional aircraft including certification constraints. In *2022 AIAA Aviation and Aeronautics Forum and Exposition*, 27 June - 1 July 2022, Chicago, Illinois. DOI: https://doi.org/10.2514/6.2022-3932.

  This paper focuses on the preliminary design of a small regional turboprop aircraft that can accommodate 19 passengers. The overall process is implemented within the framework of the AGILE 4.0 research project, using a collaborative remote multidisciplinary approach.

- J.H. Bussemaker, P.D. Ciampa, J. Singh, M. Fioriti, C. Cabaleiro, Z. Wang, D.M.J. Peeters, P. Hansmann, P. Della Vecchia and **M. Mandorino**. Collaborative Design of a Business Jet Family Using the AGILE 4.0 MBSE Environment. In *2022 AIAA Aviation and Aeronautics Forum and Exposition*, 27 June - 1 July 2022, Chicago, Illinois. DOI: https://doi.org/10.2514/6.2022-3934.

  This paper presents a MBSE design approach for a business jets family, performed using methods developed in the AGILE 4.0 project.

3

MBSE enabling technologies and Collaborative MDAO

Contents

The MBSE methodologies and technologies implemented in this thesis are introduced. Additionally, this chapter illustrates the MDAO technologies exploited to achieve the results presented in this work. The MBSE approach plays a crucial role in supporting the primary activities of a Systems Engineering Product Development process through modeling. Within the MBSE paradigm, the model serves as the specification, encompassing the modeling of development scenarios, stakeholders, needs, and requirements. It also involves modeling aircraft architecture, verifying requirements, and decision-making, verification, and validation processes. The Collaborative MDAO approach enables the design and optimization of complex engineering products. This method involves a variety of essential technologies for implementing an MDAO workflow within a cross-organizational framework.
The MBSE and MDAO technologies are implemented within an Operational Collaborative Environment (OCE) [2]. This OCE facilitates the collaborative development of complex aeronautical products by providing robust support for modeling and a Systems Engineering approach throughout all phases of development. A schema illustrating various MBSE and MDAO technologies integrated into the OCE and their utilization in every stage of a Systems Engineering Product

Development process, as shown in Figure 2.3, is presented in Figure 3.1. This environment enables the design of complex products while taking into consideration stakeholders' needs, TLARS, the scenario in which the system arises and operates, and the definition of system architecture. The process is guided by MBSE tools, which streamline the development of a MDAO workflow capable of designing enabling systems and facilitating the verification of the previously defined TLARS.

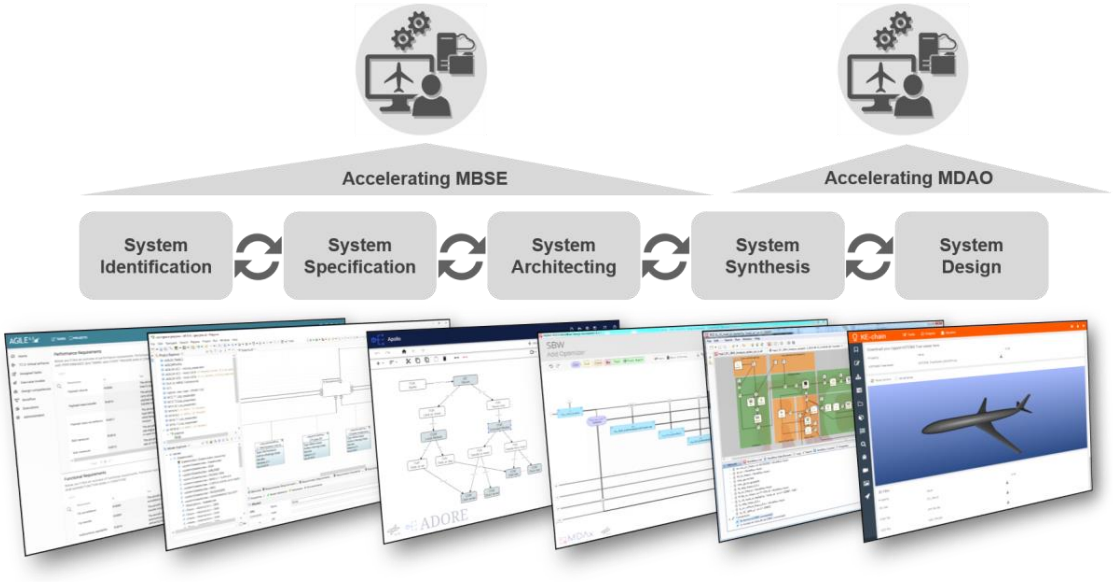

Figure 3.1: Overview of the collaborative MBSE and MDAO technologies exploited to address all the steps of a Systems Engineering Product Development process. Adapted from [15].

3.1 MBSE Approach for Collaborative Aircraft Design

The presented work introduces new methods and implementations that utilize an MBSE approach to streamline the design of an innovative ARE configuration for transport jet aircraft. Within the MBSE framework, models have been used to specify all the components and factors that influence the final configuration design of the ARE. This involves modeling development scenarios, engaging stakeholders, identifying needs and requirements, architectural modeling of the aircraft, modeling requirement verification methods, and modeling decision-making, verification, and validation processes. The methodologies outlined in this section form the framework through which the author has developed specialized expertise in the field of MBSE modeling technologies, as detailed in Section 2.3. Here, an overview is provided,

illustrating the MBSE technologies that enabled the author to leverage the MBSE environment and apply this paradigm in his research work.

3.1.1 Operational Collaborative Environment

The MBSE technologies utilized in this research are integrated into an OCE in the framework of AGILE4.0 research project [1]. The OCE is represented by a web-based process integration platform that allows for the generation of projects and corresponding design studies, management of user access, and collaborative generation of models for each design study. These models include stakeholder models, needs and requirements models, as well as architectural design spaces and MDAO workflow setups. Subsequently, the connection between MBSE and MDAO models can be established, using them to input into the executable MDAO and utilizing its outputs to validate requirements and select the results. Figure 3.2 provides an overview of the technologies integrated into the OCE, as developed in the AGILE4.0 project [150].

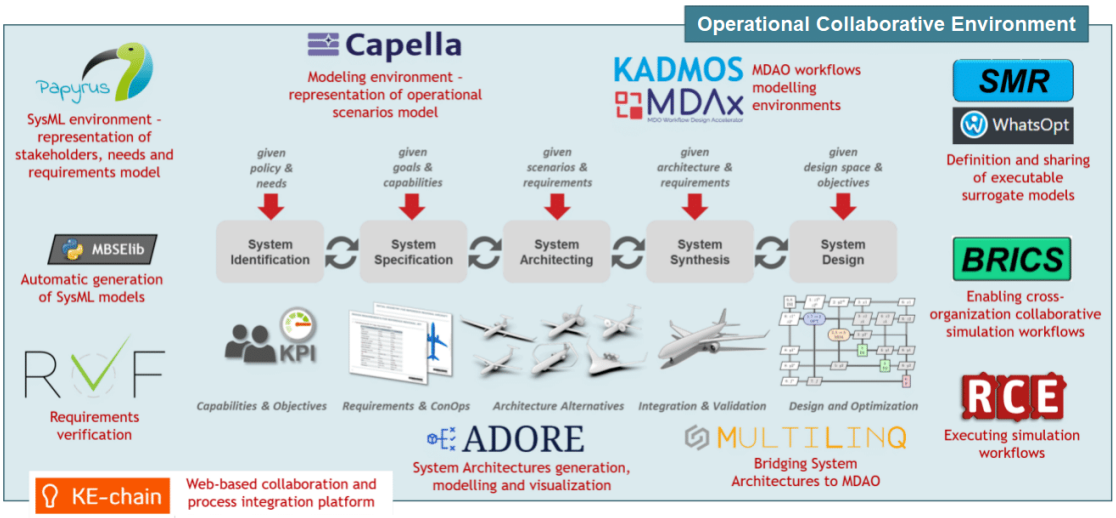

Figure 3.2: Overview of technologies integrated in the OCE exploited for the MBSE-MDAO Development Framework. Adapted from [150].

The OCE supports the collaborative development of complex aeronautical products by facilitating modeling and a Systems Engineering approach at all stages of development. The integration of MBSE technologies within the OCE aims to support the Systems Engineering Product Development process at every phase. The main goal of the OCE is to streamline and provide integrated access to expert knowledge, competencies, technologies, data, and information distributed across

[1] AGILE 4.0 Project home page: `https://www.agile4.eu/` [retrieved March 11, 2024]

engineering divisions in various organizations. Within the team of remote engineers, each engineer is equipped with a personalized dashboard to support their role in the development process.

Centralized and integrated access to the OCE is facilitated through KE-chain [2], a web-based platform for collaborative process modeling and data management. This platform offers a Graphical User Interface (GUI), designed to provide experts with access to relevant skills, technologies, data, and information while hiding the inherent complexity associated with using individual domain-specific tools. KE-chain serves as a portal, offering user-friendly collaboration for diverse teams of experts to organize and access design study data and technologies throughout the various stages defined in the Systems Engineering Product Development process and among collaborating partners. KE-chain drives the transition from traditional document-centric methodologies to a model-based paradigm. The platform enables the definition of projects and associated design studies, as well as the management of user authentication and data access. KE-chain serves as a central platform for initiating collaborative MDAO studies and defining MDAO workflows, all without requiring centralization of data storage or domain-specific tools. It enhances digital communication efficiency by centralizing information, streamlining management, automating tasks, and expediting workflows. A schematic overview of the KE-chain as the front end for the OCE is depicted in Figure 3.3. KE-chain provides access to various data standards for modeling information throughout the development process (e.g., Systems Modeling Language SysML, CPACS, CMDOWS), manages expert knowledge and tools such as ADORE, MDAx, KADMOS, supporting the collaborative application of the MBSE methodology for MDAO. These tools are either integrated into the KE-chain front end or interact with the KE-chain data model through the Python library Pykechain [3]. OCE tools are integrated as engineering services that can be executed directly on the KE-chain server using Docker containers that host dedicated Python computational environments [150]. The identification of stakeholders, needs, requirements, scenarios, and functional architectures can be directly performed through the KE-chain interface, utilizing all the engineering services depicted in Figure 3.3. In the following sections, all of these technologies are thoroughly described.

[2]Ke-Chain Platform home page: `https://ke-chain.com/` [retrieved March 11, 2024]

[3]pykechain library home page: `https://pykechain.readthedocs.io/en/stable/` [retrieved March 11, 2024]

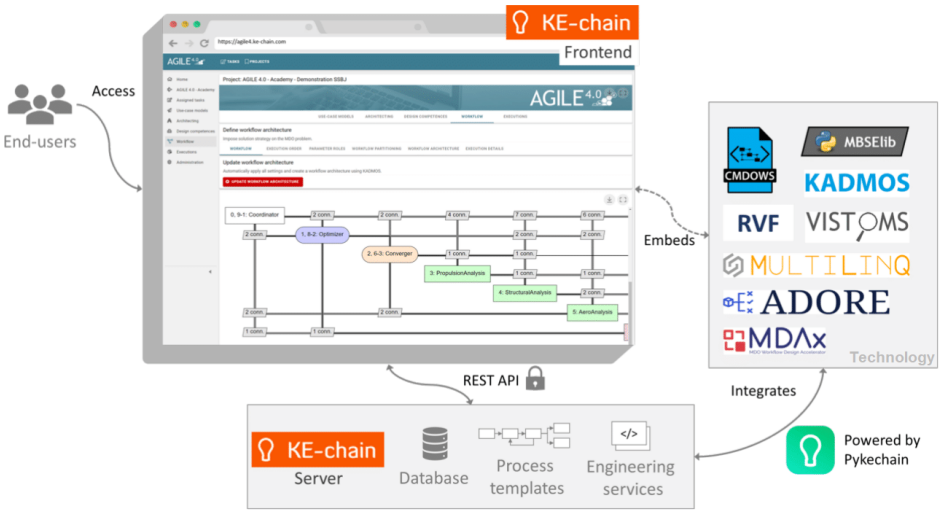

Figure 3.3: Schematic overview of the KE-chain front end which embeds and provides access to OCE technology as engineering services. Adapted from [149].

3.1.2 Stakeholders, Needs, Scenarios and Requirements

The initial phase of the Systems Engineering Product Development process focuses on the identification of system stakeholders, collecting their needs, and formulating system requirements. A stakeholder is defined as an "individual or organization having a right, share, claim, or interest in a system or in its possession of characteristics that meet their needs and expectations" [17]. When using an aircraft as an example of a system, stakeholders may include airlines, passengers, maintenance organizations, Original Equipment Manufacturers (OEMs), suppliers, regulatory authorities, and air traffic controllers. Each stakeholder has unique needs, requirements, and preferences for the system. In simpler terms, they represent various requirements, defined as "informal expressions of something that must be provided, ensured, or avoided by a system or its development project" [151]. For example, OEMs may aim to maximize performance, while regulatory authorities prioritize reducing air emissions. Since needs are usually presented in an unstructured manner using ambiguous or general terms, it is crucial to translate them into specific requirements. Requirements, in contrast, must adhere to specific patterns and rules to ensure characteristics such as clarity, comprehensiveness, achievability, verifiability, and accuracy. A requirement is defined as "a statement that translates or expresses a need and its associated constraints and conditions" [151]. The ontology depicted in Figure 3.4 defines and emphasizes the key concepts introduced earlier and their relationships, including complex systems, stakeholders, needs, and requirements. An ontology defines the fundamental concepts that make up the system architecture and their interrelationships [21]. Furthermore, the ontology

includes additional concepts, which are further explained below, such as types of requirements, rules, and attributes. One of the key elements in the ontology is the system. Within the specific context of this work, examples of a system can include a fleet, a single aircraft, or its components.

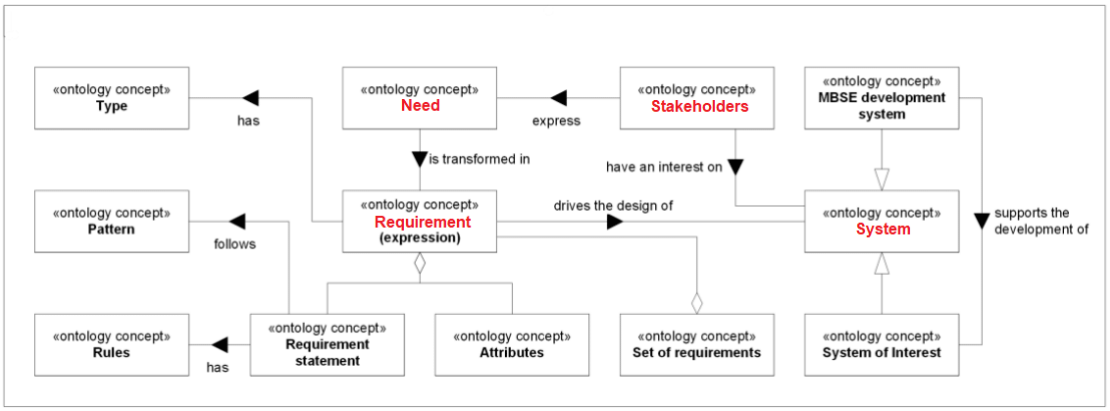

Figure 3.4: Architectural Framework Ontology representing system stakeholders, needs, requirements and their relationships. Adapted from [2].

Each requirement consists of two parts: the requirement statement and a series of attributes used for requirement management. Numerous attributes, as recommended and explained in [152], include requirement ID, author, and compliance methods. Requirements can also be categorized based on their type [153]. Depending on the type, requirement statements follow different patterns, including mandatory and optional elements such as functions, performance characteristics, durations, and conditions. Ultimately, requirement statements should adhere to several rules, such as those recommended by INCOSE [152], to ensure compliance with quality standards. Requirement statements must be complete, consistent, comprehensible, and capable of validation; otherwise, the project may encounter challenges in achieving success. To ensure these qualities, five types of patterns for modeling requirement statements are introduced. Each requirement pattern depends on the type of requirement, as outlined in Table 3.1.

The architecture of the MBSE development system described above is achieved through the combined use of Ke-Chain, MBSElibs, and Papyrus, as illustrated in Figure 3.5. Within Ke-Chain, multiple users can access the platform to specify all data related to the system under development, including stakeholders, needs, requirement elements, and requirement attributes, using tables and interfaces. Additionally, KE-chain facilitates the definition of connections between different elements, ensuring the functionality of supporting model traceability. The collected data is verified to ensure qualities such as completeness and correctness. MBSElib [20], developed by

Table 3.1: Requirement's Definition and Pattern Description. Adapted from [2,153,154].

Type	Definition and Pattern
Functional Requirement	Define what functions need to be performed to accomplish the objectives. The SYSTEM shall exhibit FUNCTION while in CONDITION.
Performance Requirement	Define how well the system needs to perform the functions. The SYSTEM shall FUNCTION with PERFO and TIMING upon EVENT TRIGGER while in CONDITION.
Design Constraint Requirement	Limit the options open to a designer of a solution by imposing immovable boundaries and limits. The SYSTEM shall exhibit DESIGN CONSTRAINTS in accordance with PERFO while in CONDITION.
Environmental Requirement	Define which characteristics the system should exhibit when exposed in specific environments. The SYSTEM shall exhibit CHARACTERISTIC during or after exposure to ENVIRONMENT for EXPOSURE DURATION.
Suitability Requirement	Include a number of the "-ilities" in requirements to include. The SYSTEM shall exhibit CHARACTERISTIC with PERFORMANCE while CONDITION for CONDITION DURATION

DLR, is used to automatically generate SysML models from this data. These models can be exported and visualized using SysML diagrams in Eclipse Papyrus [4].These automatically generated diagrams incorporates models of stakeholders, needs, and requirements. It can be opened in the Papyrus environment for inspection and verification by the designers. The Papyrus software enables the representation of stakeholders involved in the development of the system throughout its entire life cycle. It captures all the needs of various stakeholders, project requirements, and establishes connections among them. Additionally, Papyrus facilitates the creation of a traceability diagram that illustrates the relationships between requirements and needs, highlighting the potential consequences if the developed system deviates from the specified requirements. The tool also identifies the stakeholder responsible for verifying the requirement, and the attribute priority indicating the significance of the requirement to stakeholders [152].

Another instrument that is beneficial for formalizing, visualizing, and initiating the initial phases of the Systems Engineering Product Development process is represented by Capella [5]. This software serves as an open-source MBSE tool,

[4]Eclipse Papyrus home page: `https://eclipse.dev/papyrus/` [retrieved March 11, 2024]
[5]Capella home page: `https://mbse-capella.org/` [retrieved March 11, 2024]

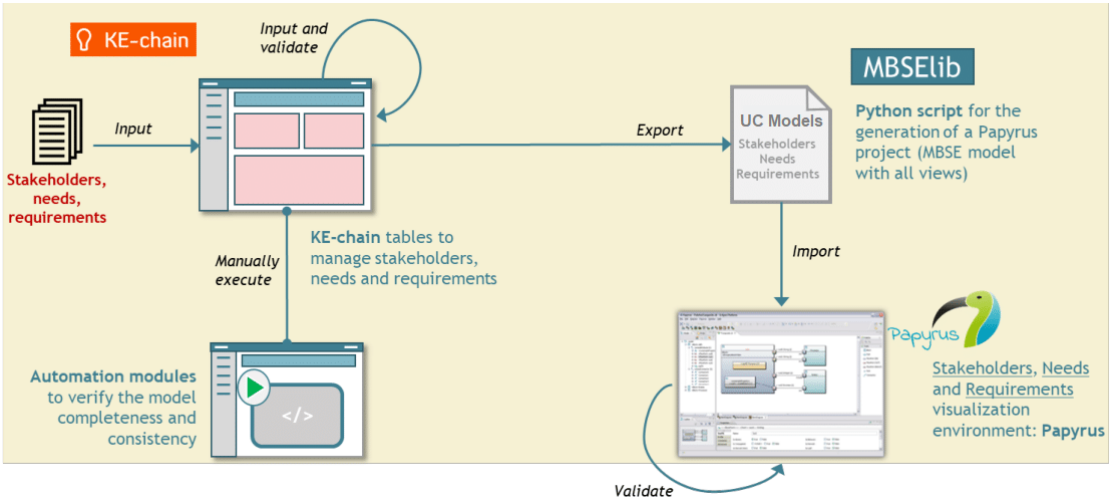

Figure 3.5: Architecture of the MBSE development system. Adapted from [2].

implementing the Arcadia method [155]. In the present study, the author utilizes Capella to perform an operational analysis, resulting in the development of an Operational Entity Scenario diagram. Capella adopts a top-down approach to system development [155] and encompasses four modeling levels: Operational Analysis (OA), System Analysis (SA), Logical Architecture (LA), and Physical Architecture (PA) [156]. Each modeling layer in Capella offers a variety of diagrams with different objectives. An example is illustrated by a System Architecture diagram, which provides a graphical representation of elements such as system functions, allocations, connections, and data flow. An additional valuable feature of Capella is its ability to navigate within model elements independently of diagrams using a contextual semantic browser. More practical than the standard hierarchical view, the semantic browser instantly provides context through meaningful queries, offering a preferred method for navigation and quick analysis of relationships between model elements as shown in Figure 3.6.

3.1.3 System Architecting and Modelling

The ISO/IEC/IEEE 42010 standard defines an architectural framework as a set of "conventions, principles, and practices for describing architectures established within a specific domain of application and/or community of stakeholders" [158]. In this context, "architecture" refers to the structure and behavior of a system. A system is defined as a "set of entities and their relationships, whose functionality is greater than the sum of the individual entities" [159]. Consequently, architecture encompasses various aspects of the system, including the composition of its parts, life cycle, operational procedures for external users, and other relevant information.

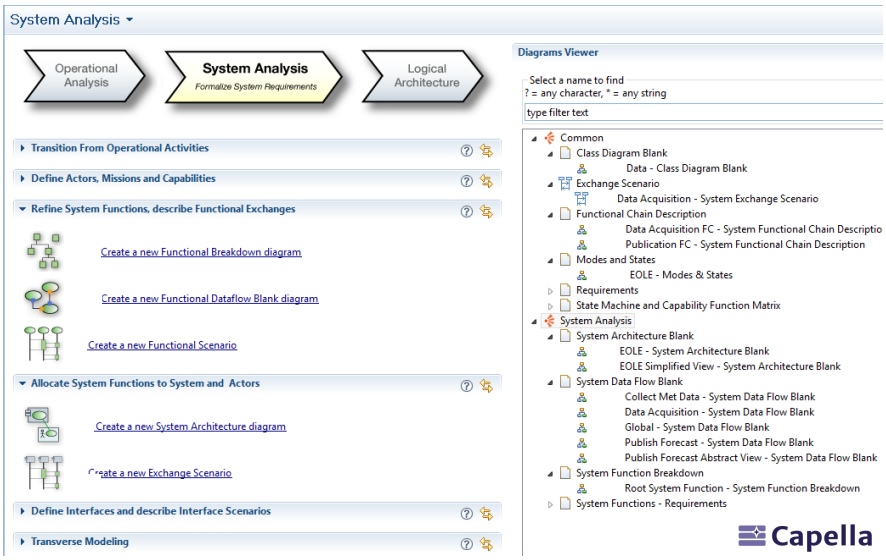

Figure 3.6: Capella Methodological Activity Browser. Adapted from [157].

A system architecture, on the other hand, is a specific design that exclusively represents the components comprising the system and their interconnections. An architectural framework establishes guidelines for the standardized representation of multiple system architectures [59]. The system architecting phase of a Systems Engineering process aims to develop a range of potential system architectures that align with stakeholder needs and adhere to the technical requirements of the system. Stakeholder expectations should include solution-neutral functions that the system must provide through its components. However, there is flexibility in selecting multiple alternative components to fulfill these functions, leading to the emergence of various system architecture options. The architectural framework discussed in this work specifically focuses on defining system architectures. The proposed architectural framework outlines the system architecting process, which is designed to derive two types of system architectures [59], functional and logical architectures. Functional system architectures aim to identify all the functions that the system, through its components, must fulfill. These functions, known as boundary functions, are determined during the architectural process, focusing on a specific level of detail of the system being designed. A boundary function specifies "what" a particular level of system elaboration should provide through its architecture, derived from functional requirements. Once all the boundary functions for that specific level are identified, the architectural process proceeds to the subsequent phase, focusing on logical architecture. The goal of the logical architecting phase in the system architecting process is to create multiple architectures with distinct logical components that satisfy all the boundary functions defined in the previous phase. Components

may also introduce other functions, known as induced functions, which are then fulfilled by additional components. The Architectural Design Space encompasses all potential system architectures that can be created through architectural design decisions. These decisions involve selecting components, specifying characterization, and determining connection options. Architectural decisions enable the selection of one or more architecture instances from the Architectural Design Space, which can be further addressed in the physical system architecture process [63]. The first step in creating a system architecture is to model and formalize the architecture design space. Within the established MBSE framework, this is accomplished through the use of the Architecture Design Space Graph (ADSG): a graph-based representation that links functions to components while also depicting component characterization and connection decisions. Figure 3.7 represents a generic example. Thanks to its function-based nature, it offers a solution-agnostic approach for modeling architectural design spaces. Moreover, function-based architecture establishes a seamless link from system requirements. A comprehensive explanation of all modeling components and the behavior of the ADSG can be found in [63].

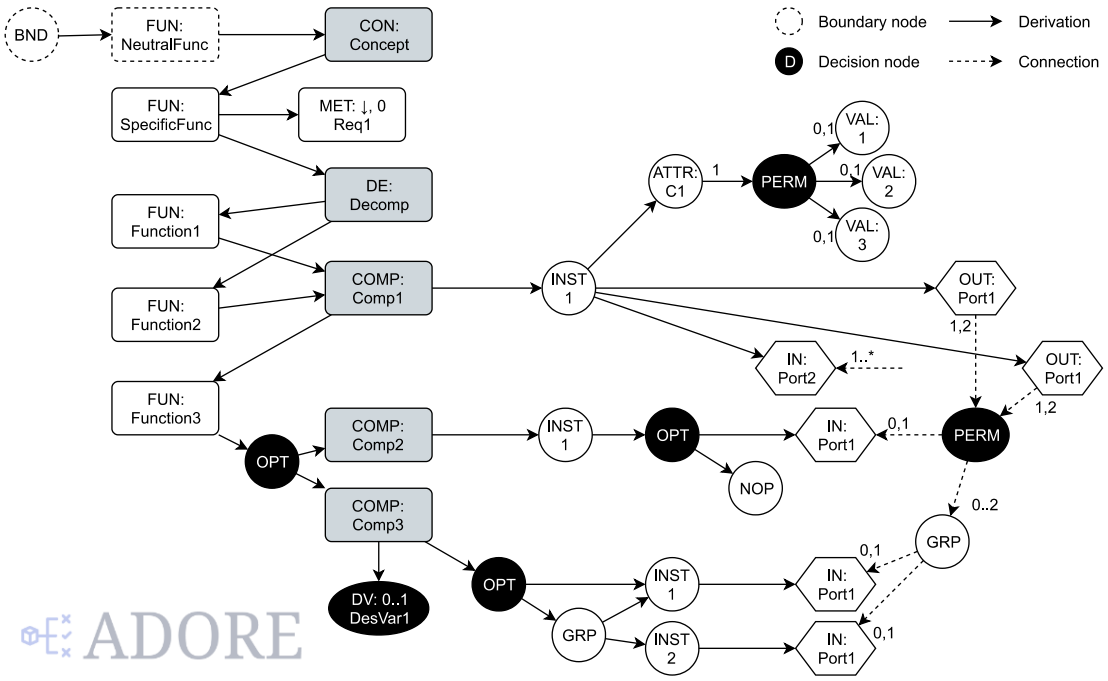

Figure 3.7: Example of Architecture Design Space Graph. Directed edges indicate derivation, decision nodes indicate a selection of mutually-exclusive options. Adapted from [63].

From the ADSG, an architecture optimization problem is formulated by mapping decision nodes to design variables. Objectives and constraints are defined using Quantities of Interest (QOIs), which represent values associated with functions or

components that serve various roles during the optimization process. In addition to serving as objectives and constraints, QOIs can also function as design variables (in conjunction with those defined from decision nodes), input parameters, and output metrics. QOIs may also refer to performance requirements, establishing a crucial link between requirements definition and architectural activities [62]. The GUI for editing the ADSG is implemented in a tool called ADORE [62]. ADORE is hosted on a central web server, and the connection to the OCE implemented in KE-chain is established using the Pykechain Python library. The connection of upstream elements to elements in the architectural design space model serves as the primary forward traceability link between upstream system engineering phases and the phase of architectural design.

3.1.4 Connecting Architecting and Collaborative MDAO

The goal of the physical architecting phase in the system architecting process is to identify appropriate physical components that meet the non-functional requirements of the system's level of elaboration. Physical architectures can be developed from logical architectures through the formulation and implementation of MDO processes. Through Means of Compliance and Test Cases it is possible to demonstrate how the designer can ensure that the system under design aligns with the collected requirements. Examples of Means of Compliance include simulations, tests, and disciplinary analyses. Test Cases, on the other hand, serve as instantiations of the Means of Compliance. Through them, it is possible to determine whether the system has undergone verification against the requirement, the outcomes of the verification process, and the individuals or groups responsible for designing the system as per the specified requirements. Before defining the MDO process, test cases must be identified. These cases may involve the execution of disciplinary competencies, such as aerodynamics and structure, necessary to verify the non-functional requirements at the system level of elaboration [7]. To evaluate the performance of generated system architectures, it is essential to establish a two-way connection between architecture design space modeling and the collaborative MDAO workflow. Initially, the connection from the generated architectures to collaborative MDAO must facilitate synchronization between the architecture definition and the central data schema instance. This is performed through QOIs indicators. Indeed, a QOI introduced in the architecture is automatically linked to an item belonging to the central data schema. After analyzing a specific architecture within the MDAO workflow, it is important to establish a feedback connection to extract performance data and communicate this information to the architecture

optimizer. The architecture-to-MDAO bridge also plays a role in supporting the selection of disciplinary tools during the workflow definition process [15]. By utilizing information from the architecture design space model, which outlines the components and associated QOIs, and the MDAO workflow model, which identifies the disciplines utilizing central data schema nodes, a mapping of components and QOIs to the central data schema reveals the associations between disciplines and architecture components. The mapping presented is accomplished by defining a Data Schema Operation (DSO) for each QOI and/or component [62].

Connecting architecture models created using ADORE to MDAO workflows for quantitative analysis of generated architectures involves associating architectural elements (e.g., components and QOI) with nodes in the central data schema. This connection is established using the MultiLinQ tool [62]. Similar to ADORE, MultiLinQ is integrated into the KE-chain collaborative environment . The KE-chain adapter for MultiLinQ provides functionality to retrieve ADORE models and import MDAO tool input/output definitions from the project's tool repository or established collaborative workflows. This process establishes the connection between components and QOIs in both the ADORE and MultiLinQ projects, facilitating integration into the architecture optimization loop. The relationship between components and QOIs to disciplinary tools is illustrated in the Component Tool (CT) matrix, as shown in Figure 3.8. The CT matrix illustrates the connections between components and their associated QOIs in relation to disciplinary analysis tools.

Once a MDO process has been formulated and successfully executed, system solutions are identified. This phase involves validating requirements at the system's elaboration level and establishing a physical architecture that is both designed and potentially optimized. The objective of the Requirement Verification Framework (RVF) is to help users integrate requirements into the design process, improve requirement traceability, and facilitate the automatic verification of requirements. To achieve these objectives, the RVF tool has been integrated into KE-Chain to enhance support for collaborative systems engineering processes [7]. The RVF establishes a connection between model-based requirements and engineering tools within the MDAO workflows, enabling the automated verification of requirements based on MDAO results. The RVF is implemented as a Python package, while KE-Chain serves as the GUI for the RVF, directly interacting with the Python code. In the context of the research activity presented, the RVF process involves the automated verification of requirements based on a predefined design. As shown in Figure 3.9, this process consists of three key steps. Initially, requirements need to be formulated in a machine-readable format. Subsequently, verification methods are defined and assigned to each requirement. In the final stage, predetermined

		Tools				
Components	QOIs	Aerodynamics	Cost	Performance	Propulsion	Structures
Engines	Base engine weight				✓	
Engines	Thrust				✓	
Fuel system	Fuel price					
Fuel system	Misc fuel weight					✓
Wings	AR	✓				✓
Wings	Reference area	✓				✓
Wings	Sweep	✓				✓
Wings	Taper ratio					✓
Wings	t/c	✓				✓
Wings structure	Load factor					✓
Wings structure	x					✓
	Altitude	✓		✓	✓	

Figure 3.8: Example of Component-Tool matrix generated through MultilinQ. Adapted from [62].

designs undergo automated verification according to the specified requirements and assigned verification methods. An automatically generated compliance report is then made available for user review. Further details about this methodology can be found in [7], where the RVF process actively utilizes requirements to guide the design process and formulate a MDAO process.

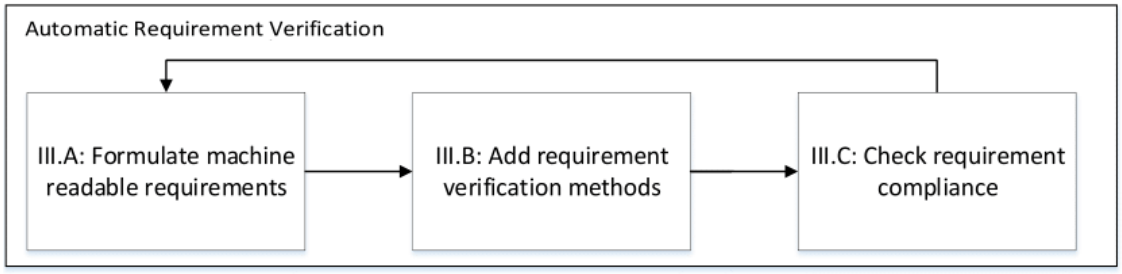

Figure 3.9: Overview of the different steps within the Requirement Verification Framework. Adapted from [7].

Assuming that stakeholders' needs and requirements have been adequately defined, especially with requirements formulated according to fixed definitions and patterns (as illustrated in Table 3.1), the application of patterns ensures the requirements' machine-readable nature. This is achieved by assigning meaning to

the various elements of the requirements, with each element in the pattern being implemented as an object within the RVF. This approach enables software programs to accurately interpret the requirements. Within the RVF, a verification method consists of two components: a means of compliance and a test case, both generated using the methodology outlined in Section 3.1.2. The means of compliance define the conditions that the verification process must meet and set the requirements for the verification process. Furthermore, a test case in the RVF includes design competencies and their corresponding input and output variables. These design competencies are implemented to assess compliance with the requirements, and their input and output parameters are the same as those used for the requirement definitions. The test case results are automatically compared with the target values specified in the requirements. The determination of compliance with requirements is made by comparing the actual values with the target values, and the results are automatically documented in a compliance report.

3.2 MDAO Approach for Collaborative Aircraft Design

The collaborative MDAO approach facilitates the integration of extensive MDAO processes across engineering disciplines by exchanging data through a central data schema. This requirement highlights the need for a shared language across disciplines, which reduces the necessity for multiple interfaces. It also enables disciplinary experts to focus on their specific tools, while the process integrator concentrates on defining the MDAO workflow. Collaborative MDAO has proven to be a powerful method for designing and optimizing complex engineering products. It involves various technologies that are essential for implementing an MDAO workflow in a cross-organizational context. Indeed, the previously described OCE offers multiple technologies for orchestrating various tools distributed across participating organizations in accordance with the collaborative workflow methodology. This framework enables tool and resource owners to ensure secure data flow among tools across different locations. These technologies actively support the development activities of the Systems Engineering approach discussed in the presented work. This section provides an overview of the MDAO technologies used to develop and implement MDAO workflows. The approaches outlined in this section form the framework through which the author has developed a comprehensive understanding of MDAO, as explained in Section 2.2. Within this context, a comprehensive overview is provided, emphasizing the MDAO technologies that enabled the author

to explore this domain and apply this paradigm in developing and executing MDAO workflows within the scope of his research pursuits.

3.2.1 MDAO formulation and execution

The formalization and methodology outlined in the author's research work establish an agile approach for specifying and manipulating MDAO systems of any scale. This task can be partially automated using a graph-based method, where information about tool interfaces is utilized to depict data flows between disciplinary tools and the nodes of the data schema [160]. This graph serves as a foundation for querying workflow properties, such as identifying input and output nodes or detecting potential collisions. This information is crucial for determining data connections between tools and establishing the optimal sequence for executing the workflow. Further specifications are added to transform it into a MDAO workflow, such as assigning design variables, objectives, constraints, and incorporating convergence and optimization elements. The graph-based workflow model is then used to create a workflow within a Process Integration and Design Optimization (PIDO) environment. While PIDO environments allow for the manual definition of MDAO workflows, the significant advantage of the graph-based MDAO workflow modeling method lies in its ease of modification and simultaneous assurance of correct data exchange. Lambe and Martins [161] introduced a type of representation for MDAO workflows known as the eXtended Design Structure Matrix (XDSM). This representation emerged as an extension of the Design Structure Matrix (DSM) approach [162], which primarily focuses on specifying the data coupling between different components. In contrast, the XDSM goes beyond by encompassing information related to the processes to be executed, providing a more comprehensive view of the MDAO system. The essential tasks described earlier are accomplished using one of two different tools integrated into the OCE: KADMOS [163] and MDAx [164].

The KADMOS software (Knowledge- and graph-based Agile Design for Multi-disciplinary Optimization System) empowers MDAO system architects to formulate extensive and complex MDAO systems. This is achieved by leveraging a repository of tools provided within the OCE by diverse design teams. More detailed information about the KADMOS software and the graph-based methodological approach integrated into the software can be found in [163]. KADMOS enables the automatic generation of a collaborative MDAO workflow, effortlessly facilitating modifications to the workflow architecture. It involves defining drivers, design variables, constraints, objective functions, and the disciplines involved. The software stores all generated graphs using the standardized CMDOWS storage format, the

VISTOMS [6] package can be utilized at any stage of the formalization process to generate necessary visualizations. The formulations produced by KADMOS are stored as CMDOWS files, which stands for Common MDO Workflow Schema, an open-source, eXtensible Markup Language (XML)-based neutral language for workflow schemas [160]. This file can be directly translated into executable workflows in a PIDO platform.

The MDAO Workflow Design Accelerator (MDAx) [164] explores a novel approach to streamline collaboration among engineering teams in large projects. Instead of predefining an MDAO problem and modeling the workflow based on predefined steps, MDAx enables workflow integrators to directly interact with an XDSM interface through drag-and-drop operations. MDAx implements the collaborative MDAO workflow modeling methodology introduced earlier, utilizing an interactive user interface. MDAx provides a web-based GUI for designing and exploring collaborative MDAO workflows, which can be exported to various formats. Similar to ADORE, its Python backend is connected to KE-chain using the KE-chain adapter principle. In addition to storing workflows and associated CMDOWS files in the OCE, it also displays available tool definitions from the OCE's tool repository in the MDAx user interface. Users can directly use the OCE tool repository to start creating workflows.

Once the MDO workflow is defined using KADMOS or MDAx, it can be exported to a neutral format, CMDOWS. The CMDOWS file can be interpreted in RCE (RCE [7]) workflow manager. RCE is an open-source platform created to integrate standalone tools into automated executable workflows [102]. RCE software can import workflow definitions in CMDOWS format, allowing for the automatic creation of local workflows . As a result, the CMDOWS file can be imported as an executable workflow and run. Figure 3.10 depicts the RCE environment along with an executable collaborative MDAO workflow.

RCE [102], or Remote Component Environment, is a comprehensive open-source application that facilitates the seamless integration of disciplinary tools. Users can intuitively establish dependencies between tools using a user-friendly graphical interface, enabling the creation and execution of complex multidisciplinary engineering workflows. RCE offers pre-defined components that provide fundamental functionalities, including controlling data flow, reading and extracting data from XML files, and executing user-supplied Python scripts. Furthermore, RCE includes

[6]VISTOMS home page: `https://www.agile-project.eu/files/VISTOMS_TUDWingDesign/` [retrieved March 11, 2024]

[7]RCE home page: `https://rcenvironment.de/pages/download.html` [retrieved March 11, 2024]

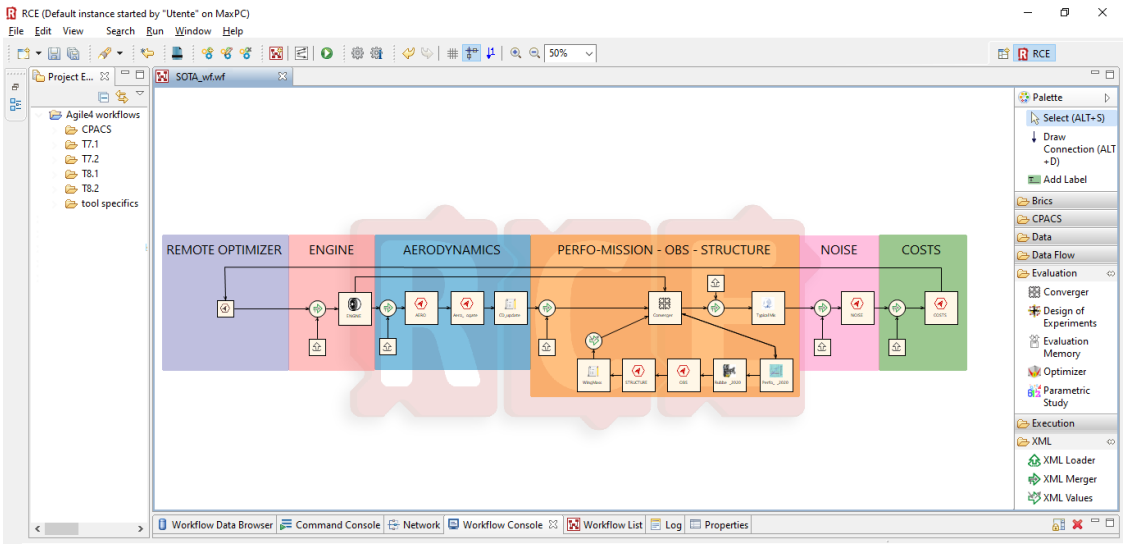

Figure 3.10: Example of collaborative MDAO workflow integrated in RCE.

components that use mathematical and statistical methods to evaluate incoming data. It facilitates the construction of design, evaluation, and optimization loops, integrating well-known frameworks such as the versatile Dakota [8] [165,166] framework.

Tools integrated into RCE, or more generally into a common MDAO workflow, must adhere to a standardized data schema for input and output definitions. The adoption of a central data schema for product representation aims to standardize communication, ensuring that all stakeholders "speak the same language". To facilitate the integration of various domain-specific tools at the data level, the previously mentioned OCE utilizes a standardized XML-based schema format for data compatibility among engineering tools known as the Common Parametric Aircraft Configuration Schema (CPACS) [9] [165, 166]. CPACS is an open-source, XML-based schema that serves as a universal format for exchanging product data. It allows for the storage of parametric definitions of aircraft geometries and analysis results from individual design disciplines in a hierarchical structure. This framework enables the consistent exchange of product data at various levels of detail. In practical terms, CPACS provides a comprehensive predefined standard dictionary that is designed to encompass all typical input and output data of the analysis tools used in conceptual and preliminary aircraft design. Another advantage is the substantial reduction in the number of data interfaces required when constructing a MDAO workflow [166]: from N(N-1) to 2N, where N represents the number of disciplinary tools, as shown in Figure 3.11.

[8] Dakota user's manual: `https://dakota.sandia.gov/manuals/` [retrieved March 11, 2024]

[9] CPACS home page: `https://dlr-sl.github.io/cpacs-website/` [retrieved March 11, 2024]

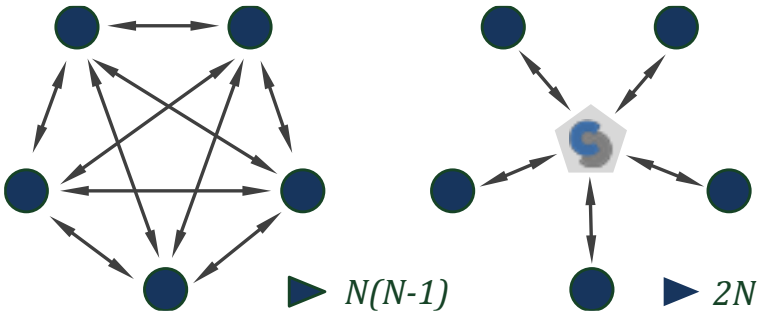

Figure 3.11: The use of CPACS central data schema like reduces the number of implemented data interfaces from N(N-1) to 2N. Reproduced from [166].

When using CPACS, each disciplinary tool within the MDAO system requires a CPACS file as input and is expected to produce output into the CPACS file. As a result, once all component providers have adapted their tools to be CPACS-compatible, the assembly of even large executable MDAO systems becomes a relatively straightforward task for the integrator. It is important to emphasize that integrating a tool with the central data model is non-intrusive, meaning that the domain specialist does not need to overhaul the code of an existing analysis module. To streamline the process of integrating analysis capabilities with CPACS and ensure the correct semantic interpretation of provided data, open-source libraries such as TiXI [10] and TiGL [11] are available [167]. These libraries provide commonly needed query functions for processing CPACS data and geometry information in popular programming languages (C, C++, Python, Java, MATLAB, and Fortran).

3.2.2 Surrogate Modelling and Response Surface Formulation

The generation of surrogate models or response surfaces is a significant facilitator in executing MDAO frameworks. They enable the maintenance of high fidelity levels of tools by introducing approximations of the outputs generated by these tools. Their utilization serves as a crucial means to address the development of multidisciplinary frameworks following an MDAO approach.

DOE methods represent techniques aimed at extracting comprehensive trend data from a parameter space, often with a limited number of sample points. Common DOE approaches, such as central composite design, Box-Behnken design, and full and fractional factorial design, typically place sample points at the extremes of the parameter space. This strategic placement enhances the reliability of trend

[10] TiXi library home page: `https://github.com/DLR-SC/tixi` [retrieved March 11, 2024]
[11] TiGL library home page: `https://dlr-sc.github.io/tigl/` [retrieved March 11, 2024]

extraction, especially when dealing with non-repeatability. The Design and Analysis of Computer Experiment (DACE) methods differ from other DOE methods in that they allow for the exclusion of the non-repeatability component, as computer simulations are involved. In these cases, space-filling designs like orthogonal array sampling and Latin hypercube sampling (LHS) are more commonly used to accurately capture trend information. Additionally, quasi-Monte Carlo sampling techniques, designed to uniformly cover the unit hypercube, can also be applied in DACE scenarios. These methods are particularly beneficial when dealing with computer simulations as they enhance the efficiency of trend extraction and eliminate the need to address non-repeatability, thanks to the consistency of results for identical experiments. The Dakota library integrated into RCE accommodates both DOE and DACE techniques. In this context, only parameter bounds are employed for selecting samples within the parameter space. Dakota incorporates various approaches to sampling and design of experiments, all implemented through included third-party software libraries. The LHS technique employed by Dakota [168] represents a versatile sampling package which provides the capability to generate Latin Hypercube designs, allowing for the creation of uniform samples between variable bounds. LHS [169–171] operates as a stratified sampling technique wherein the range of each uncertain variable is divided into N_s segments of equal probability, where N_s denotes the number of samples requested. Subsequently, a sample is randomly selected from each equal probability segment for each variable. The resulting values of N_s for each individual parameter are then combined in a shuffling operation to create a set of N_s parameter vectors with a specified correlation structure. One notable feature of the resulting sample set is that each row and column in the hypercube of partitions contains exactly one sample. This ensures comprehensive coverage of the hypercube while maintaining a balanced distribution. For a more comprehensive understanding of the implementation details of the LHS algorithm, additional information can be available on the Dakota manuals webpage [12] and in [168].

A dataset generated from DOE sampling, such as LHS, can subsequently be used to create a response surface from data distributed at widely spaced and usually irregular intervals. Scattered data approximation is a rapidly evolving field of research that addresses the challenge of reconstructing an unknown function from given scattered data. In practical applications across various disciplines, the task often involves reconstructing an unknown function, denoted as f, from a finite set of discrete data. This dataset comprises data points $X = \{x_1, ...x_n\}$ and their

[12] Dakota Manuals webpage `https://dakota.sandia.gov/manuals/` [retrieved March 11, 2024]

corresponding data values $f_j = f(x_j)$, where $1 < j < N$. The objective of the reconstruction process is to estimate the data values at the specified data sites. In essence, the objective is to find a function s that either precisely interpolates the data, satisfying $s(x_j) = f_j$ for $1 < j < N$, or provides a reasonable approximation, i.e., $s(x_j) \simeq f_j$. The latter situation is especially important when the data contains noise. In many cases, the data sites are scattered and lack a regular structure. Their number can be quite substantial, easily reaching into the millions. Furthermore, in certain applications, the data points may exist in a high-dimensional space [172] . One of the most obvious uses of scattered data interpolation and approximation is for reconstructing a surface. To efficiently explore various optimization problems by manipulating design variables, constraints, and objective functions, the author employed a methodology capable of generating a prediction model in the form of a response surface. This approach led to the results illustrated in the following section. This model predicts the trend of any possible problem's function of interest. The response surfaces can be generated using Radial Basis Function (RBF) [173,174] and can predict specific functions of interest based on the specified set of design variables.

RBFs are functions that exhibit radial symmetry, meaning they depend solely (apart from specific known parameters) on the distance $r = ||x - x_j||$ between the center of the function, x_i, and a generic point x. These functions can be broadly expressed in the form $\phi(r)$. Given this general definition, it's possible to understand that there exists an infinite variety of RBF. They can be categorized as either globally supported or compactly supported, depending on whether their support extends across the entire domain or is limited to a part of it. Among the globally supported RBFs, the following types are commonly used in high-dimensional space [172]:

$$\text{Gaussian:} \quad \phi(r) = exp\left(-\frac{r^2}{2\sigma^2}\right) \tag{3.1a}$$

$$\text{Multiquadrics:} \quad \phi(r) = \sqrt{1 + \frac{r^2}{\sigma^2}} \tag{3.1b}$$

$$\text{Linear:} \quad \phi(r) = r \tag{3.1c}$$

$$\text{Cubic:} \quad \phi(r) = r^3 \tag{3.1d}$$

$$\text{Thinplate:} \quad \phi(r) = r^2 \ln(r + 1) \tag{3.1e}$$

The parameter σ in the expressions above controls the shape of the RBFs. This parameter is sometimes referred to as the "local shape parameter". In short, interpolation with RBFs can be represented as follows:

$$s(x) = c_0 + c_1 x + \sum_{i=1}^{n} \lambda_i \phi(|x - x_i|) \tag{3.2}$$

This approximation solves for the $n + 2$ unknowns in the system of $n + 2$ linear equations of the following type:

$$s(x_i) = f(x_i) = c_0 + c_1 x + \sum_{i=1}^{n} \lambda_i \phi(|x - x_i|) \tag{3.3}$$

where $f(x_i)$ is known for a series of points x_i.

The objective of RBF interpolation is to construct an approximation of the function by selecting coefficients c_0, c_1 and λ_i to match the values of the function at the interpolation nodes.

The RBF method offers several key advantages. Firstly, its mesh-free nature makes it exceptionally flexible in adapting to various geometries within the computational domain. This characteristic makes it particularly well-suited for scenarios where data is only accessible at scattered points, enabling versatile problem-solving. Secondly, the complexity of the method does not increase for problems involving numerous spatial dimensions. This is because the only geometric property utilized is the pairwise distance between points. Consequently, the method maintains its efficiency and applicability across a variety of spatial dimensions without unnecessary complexity. Furthermore, when working with smooth functions, approximations using smooth RBFs have the potential to achieve spectral convergence. This indicates that, in specific instances, the RBF method's accuracy in approximating smooth functions reaches a level of precision comparable to spectral methods. This capability further enhances its suitability for applications involving functions that have inherent smoothness.

3.2.3 Optimization Tools and Methodologies

Two different optimization tools are employed in the context of this work to drive the optimization workflow generated through the previously described MBSE and MDAO tools: the RCE embedded optimizer and JPAD optimizer. The main optimization tool employed by the author for his thesis work is the RCE embedded optimizer, which utilizes the Dakota optimization algorithms toolkit [13].

In addition to the previously presented functionalities, Dakota includes algorithms for optimization using both gradient and non-gradient-based methods, suitable for applications in science and engineering design. Additionally, Dakota offers more advanced algorithms, such as those for handling multi-objective optimization or

[13] Dakota Manuals webpage `https://dakota.sandia.gov/manuals/` [retrieved March 11, 2024]

performing surrogate-based minimization. The following provides a brief description of the main optimization methods available through the Dakota methodology.

Optimization methods based on gradients are widely recognized for their high efficiency, as they boast faster convergence rates compared to other optimization techniques. These methods are usually preferred in situations where the problem is defined by smooth, unimodal, and well-behaved features. Their vulnerability can stem from potential inaccuracies in gradient calculations, which can lead to suboptimal search directions. It is important to note that gradient-based optimizers are effective at efficiently navigating towards a local minimum near the initial point, but they may not be suitable for discovering global optima in nonconvex design spaces. For this reason, ensuring the accuracy of the gradient becomes a crucial factor in gradient-based optimization. While analytic gradients are considered ideal, they are not always available. In practical engineering applications, optimization algorithms often rely on finite difference methods to estimate gradient values. Dakota offers users the flexibility to select the step size for these calculations and to choose between forward-difference and central-difference algorithms. For unconstrained problems, it is possible to use conjugate gradient methods that depend on first derivative information. These methods involve solving subproblems that aim to minimize a quadratic function within a space defined by the gradient and directions that are mutually conjugate with respect to the Hessian matrix. Dakota offers access to conjugate gradient methods. Specifically, the Fletcher-Reeves conjugate gradient method is accessible [175].

Non-gradient-based methods exhibit significantly slower convergence rates in the pursuit of an optimum, making them more computationally demanding compared to their gradient-based counterparts. In non-gradient optimization studies, it is crucial that the computational cost of function evaluation remains relatively low to achieve an optimal solution within a reasonable time frame. Non-gradient methods have advantages in terms of robustness and inherent parallelism compared to gradient-based approaches. Furthermore, certain non-gradient-based methods can be used for global optimization, which is a capability that standalone gradient-based techniques lack. Pattern Search methods are applicable to nonlinear optimization problems, navigating through the domain based on a defined set of search directions. These methods are excellent at efficiently maneuvering towards a local minimum in the vicinity of the initial point. In Dakota, the primary method for pattern search is the Asynchronous Parallel Pattern Search (APPS) [176]. Similar to pattern search methods, simplex methods for nonlinear optimization problems use search directions defined by triangles that are reflected, expanded, and contracted across the variable space. Two simplex methods suitable for constrained optimization available

in Dakota include the Parallel Direct Search method [177] and the Constrained Optimization BY Linear Approximations (COBYLA).

The effectiveness and efficiency of optimization methods can often be improved by incorporating surrogate models. Dakota's optimization methods are adaptable to seamlessly integrate with a globally applicable surrogate model. This strategy supports the use of surrogates trained from either static imported data or trained online through a Dakota design of experiments. Dakota offers three capabilities for multi-objective optimization: Multi-Objective Genetic Algorithms (MOGAs), the Pareto-set strategy, and a weighting factor approach for multi-objective reduction. These features expand the range of optimization applications, offering users versatile tools to tackle various challenges in the optimization and calibration fields.

The second optimization tool utilized in this study is the JPAD Optimizer, which is based on the Multi-Objective Evolutionary Algorithms (MOEA) Framework [14], and directly integrated into the JPAD library [178, 179]. The MOEA Framework is an open-source Java library designed for the development and experimentation of MOEAs and other versatile optimization algorithms. It offers a variety of pre-implemented algorithms, such as genetic algorithms, particle swarm optimization, and others. The MOEA Framework features fast and reliable implementations of numerous cutting-edge multiobjective evolutionary algorithms. It includes internally embedded algorithms , all meticulously optimized for high-performance applications. The framework extends its support beyond its native algorithms by also integrating with the JMetal and PISA libraries, providing access to a wide range of multiobjective optimization algorithms. The MOEA Framework includes a total of 26 optimization algorithms. Among its native offerings is GDE3 [180], an extension of differential evolution for multi-objective problems, which completes the roster. The MOEA Framework incorporates a diverse array of optimization algorithms from the JMetal library. Within this selection, CellDE [181] takes a unique approach by combining cellular genetic algorithms with differential evolution, restricting mating to occur solely among neighboring individuals. SMPSO [182] is a particle swarm optimization algorithm designed specifically for multi-objective optimization tasks. Furthermore, the MOEA Framework seamlessly integrates with PISA algorithms, which are provided by a third party, thereby expanding the range of optimization algorithms available for configuration and execution.

[14] MOEA Framework, a Java library for multiobjective evolutionary algorithms: `http://moeaframework.org/` [retrieved March 11, 2024]

Author contribution

The author of this thesis work has been directly involved in the development of MBSE and MDAO technologies and methodologies within the context of the AGILE and AGILE 4.0 projects. The author's work, conducted using these technologies, not only demonstrated their capabilities and constraints but also contributed to their improvement by serving as a tester, highlighting strengths and limitations. Furthermore, a method for creating a response surface using Radial Basis Function from data distributed at widely spaced and irregular intervals has been developed. The knowledge acquired during this phase has informed the implementation of MBSE and MDAO technologies for developing a multidisciplinary workflow to optimize an ARE configuration.

List of related publications

Conference papers

- E.H. Baalbergen, J. Vankan, L. Boggero, J.H. Bussemaker, T. Lefèbvre, B. Beijer, A.L.M.R.M. Bruggeman and **M. Mandorino**. Advancing Cross-Organizational Collaboration in Aircraft Development. In *2022 AIAA Aviation and Aeronautics Forum and Exposition*, 27 June - 1 July 2022, Chicago, Illinois. DOI: https://doi.org/10.2514/6.2022-4052.

  This paper reviews the collaboration challenges that arose during the AGILE 4.0 project. The importance of well-organized, multidisciplinary, multi-engineer, and multi-organizational development processes is emphasized. The paper describes how AGILE 4.0's collaboration-enabling technologies addressed these challenges. Furthermore, the applications provide details and highlight the experiences gained from using these technologies.

- N. Bartoli , T. Lefebvre , R. Lafage , P. Saves , Y. Diouane, J. Morlier, J. H. Bussemaker , G. Donelli , J. M. Gomes de Mello, **M. Mandorino** and P. Della Vecchia. Multi-Objective Bayesian Optimization With Mixed-Categorical Design Variables For Expensive-To-Evaluate Aeronautical Applications. In *AeroBest 2023 II ECCOMAS Thematic Conference on Multidisciplinary Design Optimization of Aerospace Systems*, 18-20 July 2023, Lisbon, Portugal.

  In this paper, surrogate-based optimization methods have been used in aeronautical engineering systems. The JPAD Optimizer tool has been compared with SEGOMOE, an optimization framework proposed by ONERA and ISAE-SUPAERO. The proposed methodologies' effectiveness was tested on practical aeronautical applications within the context of the AGILE 4.0 Project.

4

Methodologies for MDAO Aircraft Design

Contents

In this chapter, the methodologies employed as design disciplines in MDAO workflows are presented. The described methodologies encompass high, medium, and low-fidelity tools intended for analyzing a complex rear-end configuration, including components such as a forward-swept horizontal stabilizer, LEX, and bottleneck-shaped fuselage. These tools are categorized into three groups.

- Geometry definition tools, described in Section 4.1. This group facilitates the generation of geometric models for analysis and, consequently, the computation of structural parameters. These disciplines are essential for creating the necessary input in the correct format for the following disciplines.
- Aerodynamic tools, described in Section 4.2. These methodologies include VLM and CFD analysis, along with sensitivity analysis for aerodynamic gradients.
- Aerostructural tools, described in Section 4.3. These methodologies produce deformation results, along with the calculation of structural gradients.

It is worth to notice since the beginning a certain disciplines overlaps. Indeed, some of the tools presented can produce similar results. Specifically, structural

disciplines are approached using both high-fidelity and low-fidelity methods. The high-fidelity structural methodology, detailed in Section 4.3.1, represents a significant advancement in the state of the art of the MDAO architecture methodologies developed. Indeed, the approach can be integrated into a framework where optimization follows an IDF approach guided by adjoint optimization on macro-parameters related to the geometry and structure of the aircraft's tailplane. This represents a potentially groundbreaking innovation, as there is no reference in the state of the art of IDF adjoint optimization based on geometrical and structural macro-parameters. However, its current application is limited to analyzing an isolated tailplane. In the context of this thesis work, the author recognized the need for further advancements, especially to broaden the applicability of the methodology within an MDAO framework. Specifically, the author identified potential advancements related to extending the methodology to enable analyses of the entire aircraft or non-isolated components, as well as incorporating viscous analyses. Consequently, a low-fidelity approach is also introduced, as presented in Section 4.3.2. The low-fidelity approach can be easily integrated into a traditional MDF optimization framework. It has been used in a DOE analysis to create a surrogate model of the methods and to carry out more efficient optimizations. This is crucial because the high-fidelity structural technology, despite its advancements, is not yet fully mature for integration into an MDAO context. Therefore, a reliable low-fidelity approach is introduced to complement the high-fidelity counterpart. Similar considerations apply to the aerodynamic disciplines, where medium to high-fidelity methodologies are utilized. However, the discipline introduced in Section 4.2.2 can be integrated into the IDF optimization framework along with the structural discipline described in Section 4.3.1. This aerodynamic discipline primarily involves conducting Eulerian analyses on the isolated tailplane. In contrast, viscous analyses of the entire body-horizontal configuration, including a LEX, can be conducted by integrating the discipline presented in Section 4.2.1

4.1 Geometry Definition Tool and Methodologies

4.1.1 CAD Generator

The CAD Generator is a 3D modeling tool developed to automatically generate the external shapes of an ARE concept, which encompasses a forward-swept horizontal tailplane, a LEX body part, and an updated fuselage tailcone. The tool aims to produce watertight solid parts in various CAD formats suitable for high-fidelity analyses. It achieves this by providing wing and fuselage section

points, along with geometric macro parameters. These components can be directly transferred to another tool for CFD calculations without the need for any preliminary user operations.

The 3D modeling tool relies on JPAD [179, 183], an Application Programming Interface (API) designed by the DAF research group of University of Naples Federico II specifically for aircraft designers [1]. This API is a Java software library that can be used to construct and execute the desired analysis and optimization workflow, encompassing both conventional and unconventional aircraft systems [184–186]. This library of aircraft design and analysis methods comprises several independent modules, each dedicated to a specific thematic area. For the research project, the module dealing with 3D modeling and advanced CAD features, called JPADCAD [187, 188], was extensively used. JPADCAD's 3D modeling capabilities are based on the OpenCASCADE Technology [2] (OCCT) software library is an open-source 3D modeling kernel widely utilized by industries and integrated into several CAD programs and scientific computing environments, such as FreeCAD [3] and SALOME [4]. Following the paradigm established by JPAD and OCCT, the LEX-Modeller has been developed by the author, in collaboration with the DAF research group, using an Object-Oriented Programming (OOP) approach. For this reason, the code was organized according to the structure depicted in Figure 4.1.

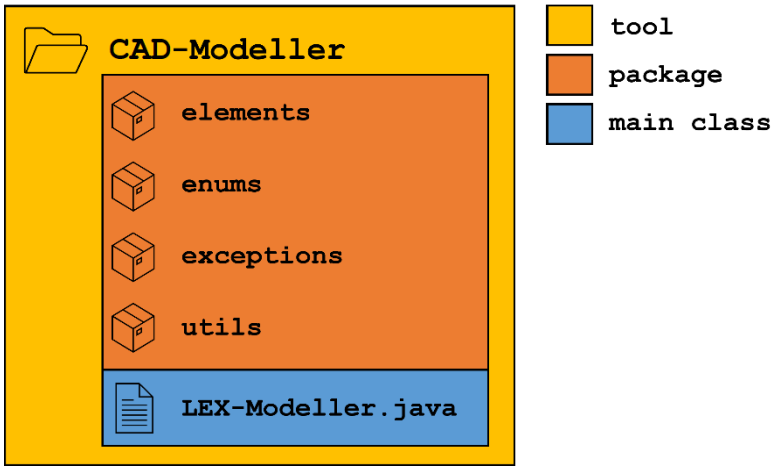

Figure 4.1: CAD-Modeller architecture overview.

All the Java classes, which are containers of data and methods for a program following an OOP paradigm were organized into four main packages based on their

[1] JPAD Modeller homepage: `https://www.smartup-engineering.com/jpad-modeller` [retrieved March 11, 2024]
[2] Open CASCADE website: `https://www.opencascade.com` [retrieved March 11, 2024]
[3] FreeCAD website: `https://www.freecadweb.org` [retrieved March 11, 2024]
[4] SALOME website: `https://www.salome-platform.org` [retrieved March 11, 2024]

scope. The "elements" package includes all the classes dealing with the abstraction of aircraft components, such as airfoils, lifting surfaces, lifting surface tips, fuselage cross-sections, and fuselage trunks. It also includes the Java class that handles general directives, such as specifying which 3D shapes should be exported to a file and in which file format. The "utils" package consists of classes that implement utility methods shared by multiple classes. Moreover, the 'utils' package contains the 'LEXModellerManager' class. As the name suggests, this Java class manages the tool's operations, from importing input directives to producing the 3D shapes requested by the user and writing them to a file. The "exceptions" package includes exception classes that enable more efficient management of all potential warnings and errors arising from incorrect user inputs or from unpredictable behavior of the CAD kernel. Finally, the 'enums' package facilitates the smoother management of various options provided by the tool (e.g., output file extensions, lifting surface tip types), as well as the rigid tree structure of input and output folders.

The input files for this 3D modeling tool were organized to facilitate its integration into an RCE workflow and to generate the analysis and optimization framework mentioned in the introduction of this section and described in Chapter 5. All input files are in XML format, which makes them more human-readable and easy to interpret and modify using an external tool or script. In this way, the XML file can also be integrated into the CPCAS format to better specify the selected input for the CAD Generator tool.

The input for the tool consists of four primary groups of items. General input directives include user requirements for exporting 3D shapes to a file and specifying the file format for the generated CAD files. These directives allow users to customize the export of 3D shapes produced with the CAD Modeller to a file. The user can choose whether to include the output 3D shapes in a single CAD file, allowing for the selection of specific components to be exported to the file. Tail plane inputs include data related to the geometry of the Horizontal Tail Plane (HTP). To define the geometry of this component, the user must provide the airfoil geometry, including x and y coordinates in a unitary chord reference frame. Figure 4.2 provides visual examples of potential inputs used to define the output geometry. The position of the tailplane can be specified, along with basic shape parameters related to planform geometry, twist, and dihedral angles. Other customizable parameters include tip type (e.g., rounded or flat), airfoil curve discretization, and the number of airfoil curves to be generated spanwise.

The LEX input includes parameters that define the geometry of the LEX. Key input parameters related to the planform shape of the LEX and the average thickness of the LEX must be provided. Furthermore, input data pertaining to the shape of

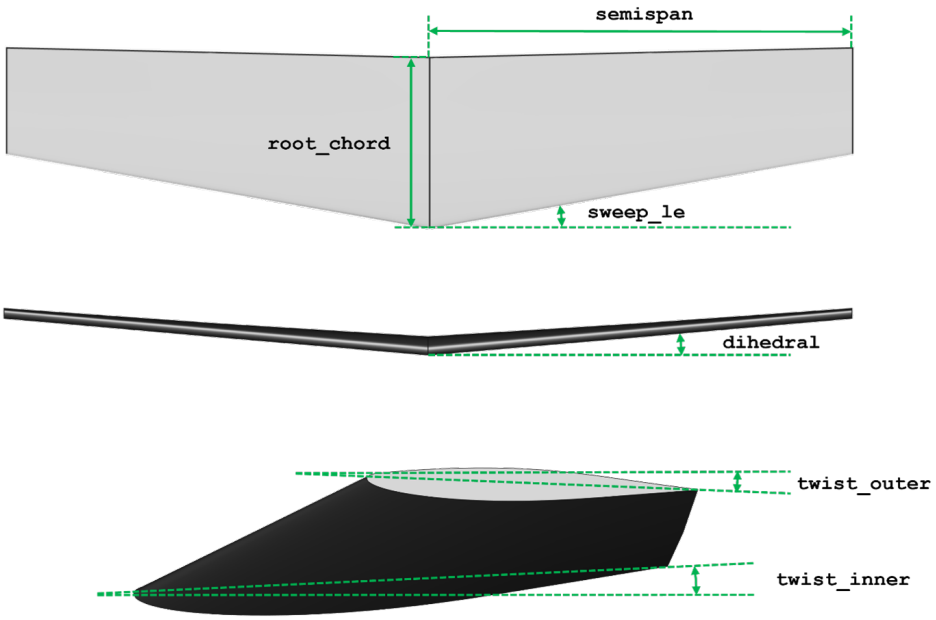

Figure 4.2: CAD-Modeller architecture overview.

the LEX guide curve is required. The guide curve is a Bézier curve defined by five control points. A representation of this curve (i.e., the one visible from a top view) is provided in Figure 4.3, along with its five control points, which are defined as follows:

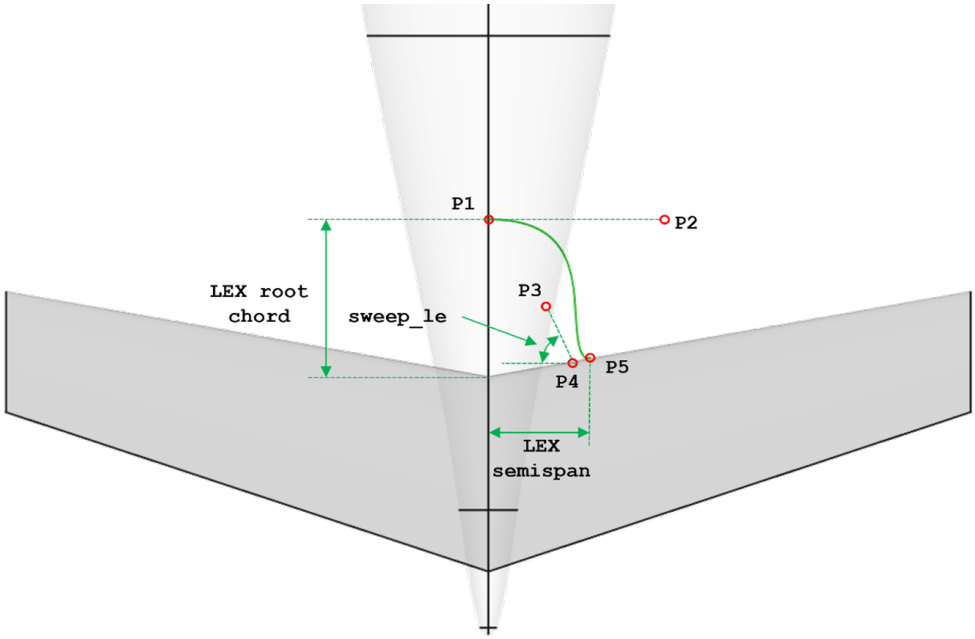

Figure 4.3: Summary of the LEX parametrization implemented by CAD-Modeller.

- Control point P1 coordinates match those of the tail plane apex, except for the x-coordinate, which is forward-shifted using the root chord ratio variable.

- Control point P2 has an x-coordinate that matches that of P1, while its z-coordinate matches that of the tail plane at the same spanwise location. The y-coordinate is determined by a control parameter ratio, y_2, multiplied by the LEX semispan.
- Control point P3 has a y-coordinate set by a y_3 control parameter ratio multiplied by the LEX semispan. The x-coordinate is adjusted to align with the assigned sweep at the leading edge, while the z-coordinate matches that of the tail plane at the same spanwise location.
- Control point P4 has a y-coordinate determined by the complement of 1.0 of a y_4 control parameter ratio multiplied by the LEX semispan, while its x- and z-coordinates are set so that P4 is located on the HTP leading edge.
- Control point P5 is located on the leading edge of the tail plane at a spanwise location dictated by the assigned LEX span ratio.

A separate 3D shape for the LEX, distinct from the HTP, can be generated.

The tail cone input encompasses all parameters related to the tail cone geometry and the fuselage in general. The initial fuselage geometry can be defined by its series of longitudinal cross sections or through the fuselage parameterization provided by JPAD Modeller. In the latter case, the cross sections will be generated automatically. The fuselage is defined as the combination of three distinct sections: the nose, the cylinder, and the tail. For each defined trunk, various cross-sectional shape parameters can be specified. These parameters relate to the fundamental shape of the entire fuselage or a specific section of it. The cross-sectional parameters impact the relative positions of Bezier curve control points. Figure 4.4 provides an explanation of the required input parameters and illustrates the placement of control points. The tail cone of a fuselage, defined by cross-sections, can be adjusted using CAD-Modeller through a set of input parameters. This set includes fundamental shape parameters that determine the position in the Body Reference Frame (BRF) of the updated fuselage tail cone. It also includes advanced parameters that enable the individual definition of the shape of the new cross-sections of the tail cone and the management of their number and spacing.

In addition to the specified input boundaries, the code includes several checks to ensure the consistency of the results generated by the CAD-Modeller application and to minimize the risk of crashes or unexpected behaviors. Figure 4.5 depicts a visualization in FreeCAD of the aircraft's 3D shapes created using the CAD Generator tool.

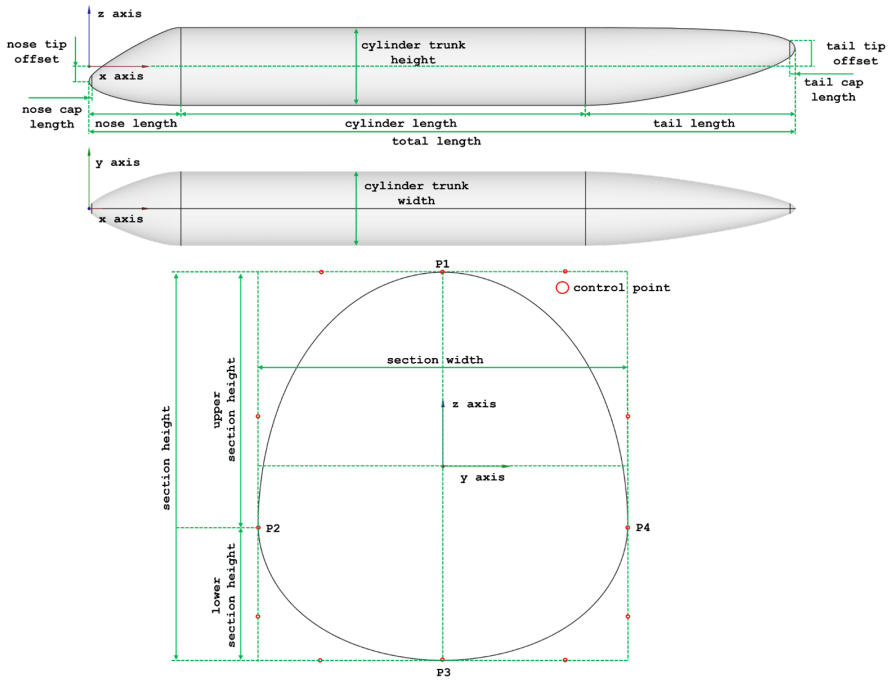

Figure 4.4: Synthesis of CAD generator fuselage parameters.

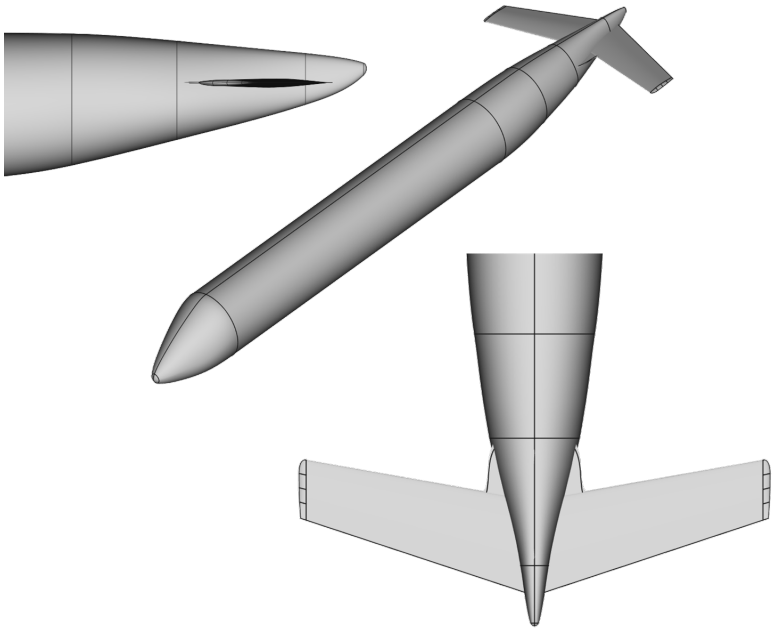

Figure 4.5: Visualization in FreeCAD of the 3D shapes generated with the application example.

4.1.2 STAR-CCM+ Mesh Generator

The STAR-CCM+ Mesh Generator is a comprehensive CFD pre-processing tool designed to generate an aerodynamic mesh ready for immediate use. Its purpose is to streamline and improve the workflow for efficiently conducting complex aerodynamic analyses. This seamlessly integrated software establishes a strong connection with Siemens Simcenter STAR-CCM+ [5] platform, offering an automated process for importing geometry and generating meshes. The main purpose of this tool is to automatically generate a mesh from a pre-defined CAD geometry, specifically designed to tackle aerodynamic challenges across different fluid domain conditions, such as variations in the angle of attack. The tool's effectiveness depends on its ability to adjust the mesh to match the specific characteristics of the analysis scenario, thereby ensuring accurate and reliable results. To start the CFD analysis process, input parameters defining the fluid domain are required. These parameters provide essential information for generating an optimized aerodynamic mesh. Furthermore, the tool requires a specified folder containing CAD files that represent the solution being examined.

The STAR-CCM+ software utilizes a wide range of capabilities within the Simcenter STAR-CCM+ environment, seamlessly integrating them to optimize both surface and volume meshing operations for aerodynamic analyses. This comprehensive tool utilizes a versatile mesh framework with a wide range of features designed for flexibility and reusability. The mesh framework supports various operations, such as local mesh modification for wrapped and remeshed surfaces, surface preparation for manual repair and pre-meshing, and surface wrapping for creating closed and non-intersecting surfaces from imperfect CAD data. Volume mesh generation is facilitated by specialized meshers that can be adapted to specific geometries. These include the thin mesher, generalized cylinder mesher, extruder mesher, offset mesher, and directed mesher for swept geometries.

To initiate the tool, a CAD file representing the geometry being analyzed is required. This file is used to create a Java-based macro file that is compatible with STAR-CCM+. It serves as the core of the tool by orchestrating a sequence of operations within the STAR-CCM+ environment. The first step involves importing the CAD files that represent the geometry of interest, which serve as the blueprint for the following macro operations. The code efficiently handles tasks such as importing geometry, defining parts, customizing surfaces, and initiating the computation process. The following operation involves subtracting parts to isolate specific

[5] Simcenter STAR-CCM+ Software home page: `https://plm.sw.siemens.com/en-US/simcenter/fluids-thermal-simulation/star-ccm/` [retrieved March 11, 2024]

components, enabling a focused approach to meshing. This step is crucial for refining the mesh in specific areas of interest, such as the fuselage, horizontal tail, and LEX. The subtraction operation allows for the precise definition of the geometry objects involved in the process of subtraction. The tool's workflow focuses on automated mesh generation, allowing users to customize mesh controls for specific surfaces to a high degree. The assignment of the region is another crucial step in defining the simulation domain. The code demonstrates how to establish boundaries and regions corresponding to different components of the geometry. Surfaces are defined for each system component, including the far-field, symmetry zone, inflow, and outflow zones. The mesh is then customized by adding a refinement volume of interest in areas where the mesh needs to be tightened, such as the horizontal tailplane and LEX, specifically focuses on the trailing edge of both surfaces. Figure 4.6 illustrates a flowchart summarizing the primary steps taken by the tool to automatically generate a mesh from CAD input files.

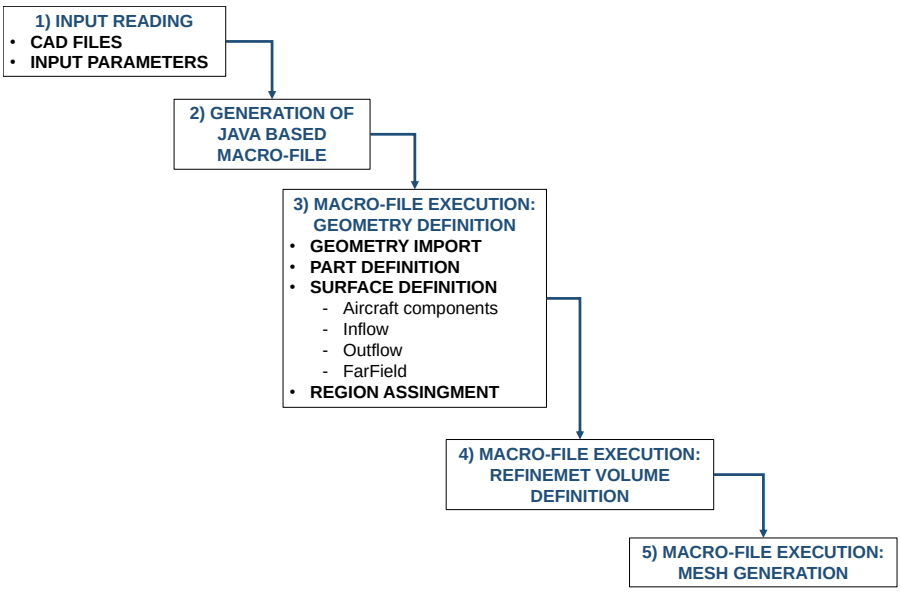

Figure 4.6: Flowchart illustrating the steps taken from the STAR-CCM+ Mesh Generator tool to automatically generate a mesh from CAD input files.

In summary, the STAR-CCM+ Mesh Generator and Solver emerge as an automated solution to employ in the field of aerodynamic simulations. The seamless integration with CAD geometries, combined with its automated mesh generation capabilities, positions it as a versatile tool in the field of aerodynamics research and engineering. In addition to its automation capabilities, the tool's inherent adaptability to complex geometries, combined with a set of custom mesh controls, ensures the creation of a reliable simulation process.

4.1.3 SU2 Mesh Morphing

SU2 Mesh Morphing is a tool designed to streamline the integration between CFD and FEA in the context of aerodynamic and structural simulations. The main goal of this tool is to automate the process of morphing SU2 meshes, starting with a basic set of point deformations that include translations and rotations. This capability plays a crucial role in improving the efficiency of the design optimization process by ensuring a consistent representation of physical solutions across both aerodynamic and structural domains. The tool's methodology involves using RBF interpolation to facilitate simultaneous deformation of aerodynamic and structural meshes.

Indeed, integrating SU2 and MSC Nastran poses significant challenges due to their different computational domains. Achieving coupling between CFD and FEA domains requires accurate data exchange and a robust coupling scheme for a fully integrated analysis. Considering the complexities of developing MDA capability, the IDF strategy emerges as a more efficient solution. Indeed, the IDF approach replaces the complex coupling required between disciplines with surrogate variables. In the context of this thesis work, these variables are essential for considering the reciprocal effects of structural flexibility on aerodynamics and loads. To comply with the IDF architecture, the tool accepts a geometrically warped input based on structural deformation expressed through surrogate structural degrees of freedom. These degrees of freedom, which represent structural displacements and rotations, need to be interpolated on the CFD mesh to ensure consistent geometry warping. RBF interpolation, commonly used for black box multi-physics applications [189], establishes a mapping between the two computational domains. Accuracy depends on selecting the appropriate parameters for RBF, including the basis functions' radius and the number of interpolating points. The latter, which could be substantial, can increase the magnitude of the consistency constraint. To tackle this task, a virtual structural line is introduced inside the wingbox, as illustrated in Figure 4.7. The structural response at these grid points is then reconstructed using rigid kinematic modeling, assuming an infinitely rigid wing section in-plane. The degrees of freedom of this structural line, specifically the vertical translations and axial rotations, will be related to those of the wingbox as

$$\mathbf{x_s} = \mathbf{x_{s,0}} + \mathbf{u^{(tr)}} + \mathbf{u^{(rot)}} \times \mathbf{d_s} \tag{4.1}$$

where $\mathbf{x_s}$ and $\mathbf{x_{s,0}}$ are the locations of the surrounding wingbox nodes in the deformed and undeformed configurations, respectively, $\mathbf{u^{(tr)}}$ and $\mathbf{u^{(rot)}}$ represent the vertical translations and axial rotations of the structural line, and $\mathbf{d_s}$ the

distance vector between the structural line nodes and the nodes on which the deformation is reconstructed.

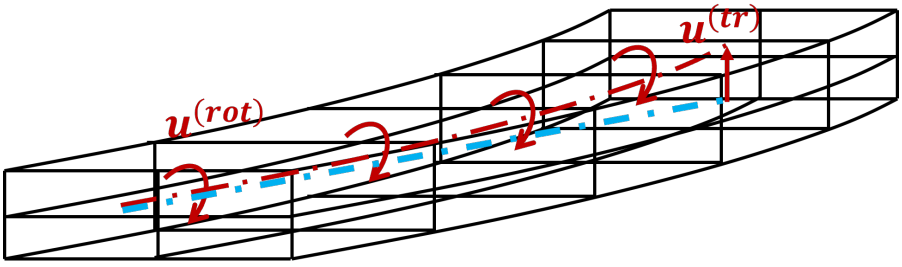

Figure 4.7: Schematic of a structural line and a deformed wingbox.

Consequently, the structural surrogates needed for the IDF method represent the vertical translations and axial rotations of the structural line. The mesh depicting the wing geometry is deformed using RBF interpolation. While this interpolation directly controls the surface mesh points to reshape the wing, the volume mesh undergoes distortion using the embedded SU2 DEF solver [190]. This method treats the volume mesh as a physical net subject to displacement based on linearly elastic relationships, similar to a FEA approach.

This approach can be easily applied to both CFD and FEA mesh domains. Consequently, it allows for simultaneous deformation of both the aerodynamic mesh and the finite element model for the structure, making it easier to define shared design variables for modifying the wing's geometry. This ensures that if a geometric variable needs to be modified during the design process, the structural model can be rebuilt using a dedicated routine, and the aerodynamic mesh is deformed concurrently. This step is crucial to ensure that aerodynamic and structural analyses are performed on identical geometries. Furthermore, integrating aerodynamic and structural models in this way improves the efficiency and effectiveness of the design optimization process. Rapid assessments of the impact of structural geometry changes on both aerodynamic and structural performance become feasible. The utilization of shared variables and automated routines for rebuilding the model streamlines the design optimization process, reducing the risk of errors or inconsistencies. This integrated approach not only improves computational efficiency but also ensures synchronized and efficient design evaluations, proving valuable in multidisciplinary optimization scenarios.

4.1.4 HTP Sizing

The HTP sizing tool utilizes a structural sizing method based on a semi-analytical approach. Its main goal is to establish an initial rigid tail shape by utilizing a set of macro design variables, mainly associated with planform parameters. The external

rigid shape determines the masses and characteristics of important structural elements by taking into account elasticity and stiffness, in line with specific layout and sizing conditions. These sizing conditions are determined based on the flight envelope diagram [191], which covers a range of maneuvering scenarios starting from a standard aircraft configuration. The design of the horizontal stabilizer typically aims to ensure static stability and provide effective control by achieving an appropriate maximum lift coefficient during downward lift, which is required to stabilize the aircraft in case of positive wing lift. Key factors influencing the size of the tailplane include stability during cruise conditions and the control requirements for landing. In the preliminary sizing phase, a common approach to determine the tail area involves establishing two relationships: one between wing and tailplane area ratio, denoted as S_H/S_W, and the other involving the longitudinal distance between the Center of Gravity (CG) and the Aerodynamic Center (AC), expressed as $(X_{cg} - X_{ac_{wf}})/C_{mac}$. These relationships are used to satisfy the sizing conditions outlined above. Referring to the force and moment diagram in Figure 4.8, the sizing conditions can be formulated using Equations 4.2 and 4.3.

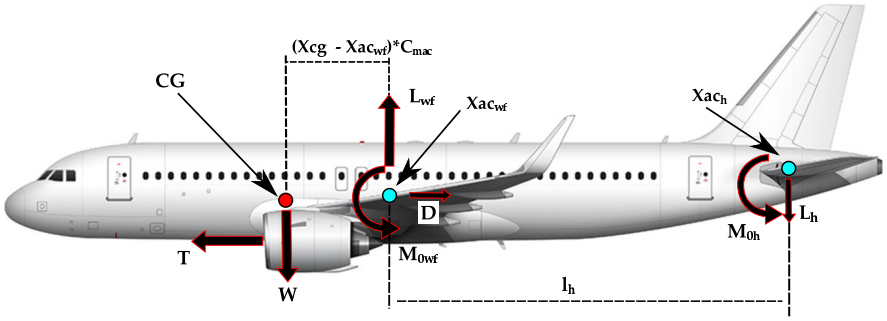

Figure 4.8: Forces, moments, and lever arms are used to calculate the pitching moment of an aircraft [192].

$$\frac{S_H}{S_W} = \frac{\left[C_{m_{0_{wf}}} + C_{m_{0_e}} + C_{L_{wf}}\left(X_{cg} - X_{ac_{wf}}\right)\right] C_{mac}}{\eta_h \left\{C_{L_h}\left[l_h + \left(X_{cg} - X_{ac_w}\right) C_{mac}\right] - C_{mac} C_{M_{0_h}}\right\}} \tag{4.2}$$

$$\frac{S_H}{S_W} = \frac{C_{L_{\alpha_{wf}}}\left(X_{cg} - X_{ac_{wf}}\right)}{\eta_h C_{L_{\alpha_h}}\left(1 - \frac{d\epsilon}{d\alpha}\right)\left[\left(X_{cg} - X_{ac_{wf}}\right) + \frac{l_h}{C_{\text{mac}}}\right]} \tag{4.3}$$

These equations are commonly represented in a unified graph known as the scissor plot [193], as depicted in Figure 4.9, showcasing a qualitative representation. Within these limitations, and considering a specific range of center of gravity excursion, it is possible to estimate the minimum tail planform area. The area of interest is located above the horizontal dashed line in Figure 4.9. Additionally, it is essential to

note that the aft center of gravity is typically positioned at a safe distance from the neutral stability limit. For conventional jet transport aircraft, this limit typically falls between 3% and 5% of the wing's mean aerodynamic chord [194–196].

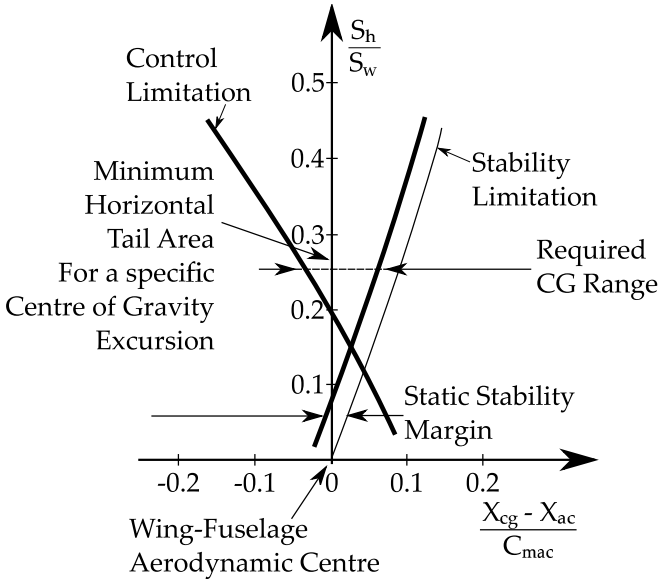

Figure 4.9: Qualitative representation of the scissor plot diagram [192].

Ensuring longitudinal stability and control in all operational scenarios of an aircraft is a crucial function of the tailplane. The first step in determining the critical loading condition on the tail and guiding the structural sizing process involves creating the classical V-n diagram for the specific aircraft. Depending on the aircraft category, specific regulations may be applied to define the flight envelope and subsequently estimate the balancing loads required for the tailplane, covering the most critical maneuvering conditions. An illustration of this diagram, as described in the FAR25 regulation [137], can be found in Figure 4.10.

The flight envelope is a diagram used to determine limit loads for aircraft structures, ensuring that an aircraft operates within the defined flight envelope throughout its service life. Consequently, the most extreme flight conditions are within these limitations. Calcara and Megson [197, 198] provide detailed discussions on constructing the flight envelope. Solving the longitudinal equilibrium equation enables the estimation of the necessary aerodynamic load on the tail to balance the aircraft for each condition on the V-n diagram. Identifying the most critical loading condition for the tail involves considering all steady flight levels and complementary conditions (where the pitching acceleration is not zero), as illustrated by Calcara [197].The critical sizing condition for the tailplane, which are typically one of the points from A to H indicated in Figure 4.10, is then converted into

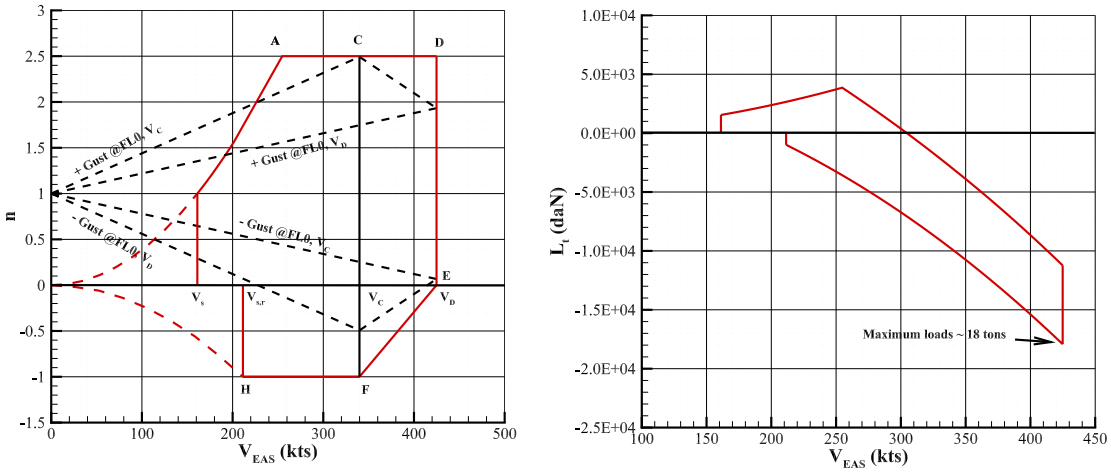

Figure 4.10: Example of a V-n diagram (left) for an A320-like aircraft according to FAR25 [137] and balancing loads on the horizontal tailplane (right) [192].

a spanwise load distribution, which facilitates structural sizing and deformation analysis. Among various methods available, the Schrenk method [199] has been applied, with enhancements for the sweep effect provided by the Pope and Haney correction [200]. Once the structural loads have been characterized, the tailplane structural element can be sized.

The HTP sizing tool's primary inputs include macroparameters for the wing and tailplane, details about the tailplane's structural layout and material, and the aircraft's weight and balance information. For a more detailed explanation of the methodology, including validation analysis and an application example, refer to [192], where it is possible to notice how all the formulas presented in this section can be applied to both the wing and tailplane. The tailplane is composed of primary and secondary structures. The mass of the primary structure is determined through fundamental structural analysis, which relies on stress and deformation measurements. This structure is designed to withstand significant loads and deformations. The calculation of the primary structure mass takes into account factors such as relief from bending moments, material properties, and weight penalties. However, the mass of the secondary structure is statistically estimated, as outlined in [201]. The tailplane weight model involves an initial categorization of primary and secondary weight contributions. The primary structure typically includes upper and lower stiffened skin panels, spars, ribs, and the "Non-Optimum Weight," which accounts for penalties such as joints, attachments, and cut-outs. The primary structure bears the main loads applied to the tailplane. The weight contribution of the former is analytically computed to the greatest extent possible through optimal sizing, while the weight contribution of the latter is estimated

empirically. The secondary structure includes fixed leading and trailing edges and control surfaces, with their weight estimated using geometry-dependent statistical methods. As previously discussed, the issue of tail mass is expressed as the combined mass of primary and secondary structures. The primary structure comprises various components, all of which contribute to bearing loads under stress, with some specialized for specific tasks. A simplified approach treats the wing box as a statically determined equivalent system, with each component supporting a specific type of load. The caps of the spars are designed to withstand the bending moment M_b, while the web of the front and back spars supports the vertical shear forces S_f. The wing's skin covering handles the torsion moment M_t, while the ribs prevent buckling of the tail panels and maintain the external shape. Complex structural phenomena, such as the effects of combined loads and dynamic forces, are often overlooked. Cross-sectional distortion is not considered; flat sections maintain their shape after the application of load. A spar consists of a web and cap. In the sizing method, a unique average height h_m, as detailed in Equation 4.4, is assumed. This average is calculated using a weighted average with a coefficient α_b, which represents the contribution of one spar to the overall absorption.

$$h_m = h_1 c(y)\alpha_b + h_2 c(y)(1 - \alpha_b) \tag{4.4}$$

The spar cap is designed to absorb the stress σ generated by the increase in bending moment M_b, and this is further multiplied by the assumed safety margin S_M. The overall spar cap area, denoted as A_{cap}, should be able to withstand a uniform stress distribution denoted by σ_y. This stress distribution, when multiplied by the lever arm h_m, generates the bending moment M_b. Therefore, the area of the unknown spar caps can be determined using Equation 4.5.

$$A_{cap}(y) = \frac{S_M M_b(y)}{\sigma_y h_m(y)} \tag{4.5}$$

The estimated value of A_{cap} could result in impractical thickness values. Indeed, there is a technological limit set for the maximum allowable thickness. If the thickness falls below this limit, it will be replaced with the minimum allowable value. With knowledge of the distribution of the area of the spar caps and material properties, including material density ρ_{mat}, it becomes possible to estimate the mass of the cap using Equation 4.6, where g denotes gravitational acceleration. Parameters that are useful for estimating the distribution of the wing box moment of inertia include the cap thickness, as defined in Equation 4.7, and the cap span, as outlined in Equation 4.8.

$$w_{cap}(y) = gA_{cap}(y)\rho_{mat} \tag{4.6}$$

$$t_{cap}(y) = \frac{\sqrt{A_{cap}(y)}}{2} \tag{4.7}$$

$$b_{cap}(y) = 4t_{cap}(y) \tag{4.8}$$

During the conceptual-preliminary design phase, the spar webs are specifically engineered to withstand the vertical shear stresses resulting from aerodynamic and inertial loads. In this context, the sizing of spar webs utilizes the von Mises method, focusing exclusively on shear stress considerations. The spar web is assumed to have a rectangular shape with a height equal to h_m and an unknown area A_{web}. Similar to the approach taken for spar caps, the value of A_{web} can be determined as the area that exhibits a uniform τ_y, multiplied by the safety margin, effectively absorbing the designated shear load S.

$$A_{web}(y) = \frac{S_M S_f(y)}{\tau_y} \tag{4.9}$$

By knowing the area of the spar web, its mass can be estimated using Equation 4.10.

$$w_{web}(y) = gA_{web}(y)\rho_{mat} \tag{4.10}$$

The box's skin must withstand the torque generated by torsion. The wing-box is conceptualized as a closed, thin section that responds to torsion according to Bredt's theory. The area of the box can be calculated using Equation 4.11, assuming the chord extension of the wing box is c_{box}.

$$A_{box} = c_{box}c(y)\left[h_1(y) + h_2(y)\right] \tag{4.11}$$

By using the box area, the thickness distribution can be approximated using Bredt's first theorem, which establishes a relationship between thickness and torsional stress, as depicted in Equation 4.12.

$$t_{skin} = \frac{1}{2}\frac{M_t(y)}{\tau_y A_{box(y)}} \tag{4.12}$$

In this instance, a technological limit has been established for the minimum allowable skin thickness. Once the skin thickness is determined, the area of the panel skin can be approximated using Equation 4.13. This estimation, in turn, facilitates the calculation of the skin mass using Equation 4.14.

$$A_{skin} = 2c_{box}c(y)t_{skin}(y) \tag{4.13}$$

$$w_{skin}(y) = gA_{skin}(y)\rho_{mat} \tag{4.14}$$

The moment of inertia I for the wing box depends on the dimensions of the box elements and is calculated as the sum of the moments of inertia of both the spar and skin, as detailed in Equations 4.15 and 4.16.

$$I_{spar}(y) = \frac{b_{cap}(y)h_m(y)^3}{12} - \frac{b_{cap}(y) - 2\left[\frac{A_{web}(y)}{h_m(y)}\right][h_m(y) - 2t_{cap}(y)]^3}{12} \tag{4.15}$$

$$I_{skin}(y) = \frac{c_{box}c(y)h_m(y)^3}{12} - \frac{c_{box}c(y)\left[h_m(y) - 2t_{skin}(y)\right]^3}{12} \tag{4.16}$$

The model assumes that all ribs have uniform thickness, set at the minimum required to prevent instability. However, there is a slight variation in the geometric pitch along the wingspan, and ribs are only present in the working chamber. The wings are considered to be panels, sharing an area equivalent to that of the box. The specified thickness and spacing of the wings are provided as input data for the wing box layout. Spacing refers to the total number of ribs, denoted as N_{rib}, along the span. Consequently, the rib volume V_{rib_i} can be determined using Equation 4.17. The mass of the rib is calculated by multiplying the rib volume by the assumed material density, as shown in Equation 4.18.

$$V_{rib_i} = A_{box_i}t_{rib} \tag{4.17}$$

$$M_{rib_i} = A_{box_i}t_{rib}\rho_{rib} \tag{4.18}$$

The bending and torsional stiffness of each section of the wing is calculated. Specifically, the torsional stiffness can be divided into two components, primarily associated with pure torsion stiffness (following Bredt's theory) and torsion-bending stiffness (based on a non-linear theory relying on root boundary conditions), as illustrated in Equation 4.19.

$$J = J_t + J_b \tag{4.19}$$

In conclusion, these stiffness characteristics are used to discretize a beam-like model, where the stiffness of the shoes is aligned with that of the wing-box.

Subsequently, the rotation and deformation of each section are checked to account for wing flexibility and determine if they exceed critical values.

The secondary structure includes fixed leading and trailing edges, control surfaces, and high-lift devices. Estimating the weight of these components depends on statistical methods that take into account their geometry. The goal is to evaluate the mass of the secondary structure in order to complete the calculation of the lifting surface mass. Typically, the secondary mass contributes around 30% of the total wing mass and significantly influences inertial relief. Given the complexity of these components, a statistical approach is valuable for estimating the secondary mass contribution. The method used is based on Roux's assumptions [202]. It suggests that the mass of the secondary structure is proportional to the wing's lifting surface reference area. This approach is considered reliable because it allows for precision in the collection of surface mass data. Following this approach, Equation 4.20 can be utilized.

$$\begin{aligned} &M_{secondary} = 0.488 K S_{ref}^{n} \\ &Where: \\ &K = 25.9 \; and \; n = 1.097 \; if \; W_{MTO} \geq 10000N \\ &K = 4.39 \; and \; n = 1.358 \; if \; W_{MTO} \leq 10000N \end{aligned} \tag{4.20}$$

4.2 Aerodynamic Tool and Methodologies

4.2.1 STAR-CCM+ CFD Solver

The STAR-CCM+ Solver is a CFD tool designed to improve the efficiency of aerodynamic analyses within a seamlessly integrated workflow. Specifically designed to integrate with the Siemens Simcenter STAR-CCM+ platform, this software provides an automated solution for addressing intricate fluid dynamics problems. Its main goal is to simplify the CFD analysis process by addressing aerodynamic challenges in various fluid domain conditions, including variations in the angle of attack. The tool's primary input parameters relate to characterizing the fluid domain. Each parameter can be specified as a single value or in vector form, allowing for the automatic initialization of a DOE that comprehensively covers all input variables. The analysis systematically unfolds for every combination of input parameters, including factors such as the angle of attack, Mach number, flight altitude, and other crucial elements for aerodynamic assessment. In addition to the specified parameters, the tool requires the provision of a STAR-CCM+ .sim file. This file contains a pre-defined mesh that is essential to the analysis

process. The mesh serves as the foundation for the comprehensive evaluation of aerodynamic behavior, ensuring accurate and insightful results. Expanding on the capabilities of the STAR-CCM+ Solver, it is noteworthy that its integration with the Siemens Simcenter STAR-CCM+ platform enhances the overall user experience. The seamless connectivity streamlines the workflow, enabling engineers and analysts to concentrate on the complexity of aerodynamic analyses without being burdened by manual processes. Furthermore, the automated initialization of a DOE not only speeds up the analysis but also guarantees a systematic exploration of the entire parameter space, leading to a more comprehensive understanding of the aerodynamic phenomena being studied.

The Simcenter STAR-CCM+ software is a simulation environment capable of encompassing every stage required to conduct comprehensive engineering analyses. This involves tasks such as importing and creating geometries, generating meshes, solving governing equations, analyzing results, and automating simulation workflows for design exploration studies. Simcenter STAR-CCM+ offers a wide range of capabilities for modeling fluid flow and energy. Its core functionalities cover various flow characteristics, accommodating scenarios of inviscid, laminar, or turbulent flows, as well as considerations for Newtonian and non-Newtonian viscosities, incompressible, and compressible conditions. The software offers a variety of options for equations of state, including constant density, ideal gas law, real gas laws, polynomial density, and user-defined alternatives. Simcenter STAR-CCM+ offers a wide range of turbulence models, including Reynolds-Averaged Navier Stokes (RANS) models, among others. Parallel execution is facilitated through automatic decomposition, with support for various MPI implementations. For analyzing simulation results, Simcenter STAR-CCM+ provides a comprehensive range of tools, including various types of reports, monitors for sampling and saving summary information during the simulation, and field monitors that gather data samples from the solution domain. The software enables users to take advantage of a built-in automation framework, which provides operation blocks for conditional branching, looping, and setting scalar parameters. Additionally, the software supports Java scripting, allowing users to journal User Interface actions and play back scripts for increased flexibility and automation.

As previously discussed in Section 4.1.2, the integrated STAR-CCM+ CFD Solver tool generates a Java-based macro file that is compatible with STAR-CCM+. The code serves as the core of the tool, orchestrating a sequence of operations within the STAR-CCM+ environment. The Java code defines parameters such as altitude, Mach number, pressure, temperature, viscosity, and density, which are crucial for governing fluid dynamics behavior during the simulation. The tool's flexibility is

evident in its ability to adapt to diverse scenarios and operating conditions. An iterative process, powered by a loop over the array of fluid domain inputs (e.g., angles of attack), coordinates the simulation for each specified input. The solver is configured to handle a specified number of iterations or to stop earlier if all residuals reach a predefined threshold value. The simulation output data, including aerodynamic coefficients and derivatives, are collected and stored in a specific report. Exporting data from the simulation is facilitated through the final section of the Java code, which saves essential aerodynamic coefficients in a Comma-Separated Values (CSV) file for easy handling in the RCE environment.

4.2.2 SU2 CFD Solver and Sensitivity Analysis

The SU2 CFD Solver and Sensitivity Analysis tool is designed to perform high-fidelity aerodynamic analysis, with a focus on inviscid flow around a wing. Furthermore, a methodology has been implemented for computing aerodynamic gradients with respect to wing geometry parameters and parameters from other disciplines involved in the optimization problem. The tool requires a mesh that is compatible with SU2, as well as the fluid domain conditions for conducting the analysis and optimization. For aerodynamic analysis, this tool utilizes SU2 [203], an open-source Multi-Physics tool equipped with CFD solvers. SU2 is designed for conducting Partial Differential Equation (PDE) analysis and solving PDE-constrained optimization problems on general unstructured meshes. Its C++ executables provide functionality for solving direct, adjoint, and linearized problems for various sets of equations. SU2 supports various techniques for design sensitivity analysis, catering to aerodynamic shape optimization. It incorporates both discrete and continuous adjoint methods. The suite includes modules for mesh deformation, gradient projection, geometry definition and constraints, mesh adaptation, and solution export. These tools are integrated into a Python framework that enables seamless integration with a gradient-based optimizer. Shape optimization relies on calculating surface sensitivity, which is then used to determine the gradient of the objective function and constraints by projecting it onto the shape design variables. Geometry control is achieved through parameterization using either FFD or Hicks-Henne-Bump (HHB) functions [203].

The CFD Solver and Sensitivity Analysis tool's methodology is designed to calculate the elements required to solve a general aero-structural problem formulated using the IDF architecture. A potential objective function for this problem can be expressed as a linear combination of an aerodynamic quantity C_f and a structural quantity C_s, given by $J = \beta_1 C_f + \beta_2 C_s$, where β_1 and β_2 are arbitrary weights.

The set of design variables includes parameters that affect the external wing shape, which will be shared design variables, as well as internal structural properties of the FE model or the airfoil section, which are specific to the FEA or CFD, respectively. The design variables that are shared determine the planform shape of the wing and are gathered in two vectors denoted as $\mathbf{p}$ for the macro parameters of the wing geometry and $\mathbf{t}$ for the structural properties. A generalized formulation for this type of IDF aero-structural problem can be expressed as follows:

$$\begin{aligned} \text{minimize} \quad & J = \beta_1 C_f(\mathbf{p}, \mathbf{u}^*) + \beta_2 C_s(\mathbf{p}, \mathbf{t}) && \text{(4.21a)} \\ \text{with respect to} \quad & \mathbf{p}, \mathbf{t}, \mathbf{u}^* && \text{(4.21b)} \\ \text{subject to} \quad & \mathbf{g}_j^{IDF} = \mathbf{u}^* - \mathbf{u} = 0 && \text{(4.21c)} \end{aligned}$$

being $\mathbf{u}$ and $\mathbf{u}^*$ the structural displacements and their surrogates, respectively.

The method for evaluating aerodynamic optimization gradients, also known as sensitivity analysis, is described here. The optimization algorithm uses gradients of the objective function and constraints to guide the evolution of the design variables through successive iterations. Not only is a correct estimation of the gradients essential for converging to a solution, but also the higher the accuracy, the fewer iterations will be required to find a design. For a general gradient-based optimization problem, the aerodynamic objective functions need to be differentiated with respect to each design variable independently. An ad-hoc method for computing these gradients has been developed and validated. To further reduce the computational burden and converge to a solution in a reasonable amount of time, it is essential to carefully consider the cost of differentiating such functions.

Based on Eq. 4.21a, where the objective function is a combination of structural and aerodynamic coefficients, its differentiation can be expanded as

$$\frac{dJ}{d\gamma} = \beta_1 \frac{dC_f}{d\boldsymbol{\gamma}} + \beta_2 \frac{dC_s}{d\boldsymbol{\gamma}} \tag{4.22}$$

being $\boldsymbol{\gamma} = [\mathbf{p}, \mathbf{t}, \mathbf{u}^*]^\mathsf{T}$, a vector that collects all the design variables of interest. For the calculation of the gradient of a generic aerodynamic contribution, represented by $dC_f/d\boldsymbol{\gamma}$, the capabilities of the discrete adjoint solver available in SU2 (described by [204]) are utilized. This tool calculates the sensitivity of any aerodynamic coefficient, such as drag, lift, or moment, with respect to the coordinates of the surface mesh points. This quantity, also known as surface sensitivity, will be denoted as $dC_f/d\mathbf{x}_f$, where $\mathbf{x}_f$ represents the points of the surface mesh. It is independent of the design of any variable, as it solely depends on the characteristics of the flow around the current geometry. The differentiation of an aerodynamic

coefficient with respect to the shape of shared design variables can be expressed by applying the chain rule as follows:

$$\frac{dC_f}{d\mathbf{p}} = \frac{dC_f}{d\mathbf{x_f}} \cdot \frac{d\mathbf{x_f}}{d\mathbf{p}} \tag{4.23}$$

where $d\mathbf{x}_f/d\mathbf{p}$ is computed by differentiating the function that warps the geometry according to the chosen design variables, using an Automatic Differentiation (AD) tool based on the Algopy library [205]. This essentially corresponds to a dot product expressing the projection of the surface sensitivity on the chosen design variable.

A similar approach is followed for the derivative aerodynamic coefficients with respect to external surrogate variables, such as structural surrogates. The derivative is here represented as $dC_f/d\mathbf{u}^*$, which quantifies the impact of an external variable on the aerodynamic characteristics. In analogy with Eq. 4.23, this is expressed as

$$\frac{dC_f}{d\mathbf{u}^*} = \frac{dC_f}{d\mathbf{x_f}} \cdot \frac{d\mathbf{x_f}}{d\mathbf{u}^*} \tag{4.24}$$

where $d\mathbf{x}_f/d\mathbf{u}^*$ depends on the interpolation of the external surrogates on the surface mesh. The sensitivity analysis tool has been developed to consider these external surrogates as structural substitutes. In this particular case, $\mathbf{u}^*$ represents the degrees of freedom of the internal structural line, whose nodes are not used to construct the RBF mapping between the CFD and FEM domains. Consequently, an alternative method of interpolation must be introduced. This is accomplished using HHB functions, which impose a distortion on the wing that locally replicates the displacement of each of the structural line nodes. This can be better visualized in Figure 4.11, which illustrates how the geometry is warped around the axial rotation of one of the underlying structural nodes.

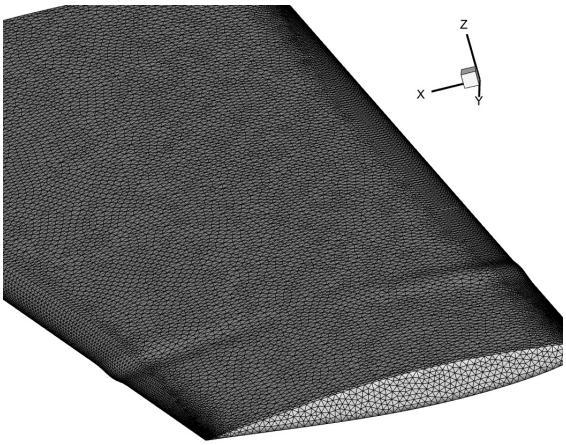

Figure 4.11: HHB for interpolation of external surrogate variables.

As described by [206], this local deformation is expressed as

$$\mathbf{x_f} = \left[\sin\left(\pi\, \mathbf{x_{f,0}}\right)^{\frac{\log \mathbf{0.5}}{\log \mathbf{t_2}}} \right]^{\mathbf{t_1}} \tag{4.25}$$

where t_1 and t_2 are parameters that control the amplitude and width of the HHB function, respectively, while $\mathbf{x}_{f,0}$ represents the position of the surface mesh points of the undeformed geometry. Specifically, t_1 will represent the magnitude of the n-th component of $\mathbf{u}^*$, so that differentiating Equation 4.25 using AD will yield $d\mathbf{x}_f/d\mathbf{u}^*$ for Eq. 4.24.

In conclusion, there is no need to calculate the derivative of the aerodynamic objective function with respect to the structural properties. In an IDF optimization problem, there is no direct connection between this variable and the function.

4.2.3 Enhanced VLM Solver

The methodology presented in this section relies on an enhanced VLM approach for aerodynamic calculations. The main goal of the tool is to calculate aerodynamic loads under specific conditions and varying angles of attack, including nonlinear lift regimes. The process involves efficiently estimating the aerodynamic load for the tailplane configuration by determining the spanwise lift distribution, which is represented as $C_l(y)$. In this approach, the tailplane surface is divided into multiple spanwise panels. Each panel contains a single horseshoe vortex positioned at one-quarter of the local chord, with its free-stream sections extending to infinity. Control points are positioned at three-quarters of the chord length to facilitate the calculation of the unit normal vector. Key inputs for the tool include macro-parameters for the wing and tailplane, data on the aerodynamic characteristics of the airfoil section, and fluid domain conditions. Additional information regarding the proposed methodology can be found in [207]. The core of the methodology shares similarities with classical vortex methods, such as the one developed by the NASA research center and detailed in [208]. However, classical vortex methods encounter certain challenges. One notable issue is that their reliability is limited to the linear range of the lift curve. Moreover, these methods overlook the actual airfoil lift coefficient slope, assuming a slope equal to $2\pi(\text{rad}^{-1})$ based on the Glauert theory. The VLM approach used in this study is based on Blackwell's method [208], but the aerodynamic load distribution is usually obtained from either experimental data or high-fidelity airfoil curves. This approach facilitates the extrapolation of aerodynamic results to nonlinear lift regions, including the stall. The method unfolds in two main phases. In the initial phase, a conventional VLM is used to

calculate the spanwise lift and induced angle distributions of the wing for a specific angle of attack, denoted as α. The next phase expands the applicability of the VLM approach to the non-linear range of the lift curve by accessing an external database that contains 2D airfoil aerodynamic curves. To account for 3D effects, adjustments are made to the 2D airfoil data, with a crucial focus on sweep. Sweep induces a spanwise flow in the boundary layer. Backward sweep promotes stall from the tip, while forward sweep promotes stall from the root, as demonstrated in NACA studies detailed in the technical note [209]. The 2.5D aerodynamic characteristics of the wing section (perpendicular to the sweep line) are estimated using fundamental sweep theory [210], following the recommendation to analyze the wing section normal to the sweep line, as proposed by Mariens et al. [211]. In practical applications, Obert [212] suggests using the velocity component perpendicular to the quarter-chord line for subsonic wing analysis. This choice is consistent with the fact that pressure drag acts perpendicular to the isobars [213] (or shock wave line). For transonic wing analysis, the sweep line is positioned at the half-chord to closely align with the shock wave line, ensuring accurate analysis [214]. The procedure for estimating the lift coefficient distribution using the VLM approach is illustrated in Figure 4.12, and it is repeated for each angle of attack.

The developed method adjusts the load distribution obtained from Blackwell's approach. The wing semispan is discretized into n control/vortex points, typically set at 50. Each of these n points corresponds to an intermediate airfoil with its own unique lift characteristics. The calculation procedure can be outlined as follows: for each angle of attack, the inviscid lift distribution is computed using the selected vortex-lattice approach, which determines the local C_l at n points along the semispan. Subsequently, for all sections, armed with the local C_l, one can refer to the 2D linear lift coefficient chart to determine the local angle of attack of the airfoil using Equation 4.26.

$$(\alpha_{eff})_j = (\alpha_w + \epsilon_j) + (\alpha_{induced})_j \tag{4.26}$$

Subsequently, by utilizing this angle of attack, it is possible to extract the airfoil aerodynamic dataset to obtain a new local C_l that accounts for both viscous and three-dimensional effects. This process results in a modified lift distribution along the semispan, addressing the two-dimensional non-linearity. The revised lift coefficient distribution, in turn, produces a new distribution of the induced angle of attack, estimated using Prandtl's theory [215]. The induced angle of attack then results in a new C_l distribution. Following the approach outlined in [208], the lifting surface is divided into several rectangular horseshoe vortices

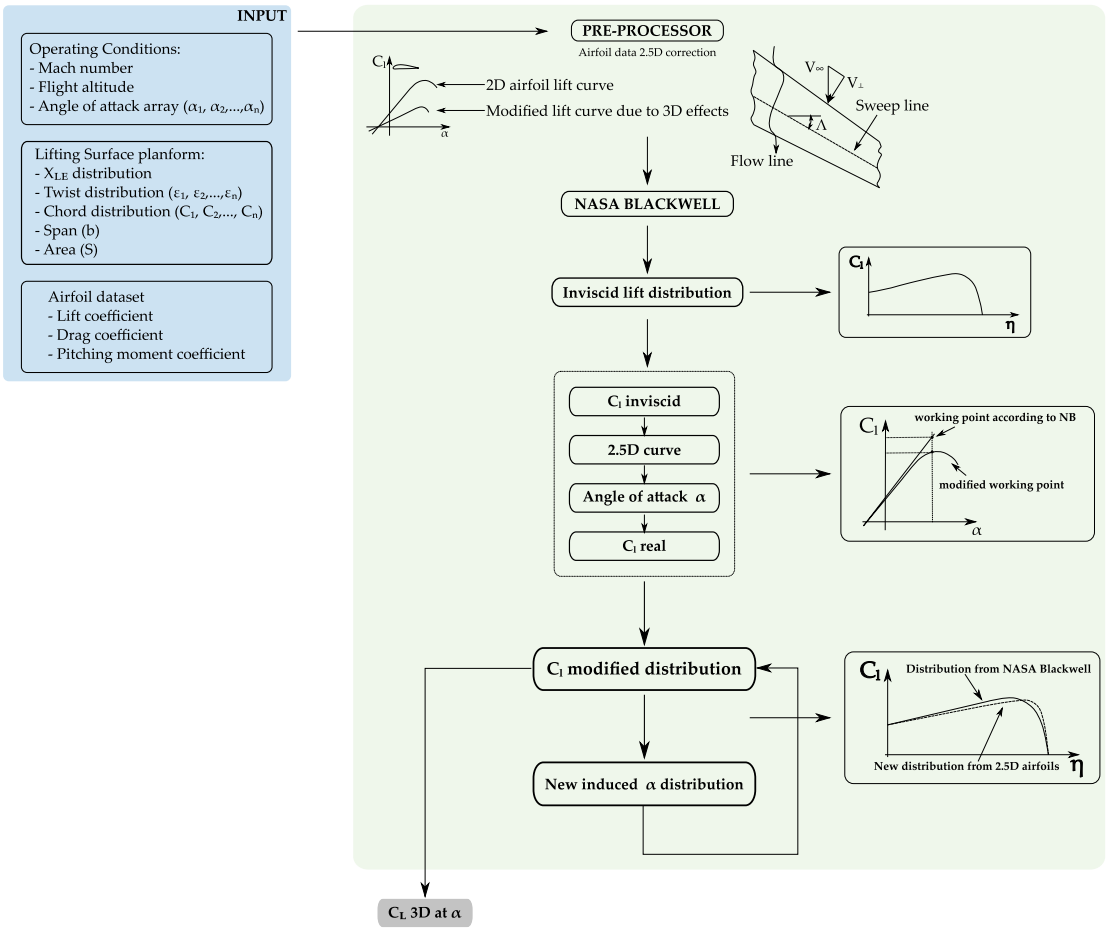

Figure 4.12: Flow chart of lift coefficient distribution computed through the improved VLM approach. Adapted from [192].

along the span, with one horseshoe vortex along the chord being utilized. This means that the midpoints of the vortices are exclusively positioned at points along the quarter-chord lines. An equal number of control points are located along the three-quarter-chord lines. The velocity of the entire vortex system is equal to the component of the free-stream velocity that is perpendicular to the lifting surface chord at each control point. The downwash velocity at any of the control points P, resulting from the 2N horseshoe vortices, is

$$w = \frac{1}{4\pi} \sum_{n=1}^{N} \Gamma_N F'_{w,v_N} \tag{4.27}$$

With the updated knowledge of the induced angle of attack distribution, it becomes feasible to calculate the new angle of attack and lift coefficient distribution. An iterative process is essential from the second step to the last step. Once convergence is achieved, the lift coefficient (C_L) of the lifting surface can be

determined by integrating the final lift distribution. This method facilitates the calculation of a more reliable achievable $C_{L_{\mathrm{MAX}}}$ compared to an unmodified stall path procedure, by incorporating local viscous effects.

4.2.4 ICE Effect

The ICE Effect tool outlines a CFD-based methodology designed by Austrian Institute of Technology to explore the impact of geometric parameters on the aerodynamic performance of an innovative forward-swept horizontal stabilizer concept under icing conditions. Ice accumulation on the horizontal stabilizer of the empennage is assessed using the commercial software Ansys FENSAP-ICE [6], conducting three-dimensional multishot in-flight icing simulations. Each simulation comprises four sequential calculation steps that collectively evaluate the ice accretion on an aerodynamic surface over a typical duration of one or a few minutes. The steps involved are:

1. Calculation of the turbulent flow field, considering surface roughness.
2. Eulerian droplet field and impingement calculation.
3. Eulerian surface water runback, ice accretion, and updated geometry calculation.
4. Remeshing.

These four steps, when performed in succession, constitute a "shot." Shots are taken sequentially to capture the passage of time and the accumulation of ice on the surface. For more information about FENSAP-ICE and the multishot methodology, please refer to the references [216–218]. Further details regarding the methodology described can be found in the referenced [219].

To streamline the icing analysis, only the tail is subjected to icing, while the wing and the rest of the fuselage are kept ice-free. This assumption is based on the belief that any ice accumulation on the thick wing inboard section would minimally impact the tail's ability to collect ice. In the quasi-steady multi-shot icing approach, the entire computational domain is remeshed and recalculated after each surface displacement. Since there are no intended changes in the wing and fuselage geometry, these components are excluded from the initial solution. Only a subsection of the complete computational domain, which includes the tail and the aft section of the fuselage, is used for the icing simulation. CFD-based, in-flight icing simulations are conducted for each aircraft geometry, simulating a 45-minute holding flight condition in accordance with the cloud conditions specified in FAR

[6] Ansys FENSAP-ICE Software home page: `https://www.ansys.com/products/fluids/ansys-fensap-ice` [retrieved March 11, 2024]

25 Appendix C. Subsequently, CFD is used to determine lift versus angle of attack curves for each geometry, both with and without icing. The total icing duration of 45 minutes is divided into 20 intervals, each lasting 135 seconds. Fluent Meshing is used to remesh around the new ice surface within the reduced computational domain at the end of each shot.

In summary, the process for conducting a multishot icing simulation on the tail with full aircraft effects involves the following stages:

1. Employing a fully scripted automatic CAD model of the entire aircraft for mesh generation, and then applying an automatic solution error-based anisotropic adaptation to the full aircraft mesh. This adjustment is made for pressure, velocity components, and liquid water gradient in a FENSAP-DROP3D-Optigrid loop.
2. Deriving boundary condition profiles from the adapted full aircraft CFD and Liquid Water Content (LWC) solutions specifically for the related pertaining to the empennage.
3. Extracting the geometry and domain specifically solely for the empennage.
4. Conducting a multi-shot in-flight icing simulation focused on the empennage. The remeshing sizing during this process is not adapted, but rather suggested by the non-adapted full aircraft mesh and the complexity of the evolving ice shape.

Figure 4.13 depicts a diagram of the workflow with four stages.

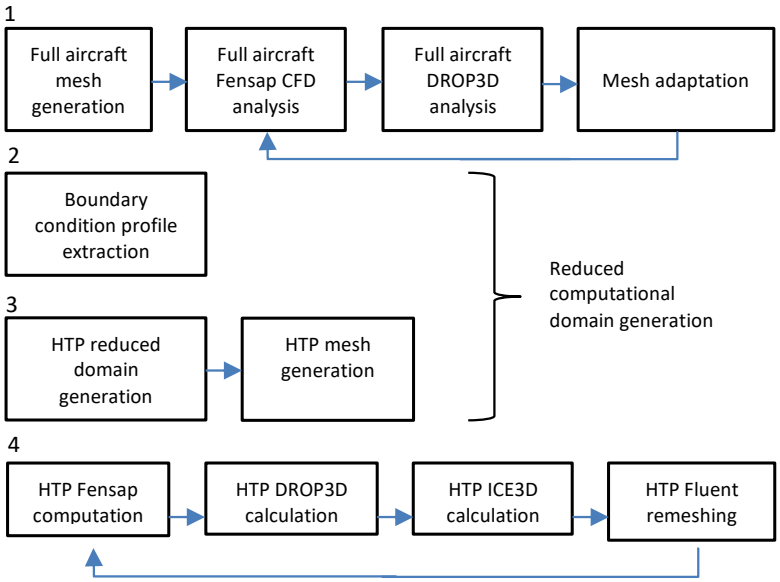

Figure 4.13: Flowchart showing four stages of a full aircraft-based HTP in-flight icing simulation. Adapted from [219].

4.3 Aerostructural Tool and Methodologies

4.3.1 MSC Nastran FEM Solver and Sensitivity Analysis

The MSC Nastran FEM Solver and Sensitivity Analysis tool is designed by the author in collaboration with University of Southampton for conducting high-fidelity structural and aerostructural analyses on wings. Furthermore, a method has been implemented for calculating structural gradients in relation to wing geometry and structural parameters. The primary inputs for the tools include wing geometry, structural parameters, and fluid domain conditions for conducting the analysis and optimization. Structural analyses are conducted using MSC Nastran [7], a commercial FEA software widely used in aeronautical applications for structural analysis. In addition to its structural capabilities, the software offers aeroelastic solvers that are based on a built-in Doublet Lattice Method (DLM) for aerodynamics. The FEM solver tool utilizes the static aeroelastic solver (SOL 144) to evaluate the structural response to aerodynamic loads. Conversely, the design analysis tool (SOL 200) is used to calculate derivatives of specific structural parameters. To facilitate integration into a multidisciplinary workflow, toolkits have been developed for reading and writing input and output files, enabling automated data transfer. These toolkits also provide flexibility for customizing MSC Nastran outputs and enable the capability to modify the finite element model (FEM) based on the design variables of interest.

The methodology of the tool is designed to calculate the components required to solve a general aero-structural problem formulated using the IDF architecture, similar to the one outlined in Equation 4.21a. A plausible objective function for such a problem can be expressed as the linear combination of an aerodynamic function C_f and a structural function C_s, denoted as $J = \beta_1 C_f + \beta_2 C_s$, where β_1 and β_2 act as arbitrary weights. In an IDF architecture optimization problem, the structural solver is required to evaluate the structural response under specified surrogate loads. The consistency constraint requires the surrogate variables to align with the output of each disciplinary solver, ensuring that the final design reflects a physically plausible solution. For a large-scale problem, the size of the consistency constraint grows significantly, which could potentially impact the computational efficiency of the algorithm. Nevertheless, MSC Nastran offers a fast and efficient aerodynamic analysis based on DLM aerodynamics. Consequently, there is no longer a need for surrogates of the aerodynamic loads, as the FEA response will be computed using the aerodynamic forces determined by this solver. Consequently, only structural

[7] MSC Nastran Software home page: `https://hexagon.com/products/product-groups/computer-aided-engineering-software/msc-nastran` [retrieved March 11, 2024]

substitutes are necessary in the problem formulation. The aerodynamic solver, as described in Section 4.2.2, will handle these surrogates. With this approach, if a geometric variable needs to be modified during the design process, the structural model can be reconstructed using a dedicated routine specifically generated to define a new FEM model representing the geometry introduced through the tool's inputs. The structural component of the objective function depends solely on the wing geometry and its structural properties, such as element thicknesses, as explained in Eq. 4.21a. Hence, the derivatives $dC_s/d\mathbf{p}$ and $dC_s/d\mathbf{t}$ need to be assessed to compute the element $dC_s/d\boldsymbol{\gamma}$ represented in Equation 4.22. This can be readily obtained from the MSC Nastran design and optimization solver (SOL200), which is capable of computing the derivative of a structural function, such as weight or stresses, with respect to structural element properties. However, these derivatives do not include the common design variables that are defined to control the wing geometry. Consequently, the derivative $dC_s/d\mathbf{p}$ will be calculated using an FD scheme, expressed as

$$\frac{dC_s}{d\mathbf{p}} = \frac{C_s(\mathbf{p} + \mathbf{dp}) - \mathbf{C_s}(\mathbf{p})}{d\mathbf{p}}, \tag{4.28}$$

where $d\mathbf{p}$ is the step size, chosen to be sufficiently small to limit the truncation error.

The success of a constrained gradient-based optimization also depends on accurately estimating the constraint gradients. In the IDF approach, these gradients guide the optimizer to ensure that the consistency constraints are satisfied upon convergence, thereby guaranteeing that the final design is a physically feasible aero-structural solution. The gradients to be computed are related to the function represented in Equation 4.21c. Initially, the derivative $d\mathbf{g^{IDF}}/\mathbf{dp}$ is discussed. Assuming that the design variables are independent of each other, this expression can be expanded and simplified as

$$\frac{d\,\mathbf{g^{IDF}}}{d\mathbf{p}} = \frac{d}{d\mathbf{p}}(\mathbf{u}^* - \mathbf{u}) = -\frac{\mathbf{du}}{\mathbf{dp}}, \tag{4.29}$$

Equation 4.29 expresses the relationship between the structural response, specifically the displacements $\mathbf{u}$, and the wing's geometry, which is controlled by $\mathbf{p}$. Similarly, the derivative $d\mathbf{g^{IDF}}/\mathbf{dt}$ can be simplified to

$$\frac{d\mathbf{g^{IDF}}}{d\mathbf{t}} = -\frac{d\mathbf{u}}{d\mathbf{t}} \tag{4.30}$$

Both Equations 4.29 and 4.30 are computed using finite difference (FD) schemes, where the structural deformation is calculated in a manner similar to Equation 4.28.

This calculation utilizes the static aeroelastic solver of MSC Nastran, with the aerodynamic loads being updated following the application of the step size on $\mathbf{p}$). Finally, when differentiating the consistency constraint with respect to the surrogate structural variables, it is important to note that they will not depend on the corresponding physical ones $\mathbf{u}$. This leads to the following expression:

$$\frac{d\mathbf{g}^{\mathbf{IDF}}}{d\mathbf{u}^*} = \frac{d\mathbf{u}^*}{d\mathbf{u}^*} = \mathrm{I}, \tag{4.31}$$

where I is the identity matrix of size $2N_{el} \times 2N_{el}$, with N_{el} representing the number of nodes where the surrogate displacements are defined (equivalent to $2N_{el}$ for each node's vertical translation and axial rotation).

In conclusion, the tool also provides the distribution of Von Mises stresses in the final design to verify if the solution of the problem exceeds certain stress levels.

4.3.2 HTP Flexible Deformation

The deformation analysis tool presented here utilizes a semi-analytical approach to evaluate the structural response of an aircraft to aerodynamic forces. The tool specifically calculates the elastic deformation of the tail for different angles of attack. In this analysis, aerodynamic loads are systematically transferred to the structural configuration, enabling the estimation of the tail's deformation. The distribution of weight, lift, torque from pitching, and other forces acting on the structure induces stress, which leads to specific strain patterns. These strain patterns encompass a range of vertical displacements and twist angles, which are typical parameters that are useful for understanding the structural behavior under aerodynamic forces. The tool's primary inputs include macroparameters for both the wing and tailplane, as well as detailed information about the tailplane's structural characteristics, such as inertia, weights, and material properties. Additionally, the weight and balance details of the aircraft are crucial factors for accurate deformation predictions. For a thorough understanding of the tool, including its underlying principles and application, readers are encouraged to refer to [192]. The cited work offers a comprehensive explanation of the tool's methodology, supported by a validation analysis and a practical application example, providing valuable insights into its reliability and versatility.

The elastic behavior of the lifting surface is analyzed using De Saint Venant's (DSV) elementary beam theory [220]. According to the DSV theory, the structural sizing of a tailplane, conceptualized as a cantilever beam, is influenced by N_x, the normal stress along the beam axis, S_y and S_z, the shear stresses along transverse axes, M_t, the torsional moment about the beam axis, M_{b_y} and M_{b_z}, the bending

moment about transverse axes. The proposed low-fidelity model considers S_z, M_b around the longitudinal axis, and M_t as the primary stresses affecting the deformation of the lifting surface. The elastic axis, which represents the locus of the cross-section shear centers, is assumed to be a straight line. This assumption implies that both geometric and inertial properties are uniformly distributed along the span. Loads on the tail structure result from aerodynamics and mass distribution. The presented approach considers the following loads: lift distribution $l_d(y)$, applied at 25% of the local chord, aerodynamic pitching torque $t_d(y)$, applied at the sectional quarter point, and the weight force $w(y)$. These three loads can be calculated using the following equations.

$$l_d(y) = \frac{1}{2}\rho V_d^2 c(y) C_{l_d}(y) \tag{4.32}$$

$$t_d(y) = \frac{1}{2}\rho V_d^2 c(y)^2 C_{m_{ac}}(y) \tag{4.33}$$

$$w_d(y) = n_z m(y) g \tag{4.34}$$

Since the analysis focuses on static aeroelastic phenomena, it is important to note that vibratory inertial forces are excluded from the equilibrium equations. An essential factor to consider when evaluating the deformation of a swept lifting surface is the interaction between bending and torsion stresses. In a swept wing, the lateral axis does not align with the elastic axis. To address this, a new axis system is introduced by rotating both the x and y axes around the vertical axis by an angle equal to the sweep angle of the elastic axis (Λ_{EA}). In this updated reference system, denoted as $\overline{xy}$, the lateral axis aligns with the elastic axis, as depicted in Figure 4.14.

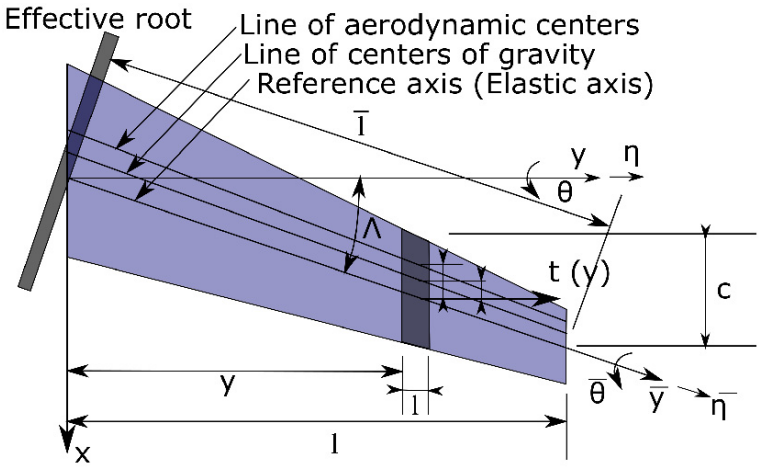

Figure 4.14: Reference coordinate systems for a swept lifting surface [192].

In this revised reference frame, the distribution of shear, bending moment, and torsional moment along $\bar{y}$ can be approximated using Equations 4.35, 4.36, and 4.37, respectively. In these equations, $\bar{s}$ represents the curvilinear abscissa in the new reference frame.

$$S_f(\bar{y}) = \int_{\bar{y}}^{\frac{\bar{b}}{2}} \left[l_d(\bar{s}) + w_d(\bar{s}) \right] \bar{s} \tag{4.35}$$

$$M_b(\bar{y}) = \int_{\bar{y}}^{\frac{\bar{b}}{2}} S_f(\bar{s}) d\bar{s} \tag{4.36}$$

$$M_{t_a}(\bar{y}) = \int_{\bar{y}}^{\frac{\bar{b}}{2}} t_d(\bar{s}) d\bar{s} \tag{4.37}$$

M_b and M_t are functions of $\bar{y}$, but from a physical perspective, they are still considered moments about the x and y axes, respectively. Hence, a rotation matrix is necessary to transform these quantities into moments $\bar{M}_b$ and $\bar{M}_{t_a}$ about the $\bar{x}$ and $\bar{y}$ axes. This relationship emphasizes the significant connection between torsion and bending moments in the context of a swept lifting surface [221], as demonstrated by Equations 4.38 and 4.39.

$$\bar{M}_b(\bar{y}) = M_b(y) \cos \Lambda_{EA} - M_{t_a}(y) \sin \Lambda_{EA} \tag{4.38}$$

$$\bar{M}_{t_a}(\bar{y}) = M_b(y) \sin \Lambda_{EA} + M_{t_a}(y) \cos \Lambda_{EA} \tag{4.39}$$

Similar considerations must also be made when estimating the lever arms of lift and weight forces to account for the sweep angle, as indicated by Equations 4.40 and 4.41.

$$\bar{e}_l(\bar{y}) = \left[x_{ec}(y) - x_{ac}(y) \right] \cos \Lambda_{EA} \tag{4.40}$$

$$\bar{e}_w(\bar{y}) = \left[x_{ec}(y) - x_w(y) \right] \cos \Lambda_{EA} \tag{4.41}$$

Thus, the contributions of lift and weight to torsion can be determined using Equations 4.42 and 4.43.

$$\bar{M}_{t_l}(y) = \int_{y}^{\frac{\bar{b}}{2}} l_d(\bar{s}) \bar{e}_l(\bar{s}) d\bar{s} \tag{4.42}$$

$$\bar{M}_{t_w}(y) = \int_{y}^{\frac{\bar{b}}{2}} w_d(\bar{s}) \bar{e}_w(\bar{s}) d\bar{s} \tag{4.43}$$

Finally, the torsional moment is calculated as the sum of all contributions, as shown by Equation 4.44.

$$\bar{M}_t(\bar{y}) = \bar{M}_{t_a}(\bar{y}) + \bar{M}_{t_l}(\bar{y}) + \bar{M}_{t_w}(\bar{y}) \tag{4.44}$$

The lifting surface is conceptualized as a wing box designed to withstand only S, M_b, and M_t. Additionally, the distribution of shear strain is disregarded because its effects are considered second-order. By using the distributions of bending and torsion stiffness, it is possible to calculate the two main types of deformation. v represents the displacement along the Z-axis, and Θ represents the rotation around the beam axis. Calculations for these variables are performed for points located along the beam axis, representing the lifting surface itself. A simplifying assumption is made that the cross-section shape does not cause distortion of the camber line, implying that the section airfoil aerodynamics remain unchanged due to lifting surface deformation. The impact is on the three-dimensional surface. The elastic deformation around the beam axis, as interpreted through torsion, causes distortions in the distribution of aerodynamic loads (i.e., torsion alters the local geometric twist along the span, affecting local angles of attack). The resulting J is used to calculate Θ as a function of the beam axis coordinate, y, for a straight wing based on the fixed reference system. The relationship between the first derivative of the torsion angle arises from the equilibrium of the beam element under the influence of M_t, as demonstrated in Equation 4.45. Meanwhile, the bending moment causes vertical displacements according to the Euler-Bernoulli relation presented in Equation 4.46, where $I(y) = I_{spar(y)} + I_{skin(y)}$.

$$\frac{\partial \theta}{\partial y} = -\frac{M_t(y)}{GJ(y)} \tag{4.45}$$

$$\frac{\partial^2 z}{\partial y^2} = -\frac{M_b(y)}{EI(y)} \tag{4.46}$$

Sweep introduces a significant relationship between bending and torsion. This interdependence is also apparent in terms of kinematic variables. Consequently, it is essential to consider various perspectives in both the streamwise and chordwise directions. Due to the rotation of the beam axis about the y-axis, particularly in the context of a swept lifting surface, this relationship is represented by Equation 4.47.

$$\frac{\partial \bar{\theta}}{\partial \bar{y}} = -\frac{\bar{M}_t(\bar{y})}{GJ(\bar{y})} \tag{4.47}$$

In the case of a swept lifting surface, rotations occur around the $\bar{y}$ axis. However, an additional factor that needs to be considered is the flow incidence angle, in

order to assess the distortion of aerodynamic loads caused by elastic deformations. It's crucial to emphasize that the incidence angle is measured with respect to the y-axis. Consequently, twist angles must be transformed into the initial reference system using Equation 4.48.

$$\theta(y) = \bar{\theta}(\bar{y}) \cos \Lambda_{EC} - \frac{\partial z}{\partial \bar{y}} \sin \Lambda_{EC} \tag{4.48}$$

Author contribution

The SU2 mesh morphing, CFD solver, and sensitivity computation methodologies, along with the MSC Nastran FEM solver and sensitivity analysis methodology, were collaboratively developed with the Aerodynamics and Flight Mechanics Department of the University of Southampton. The author of this thesis gained international research experience as a visiting research student, contributing to the development, validation, and integration of these tools in a multidisciplinary environment. The main goal was to develop an adjoint-driven aero-structural optimization workflow using macro parameters for an innovative forward-swept horizontal tailplane, employing an IDF architecture approach, as part of the IMPACT Clean Sky 2 European Project. The Ice Effect tool was developed by the Austrian Institute of Technology in collaboration with ANSYS. The author utilized the described methodology to develop a Response Surface Model (RSM) within the framework of the IMPACT Clean Sky 2 European Project.
In this chapter, the author independently developed and implemented all methodologies, as reported, in collaboration with the DAF research group at the University of Naples Federico II, where the author was a member of the research group.

List of related publications

Conference papers

- C. Conti , **M. Mandorino**, A. Da Ronch and A. Elham. High-fidelity Aero-Structural Optimisation using Individual Discipline Feasible Strategy. In *2023 AIAA Aviation and Aeronautics Forum and Exposition*, 12-16 June 2023, San Diego, California. DOI: https://doi.org/10.2514/6.2023-3317.

  In this paper, an IDF technique is proposed to solve an adjoint-driven high-fidelity aero-structural optimization problem using a monolithic approach. The formulated IDF problem is presented. Additionally, the methodology developed to calculate the gradients of the objective functions and constraints with respect to structural and geometrical macroparameters is outlined.

5

Application: Advanced Rear End Design on Large Passenger Jet Aircraft

Contents

5.1 Case Study

The innovative concept involves the implementation of a Forward-Swept Horizontal Tailplane (FSHTP) attached to the rear of the fuselage in a way that eliminates the need for a structural opening at the back of the aircraft (also known as cut-out), as illustrated in Figure 5.1 [222]. The main advantage of the proposed horizontal stabilizer configuration, compared to the traditional design, is the potential to eliminate the structural opening in the fuselage. This opening is typically located in a highly stressed area due to the forces exerted by both the vertical and horizontal stabilizers. As a result, the structural weight of the fuselage is reduced by eliminating the need for reinforcements associated with the opening. Simultaneously, the rigidity of the fuselage is enhanced in the area where the horizontal stabilizer is installed, leading to improved effectiveness of the stabilizer in reducing tailcone deformations caused by aerodynamic loads. This configuration enhances the fuel efficiency of the aircraft, primarily due to the reduction in structural weight. Furthermore, a forward-swept tail exhibits improved aerostructural characteristics compared to conventional configurations, where structural deformation tends to reduce the generated lift of the lifting surface. Assuming the aerodynamic center position of a conventional aircraft's horizontal tailplane remains unchanged with reference to a forward sweep configuration, the necessary stabilizing performance of the tail could be achieved with a reduced tail surface, thanks to the aforementioned improvement in lifting characteristics. These factors would result in further weight reduction and reduced aerodynamic drag.

The innovative design must meet the certification requirements specified in the Certification Specifications and Acceptable Means of Compliance for Large Aeroplanes CS-25 [223]. Section 25.143(a) and (b) stipulate that:

CS-25.143 a): *The aeroplane must be safely controllable and manoeuvrable during: take-off, climb, level flight, descent, approach and go-around, approach and landing.*

CS-25.143 b): *It must be possible to make a smooth transition from one flight condition to any other flight condition without exceptional piloting skill and without danger of exceeding the aeroplane limit-load factor under any probable operating conditions.*

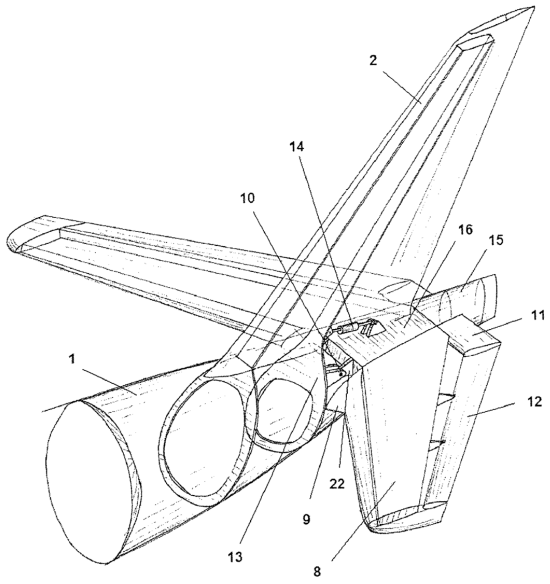

Figure 5.1: Concept of forward–swept tail plane configuration [222].

For this reason, it is crucial to ensure a high level of lift capability for the tailplane, especially in the most critical conditions where tailplane stall is likely. To improve the lift capabilities of the tailplane, the FSHTP should be equipped with a LEX. This device is designed to further reduce the size of the horizontal stabilizer by enhancing the non-linear characteristics of the stabilizer surface while keeping the linear characteristics constant. The LEX is designed to create vortices at high angles of attack (both positive and negative) that interact with the airflow around the tail surfaces, thus inhibiting the spread of flow separation from the outer part to the inner part of the horizontal tail surface. This ensures that the linear aerodynamic characteristics remain unchanged, while the lift achievable in the non-linear zone is significantly increased by such a device.

Additionally, CS-25 Section 25.143 (c), (i), and (j) require that:

CS-25.143 c): *The aeroplane must be shown to be safely controllable and maneuverable with the critical ice accretion appropriate to the phase of flight defined in appendix C and O: 1) At the minimum V_2 for take-off; 2) During an approach and go-around; 3) During an approach and landing.*

CS-25.143 i): *When demonstrating compliance with CS-25.143 in icing condition, controllability must be demonstrated with the most critical of the ice accretion(s) for the particular phase of flight as defined in appendix C and O.*

CS-25.143 j): *For flight in icing condition before the ice protection system has been activated and is performing its intended function, it must be demonstrated in*

flight with the most critical of the ice accretion(s) defined in Appendix C part II(e) and Appendix O part II(d) that the airplane is controllable in a pull-up maneuver up to 1.5g load factor.

Appendix C to part 25 - part II(e): *The ice accretion before the ice protection system has been activated and is performing its intended function is the critical ice accretion formed on the unprotected and normally protected surface before activation and effective operation of the ice protection system in continuous maximum atmospheric icing condition.*

For these reasons, the most critical icing accretion conditions must be evaluated according to CS-25 Appendix C. Controllability and maneuverability in icing conditions must be ensured by minimizing the aerodynamic penalty introduced by ice accretion. To achieve this, the rear end of the fuselage has a distinctive shape, creating significant aerodynamic restrictions in the area of the horizontal tailplane. This specific fuselage shape reduces the effective flow sweep angle in comparison to a tailplane with a positive sweep angle. The adoption of a bottleneck shape for the rear end of the fuselage may help reduce the tail area affected by ice accretion. The curvature resulting from the fuselage's bottle-neck shape can cast a shadow over the inner sections of the tailplane, reducing the efficiency of ice collection or catch rate. The tapering of the fuselage's rear end creates a local region near its surface that is mostly free of droplets. The LEX is positioned within the shadow zone of this droplet to provide passive ice protection.

In this proposed scenario, where weight reduction is primarily achieved by eliminating the fuselage structural opening, the FSHTP must be designed to at least match the aerodynamic drag generated by a conventional tailplane solution. Additionally, it is crucial to ensure proper stalling behavior with a high level of maximum lift achievable and to minimize the aerodynamic penalty caused by ice accretion. To evaluate the potential benefits of the FSHTP in terms of weight, flexibility, and aerodynamics, a reference geometry was chosen for assessment. The key geometric parameters of this configuration represent an aircraft similar to the Airbus A320neo, which was provided by Airbus as part of the European project IMPACT [1], are summarized in Table 5.1. Figure 5.2 illustrates a comparison between the conventional tail arrangement and the advanced rear-end, with a forward-swept horizontal empennage. Additionally, Table 5.2 presents information about the wing-fuselage configuration to which the tailplane must be integrated. Finally, Table 5.3 presents the high-speed and low-speed flow conditions during the analysis of the

[1]IMPACT, Impact EU project website: `https://www.impact-cleansky-project.eu/` [retrieved March 11, 2024]

tailplane, which led to the following results. Following the procedure described in Section 4.1.4, it was possible to accurately determine the size of the reference conventional tailplane structure based on the specific load scenario derived from the representative maneuvering envelope for the primary structure. Tables 5.4 and 5.5 present the data for the materials used and the wing box characteristics, respectively.

Table 5.1: Geometric data for the reference conventional configurations.

Symbol	Value	Unit	Description
b	12.45	m	Tail Span
c_r	3.74	m	Root Chord
c_t	1.36	m	Tip Chord
Λ_{le}	32.30	deg	Sweep Angle at l.e.
Γ	6.00	deg	Dihedral Angle
λ	0.331		Taper Ratio
S_h	30.99	m^2	Tail Surface
AR_h	5.00		Aspect Ratio

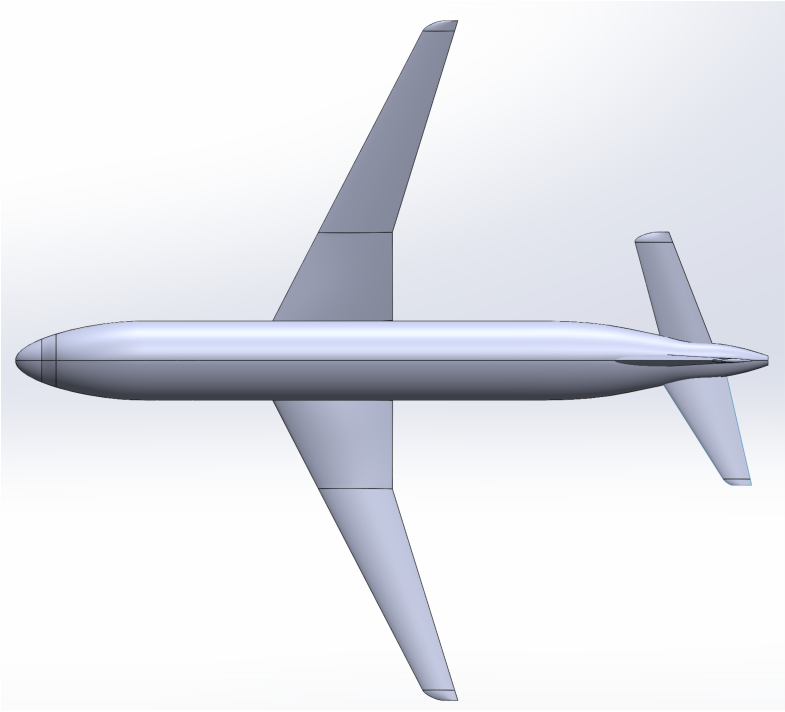

Figure 5.2: A320neo like reference aircraft: conventional tailplane versus the forward-swept arrangement.

Table 5.2: Reference Aircraft Characteristic.

Symbol	Value	Unit	Description
S_w	125.0	m^2	Wing Surface
c_{mac}	4.29	m	Wing m.a.c.
l_h	17.19	m	Wing-Tailplane a.c Distance
$C_{L_{max_{WB}}}$	1.337		WB Maximum Lift Coefficient
$\overline{x}_{ac_w}$	0.25		Position of the Wing a.c.
W_{MTO}	724.9	kN	Maximum Take Off Weight
$\overline{x}_{CG_f}$	0.17		Maximum Fwd Position of CG (% of wing C_{mac})
$\overline{x}_{CG_b}$	0.37		Maximum Bwd Position of CG (% of wing C_{mac})

Table 5.3: Flight conditions for aerodynamic and aeroelastic analysis.

	Altitude	Mach Number
High Speed-Condition	11000 m	0.78
Low Speed-Condition	Sea Level	0.2

Table 5.4: Characteristics of the material.

Symbol	Value	Unit	Description
ρ	1500	Kg/m^3	Density
s_y	200	MPa	Yielding stress
E	84	GPa	Young modulus
G	14.5	GPa	Shear modulus
ν	0.35		Poisson modulus
S_M	2.0	kN	Safety margin

Table 5.5: Characteristics of the wing box.

Symbol	Value	Unit	Description
h_1	0.14		Height of first spar (chord percentage)
h_2	0.08		Height of second spar (chord percentage)
α_b	0.70		Percentage of absorption contribution of first spar
c_{box}	0.45		Wing box length (chord percentage)
t_{rib}	2.00	mm	Rib thickness
Δ_{rib}	0.5	m	Rib spacing
x_{ac}	25%		Aerodynamic centre position (chord percentage)
x_{cg}	35 %		Centre of gravity position (chord percentage)
x_{ec}	40%		Elastic centre position (chord percentage)

5.2 Systems Engineering Product Development process: From Stakeholders' Needs and System's Requirements to MDAO workflow formulation

As mentioned in Chapter 3, the MBSE development system aims to assist designers in developing complex systems through a dedicated framework. The objective of this section is to provide an example of applying the MBSE development system for the initial design of the advanced rear-end concept introduced in Section 5.1. Following the systems engineering approach, the requirements are derived from the needs addressed by various system stakeholders. The scenario clarifies the definition of needs by describing the interactions between the product and the stakeholders in a specific situation. Another purpose of the scenario is to illustrate how the needs are validated and which stakeholders are involved in the validation process. Subsequently, a single architectural model representing different systems under analysis is generated to describe how each system's components fulfill the requirements. The system to be analyzed is constructed through a decision-making process facilitated by the generated architecture, enabling the designer to select the desired components to fulfill all the specific functions generated. In conclusion, the systems are designed and analyzed using multiple MDAO workflows, which include only the disciplines relevant to the requirements involved. After completing these steps, methods for verifying requirements, and validate the final solutions and the whole process can be carried out to select the best solution and confirm that the previously defined requirements are met.

5.2.1 Stakeholders and Needs Definition

The first phase of the Systems Engineering Product Development process involves collecting the requirements of the stakeholders involved in the design process. The stakeholders and their requirements for the Advanced Rear End Design Concept have been modeled in the OCE through the user interface implemented in KE-chain, as shown in Figure 5.3.

As it can be observed, ten different stakeholders who can interact with the Advanced Rear End Concept and its components have been identified.

- OEM: Collects needs from all stakeholders to design the advanced rear end accordingly. Takes into account new government regulations, airline schedules, economic requirements, and equipment availability. Determine the best design strategy solution based on this information.

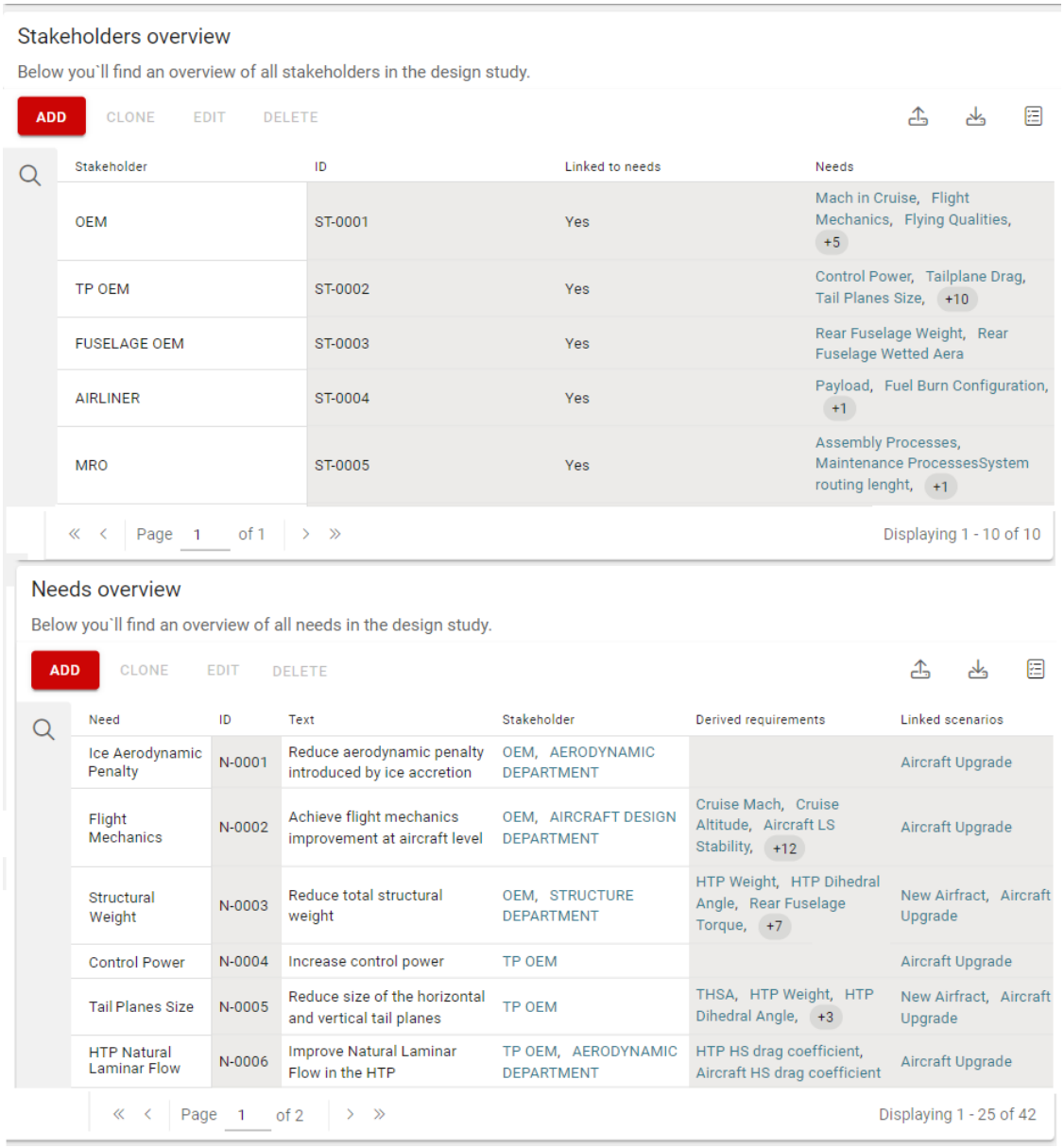

Stakeholders overview

Below you'll find an overview of all stakeholders in the design study.

ADD CLONE EDIT DELETE

Stakeholder	ID	Linked to needs	Needs
OEM	ST-0001	Yes	Mach in Cruise, Flight Mechanics, Flying Qualities, +5
TP OEM	ST-0002	Yes	Control Power, Tailplane Drag, Tail Planes Size, +10
FUSELAGE OEM	ST-0003	Yes	Rear Fuselage Weight, Rear Fuselage Wetted Aera
AIRLINER	ST-0004	Yes	Payload, Fuel Burn Configuration, +1
MRO	ST-0005	Yes	Assembly Processes, Maintenance ProcessesSystem routing lenght, +1

Page 1 of 1 Displaying 1 - 10 of 10

Needs overview

Below you'll find an overview of all needs in the design study.

ADD CLONE EDIT DELETE

Need	ID	Text	Stakeholder	Derived requirements	Linked scenarios
Ice Aerodynamic Penalty	N-0001	Reduce aerodynamic penalty introduced by ice accretion	OEM, AERODYNAMIC DEPARTMENT		Aircraft Upgrade
Flight Mechanics	N-0002	Achieve flight mechanics improvement at aircraft level	OEM, AIRCRAFT DESIGN DEPARTMENT	Cruise Mach, Cruise Altitude, Aircraft LS Stability, +12	Aircraft Upgrade
Structural Weight	N-0003	Reduce total structural weight	OEM, STRUCTURE DEPARTMENT	HTP Weight, HTP Dihedral Angle, Rear Fuselage Torque, +7	New Airfract, Aircraft Upgrade
Control Power	N-0004	Increase control power	TP OEM		Aircraft Upgrade
Tail Planes Size	N-0005	Reduce size of the horizontal and vertical tail planes	TP OEM	THSA, HTP Weight, HTP Dihedral Angle, +3	New Airfract, Aircraft Upgrade
HTP Natural Laminar Flow	N-0006	Improve Natural Laminar Flow in the HTP	TP OEM, AERODYNAMIC DEPARTMENT	HTP HS drag coefficient, Aircraft HS drag coefficient	Aircraft Upgrade

Page 1 of 2 Displaying 1 - 25 of 42

Figure 5.3: Stakeholder and Need's definition implemented in the OCE through KE-Chain. Poor image quality due to acquisition from OCE.

- Tailplane OEM: Involved as a first-level supplier or higher for tailplane manufacturing. Collects overall aircraft OEM requirements and strives to accomplish all tasks with innovative products.
- Fuselage OEM: Similar to the Tailplane OEM, it could be engaged as a first-level supplier (or more) for fuselage manufacturing. Collects overall aircraft OEM requirements with the aim of delivering a functional product.
- Airliners: Directly operate aircraft to maximize profit, ensure passenger comfort, and comply with regulations. Specify the fleet on which operations

are applied and pay for the final product.

- MRO: After aircraft production, MRO must be considered to avoid subsequent issues. Their needs influence design solution choices, impacting aircraft and OEM activities.
- Certification Authority: Aircraft design involves certification authorities at various levels. Their guidelines influence aircraft design and the subsequent testing activities.
- Passengers: As the ultimate users of the aircraft, passengers are concerned with comfort and emissions. They also consider ticket price adjustments made by airlines.
- Aircraft Design Department: Drives the Advanced Rear End design, taking into account manufacturing, certification, maintenance, and economic requirements from all stakeholders involved. This department is responsible for making key configuration decisions to produce the final product.
- Aerodynamic Department: Influences the Advanced Rear End design based on performance and certification needs. Introducing new potential solutions and configurations to meet these needs.
- Structural Department: Influences the Advanced Rear End design based on structural, weight, and certification needs. Introducing new potential solutions and configurations to meet these requirements.

Each stakeholder has multiple needs, which are identified and added to KE-chain. The model syntax correctness is verified using the OCE features, as illustrated in Figure 5.3. This process resulted in the identification of 42 distinct needs, each associated with one or multiple specific stakeholders. The modelling of these needs automatically produces a summary of the needs for each stakeholder, presented in the fourth column of the needs overview table in the figure. KE-chain also conducts an automatic check to ensure that each stakeholder is connected to at least one need, as indicated in the third column of the figure, confirming that all stakeholders have linked needs. In Figure 5.3, only a partial representation of the needs considered in the process is depicted. For greater clarity, Table 5.6 presents all the needs introduced in the OCE and their connection to the respective stakeholders.

As already explained in Section 3.1.2, stakeholders and their needs can be transformed into models using the OCE. The OCE also provides the capability to define parent stakeholders, enabling users to establish hierarchical structures as needed. Once all stakeholders, including their needs, descriptions, and hierarchy, are defined and validated within the KE-Chain framework, the entire model containing this comprehensive information can be exported as a Papyrus MBSE model. This facilitates easy visualization and management of the information. The stakeholder

Table 5.6: Stakeholders and Need's defined in the OCE.

Stakeholder	Needs
OEM	Improve aircraft's flight and performance characteristics Ensure good flying qualities (stability, handling and balance) in all flying conditions The aircraft must remain stable whatever in all flying conditions The aircraft must be able to provide the pitch necessary for carrying out the desired manoeuvres
TP OEM	Increase control power Reduce size of the horizontal and vertical tail planes Improve the efficiency of the empennage Guarantee a good aeroelastic efficiency Increase of HTP rigid lift slope Improve the non-linear characteristics of the stabiliser surface while keeping the linear characteristics constants Prevent the propagation of flow separation towards the inner part of the stabiliser Reduce the weight of the horizontal stabilizer
FUSELAGE OEM	Reduce weight of the rear fuselage Reduce the wetted area of the rear fuselage
AIRLINER	Reduce the fuel burn Ensure enough Payload Obtain a compact configuration Achieve performance improvement at aircraft level Guarantee high Mach number during cruise
MRO	Reduce length of systems routings Simplify assembly processes Simplify maintenance processes
CERTIFICATION AUTHORITY	Ensure a safety level of Stability and Control Ensure a good stall behaviour Ensure enough space for fire compartment Ensure protection from bird strike Reach favourable aeroelastic behaviour for stability The airplane must be safely controllable and manoeuvrable in all flying conditions The airplane must be safely controllable with critical ice accretion The airplane is controllable in a pull-up manoeuvre
PASSENGERS	Affordable ticket price Would like to pay for a "green" flight
AERODYNAMIC DEPARTMENT	Improve Natural Laminar Flow in the HTP Increase HTP maximum negative lift coefficient Reduce aerodynamic penalty introduced by ice accretion Reduce the tailplane drag
AIRCRAFT DESIGN DEPARTMENT	Achieve flight mechanics improvement at aircraft level Guarantee the desired attitude of the aircraft (in terms of balance) in all flying conditions with a forward centre of gravity Guarantee the desired attitude of the aircraft (in terms of balance) in all flying conditions with an aft centre of gravity
STRUCTURE DEPARTMENT	Reduce total structural weight Reduce number of structural parts

hierarchy, modeled in SysML and visualized in Papyrus, is depicted in Figure 5.4. Notably, in this particular use case, there are no hierarchical relationships among the stakeholders, which results in their presentation on the same level beneath the overarching "Stakeholder" element. A further example of MBSE visualization is illustrated in Figure 5.5, which displays all the needs associated with the stakeholder "Tailplane OEM" are displayed. Indeed, Papyrus enables the filtering and visualization of specific user-selected information. In this instance, details about the title, text, ID number, and relevant stakeholders are provided.

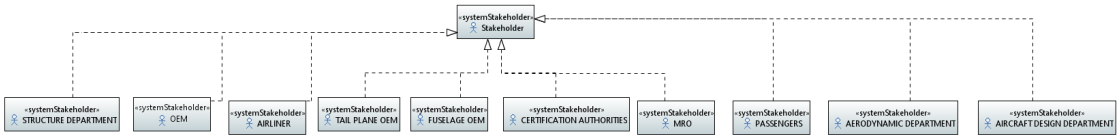

Figure 5.4: Stakeholder's hierarchy model visualized in Papyrus software.

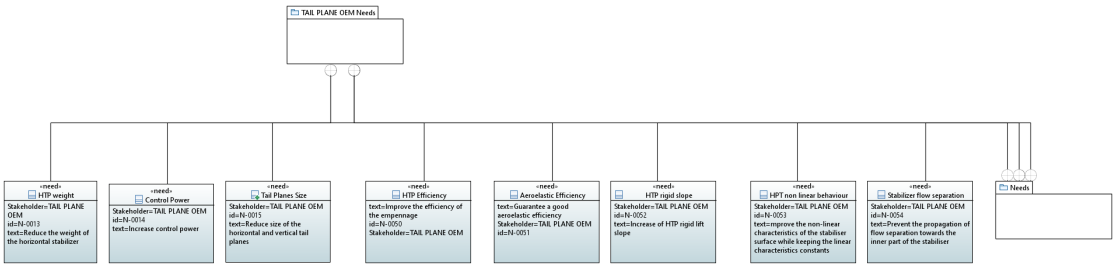

Figure 5.5: HTP OEM needs model visualized in Papyrus software.

5.2.2 Scenario Definition

To gain a better understanding of the context in which stakeholders and their needs are situated, it is essential to model the scenario in which the system of interest operates or is designed. Among the various scenarios that can be modeled for this use case, two distinct design activities have been considered. The first scenario has been created to simulate aircraft upgrade activities, which include replacing the horizontal empennage of a large commercial passenger jet with an advanced rear-end configuration. The second scenario involves representing the entire process of designing, manufacturing, certifying, and operating a new aircraft with an advanced rear-end configuration. In the Systems Engineering Product Development process described in this section, the latter scenario has been taken into consideration. Since the scenario represents the entire process of developing a new aircraft, it includes all the stakeholders as defined in Section 5.2.1. Furthermore, new systems such as the

HTP, the fuselage, and the entire aircraft are encompassed. The various activities included in this scenario are also added to the KE-Chain, as depicted in Figure 5.6.

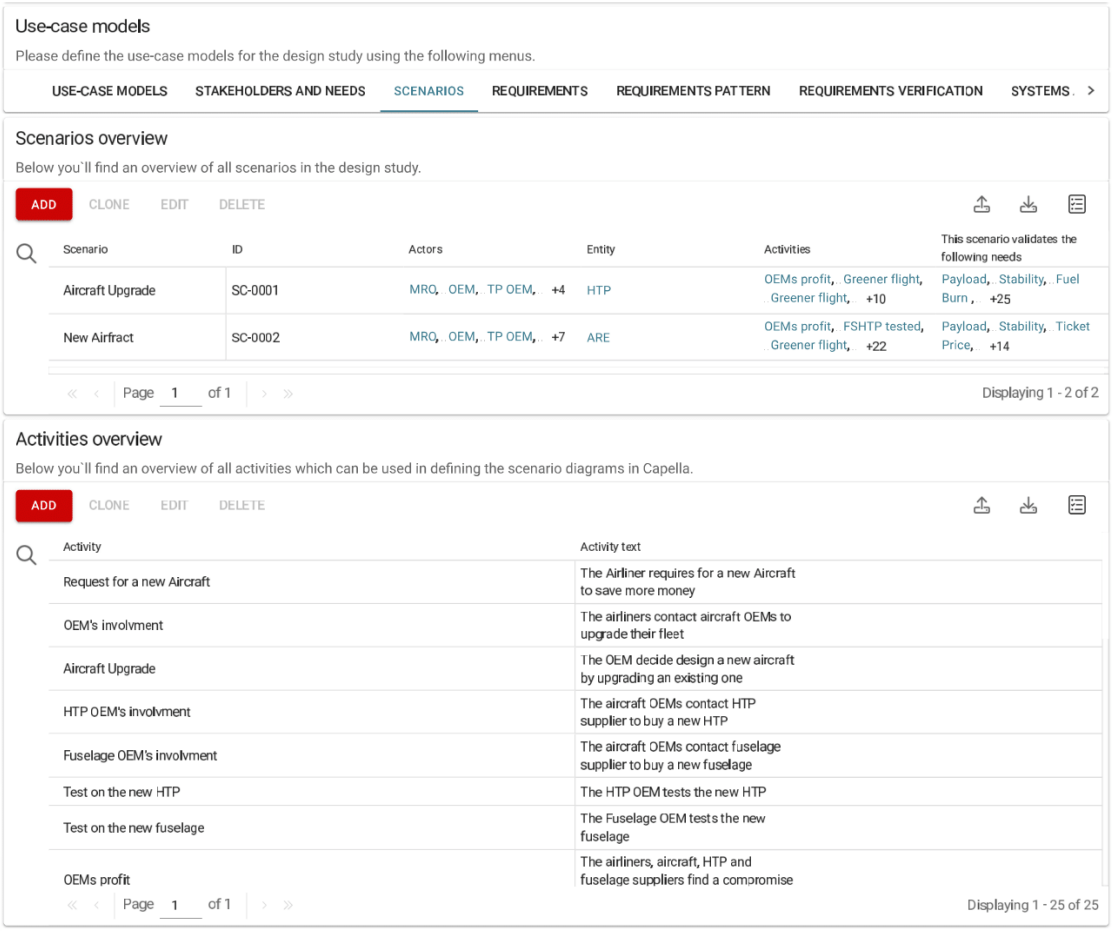

Figure 5.6: Overview of the Scenario and Activities defined in KE-Chain. Poor image quality due to acquisition from OCE.

Each activity corresponds to a step that must be performed in the scenario. Several activities combined form the complete scenario, as indicated in the fifth column of the scenario overview table, where multiple activities are associated with the scenario. In addition to the activities, the scenario is also associated with several needs, as indicated in the sixth column of the table. The second and third columns indicate the actors (i.e., the stakeholders) and the entity (i.e., the system considered in the scenario) defined in the OCE and included in the scenario. In Figure 5.6, both defined scenarios are visible, generated from a combination of various activities outlined in the activities overview table. Once all the items are defined and allocated within the OCE, KE-Chain automatically generates a preliminary version of the MBSE model that can be imported into Capella software. Capella is used to define various diagrams. First, an Operational Activity Diagram must be generated. In this

diagram, all the activities included in the scenario must be inserted and connected to each other through interactions, indicating the exchanges between operational activities. Following that, an Operational Architecture Diagram must be generated. This diagram allows for the linking of activities to specific entities or actors, providing a comprehensive overview of all interactions between stakeholders and the system through the execution of actions. In conclusion, the Operational Entities Scenario (OES) can be developed. The OES describes the behavior of entities and/or operational activities. OES are commonly represented as sequence diagrams, with the vertical axis representing time. Operational entities and actors are depicted with vertical lines to illustrate the chronological sequence of operational activities assigned to them. For this reason, this diagram is also referred to as a sequence diagram. The Operational Architecture Diagram and Operational Entities Scenario generated for the current use case are represented respectively in Figures 5.7 and 5.8. These two diagrams provide a comprehensive representation of the advanced rear-end aircraft generation process. They are useful for understanding the interconnections between stakeholders and their activities during the design, production, and certification phases. Additionally, they offer feedback from industrial partners to verify if the process has been correctly modeled in the MBSE framework.

As previously indicated, the systems considered in the scenario include the entire aircraft and two of its components: the horizontal tailplane and fuselage. The stakeholders involved are those previously defined. Actions are depicted by yellow boxes along the timeline, while interactions representing data exchanged among stakeholders are illustrated by arrows in the model. The scenario begins with the airline requesting a new aircraft. Airliners will request a solution from the aircraft OEM to enhance performance, and they will choose to engage in a new design activity to introduce innovative solutions in the new system, aiming to reduce fuel consumption and air emissions. This request involves the task of reducing the aircraft weight compared to the conventional configuration. The aircraft design department will collaborate with the structural department to develop a solution that has a lower structural weight. Weight reduction is achieved by eliminating the fuselage cutout, which is accomplished by shifting the horizontal tailplane backward. To fulfill this request, an innovative HTP with a negative sweep must be designed. As a result, the tailplane OEM is involved in the manufacturing and testing of the innovative configuration. The certification process, which involves certification authorities, will require acceptable stalling behavior that can be compromised by the introduction of negative sweep. For this reason, the aerodynamics department will introduce a LEX device in the HTP system, which will be installed on the new tailplane. The innovative tailplane will undergo testing and certification. A

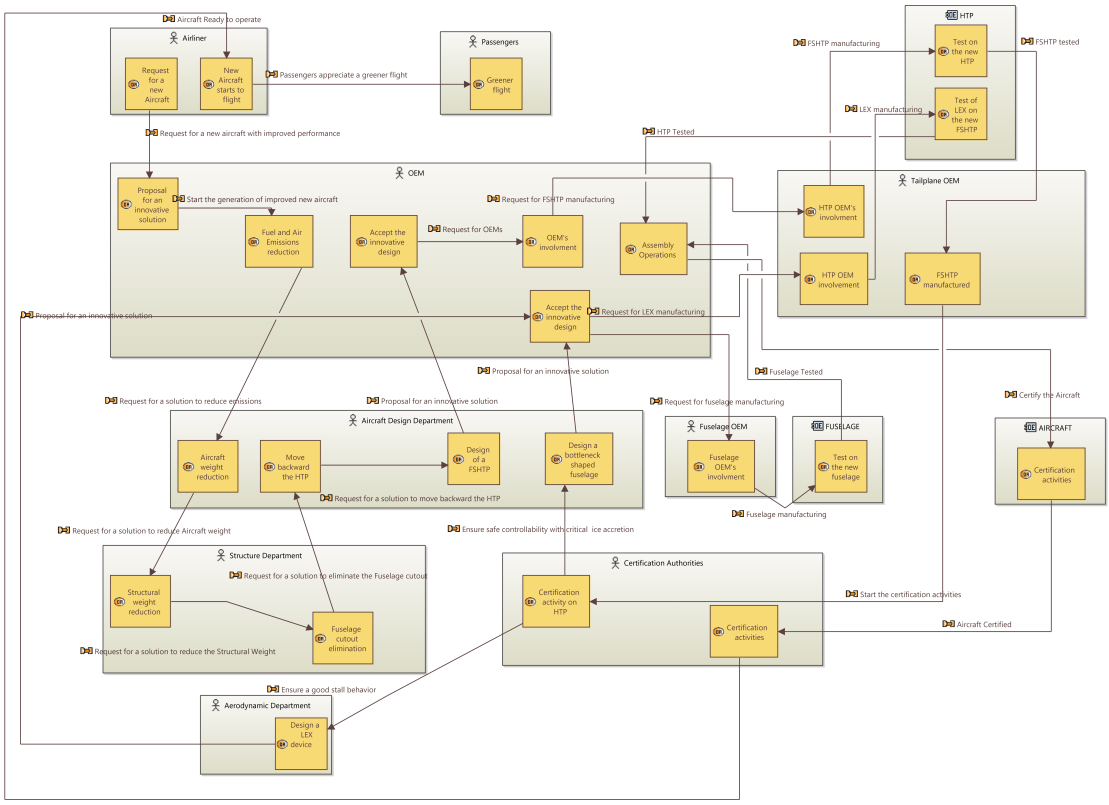

Figure 5.7: Operational Architecture Diagram representing the advanced rear end design activity generated in KE-Chain.

similar process is followed by the fuselage OEM. An innovative fuselage design is needed to ensure safe controllability in critical ice accretion situations. The innovative equipment (HTP and fuselage) will be acquired from the OEM, who will develop and test their products before selling them to the aircraft OEM. Once the availability and features of the innovative equipment are confirmed, the aircraft OEM will definitively commence the assembly process. A certification phase is then necessary, which involves certification authorities. After completing tests on the entire aircraft and obtaining the type certificate from the authorities, airlines will be able to offer their passengers a more environmentally friendly and comfortable flight, with a potential adjustment to the ticket price, another fundamental aspect perceived by passengers. The presented scenario can be used to validate the applicability and consistency of several requirements. Indeed, it allows the designer to have an overview of all the activities executed by stakeholders, from which the requirements are validated. For example, requirements related to achieving flight and improving performance at the aircraft level, reducing total structural weight, ensuring good stall behavior, minimizing aerodynamic and controllability penalties in the event of critical ice accretion, and lowering ticket prices are all predefined needs

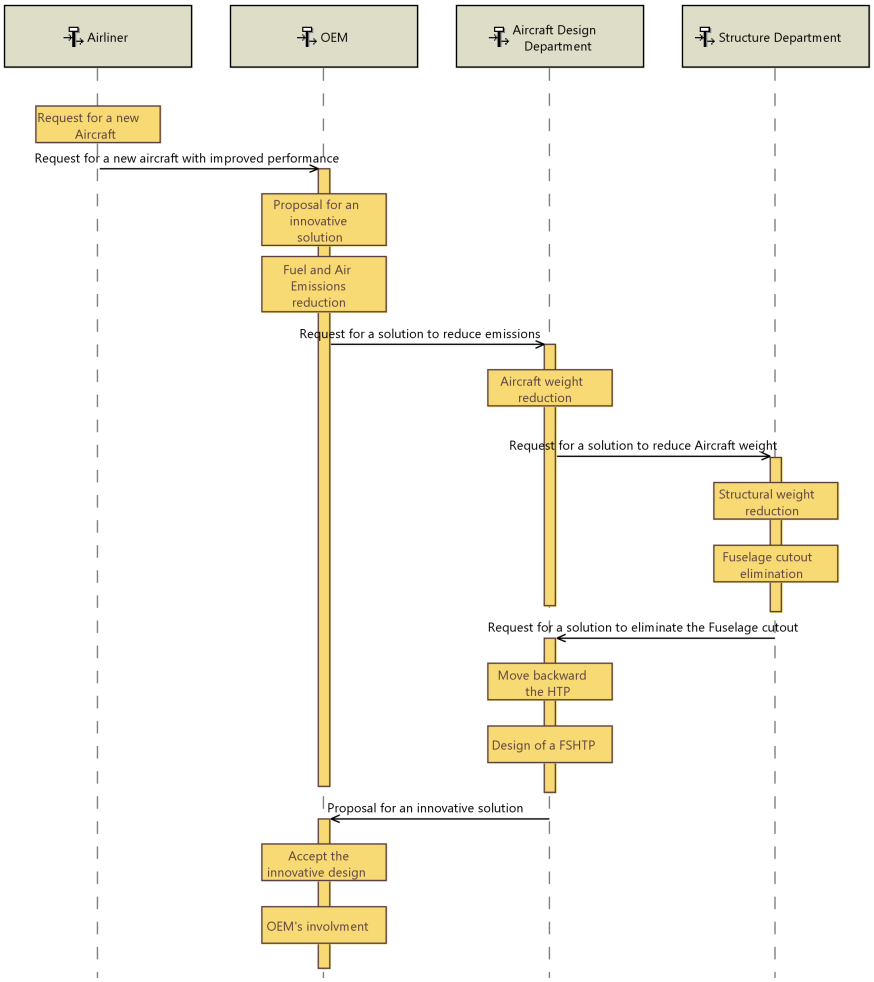

(a) Operational Entities Scenario part 1.

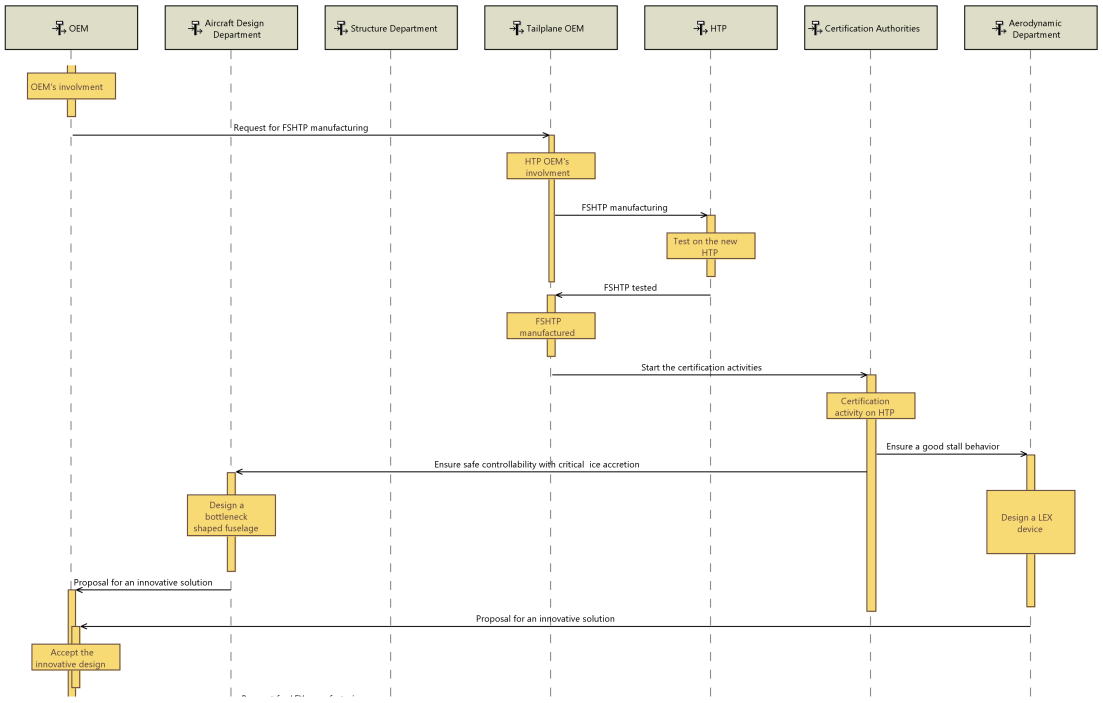

(b) Operational Entities Scenario part 2.

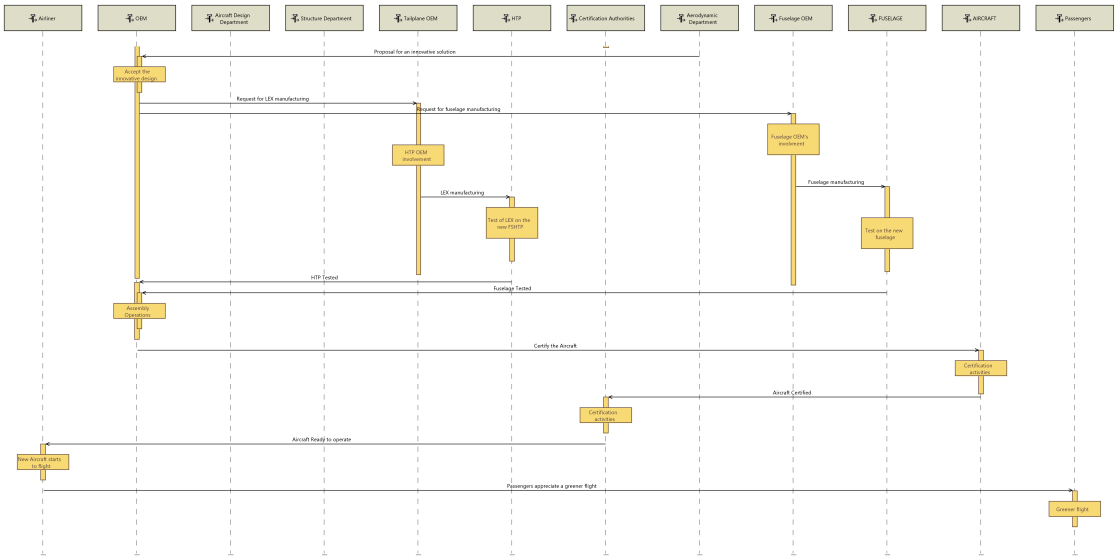

(c) Operational Entities Scenario part 3.

Figure 5.8: Operational Entities Scenario representing the advanced rear-end design activity generated in KE-Chain. The diagram has been split into multiple parts to allow for better visualization.

connected to the OEMs, Airlines, certification authorities, passengers, structural, and aerodynamic departments. The process for meeting these needs is depicted in the scenario diagram shown in Figure 5.8.

5.2.3 Requirements Definition

Requirements are a transformation of stakeholder needs to make them unambiguous and consistent. Each requirement is directly derived from a need or from a parent requirement, enabling traceability. Requirements consist of attributes and a statement of requirements. As explained in Section 3.1.2, the statement has a type (e.g., functional, performance, etc.), a pattern, and is subject to specific rules. The pattern and rules ensure completeness, consistency, unambiguity, and automatic verification. The requirements are derived from the needs and contain the same information, but they adhere to strict syntax rules that compel them to clarify and better define the information contained in the parent need. In this manner, needs are transformed into requirements according to specific rules and patterns. The shift from needs to requirements eliminates any ambiguity in interpretation. From each requirement, it is then possible to derive additional ones. Forty-five requirements have been formulated for the current use case, following the previously described rules. For greater clarity, Table 5.7 lists all the requirements introduced in the OCE, along with their type. Most of the quantities in the requirement text

are referenced to the values achieved for the conventional HTP. These values have been subsequently translated into quantities when the requirements were inserted into the KE-chain environment, as depicted in Figure 5.9. The table provides the ID, description text, and type for each requirement. Each requirement is derived from one or more needs or a parent requirement, as depicted in the sixth and seventh columns of the requirements overview table.

Table 5.7: Requirements defined in the OCE together with their type.

Requirement Description	Type
The Aircraft shall ensure safe level of stability for condition: pushover maneuver The Aircraft shall have a payload capacity which allows for the transportation of passengers for condition: typical mission The HTP shall be protected by bird strike for condition: low altitude flight phases The Aircraft shall shall have acceptable level of recurring cost to generate profit for condition: typical mission The ARE shall decrease its lead time with respect to reference Aircraft for condition: operative life The Fuselage shall notpossess a cutout The Fuselage shall keep space for fire compartment in section 19 The Fuselage shall include presence of THSA The Aircraft shall comply CS-25 regulations The ARE shall possess HPT pivots points in closed fixed fuselage section The ARE shall avoid presence of ice for condition: cruise condition	Functional Requirement
The HTP shall achieve at least reference HTP negative stall angle of attack for condition: pushover maneuver The HTP shall achieve at least reference HTP maximum negative lift coefficient for condition: pushover maneuver The HTP shall achieve at least reference HTP lift coefficient derivative for condition: pushover maneuver The HTP shall achieve at least reference HTP moment coefficient derivative for condition: pushover maneuver The HTP shall achieve at least reference HTP lift coefficient for condition: pushover maneuver The Aircraft shall match at least reference Aircraft drag coefficient for condition: cruise condition The HTP shall match at least reference HTP drag coefficient for condition: cruise condition The HTP shall match at least reference HTP lift coefficient derivative for condition: cruise condition The Aircraft shall match at least reference Aircraft moment coefficient derivative for condition: cruise condition The HTP shall match at least reference HTP moment coefficient derivative for condition: cruise condition The Aircraft shall have at least reference Aircraft lift curve slope for condition: cruise condition The HTP shall increase the rigid lift slope by 7% of the reference HTP for condition: pushover maneuver The Aircraft shall increase by the flexible pitching moment derivative by 7 % for condition: pushover maneuver The Aircraft shall reduce fuel consumption by 2 % with respect to reference aircraft for condition: typical mission The Aircraft shall increase the aerodynamic efficiency by 2 % with respect to reference aircraft for condition: cruise condition The Aircraft shall increase the aerodynamic effectiveness by 2 % with respect to reference aircraft for condition: cruise condition The ARE shall increase its elastic efficiency by 2 % with respect to reference aircraft for condition: pushover maneuver The Aircraft shall fly at MLR equal to 0.78 Mach for condition: cruise condition The Aircraft shall fly at MLR equal to 0.2 Mach for condition: pushover maneuver The HTP shall not exceed a reduction of CL max due to ice equal to 0.2 for condition: pushover maneuver The HTP shall achieve at least reference HTP flexible pitching moment derivative for condition: pushover maneuver The HTP shall achieve at least reference HTP flexible pitching moment derivative for condition: cruise condition The HTP shall achieve at least reference HTP flexible lift derivative for condition: pushover maneuver The HTP shall achieve at least reference HTP flexible lift derivative for condition: cruise condition The HTP shall achieve at least reference HTP flexible maximum negative lift coefficient for condition: pushover maneuver The ARE shall increase its elastic efficiency by 5% with respect to reference Aircraft for condition: cruise condition The Aircraft shall fly at flight level equal to 39000 ft for condition: cruise condition The Aircraft shall fly at flight level equal to 0 ft for condition: pushover maneuver	Performance Requirement
The Fuselage shall withstand at least reference Aircraft rear fuselage torque for condition: pushover maneuver The HTP shall withstand at least reference Aircraft HTP and VTP loads for condition: pushover maneuver The HTP shall withstand at least reference Aircraft HTP and VTP loads for condition: CEV maneuver The Aircraft shall have at least reference Aircraft payload for condition: typical mission The HTP shall possess a dihedral angle equal to 0 degree The HTP shall not be placed backwards with respect to reference HTP The HTP shall not exceed reference HTP weight	Design Constraint Requirement

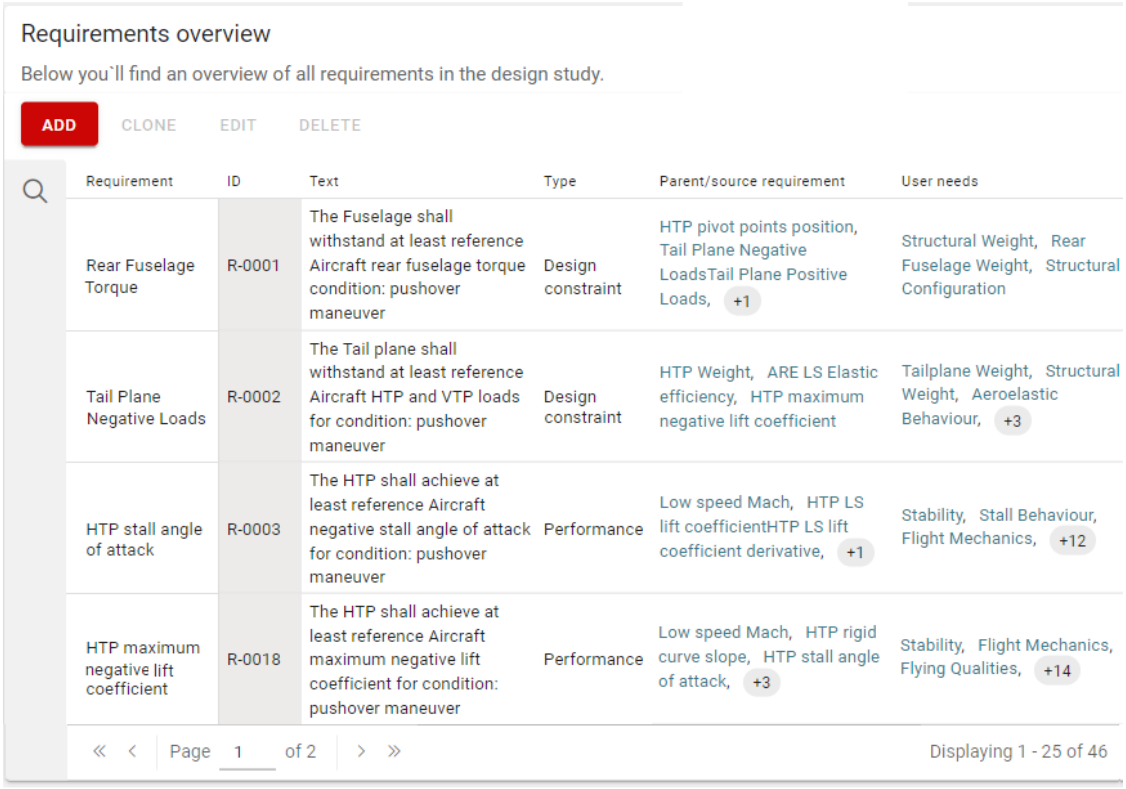

Requirements overview

Below you`ll find an overview of all requirements in the design study.

ADD CLONE EDIT DELETE

Requirement	ID	Text	Type	Parent/source requirement	User needs
Rear Fuselage Torque	R-0001	The Fuselage shall withstand at least reference Aircraft rear fuselage torque condition: pushover maneuver	Design constraint	HTP pivot points position, Tail Plane Negative LoadsTail Plane Positive Loads, +1	Structural Weight, Rear Fuselage Weight, Structural Configuration
Tail Plane Negative Loads	R-0002	The Tail plane shall withstand at least reference Aircraft HTP and VTP loads for condition: pushover maneuver	Design constraint	HTP Weight, ARE LS Elastic efficiency, HTP maximum negative lift coefficient	Tailplane Weight, Structural Weight, Aeroelastic Behaviour, +3
HTP stall angle of attack	R-0003	The HTP shall achieve at least reference Aircraft negative stall angle of attack for condition: pushover maneuver	Performance	Low speed Mach, HTP LS lift coefficientHTP LS lift coefficient derivative, +1	Stability, Stall Behaviour, Flight Mechanics, +12
HTP maximum negative lift coefficient	R-0018	The HTP shall achieve at least reference Aircraft maximum negative lift coefficient for condition: pushover maneuver	Performance	Low speed Mach, HTP rigid curve slope, HTP stall angle of attack, +3	Stability, Flight Mechanics, Flying Qualities, +14

« ‹ Page 1 of 2 › » Displaying 1 - 25 of 46

Figure 5.9: Requirements overview as defined in KE-chain. Poor image quality due to acquisition from OCE.

After the requirements have been inserted into the OCE, they can be exported to Papyrus in the form of SysML diagrams, as previously described for the stakeholders' needs. The framework described enables the automatic generation of the requirements model and its connection with the stakeholders and needs models. The model-based approach described enhances the traceability and consistency of the entire requirement definition process. For instance, the requirements can be easily categorized based on a specific criterion (e.g., the requirement type), and the linkage of the requirement with the parent need and the associated stakeholder can be consistently tracked. An example is shown in Figure 5.10, where an excerpt of the requirements related to the tailplane OEM stakeholders is illustrated. The figure also illustrates how some requirements are derived from others. This overview clearly illustrates the connection between the various requirements.

In KE-Chain, it is possible to fill in the requirement pattern for each requirement. An example of the patterns filled in the KE-chain for certain performance constraint requirements can be seen in Figure 5.11. Each design requirement is associated with a system object, as indicated in the fifth column of the performance requirement table. In this example, all the requirements are linked to the HTP. Each performance

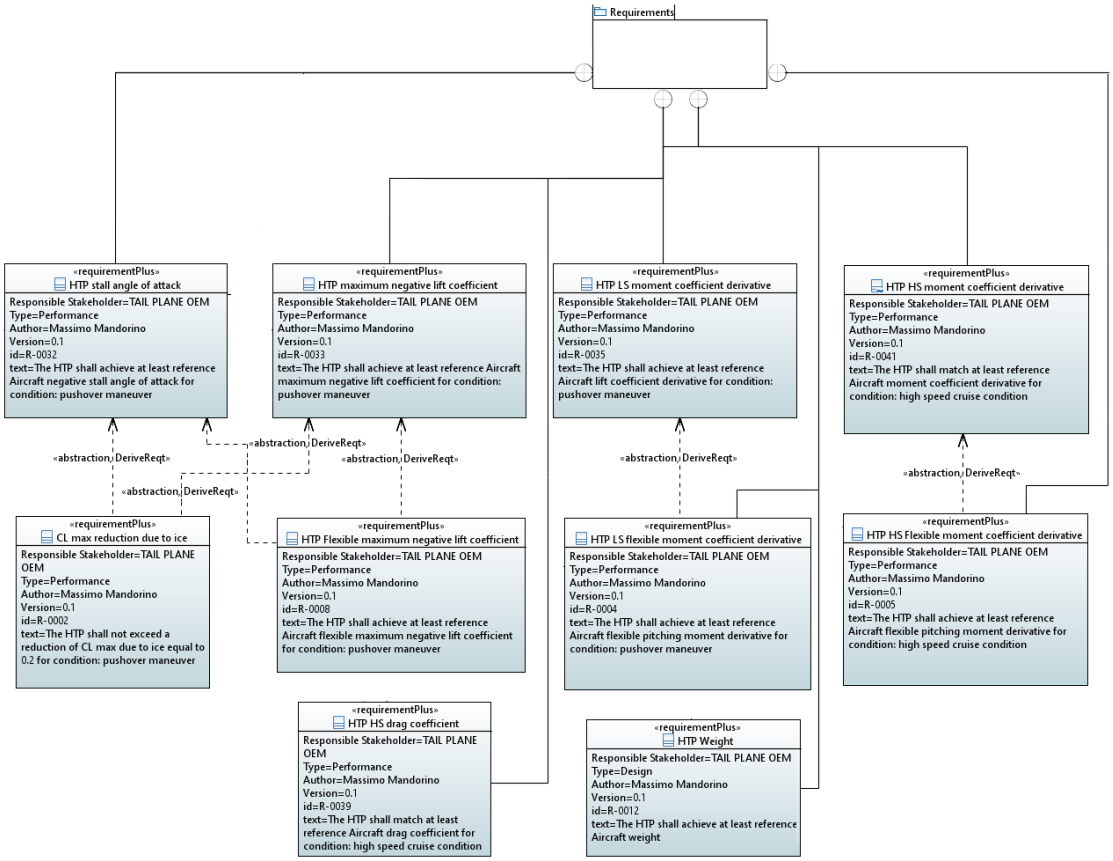

Figure 5.10: Requirements overview as generated in Papyrus. Only a small subset of the requirement related to the tail plane OEM stakeholders are shown.

Performance Requirements

Below you`ll find an overview of performance requirements. Performance requirements: define how well the system needs to perform the functions

EDIT

Requirement	ID	Text	Type	System	Performance parameter	Performance target value	Performance unit of measure	Performance constraint
HTP stall angle of attack	R-0003	The HTP shall achieve at least reference Aircraft negative stall angle of attack for condition: pushover maneuver	Performance	HTP	HTP Stall angle of attack	-10	deg	Maximal or equal
HTP maximum negative lift coefficient	R-0018	The HTP shall achieve at least reference Aircraft maximum negative lift coefficient for condition: pushover maneuver	Performance	HTP	HTP Maximum Negative lift coefficient	-0.15		Maximal or equal
HTP LS lift coefficient derivative	R-0019	The HTP shall achieve at least reference Aircraft lift coefficient derivative for condition: pushover maneuver	Performance	HTP	HTP LS CL derivative	0.0145	1/deg	Minimal or equal

« ‹ Page 1 of 2 › » Displaying 1 - 25 of 29

Figure 5.11: Requirements patterns as generated in KE-chain for some performance constraint requirements. Poor image quality due to acquisition from OCE.

requirement is associated with a parameter, a value, and a unit, as indicated in columns six through nine. In the last column, it is possible to visualize the constraint, which represents the condition the designer wants to avoid. Similar patterns were also created for the other types of requirements (design, functional, environmental, and suitability requirements). Once all the patterns are filled in the KE-chain, they can be imported and visualized in Papyrus.

A summary view that can be generated in Papyrus is the requirements traceability view. This view displays the entire trace from the need, stakeholder, requirement to the consequences. In this case, "consequence" refers to the result of not meeting the requirement. Figure 5.12 displays a segment of a requirements traceability view. It is evident that a single requirement can fulfill multiple needs, but each requirement is linked to at least one need. The requirements traceability view is valuable for understanding the connections between various requirements, needs, and stakeholders, as well as for identifying gaps in the model. The link with the scenario is represented by the needs and stakeholders imported into the presented models. Their characteristics and connections are modeled here based on the information presented in the scenario, which allowed for the definition of stakeholders and related actions that can be converted into needs.

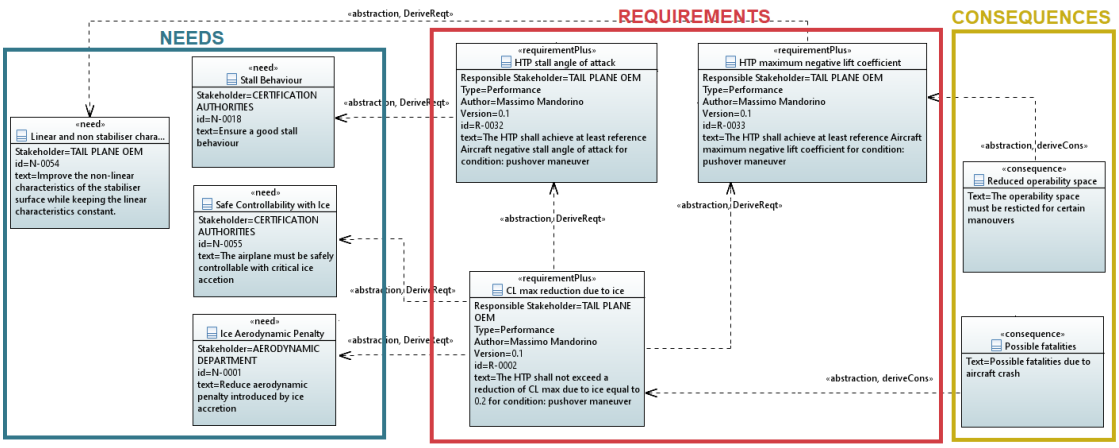

Figure 5.12: Example of a requirement traceability view in Papyrus.

5.2.4 Architecture modelling

Within the OCE, it has been possible to easily model a system architecture that represents both the conventional HTP described in Table 5.1 and the system of interest under analysis. The composition of the system of interest arises after the architecture modeling phase is completed. The architecture modeling process begins with defining the boundary functions, which are derived from the functional

requirements. Beginning with the functional requirements outlined in Table 5.7, all the components that can be part of the conventional HTP and final systems are integrated into the model as elements capable of fulfilling specific functions. Of course, a component will also need to fulfill one or more functions, which, in turn, will require other components. In this way, a comprehensive system architecture can be developed, considering all design choices and solutions. Indeed, with an automatically generated decision panel, it is possible to select how to meet each specific requirement and thus obtain the architectural model for a new solution.

Ax excerpt of the architectural model is depicted in Figure 5.13. The architecture begins with the boundary functions "Provide stability," "Transport passengers," and "Generate profit," fulfilled by the HTP system, the fuselage, the entire aircraft, and particularly by their components. Starting from the formalized requirements and needs, it is possible to trace the origin of these functions back to the stakeholders' needs. Firstly, these functions are derived from the following requirements:

- The Aircraft shall have a payload capacity which allows for the transportation of passengers for condition: typical mission.
- The Aircraft shall have acceptable level of recurring cost to generate profit for condition: typical mission.
- The ARE shall decrease its recurring costs by 5% with respect to reference Aircraft for condition: typical mission.

Secondly, these requirements are derived from the following needs:

- Ensure good flying qualities (stability, handling and balance) in all flying conditions.
- Ensure enough Payload.
- Affordable ticket price.

All functions are derived from boundary functions that represent the use cases of the system considered. The functions are successively decomposed and assigned to components for function fulfillment.

The model presented represents a portion of the primary design challenge to be addressed in the case of advanced rear-end design. Ice accretion, a phenomenon that must be considered for certification purposes, is addressed through various solutions, including active ice protection systems and the implementation of anti-ice shapes, which represent relevant architectural variants. These measures have led to the development of the innovative bottleneck fuselage rear-end shape. Similarly, the requirement for good stall behaviors can result in the design of a negatively swept horizontal tailplane. In this case, the conventional tailplane is also included in the model, allowing the user to select which system to analyze. The FSHTP is also considered a solution for reducing the loads on the rear part of the fuselage

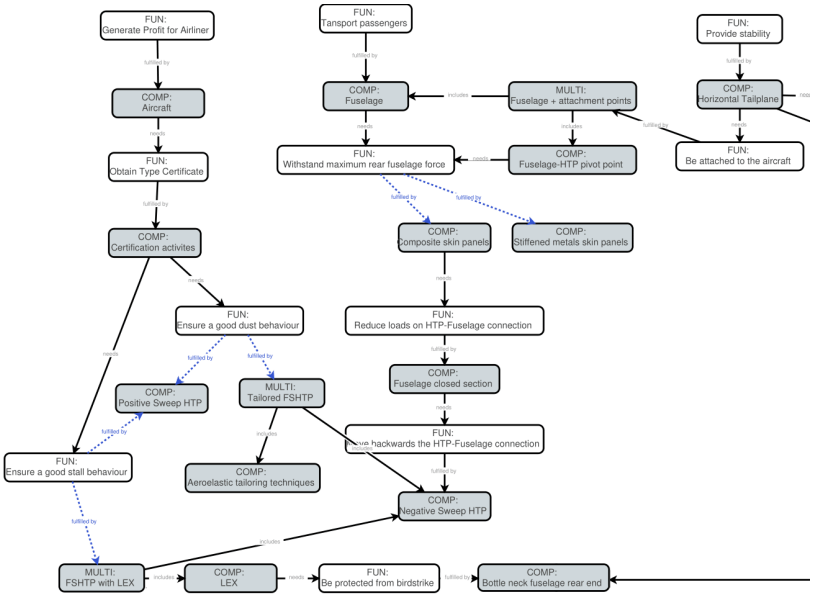

Figure 5.13: Excerpt of the architecture model of the Conventional and Advanced Rear End modelled in ADORE. Poor image quality due to acquisition from OCE.

by eliminating the fuselage cutout. Once the overall architecture is modeled, several architectural decisions could be identified. The architecture decisions are automatically determined by ADORE, which summarizes all the potential decisions that can be made within the complete architecture through the Architecture Decisions panel. An example of this panel is presented in Figure 5.14, where the list of architectural decisions for the above-described architecture model is illustrated. The decision panel columns list the following information: decision ID number, computed operation, decision objective, and decision options.

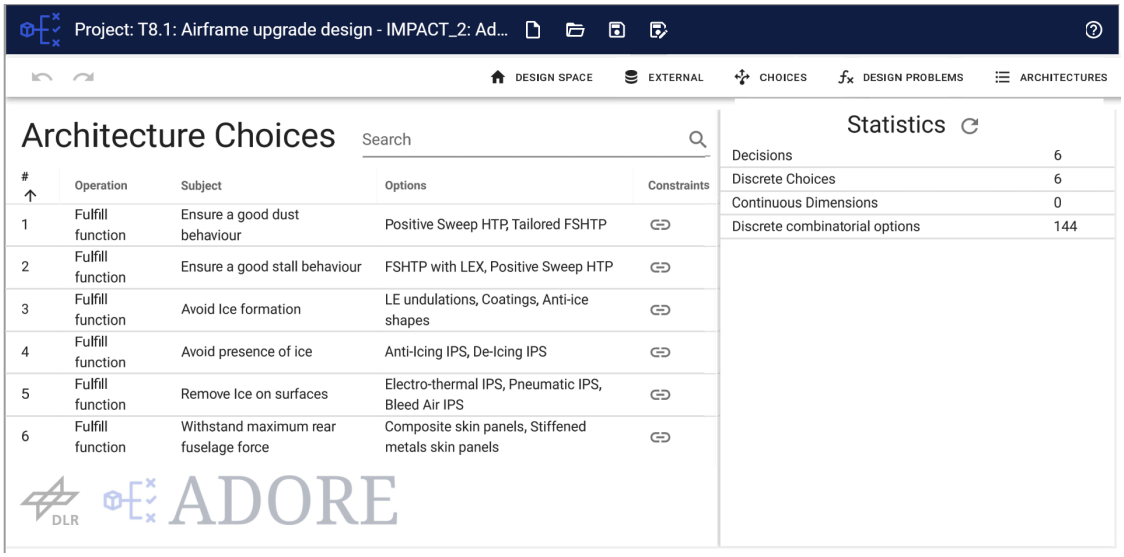

Figure 5.14: Architecture Decisions panel automatically generated in ADORE.

The main choices include various adoptable configurations for conventional or forward HTP, with or without the addition of LEX, bottleneck fuselage shape, and materials selection. The various combinations of decisions that can be made result in different architectures. A specific architecture can be defined by making a specific choice for each decision point. Two distinct architectures have been generated through the decision panel. The configuration includes all the innovative solutions of the advanced rear end, resulting in an FSHTP configuration with LEX and bottleneck fuselage shape. The second configuration consists of a more conventional design, featuring a negatively swept HTP, electro-thermal ice protection systems, and stiffened metal skin panels on the HTP. For clarification, the innovative FSHTP configuration architecture model is shown in Figure 5.15. As it is possible to notice, numerical parameters have been incorporated into the architecture as QOIs. For example, various geometry, aerodynamic, and structural parameters have been incorporated into the HTP, the fuselage, and the overall aircraft systems. These quantities of interest have been introduced to accurately formulate the MDO design problem. Indeed, in the next step, it will be possible to define all of these QoI as design variables, objectives, and constraints of the MDO problem.

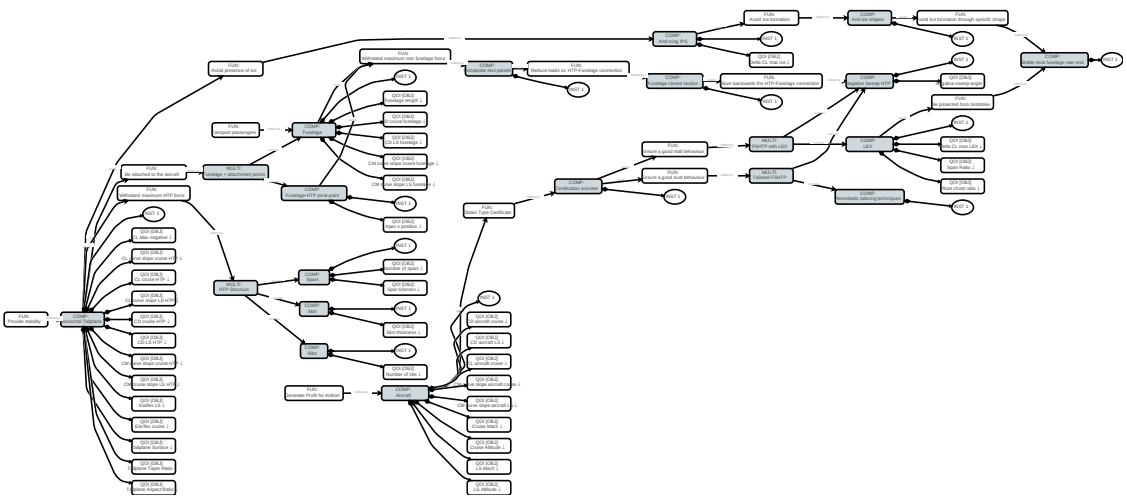

Figure 5.15: Architecture instance representing the innovative advanced rear end configuration. The model is generated in ADORE.

5.2.5 Connecting architectures to MDO

The previous section described how the system architecture model was derived from the functional requirements. Similar to how the system architecture can be derived from the functional requirements, the MDAO workflow can be derived

from the non-functional requirements. This section explains the process from non-functional requirements to the formulation of the MDAO workflow. As already explained and presented in Table 5.7, requirements must be formulated according to defined patterns. These patterns can be inserted into the OCE through a dedicated module, as illustrated in Figure 5.11. For each requirement, performance parameters and performance target value are indicated, with information about whether the parameter's value should align with the target in order to fulfill the requirement. In this manner, the OCE will have a clear way to verify whether the requirement is satisfied or not. The next step involves linking the requirement to the central data schema used in the MDAO workflow. This link will facilitate the automatic verification of the requirement after the MDAO workflow has been executed. Consequently, for each formulated parameter, an XPath is attached to indicate the link to the central data schema (in this case, CPACS). An excerpt of the defined parameters for this work can be seen in Figure 5.16. A portion of the parameters related to the HTP requirements are presented. These parameters are then used in the requirements patterns, as already illustrated in Figure 5.11.

Parameters overview

Below you'll find an overview of all parameters in the design study.

ADD CLONE EDIT DELETE

Parameter	Description	Value type	System	XPath
HTP Stall angle of attack	angle of attack at which the HTP stall occours	Continuous	HTP	/IMPACT/STAR_CCM_CFD_Solver/Output/HTP_Stall_AOA
HTP LS CM derivative	Horziontal tailplane low speed Moment Coefficient derivative	Continuous	HTP	/IMPACT/STAR_CCM_CFD_Solver/Output/HTP_CM_Der_LS
HTP Maximum Negative lift coefficient	Maximum Negative lift coefficient assumed by the HPT in stall condition	Continuous	HTP	/IMPACT/STAR_CCM_CFD_Solver/Output/HTP_CL_Max_Neg
HTP LS CL derivative	Horziontal tailplane low speed Lift Coefficient derivative	Continuous	HTP	/IMPACT/STAR_CCM_CFD_Solver/Output/HTP_CL_Der_LS
HTP ICE Maximum negative lift coefficient reduction	Reduction of maximum negative lift coefficient due to ice accretion	Continuous	HTP	/IMPACT/ICE_Effect/Output/Delta_CL_Max_ICE
HTP weight	Weight of the Horizontal Tailplane	Continuous	HTP	/IMPACT/Aircraft_Data/Structure_Output/HTP_Weight
ARE LS Elastic efficiency	Advanced Read End Elastic efficiency	Continuous	ARE	/IMPACT/Aircraft_Data/Structure_Output/Eta_flex/Low_Speed_Eta_Flex

« ‹ Page 1 of 2 › » Displaying 1 - 25 of 38

Figure 5.16: Excerpt of parameters defined in OCE and used in the requirement patterns. Poor image quality due to acquisition from OCE.

Once the requirements have been fully linked to the parameters and their associated values in the central data schema, the next step involves defining the design capabilities that will manage these parameters as tool inputs or outputs. The OCE enables the integrator to include a list of the available tools as design competences, as shown in Figure 5.17. For each design competence, it is possible to

include the name and a brief description of the tool, along with its input and output. In addition, two files must be submitted to the OCE. The files must contain the central data schema XPaths for all the input and output values of the tool. If the tool is already configured to work with the selected central data schema, the two files represent an example of an input and output file for the discipline. Figure 5.17 illustrates how all the design competences included in the OCE encompass all the tools outlined in Chapter 4, with the exception of the optimizers and RSM modeler, as they are not considered specific disciplines in the workflow. Lastly, as can be seen from the figure, a CPACS file must be provided to inform the OCE whether a specific parameter is an input defined by the users or an output generated from a specific tool. This step is essential for the automatic generation of the MDAO workflow, which is presented in the following section.

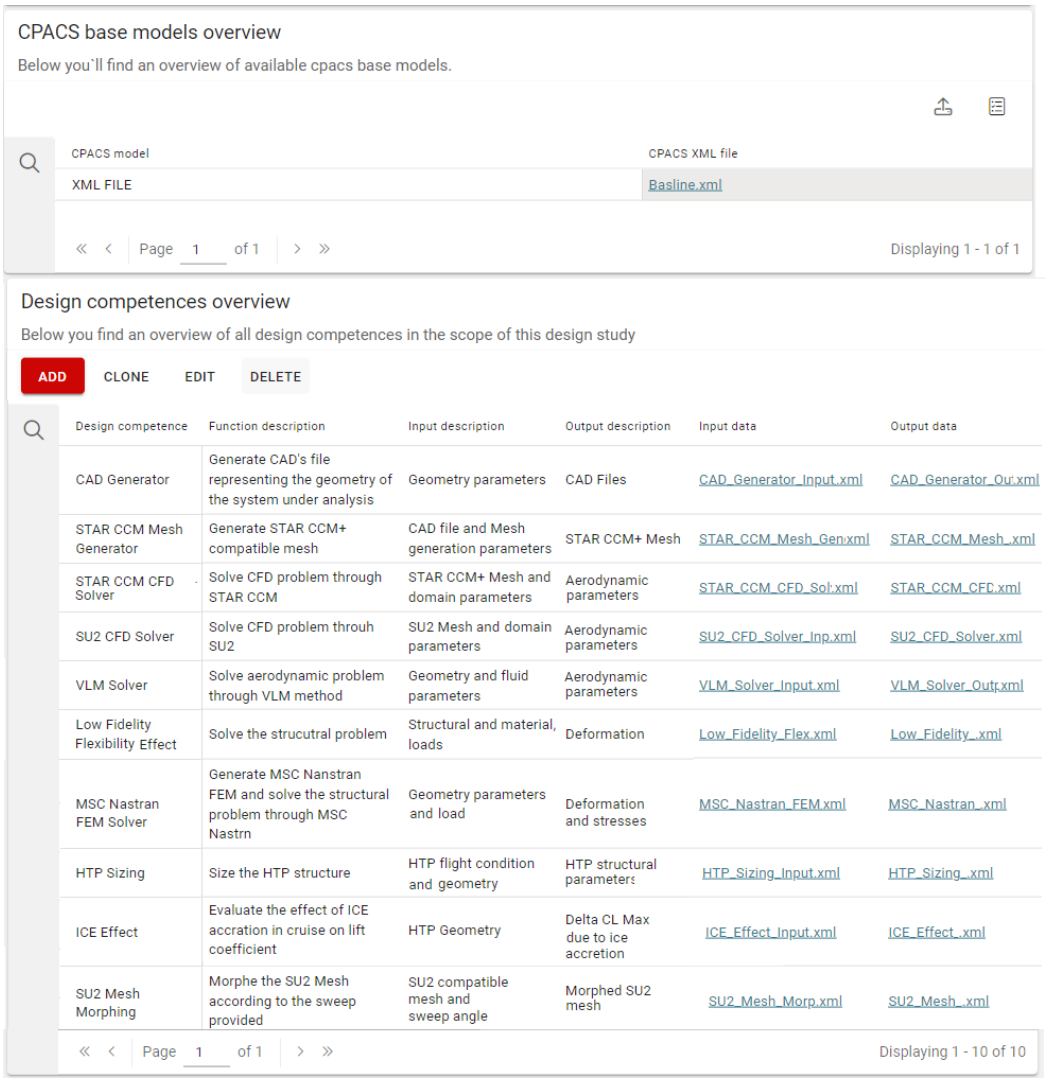

Figure 5.17: Overview of the Design Competences defined within the OCE. Poor image quality due to acquisition from OCE.

Once the design competencies have been inserted and validated in the OCE, the system architecture can be linked to them using MultiLinQ. By integrating information from the architecture model and tool input and output definitions previously described, MultiLinQ can display which tools are used to calculate specific metrics. With this tool, it is possible to verify if all the quantities of interest defined within the system architecture are addressed by the design competencies included in the optimization problem using a compliance matrix. In this work, as will be demonstrated in the following sections, several optimization problems have been defined. Each optimization problem is defined by a test case. For simplicity, Figure 5.18 presents a compliance matrix that includes all the possible tools integrated into the OCE. There will not be a defined workflow containing all the design competencies. The rows indicate the different QoIs that were assigned to the system architecture using ADORE. The columns indicate the design competencies that may be present in the MDAO workflow.

All the included QOIs can be visualized in this figure. It is easy to understand that all the QOIs are connected to at least one discipline, indicating that all the quantities introduced in the architecture model can be computed through the execution of a workflow. From this matrix, it is evident that certain tools share similar areas of expertise, and therefore, address the same QOI. In fact, these tools will be integrated into various workflows, depending on the optimizer used and the desired level of accuracy. Several test cases will be defined in the following sections, each one describing a different optimization problem that utilizes various tools. For simplicity, only this compliance matrix is shown. Furthermore, the other optimization problem sub-matrices also maintain consistent mapping, covering all QOI competences without redundancy in the analyzed QOIs.

		Tools									
Components	**QOIs**	*CAD Generator*	*HTP Sizing*	*ICE Effect*	*Low Fidelity Flexibility Effect*	*MSC Nastran FEM Solver*	*STAR CCM CFD Solver*	*STAR CCM Mesh Generator*	*SU2 CFD Solver*	*SU2 Mesh Morphing*	*VLM Solver*
Aeroelastic tailoring techniques			✓		✓	✓					
Aircraft	CD aircraft LS						✓				
Aircraft	CD aircraft cruise						✓				
Aircraft	CL aircraft cruise						✓				
Aircraft	CM curve slope aircraft LS						✓				
Aircraft	CM curve slope aircraft cruise						✓				
Anti-Icing IPS	Delta CL max ice			✓							
Anti-ice shapes				✓							
Bleed Air IPS				✓							
Bottle neck fuselage rear end		✓									
Certification activites		✓	✓	✓	✓	✓	✓		✓		✓
Coatings				✓							
Composite skin panels			✓		✓	✓					
De-Icing IPS	Delta CL max ice			✓							
Electro-thermal IPS				✓							
Flight Condition	Cruise Altitude		✓		✓	✓	✓	✓	✓		✓
Flight Condition	Cruise Mach		✓		✓	✓	✓		✓		✓
Flight Condition	Low Speed Altitude		✓		✓	✓	✓	✓	✓		✓
Flight Condition	Low Speed Mach		✓		✓	✓	✓		✓		✓
Fuselage	CD LS fuselage						✓				
Fuselage	CD cruise fuselage						✓				
Fuselage	CM curve slope LS fuselage						✓				
Fuselage	CM curve slope cruise fuselage						✓				
Fuselage	Fuselage length	✓						✓			
Fuselage closed section		✓									
Fuselage-HTP pivot point	Apex x position	✓									
Horizontal Tailplane	CD LS HTP						✓		✓		✓
Horizontal Tailplane	CD cruise HTP						✓		✓		✓
Horizontal Tailplane	CL Max negative						✓				
Horizontal Tailplane	CL cruise HTP				✓	✓	✓		✓		✓
Horizontal Tailplane	CL curve slope LS HTP				✓	✓	✓		✓		✓
Horizontal Tailplane	CL curve slope cruise HTP				✓	✓	✓		✓		✓
Horizontal Tailplane	CM cruise slope LS HTP				✓	✓	✓		✓		✓
Horizontal Tailplane	CM curve slope cruise HTP				✓	✓	✓		✓		✓
Horizontal Tailplane	Eta flex cruise				✓	✓					
Horizontal Tailplane	Etaflex LS				✓	✓					
Horizontal Tailplane	Tailplane Aspect Ratio	✓	✓		✓	✓					✓
Horizontal Tailplane	Tailplane Surface	✓	✓		✓	✓					✓
Horizontal Tailplane	Tailplane Taper Ratio	✓	✓		✓	✓					✓
LE undulations				✓							
LEX	Delta CL max LEX						✓				
LEX	Root chord ratio	✓									
LEX	Span Ratio	✓									
Negative Sweep HTP	Negative sweep angle	✓	✓	✓	✓	✓				✓	✓
Pneumatic IPS				✓							
Positive Sweep HTP	Positive sweep angle	✓	✓	✓	✓	✓				✓	✓
Ribs	Number of ribs					✓					
Skin	Skin thickness		✓		✓	✓					
Spars	Number of spars					✓					
Spars	Spar tickness		✓		✓	✓					
Stiffened metals skin panels			✓		✓	✓					

Figure 5.18: Compliance matrix defined in MultiLinQ.

5.2.6 MDAO Workflow formulation: Test Cases

The final step in formulating MDAO workflows involves generating test cases and linking them to the various requirements. A test case is defined by specifying all the design competencies needed to verify a requirement within a fixed design. After defining the test cases, they can be linked to the various requirements. The relationship between the requirement and the test cases is depicted in Figure 5.19, which illustrates the test cases defined in the OCE and provides some examples of associated requirements.

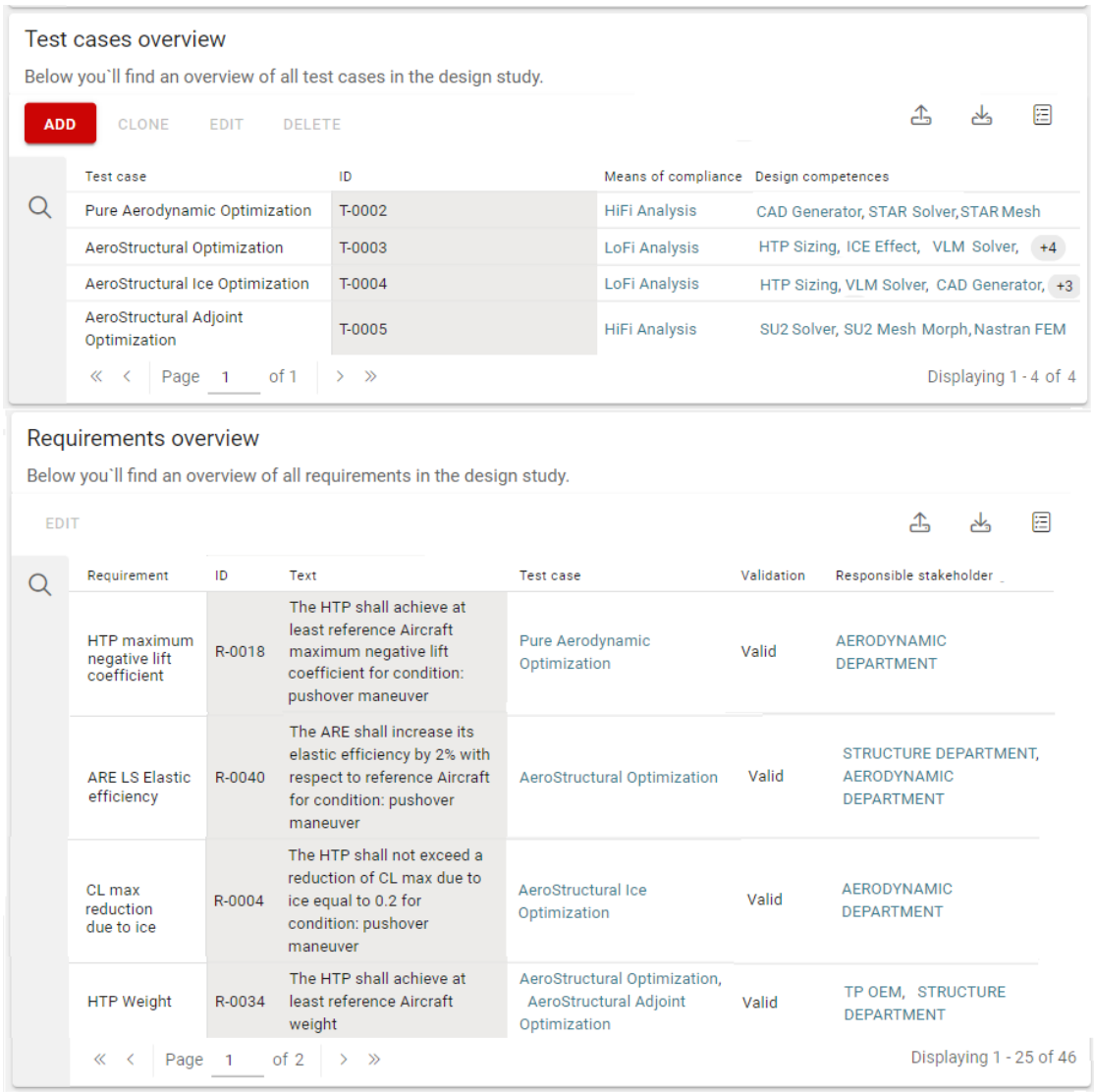

Figure 5.19: Test cases defined in OCE and examples of requirements that must be verified through the execution of these test case workflows. Poor image quality due to acquisition from OCE.

Four different test cases have been defined in the OCE:

- Pure aerodynamic optimization: It consists of high-fidelity aerodynamic analysis and optimization to verify all requirements related to aerodynamic parameters, such as drag, lift, and moment coefficient derivatives.
- Aerostructural optimization: It consists of low-medium fidelity aeroelastic analysis and optimization useful to verify all the requirements related to aeroelastic parameters such as elastic coefficient and aerodynamic parameters affected by deformation effect.
- Aerostructural ice optimization: It consists of low-medium fidelity aeroelastic analysis and optimization which includes ice effect useful to verify all the requirements related to icing aerodynamic parameters such as the aerodynamic penalty introduced by icing effect.
- Aerostructural adjoint optimization: It consists of high fidelity aeroelastic analysis and optimization useful to verify all the requirements related to aeroelastic and structural parameters such as the HTP weight.

These four test cases will be transformed into four MDAO workflows using the OCE. In the following sections, the executable workflows and the corresponding results obtained from these test cases are presented.

Once the test cases and parameters have been assigned to the requirements, the requirements must be assigned an optimization role in the OCE. Four different roles are available within KE-chain: objective, constraint, quantity of interest, and design variable bound. This work has been completed for each of the test cases illustrated. In the following sections, the role of the parameters will be presented along with the definition of the optimization problem. Note that not every requirement has a problem role assigned to it. This is also not necessary. Only the requirements with an assigned problem role will be considered in the MDAO workflow formulation. As a result, compliance with the unassigned requirements cannot be guaranteed after running the workflow. Once the roles are assigned to the requirements, KE-chain will automatically translate them into objective, design, constraint, and state variables.

5.3 Pure aerodynamic optimization: MDAO Workflow and results

5.3.1 Rigid Optimization: Problem Formulation

Upon generating the "Rigid Optimization" test case with associated design competences, parameters, and requirements, the first rigid optimization problems

were formulated and executed using a specialized optimization workflow integrated into the RCE environment. The rigid optimization problem is detailed in Table 5.8.

Table 5.8: Rigid optimization problem. Optimization function, variables, weights and constraints.

	Function/Variable
Minimize	$J = W_1 \left(\sum_{AOA=-4deg}^{AOA=4deg} \overline{CD}_{BH\,AOA} \right) + W_2 \left(\frac{1}{\lvert \overline{CL}_{max,neg.,H} \rvert} \right)$
With respect to	AR_H, S_H, Λ_{LE}, λ, X_{Apex}, $\frac{b_{LEX}}{b_H}$, $\frac{C_{Root,LEX}}{C_{Root,H}}$
Subject to	$\left(\lvert C_{M_{\alpha_H}} \rvert - \lvert C_{M_{\alpha_{H,target}}} \rvert \right)_{cruise\,and\,stall} \geq 0$
	$X_{apex,ref.\,FSHTP} - X_{apex\,FSHTP} \geq 0$
Where	$W_1 = W_2 = 0.5$
	$X_{apex,ref.\,FSHTP} = 34.756\,m$
	$C_{M_{\alpha_{H,cruise,target}}} = -0.0707 deg^{-1}$
	$C_{M_{\alpha_{H,stalltarget}}} = -0.0572 deg^{-1}$

The main objective of this optimization task was to minimize the body-horizontal drag coefficient at four specific angles of attack (-4, -2, 0, and 4 degrees) while simultaneously maximizing the tailplane's negative stall lift coefficient. Both objectives were normalized and given equal significance within the optimization function. In the optimization problem, two constraints have been introduced regarding the slope of the pitching moment curve of the tail and LEX. These constraints ensure that the tail and LEX provide a minimum level of static stability equivalent to that of the reference aircraft during both cruise and low-speed conditions. Additionally, the problem imposes a geometric constraint on the longitudinal position of the tailplane to prevent solutions that rely solely on increasing the tailplane's arm length, thereby avoiding excessive fuselage extension. The constraint value for the X-coordinate of the tailplane leading edge has been chosen to prevent the aerodynamic center of the optimized solution from exceeding that of the reference solution.

Once the MDO problem is defined, along with its parameters, their roles are formalized within the OCE environment using KE-Chain, as illustrated in Figure 5.20. Each parameter can be designated as a design variable, objective variable, or constraint by being included in a specific table. In the figure, the depicted parameters correspond to those outlined in Table 5.8. As shown in

the diagram, each parameter representing an objective variable or a constraint is connected to a requirement that needs to be validated in the test case. Furthermore, as detailed in Sections 5.2.5 and 5.2.6, each parameter is also linked to a discipline and a specific variable in the CPACS file.

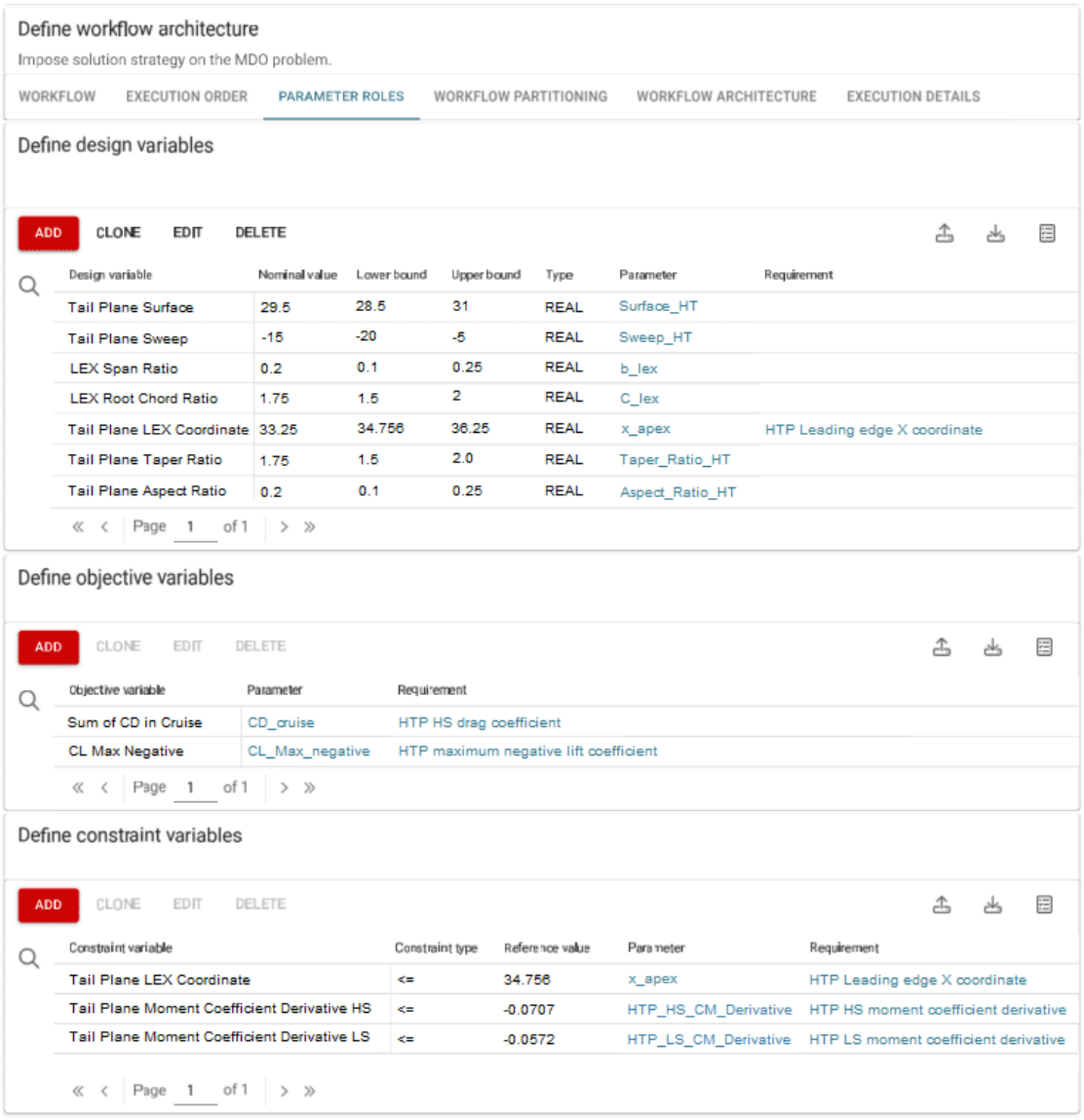

Figure 5.20: Parameters formalization executed in KE-Chain for Rigid Optimization Test Case. Poor image quality due to acquisition from OCE.

Finally, after defining the various optimization variables in KE-Chain, the MDAO workflow can be developed. Figure 5.21 illustrates the XDSM generated through KADMOS and VISTOMS for the pure aerodynamic optimization test case, highlighting the optimization functions, variables, and constraints. The main goal of this toolchain is to automatically generate and analyze an ARE concept

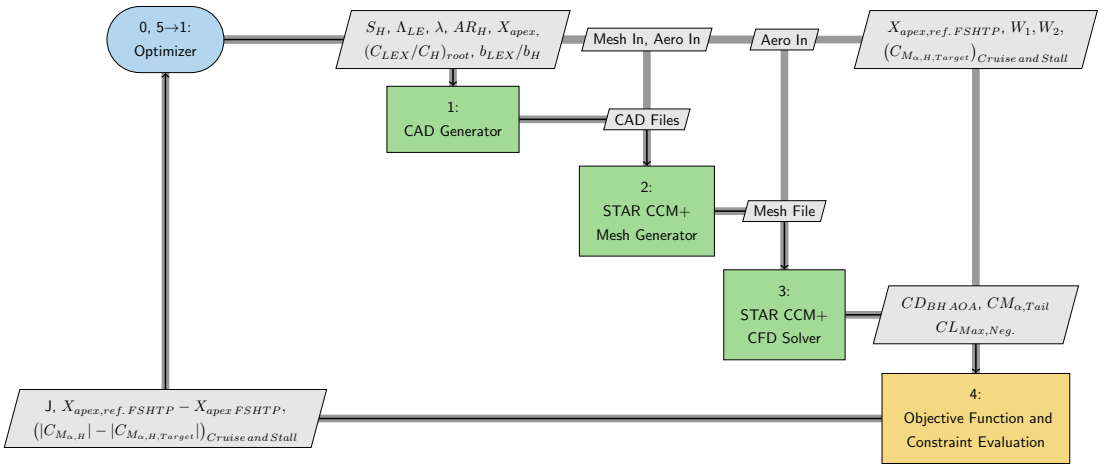

Figure 5.21: XDSM representing the MDAO workflow generated from the Pure Aerodynamic Optimization test case. "Mesh in" and "Aero in" stand for Mesh and Aerodynamic inputs.

using CFD methodology. This concept includes a FSHTP, a LEX body component, and an advanced fuselage tailcone. The primary focus of the analysis is to assess the aerodynamic and stability characteristics of different wing-body configurations. This is achieved by selecting standard aeronautical external shape parameters and analyzing different angles of attack under various flow conditions within a single workflow execution. As illustrated in Figure 5.21, the workflow consists of three primary design components, an optimization block, and a final tool that consolidates the key results obtained from the preceding tools. The first step in this workflow involves using 3D modeling software specifically designed for shaping the exterior of an ARE prototype. This conceptual design incorporates a horizontally forward-swept tailplane, a LEX element, and an innovative tailcone configuration for the fuselage. Through the provision of wing and fuselage section points, along with geometric macro parameters, the tool facilitates the automatic generation of these features in various CAD formats. The next two tools in this workflow are CFD software that utilize the STAR-CCM+ software. Their main functions are to automatically generate a mesh that is compatible with STAR-CCM+ from a pre-defined CAD geometry, thereby streamlining the CFD analysis process. This process begins with a CAD file representing the geometry under analysis, which is used to create a macro file. The macro file executed within the STAR-CCM+ software contains commands for importing the geometry, defining its components and regions, customizing the mesh, and initiating the computation. Subsequently, the analysis is conducted from multiple angles of attack, and the resulting data is stored in the output CPACS file.

5.3.2 Design of Experiment based on high-fidelity aerodynamic analysis

The workflow depicted in Figure 5.21 includes high-fidelity CFD analysis, which is computationally expensive. In such a situation, the number of iterations required to compute an optimization can become prohibitive. For this reason, two RSMs representing the high-speed and low-speed aerodynamic response of the analyzed geometry have been developed to replace the CFD workflow, offering the ability to solve the optimization problem within a reasonable timeframe. To accomplish this, a DOE workflow has been integrated and executed. Subsequently, the RSMs based on the results of the DOE have been generated. To comprehensively capture the distinctive aerodynamic features, an in-depth aerodynamic investigation of the target configuration has been conducted using high-fidelity CFD RANS calculations. To streamline this process, a DOE has been implemented in the workflow depicted in Figure 5.21. For this purpose, the optimization driver has been replaced with a DOE driver. The rest of the workflow remains unchanged. Figure 5.22 depicts examples of the geometries that can be generated using the presented workflow. As evident, the parameters of the fuselage, tailplane, and LEX can be customized for each solution.

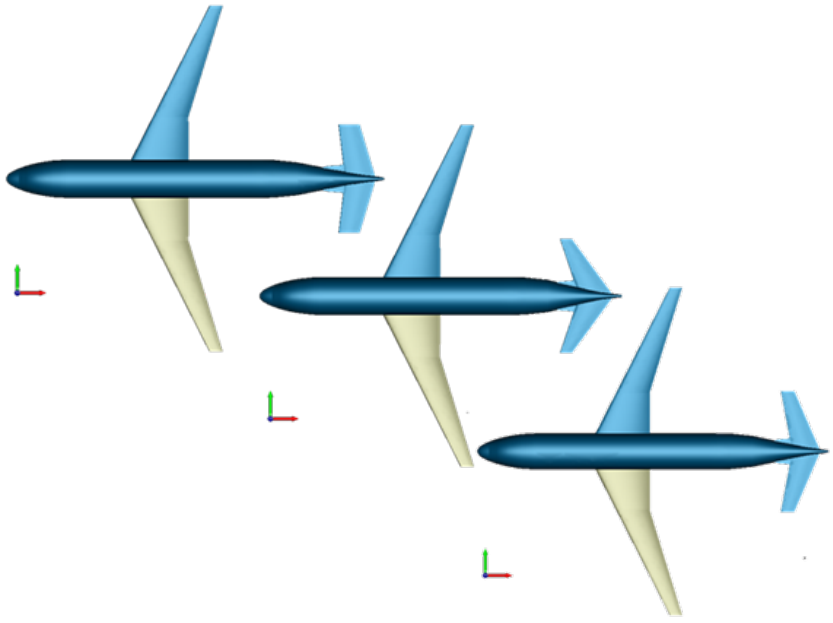

Figure 5.22: Configurations generated by the Pure Aerodynamic DOE execution.

To ensure accuracy and reliability in the high-fidelity analysis, the commercial software STAR-CCM+ has been utilized. Key details regarding the numerical model setup are presented in Table 5.9. Figure 5.23 provides a comprehensive overview of a typical fluid domain. This figure depicts the application of boundary conditions,

meticulously defined to simulate real-flight conditions. The mesh for the analysis was generated, considering only the fuselage and the horizontal tailplane, including the LEX. This strategy was pursued to reduce computational time and stay aligned with the parameters involved in the optimization problem.

Table 5.9: Numerical Model Setup for CFD-RANS Simulations.

Parameter	Value
Mesh type	unstructured polyhedral
On body minimum surface size	0.0042 m
On body target surface size	0.035 m
Number of volume cells	13 Millions
Turbulence model	SST $\kappa - \omega$
Flow model	Compressible
Mach number	0.2, 0.78
Flight altitude	sea level, 11000 m

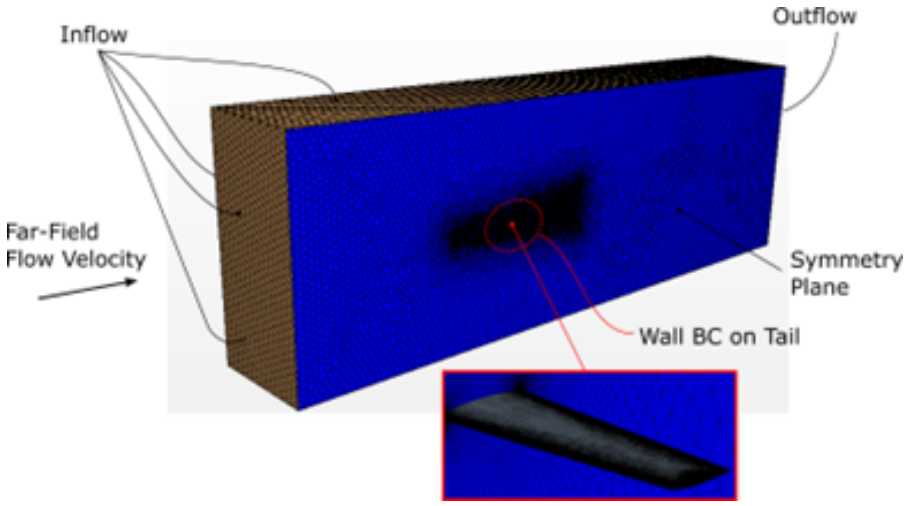

Figure 5.23: Comprehensive Overview of Fluid Domain and Boundary Conditions.

The high-fidelity aerodynamic workflow has been used to conduct a DOE focused on macro design parameters that affect the aerodynamic solution. In order to meet the time constraints, the DOE comprises 90 points, each of which must be evaluated for two different aerodynamic conditions are described in Table 5.3. LHS was used to systematically sample the specified design space. Table 5.10 presents the design parameters and their corresponding lower and upper bounds for the DOE. All aerodynamic coefficients for each angle of attack under investigation have been exported.

To effectively explore different optimization problems by adjusting design variables, constraints, and objective functions, a prediction model in the form of a

Table 5.10: DOE Variables and their range for the aerodynamic parameter estimation.

Variable	Symbol	Lower Bound	Upper Bound
Tailplane Surface	S_H	28.5 m^2	31.0 m^2
Tailplane Sweep	Λ_{LE}	-20.00 deg	- 5.00 deg
Tailplane Taper Ratio	λ	0.331	0.7
Tailplane Aspect Ratio	AR_H	4.00	6.00
Tailplane Leading Edge X coordinate	X_{apex}	33.25 m	36.25 m
LEX Root chord ratio	$(C_{LEX}/C_{tail})_{root}$	1.5	2.0
LEX Span ratio	b_{LEX}/b_H	0.1	0.25

response surface was developed for each aerodynamic parameter of interest using the RBF. These response surfaces can predict particular aerodynamic parameters based on the specified set of design variables and aerodynamic conditions. Figure 5.24 shows visual examples of these response surfaces. In addition to directly estimating aerodynamic coefficients through CFD simulations, response surfaces for crucial aerodynamic data, such as tailplane lift and pitching moment curve slopes, as well as its CLmax, have also been developed, taking into account the tailplane-body configuration.

A benchmark study was conducted to assess the performance of the presented response surface. This assessment involved conducting high-fidelity CFD analyses at both low and high speeds to evaluate various potential solutions. Table 5.11 compares the aerodynamic characteristics of three different geometries, as analyzed using both the response model and CFD simulations. The results indicate that the response model shows an error of less than 2% under high-speed conditions and a low angle of attack. However, as the angle of attack increases or under low-speed conditions, the errors also increase but they remain below 7%. The decrease in accuracy can be attributed to the highly nonlinear nature of the aerodynamic solution, which is worsened by the presence of shock waves at high speeds and the approach to stall conditions at low speeds.

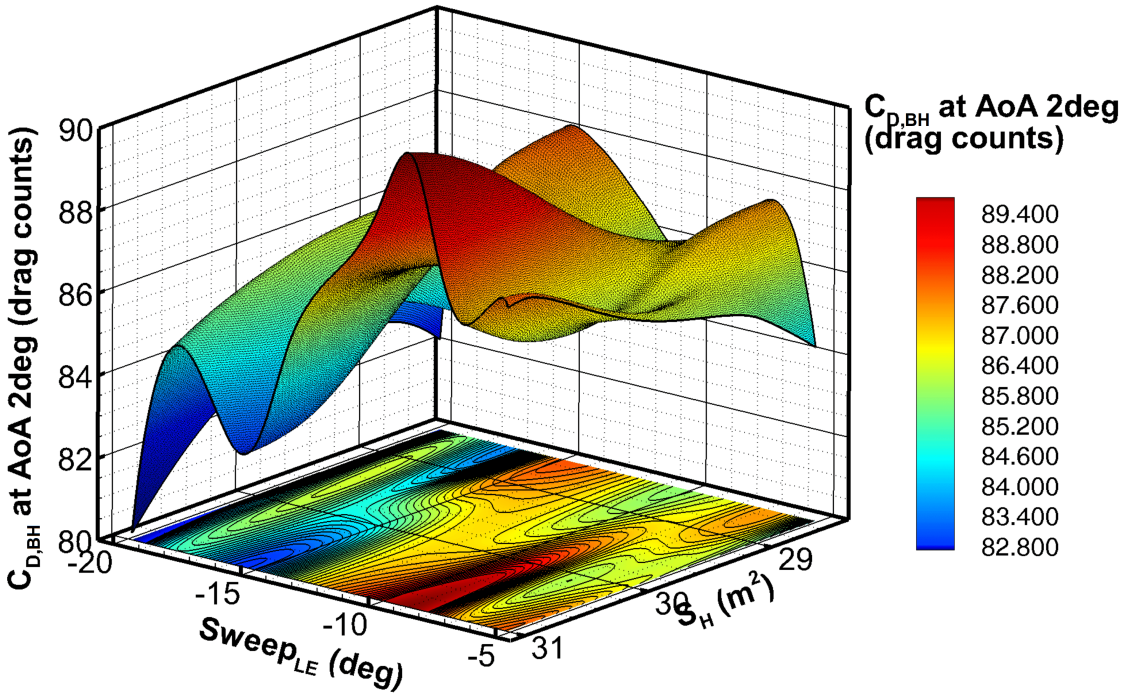

(a) Body-horizontal drag coefficient in cruise conditions (Mach number = 0.78 @FL390) at AoA = 2deg vs. Sweep and AR of the tailplane.

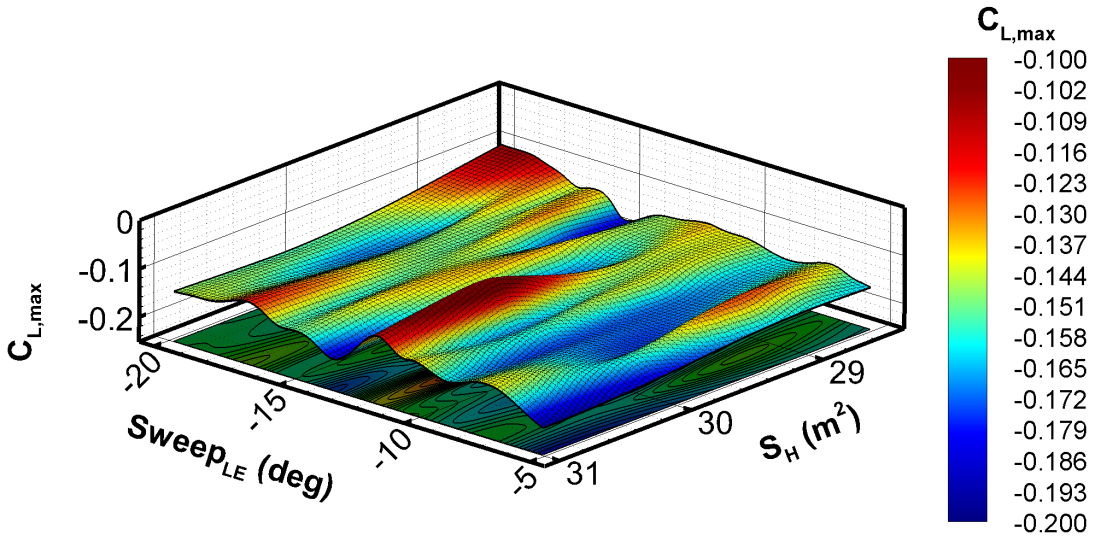

(b) Tail and LEX maximum negative lift coefficient (Mach number = 0.20 @FL0) in body-horizontal configuration vs. Sweep and Surface of the tailplane.

Figure 5.24: Examples of Response Surface for the Aerodynamic parameters over the investigated DOE.

Table 5.11: Aerodynamics comparison between solutions with same geometry achieved through the response surface shown in Figure 5.24 vs. CFD validation results. Results are referred to body-horizontal configuration.

Input Parameter	Value	Output Parameter	RSM Value	CFD Value	$\Delta(\%)$
S_H	28.504 m^2	$\mathbf{CD_{BH\,\alpha=-4deg}}$	0.01130	0.01190	5.33
Λ_{LE}	-19.734 deg	$\mathbf{CD_{BH\,\alpha=0deg}}$	0.00820	0.00822	0.30
λ	0.335	$\mathbf{CD_{BH\,\alpha=2deg}}$	0.00840	0.00843	0.34
AR_H	4.013	$\mathbf{CD_{BH\,\alpha=4deg}}$	0.01020	0.01033	1.24
X_{apex}	36.216 m	$\mathbf{CL_{max,H}}$ **neg.**	-0.152	-0.145	4.75
$(C_{LEX}/C_H)_{root}$	1.664				
b_{LEX}/b_H	0.101				
S_H	30.240 m^2	$\mathbf{CD_{BH\,\alpha=-4deg}}$	0.01324	0.01390	5.02
Λ_{LE}	-7.823 deg	$\mathbf{CD_{BH\,\alpha=0deg}}$	0.00844	0.00852	0.91
λ	0.400	$\mathbf{CD_{BH\,\alpha=2deg}}$	0.00859	0.00876	2.02
AR_H	5.070	$\mathbf{CD_{BH\,\alpha=4deg}}$	0.01093	0.01126	3.06
X_{apex}	34.617 m	$\mathbf{CL_{max,H}}$ **neg.**	-0.179	-0.168	6.13
$(C_{LEX}/C_H)_{root}$	1.969				
b_{LEX}/b_H	0.107				
S_H	29.659 m^2	$\mathbf{CD_{BH\,\alpha=-4deg}}$	0.01381	0.01304	5.60
Λ_{LE}	-5.153 deg	$\mathbf{CD_{BH\,\alpha=0deg}}$	0.00840	0.00841	0.12
λ	0.335	$\mathbf{CD_{BH\,\alpha=2deg}}$	0.00880	0.00870	1.11
AR_H	4.013	$\mathbf{CD_{BH\,\alpha=4deg}}$	0.01101	0.01074	2.50
X_{apex}	36.217 m	$\mathbf{CL_{max,H}}$ **neg.**	-0.197	-0.187	4.83
$(C_{LEX}/C_H)_{root}$	1.995				
b_{LEX}/b_H	0.101				

5.3.3 Rigid Optimization Results

Utilizing the previously introduced RSM prediction models, a variety of optimization challenges can be formulated and executed through the specialized optimization workflow depicted in Figure 5.25. The goal of this workflow is to simplify the modeling and resolution of optimization problems that utilize the output produced by the previously mentioned RSM. The response surface inputs are used as design variables for the problem. Two response surfaces have been incorporated into this workflow to predict high-fidelity aerodynamic parameters. One is designed for high-speed conditions, while the other is tailored for low-speed conditions. The main goal of this toolchain is to optimize the aerodynamic and stability characteristics of the ARE concept with reference to geometrical parameters. Furthermore, the toolchain can be used for various other optimization tasks. For example, it can be used to minimize the surface area of the tailplane while

adhering to specified constraints on performance parameters. The aerodynamic optimization workflow has been developed, integrated, and implemented within the RCE environment. This approach has been implemented to effectively handle the input and output of each tool and to conveniently formulate various optimization problems. The RCE-embedded Dakota genetic algorithm has been used to conduct the optimization process.

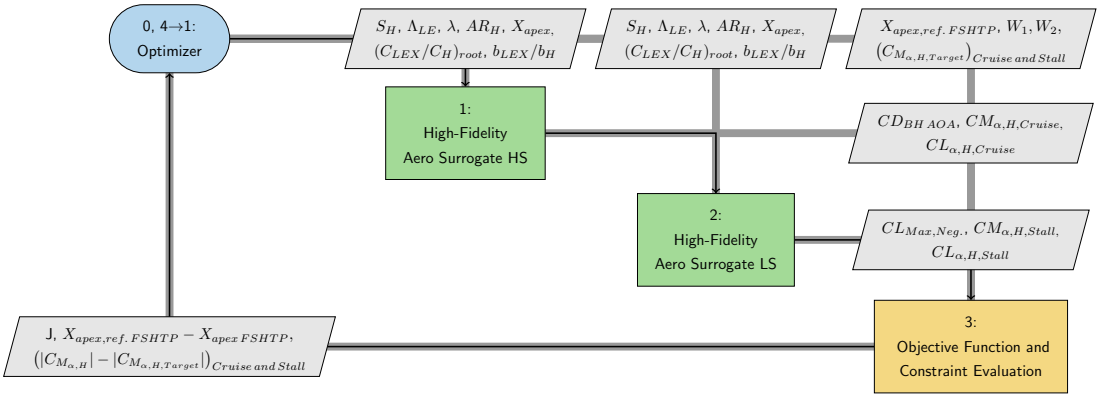

Figure 5.25: XDSM representing the Rigid Optimization executable workflow integrated in RCE enviroment.

Table 5.12 presents the geometric characteristics of the solution obtained from the optimization problem described in Table 5.8. A visual representation of this solution can be seen in Figure 5.26. A comparative analysis between the optimized solution and conventional reference geometry shows that the absolute value of the optimal sweep angle is lower than that of the reference HTP. This suggests that achieving favorable aerodynamic performance at high speeds is possible without a significant increase in the sweep angle. Furthermore, the optimization led to a 3.6% reduction in the tailplane surface area. This was accomplished by using smaller aspect ratio and similar taper ratio values, while ensuring that the tailplane's leading-edge X-coordinate does not exceed the specified value. The aerodynamic characteristics of the body-horizontal configuration solution are outlined in Table 5.13, emphasizing a significant increase in the maximum negative lift coefficient of the tailplane achievable through the optimized solution. However, the decrease in the drag coefficient of the airfoil is mainly noticed at specific angles of attack, possibly because of the formation of shock waves at high angles of attack. Both the tailplane lift and moment coefficients show improved performance compared to the reference geometry. Figures 5.27 and 5.28 visually illustrate the comparison of drag and lift characteristics between the optimized solution and the reference configurations.

Table 5.12: Comparison of the geometric characteristics of the rigid Optimization solution with respect to reference HTP.

Parameter	Ref. HTP	Rigid OPT
$\mathbf{AR_H}$	5.76	5.07 (-12%)
$\mathbf{(C_{LEX}/C_H)_{root}}$		1.969
$\mathbf{b_{LEX}/b_H}$		0.107
$\mathbf{S_H}$	31.36 m^2	30.24 m^2 (-3.6%)
$\mathbf{\Lambda_{LE}}$	32.00 *deg*	-7.82 *deg*
λ	0.336	0.400 (+19%)
$\mathbf{X_{Apex}}$	31.585 m	34.756 m (+10.0%)

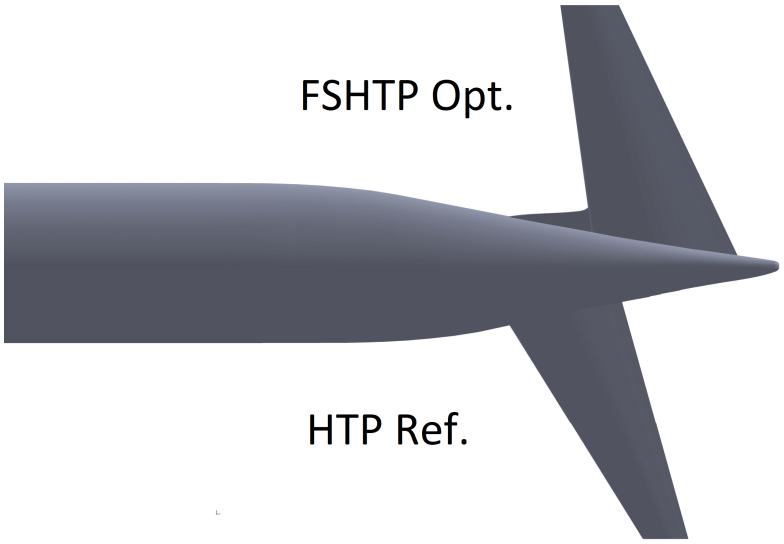

Figure 5.26: Comparison of the top views of the geometries of the rigid optimization problem and the reference conventional rear-end.

Table 5.13: Aerodynamics of rigid optimization solution vs. reference HTP. Data are referred to body-horizontal configuration. Aerodynamic conditions are described in Table 5.3.

Parameter	Ref. $\mathbf{HTP}_{Rigid}$	$\mathbf{OPT}_{Rigid}$	$\mathbf{\Delta}(\%)$
$\mathbf{CL_{max,H}}$ **negative**	-0.152	-0.179	**+18.0 %**
$\mathbf{CD_{BH\,AOA=0deg}}$	0.0086	0.0084	**-1.82 %**
$\mathbf{CD_{BH\,AOA=2deg}}$	0.0085	0.0086	**+1.03 %**
$\mathbf{CD_{BH\,AOA=4deg}}$	0.0100	0.0109	**+9.31 %**
$\mathbf{CD_{BH\,AOA=-4deg}}$	0.0129	0.0132	**+2.60 %**
$\mathbf{CM_{\alpha,H}}$ **cruise**	-0.0707	-0.0746	**+5.47 %**
$\mathbf{CM_{\alpha,H}}$ **low speed**	-0.0572	-0.0617	**+7.88 %**
$\mathbf{CL_\alpha}$ **Tail cruise**	0.0171	0.0178	**+4.19 %**
$\mathbf{CL_\alpha}$ **Tail low speed**	0.0145	0.0149	**+2.61 %**

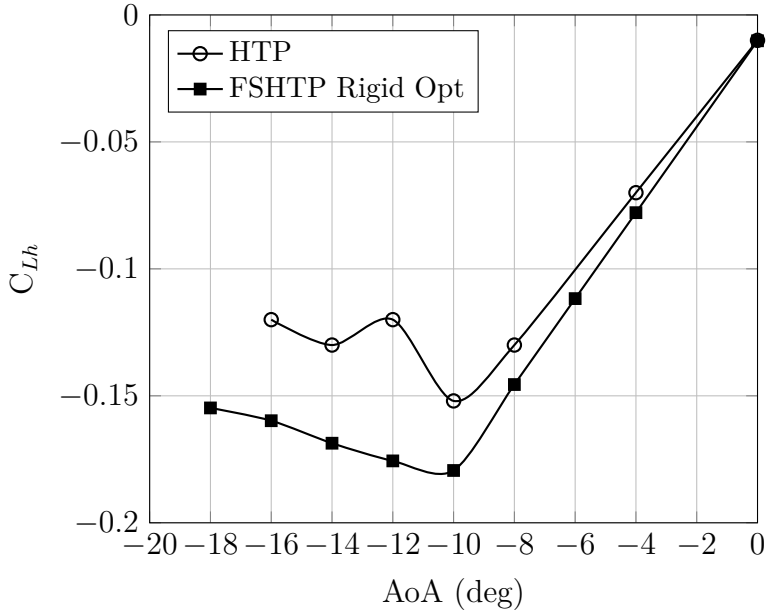

Figure 5.27: Low-speed lift curve comparison between conventional geometry and rigid optimization problem result. Data are referred to body-hotizontal configuration. Aerodynamic conditions are described in Table 5.3.

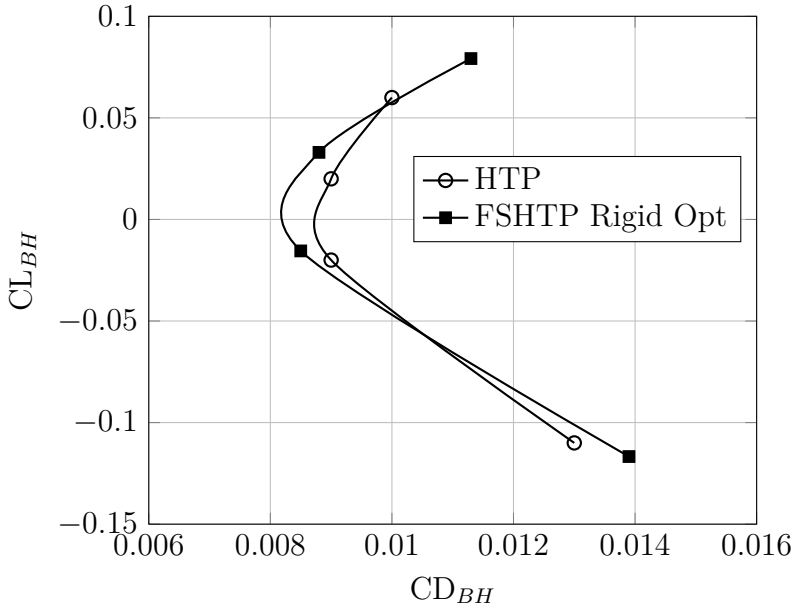

Figure 5.28: High-speed polar comparison between conventional geometry and rigid optimization problem result. Data are referred to body-hotizontal configuration. Aerodynamic conditions are described in Table 5.3.

This optimization study has revealed the potential for reducing the tail area and enhancing the tail's CLmax by approximately 12-18% (while considering the uncertainties related to CLmax estimates using RSM). It also aims to achieve a 1 to 2% reduction in drag compared to the conventional fuselage and tail arrangement. Additionally, the optimization process has produced a solution with enhanced stability characteristics, covering both tail lift and pitching moment coefficient slopes. Figure 5.28 clearly illustrates that the optimized solution shows a reduced tailplane drag coefficient while maintaining a constant lift coefficient in low incidence conditions, in contrast to the reference solution. This difference occurs even though the drag coefficient remains higher at a fixed angle of attack, due to the improved lift curve slope of the optimized solution.

5.4 Aerostructural optimization: MDAO Workflow and results

5.4.1 Aerostructural optimization: Problem Formulation

Upon generating the "Aerostructural Optimization" test case presented in Section 5.2.6 with associated design components, parameters, and requirements, a flexible optimization problem was formulated and carried out using a dedicated optimization workflow integrated into the RCE environment. The flexible optimization problem is described in Table 5.14.

Table 5.14: Aerostructural optimization problem. Optimization function, variables, weights and constraints.

	Function/Variable
Minimize	$J_{Flex} = W_1 \left(\sum_{AOA=-4deg}^{AOA=4deg} \overline{CD}_{BH\,AOA} \right) + W_2 \left(\frac{1}{\lvert \overline{CL}_{max,neg.,H_{Flex}} \rvert} \right)$
With respect to	AR_H, S_H, Λ_{LE}, λ, X_{Apex}, $\frac{b_{LEX}}{b_H}$, $\frac{C_{Root,LEX}}{C_{Root,H}}$
Subject to	$\left(\lvert C_{M_{\alpha_{H,Flex}}} \rvert - \lvert C_{M_{\alpha_{H,Flex,target}}} \rvert \right)_{cruise\,and\,stall} \geq 0$
	$X_{apex,reference\,FSHTP} - X_{apex\,FSHTP} \geq 0$
Where	$W_1 = W_2 = 0.5$
	$X_{apex,ref.\,FSHTP} = 34.756\,m$
	$C_{M_{\alpha_{H,Flex,cruise,target}}} = -0.0672 deg^{-1}$
	$C_{M_{\alpha_{H,Flex,stalltarget}}} = -0.0561 deg^{-1}$

The main objective of this optimization closely aligns with the previous one. The goal is to minimize the body-horizontal drag coefficient at four distinct angles of attack (-4, -2, 0, and 4 degrees) while also maximizing the tailplane's negative stall lift coefficient, considering the flexibility of the tailplane. Similar weighting, normalization, and constraints have been applied to this issue. The constraint in the optimization problem has been modified to account for the influence of flexibility on the aerodynamic parameters. Once the MDO problem is defined, along with its parameters, their roles are formalized within the OCE environment using KE-Chain, as illustrated in Figure 5.29.

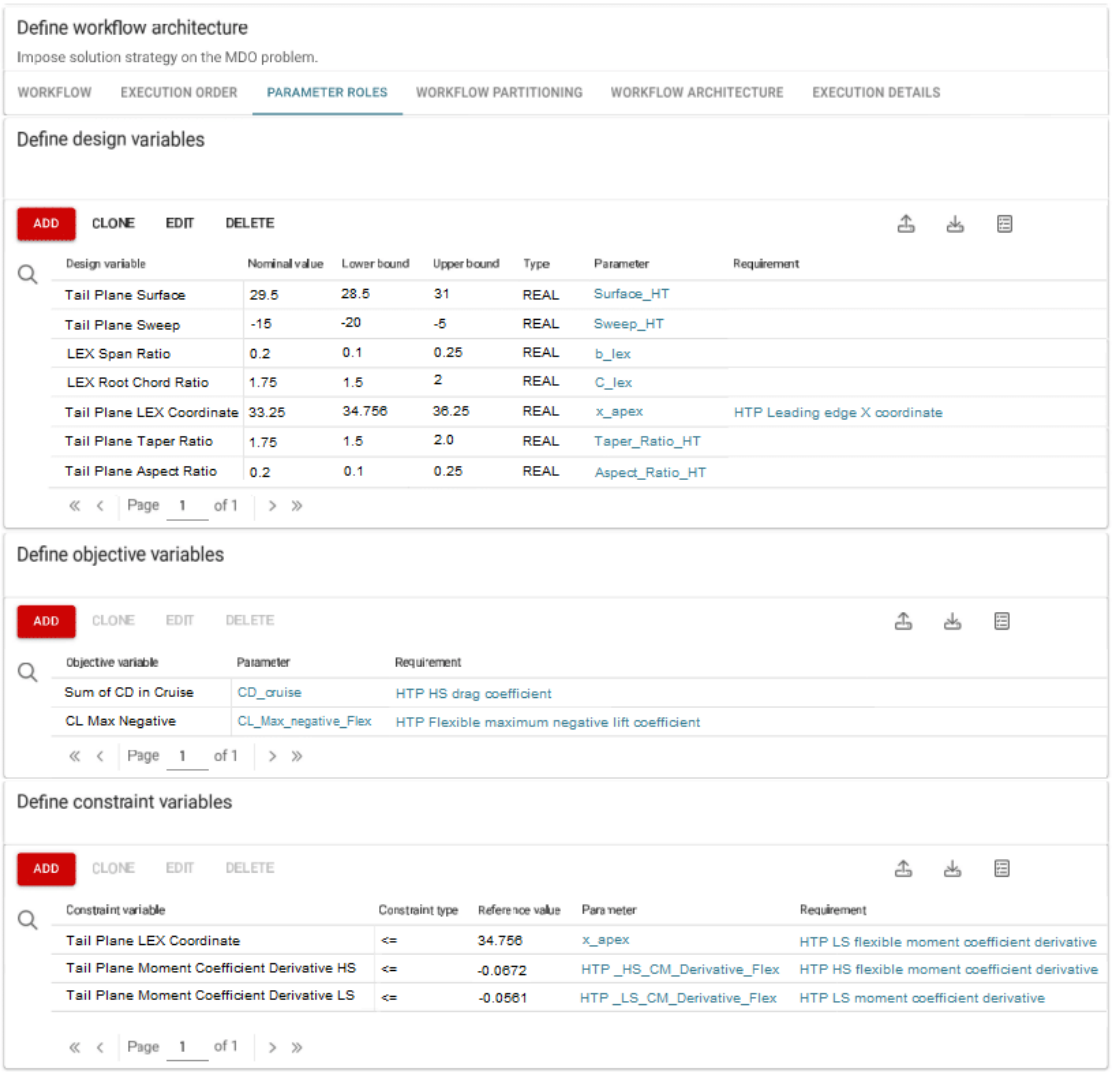

Figure 5.29: Parameters formalization executed in KE-Chain for Aerostructural Optimization Test Case. Poor image quality due to acquisition from OCE.

Each parameter can be designated as a design variable, objective variable, or constraint by being entered into a specific table. In the figure, the depicted parameters correspond to those outlined in Table 5.14. As shown in the diagram, each parameter representing an objective variable or a constraint is connected to a requirement that needs to be validated in the test case. Furthermore, as detailed in Sections 5.2.5 and 5.2.6, each parameter is also linked to a discipline and a specific variable in the CPACS file.

Once the various optimization variables have been generated by KE-Chain, the MDAO workflow can be formulated. Figure 5.30 represents the XDSM generated through KADMOS and VISTOMS for the aerostructural optimization test case. In this case, the specified objective, variables, and constraints are not highlighted in the diagram due to space limitations.

The initial stage of the workflow replicates the process depicted in Figure 5.21, which involves CAD and mesh generation, as well as high-fidelity aerodynamic computation. Furthermore, structural disciplines have been integrated. The FSI process begins with generating an initial rigid tail shape, which is determined by a set of macro design variables related to planform parameters. This rigid shape determines the masses and properties of crucial structural components using elasticity and stiffness, in accordance with specific structural layout and sizing criteria. The sizing conditions are determined from the flight envelope diagram, taking into account various maneuvering conditions, starting from a baseline aircraft. Once the structural sizing phase is completed, the tailplane's shape is input into an enhanced VLM to calculate aerodynamic forces at various angles of attack, including nonlinear lift regimes. Aerodynamic forces are then transferred to the structural analysis tool for each angle of attack in order to estimate the elastic deformation of the tail. The distorted geometry, which considers vertical displacements and sectional twists caused by torsion, is analyzed using the VLM code to adjust the aerodynamic forces. This data exchange is part of a converging loop that concludes when the tailplane lift coefficient between two consecutive iterations falls below a specified threshold. This iterative process is performed for both rigid and elastic tails across the specified array of angles of attack. The final step involves using the computed aerostructural information to adjust the aerodynamic data, in order to establish the objective and constraints for the optimization.

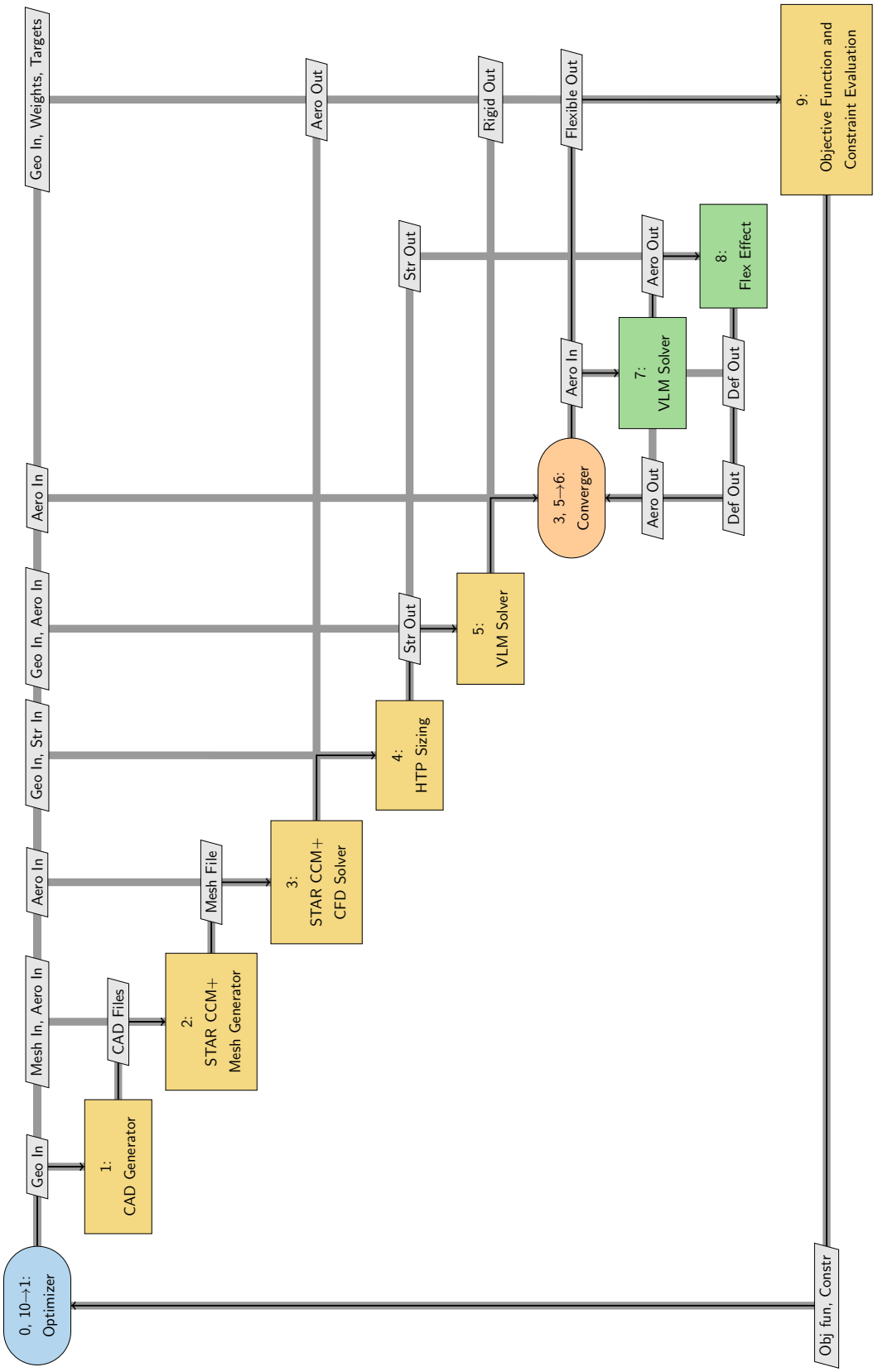

Figure 5.30: XDSM representing the MDAO workflow generated from the Aerostructural Optimization test case.

5.4.2 Design of Experiment based on low-fidelity aerostructural analysis

For the workflow depicted in Figure 5.30, the number of iterations required to compute an optimization can become prohibitive. For this reason, two additional RSMs have been developed in addition to the ones presented in Section 5.3.2. The new RSMs aim to replace aerostructural analysis, offering the potential to solve the optimization problem within a reasonable timeframe. To accomplish this, a DOE workflow has been integrated and executed. Subsequently, the RSMs based on the results of the DOE have been generated. The low-fidelity aeroelastic workflow, as illustrated in Figure 5.31, has been used to conduct an extensive DOE involving one thousand data points for two distinct aerodynamic conditions specified in Table 5.9.

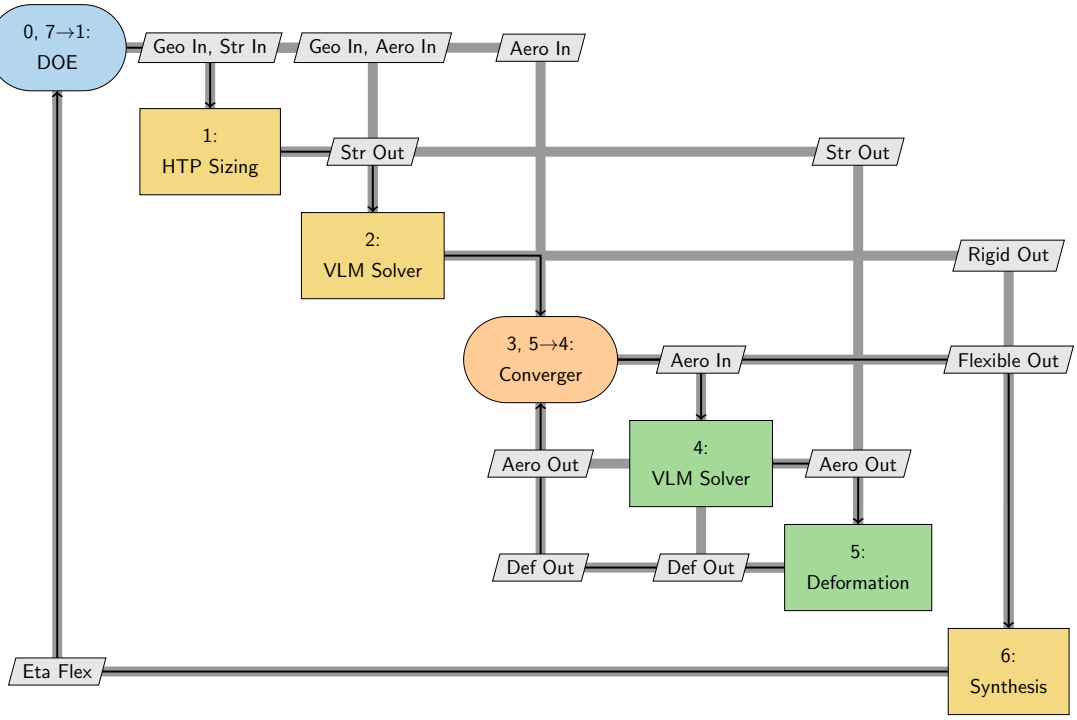

Figure 5.31: Automated DOE workflow for estimating the HTP elastic efficiency.

The DOE included variation of primary design parameters related to the tailplane. LHS was used to comprehensively sample the specified design space. A predictive model, using RBF, has been developed in the form of a response surface. This response surface enables the prediction of both the elastic efficiency parameter and the weight of the tailplane. The variables for the DOE and their corresponding ranges are detailed in Table 5.15. The results of the DOE, which where measured in terms of weight and elastic efficiency (defined as the ratio between the lift

curve slopes for the elastic and rigid configurations of the tailplane), have been visually depicted on response surfaces for both low-speed and high-speed conditions. Figure 5.32 shows graphical representations of the RSMs that were generated.

Table 5.15: DOE Variables and their range for the elastic efficiency parameter estimation.

Variable	Symbol	Lower Bound	Upper Bound
Tailplane Surface	S_H	11.70 m^2	52.89 m^2
Tailplane Sweep	Λ_{LE}	-30.00 deg	+ 30.00 deg
Tailplane Taper	λ	0.300	1.00
Tailplane Aspect Ratio	AR_H	2.160	9.825

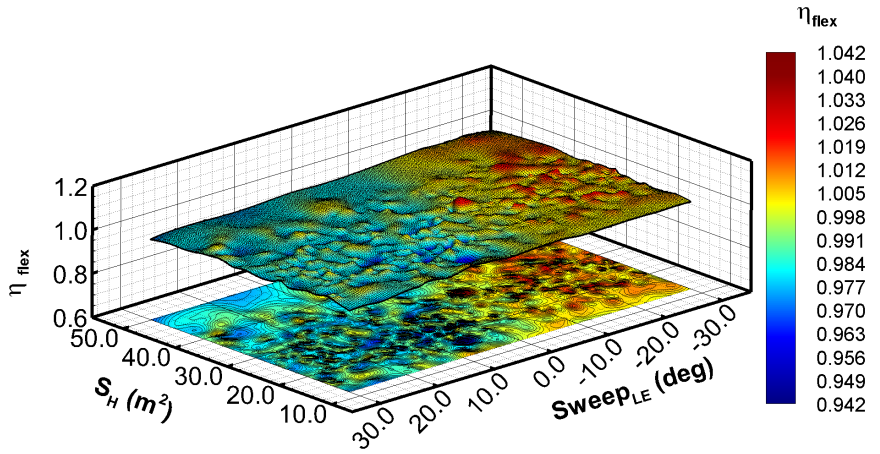

(a) Tailplane elastic efficiency in cruise conditions (Mach Number = 0.78 @FL390) vs. Sweep and AR of the tailplane.

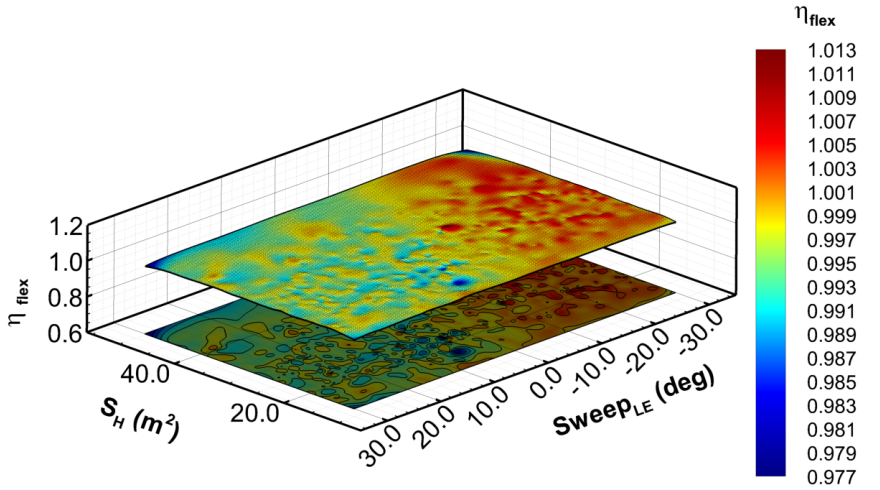

(b) Tailplane elastic efficiency in low-speed conditions (Mach number = 0.20 @FL0) vs. Sweep and AR of the tailplane.

Figure 5.32: Examples of RSM for the elastic efficiency parameter η_{flex}.

5.4.3 Aerostructural optimization Results

Utilizing the previously introduced RSM prediction models, a variety of optimization challenges can be formulated and executed through the optimization workflow illustrated in Figure 5.33. The goal of this workflow is to simplify the modeling and resolution of optimization problems that involve the outcomes produced by the previously mentioned RSM. The response surface inputs are used as design variables for the problem. Four response surfaces have been incorporated into this workflow. The first two relate to high-fidelity aerodynamic parameter predictions, one for high-speed conditions and another for low-speed conditions. The same holds true for the other two aero-structural response surfaces. The main goal of this toolchain is to optimize the aerodynamic and stability characteristics of the ARE concept by modeling its geometry and considering the impact of tailplane flexibility. Furthermore, the toolchain can be used for various other optimization tasks. The aero-structural optimization workflow has been developed, integrated, and implemented within the RCE environment. This approach has been implemented to effectively manage the input and output of each tool and to conveniently formulate various optimization problems. The RCE-embedded Dakota genetic algorithm has been used to conduct the optimization process.

Table 5.16 presents the geometric characteristics of the solution obtained from the optimization problem described in Table 5.14. A visual representation of this solution can be seen in Figure 5.34.

In this case, the optimal sweep angle is slightly lower compared to the pure aerodynamic optimization solution. Furthermore, an additional reduction in the tailplane surface area is achieved, resulting in a 4.0% decrease compared to the conventional HTP case. Additionally, the aspect ratio and taper ratio values are reduced compared to the previous optimization solution. The aerodynamic parameters of the body-horizontal configuration, related to the aero-structural rigid and flexible solutions, are documented in Table 5.17. Once again, there is a significant increase in the maximum negative lift coefficient of the tailplane. This increase is further accentuated when considering the flexible solution, due to the positive influence of the forward-swept configuration on aeroelastic behavior, as indicated by the elastic coefficient η_{flex} value. Consequently, the derivatives of the tailplane lift and moment coefficients are increased when considering the flexible solution, resulting in improved performance. In the aero-structural optimal solution, the body-horizontal drag coefficient is reduced for two out of four angles of attack. In the remaining cases, the reduction can be attributed to the formation of shock waves at high angles of incidence. Table 5.17 also provides information on the

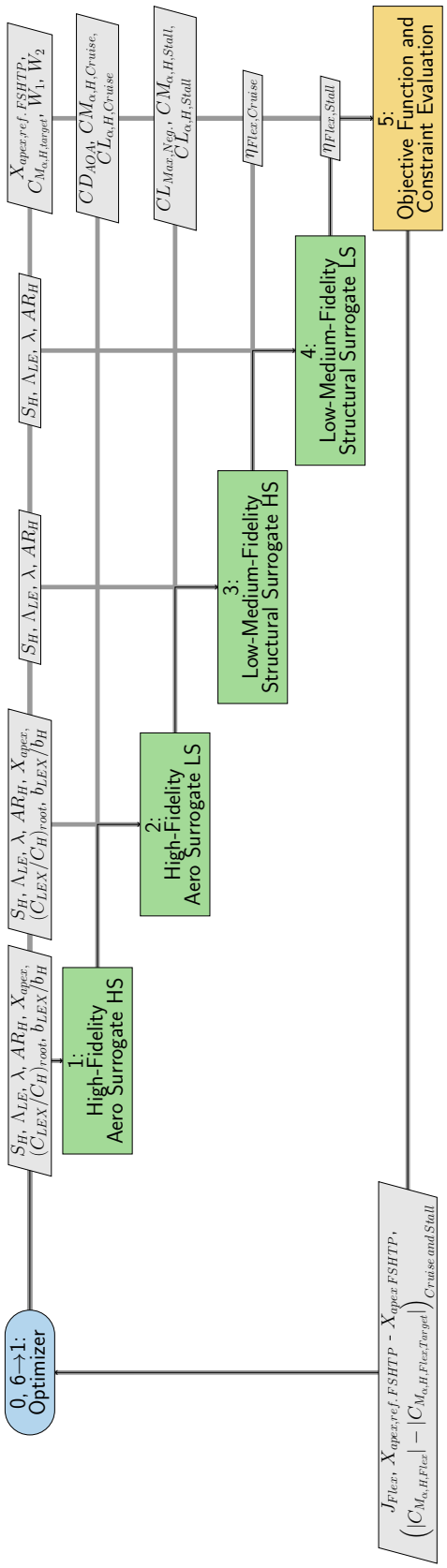

Figure 5.33: XDSM representing the Aerostructural Optimization executable workflow integrated in RCE enviroment.

total weight of the optimized and conventional solutions. As can be observed, a reduction of approximately 16% can be achieved by utilizing the forward-swept solution and reducing the dimensions of the tailplane.

Table 5.16: Comparison of the geometric characteristics of the flexible Optimization solution with respect to reference HTP and FSHTP.

Parameter	Ref. HTP	Flex. OPT
$\mathbf{AR_H}$	5.76	4.83 (-16%)
$(\mathbf{C_{LEX}/C_H})_{\mathbf{root}}$		1.985
$\mathbf{b_{LEX}/b_H}$		0.119
$\mathbf{S_H}$	31.36 m^2	30.11 m^2 (-4.0%)
$\mathbf{\Lambda_{LE}}$	32.00 deg	-7.45 deg
λ	0.336	0.335 (-0.3%)
$\mathbf{X_{Apex}}$	31.585 m	34.756 m (+10.0%)

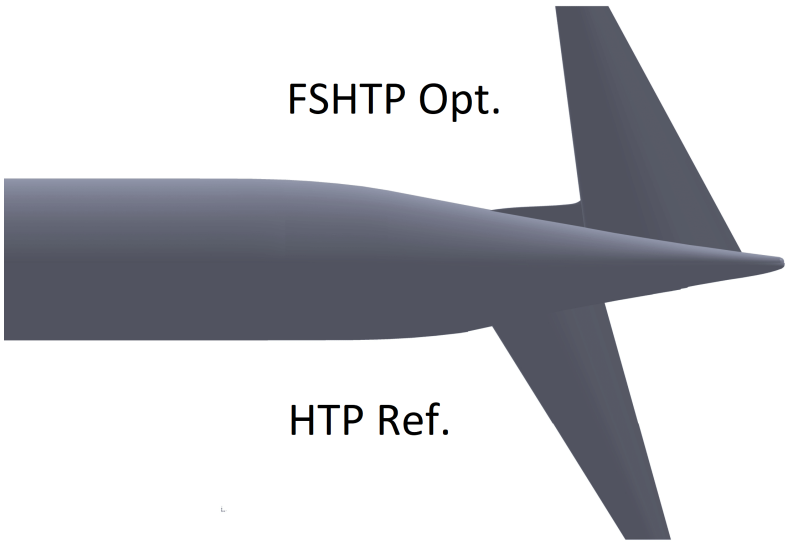

Figure 5.34: Comparison of the top views of the geometries of the flexible optimization problem and the reference conventional rear-end.

Table 5.17: Aerodynamics of flexible optimization solution vs. reference HTP. Data are referred to body-horizontal configuration. Aerodynamic conditions are described in Table 5.3.

Parameter	Ref. $\mathbf{HTP}_{Flex.}$	$\mathbf{OPT}_{Flex.}$	$\mathbf{\Delta}(\%)$
$\mathbf{CL_{max,H}}$ **negative**	-0.152	-0.181	**+19.01 %**
$\mathbf{CL_{max,H}}$ **negative flex.**	-0.149	-0.181	**+22 %**
$\mathbf{CD_{BH\,AOA=0deg}}$	0.0086	0.0084	**-2.42 %**
$\mathbf{CD_{BH\,AOA=2deg}}$	0.0085	0.0085	**-0.10 %**
$\mathbf{CD_{BH\,AOA=4deg}}$	0.0100	0.0107	**+7.24 %**
$\mathbf{CD_{BH\,AOA=-4deg}}$	0.0129	0.0131	**+1.74 %**
$\mathbf{CM_{\alpha,H}}$ **cruise**	-0.0707	-0.0692	**+2.18 %**
$\mathbf{CM_{\alpha,H}}$ **cruise flex.**	-0.0672	-0.0697	**+3.76 %**
$\mathbf{CM_{\alpha,H}}$ **low speed**	-0.0572	-0.0579	**+1.22 %**
$\mathbf{CM_{\alpha,H}}$ **low speed flex.**	-0.0561	-0.0580	**+3.52 %**
$\mathbf{CL_{\alpha,H}}$ **cruise**	0.0171	0.0169	**-1.32 %**
$\mathbf{CL_{\alpha,H}}$ **cruise flex.**	0.0162	0.0170	**+4.68 %**
$\mathbf{CL_{\alpha,H}}$ **low speed**	0.0145	0.0143	**-1.54 %**
$\mathbf{CL_{\alpha,H}}$ **low speed flex.**	0.0142	0.0143	**+0.70 %**
$\eta_{\mathbf{Flex}}$ **low speed**	0.9800	1.0023	**+2.28 %**
$\eta_{\mathbf{Flex}}$ **high speed**	0.9500	1.0077	**+6.07 %**
$\mathbf{W_{HTP}}$ **[Kg]**	555	467	**-16 %**

5.4.4 Multi-Objective Optimization: Requirements' Effect

This section investigates the impact of specific requirements on the final solution. The entire process outlined in this chapter has been executed once again, this time excluding certain requirements. This step was taken to demonstrate the flexibility of the process, showcasing its ability to automatically convert the requirements model into a new MDAO problem and workflow. The model excludes the following requirements.

- The HTP shall achieve at least reference HTP moment coefficient derivative for condition: pushover maneuver.
- The HTP shall match at least reference HTP moment coefficient derivative for condition: cruise condition.

After this modification, the optimization problem described in Table 5.14 has undergone minor adjustments. The optimization objectives and weights remain unchanged from those applied to the original optimization problem. The only difference lies in the exclusion of constraints on the derivative of the moment coefficient, which were generated from the excluded requirements. Furthermore, a multi-objective optimization has been conducted to tackle the optimization

issue. The only variation involves decomposing the optimization function J_{Flex} into two distinct functions: the sum of the drag coefficients at different angles of attack and the inverse function of the maximum flexible lift coefficient. The JPAD Optimizer was used as the optimization tool. Results from three different algorithms (GDE3, CellDE, and SMPSO) are presented. The utilization of various optimization algorithms led to the formation of the Pareto front, as depicted in Figure 5.35. The blue points represent the analyses required to conduct the optimization and define the design space of interest. Multiple Pareto fronts were generated from this set using the previously mentioned optimization algorithms. Figure 5.35 depicts the results obtained from three distinct algorithms.

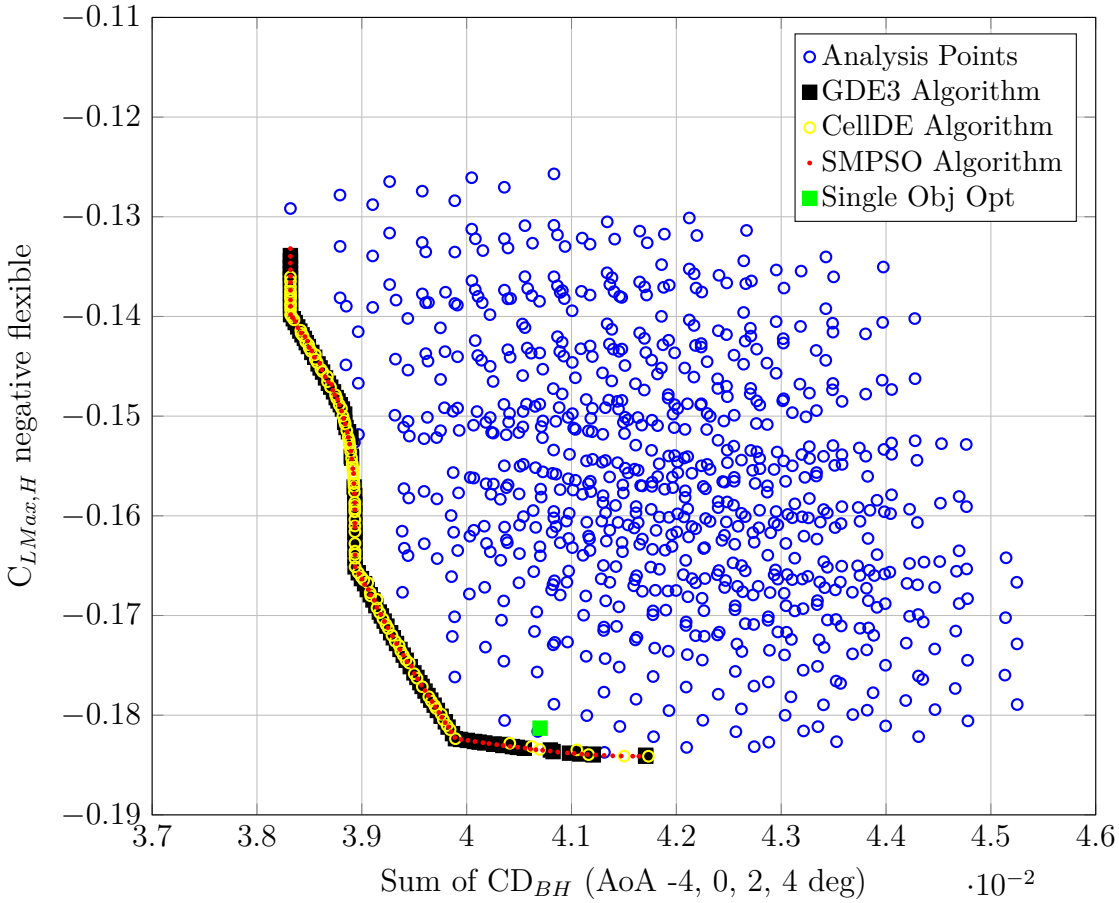

Figure 5.35: Flexible Optimization solution results. Comparison between single-objective solution and multi-objective pareto front results. Data are referred to body-horizontal configuration. Aerodynamic conditions are described in Table 5.3.

Noticeably, the results are quite similar, confirming the consistency of the final outcomes. The green dot represents the results of the single-objective optimization as shown in Table 5.17. This result was achieved by using specific weights for the two optimization objectives, and the solution is located near the Pareto frontier. This

implies that by using different weights, all the points that make up the frontier can be attained as potential solutions for the optimization problem outlined in Table 5.14.

Furthermore, to offer a clearer illustration of the impact of the excluded requirement, the multi-objective optimization was conducted by including the aforementioned requirement. Consequently, constraints were added to the derivatives of the moment coefficient. The results are displayed in Figure 5.36. It is evident that the Pareto frontier is significantly constrained to a limited area compared to unconstrained optimization. This reduction indicates that in order to meet the constraint on the moment coefficient, several solutions must be discarded, which prevents the achievement of lower drag values in cruise conditions. Consequently, all the analysis points located to the left of the Pareto frontier can be considered as points to be excluded due to the constraint on the moment coefficient.

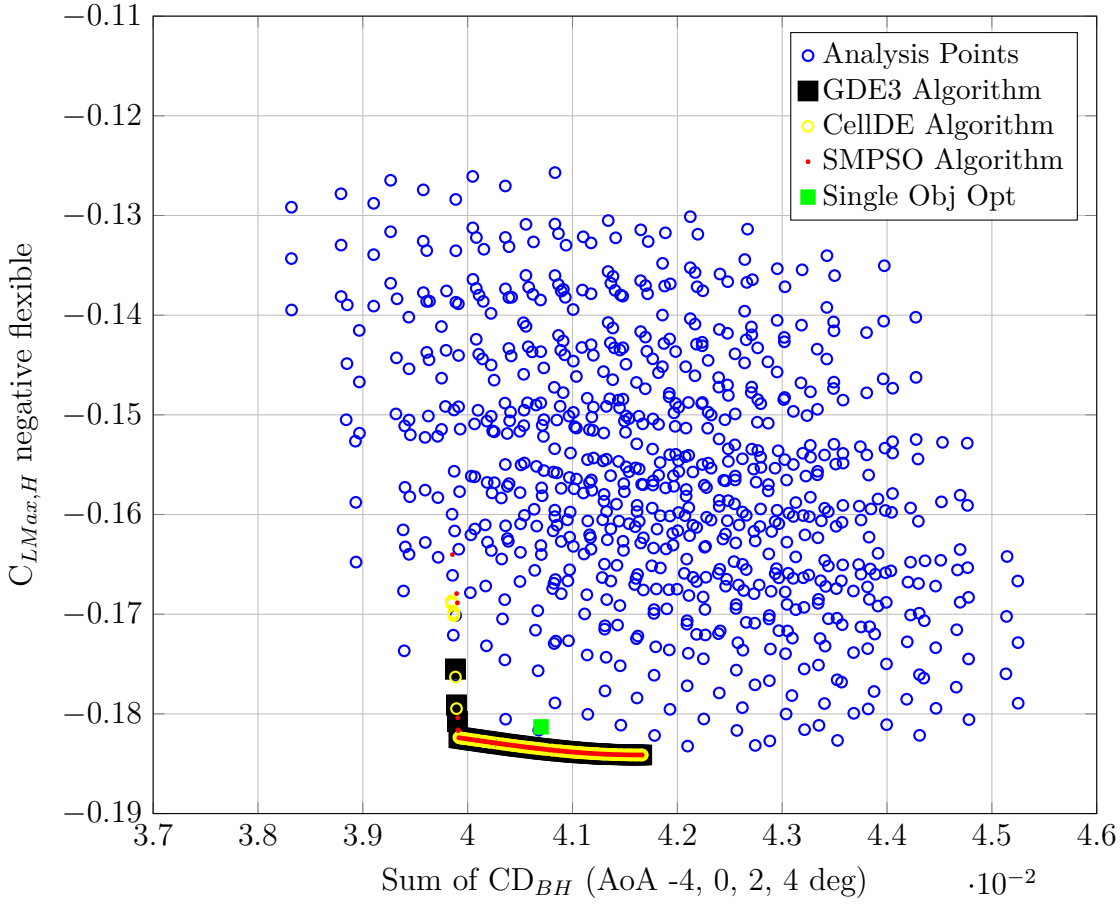

Figure 5.36: Constrained Flexible Optimization solution results. Comparison between single-objective solution and multi-objective pareto front results. Data are referred to body-horizontal configuration. Aerodynamic conditions are described in Table 5.3.

5.5 Aerostructural optimization including ice effect: MDAO Workflow and results

5.5.1 Aerostructural Optimization including Ice Effect: Problem Formulation

Upon creating the "Aerostructural ice optimization" test case with related design competences, parameters, and requirements, an aerostructural optimization problem incorporating ice effects was formulated and executed using a specialized optimization workflow integrated into the RCE environment. The optimization problem is detailed in Table 5.18.

Table 5.18: Aerostructural optimization problem including ice effects. Optimization function, variables, weights and constraints.

	Function/Variable
Minimize	$J_{Flex} = W_1 \left(\sum_{AOA=-4deg}^{AOA=4deg} \overline{CD}_{BH\,AOA}\right) + W_2 \left(\frac{1}{\lvert\overline{CL}_{max,neg.,H_{Flex}}\rvert}\right) +$
	$+W_3 \left(\Delta\overline{CL}_{Max,H,ICE}\right)$
With respect to	AR_H, S_H, Λ_{LE}, λ, X_{Apex}, $\frac{b_{LEX}}{b_H}$, $\frac{C_{Root,LEX}}{C_{Root,H}}$
Subject to	$\left(\lvert C_{M_{\alpha_{H,Flex}}}\rvert - \lvert C_{M_{\alpha_{H,,Flex,target}}}\rvert\right)_{cruise\,and\,stall} \geq 0$
	$X_{apex,reference\,FSHTP} - X_{apex\,FSHTP} \geq 0$
Where	$W_1 = W_2 = W_3 = 0.33$
	$X_{apex,ref.\,FSHTP} = 34.756\,m$
	$C_{M_{\alpha_{H,Flex,cruise,target}}} = -0.0672 deg^{-1}$
	$C_{M_{\alpha_{H,Flex,stall,target}}} = -0.0561 deg^{-1}$

The main goal of this optimization closely resembles the previous one, aiming to minimize the body-horizontal drag coefficient at four distinct angles of attack (-4, -2, 0, and 4 degrees) while simultaneously maximizing the tailplane's negative stall lift coefficient. In addition, the optimization takes into account the flexibility of the tailplane and aims to minimize the aerodynamic penalty caused by icing effects. Similar weighting, normalization, and constraints have been applied to this problem. Once the MDO problem is defined, along with its parameters, their roles are formalized within the OCE environment using KE-Chain, as illustrated in Figure 5.37.

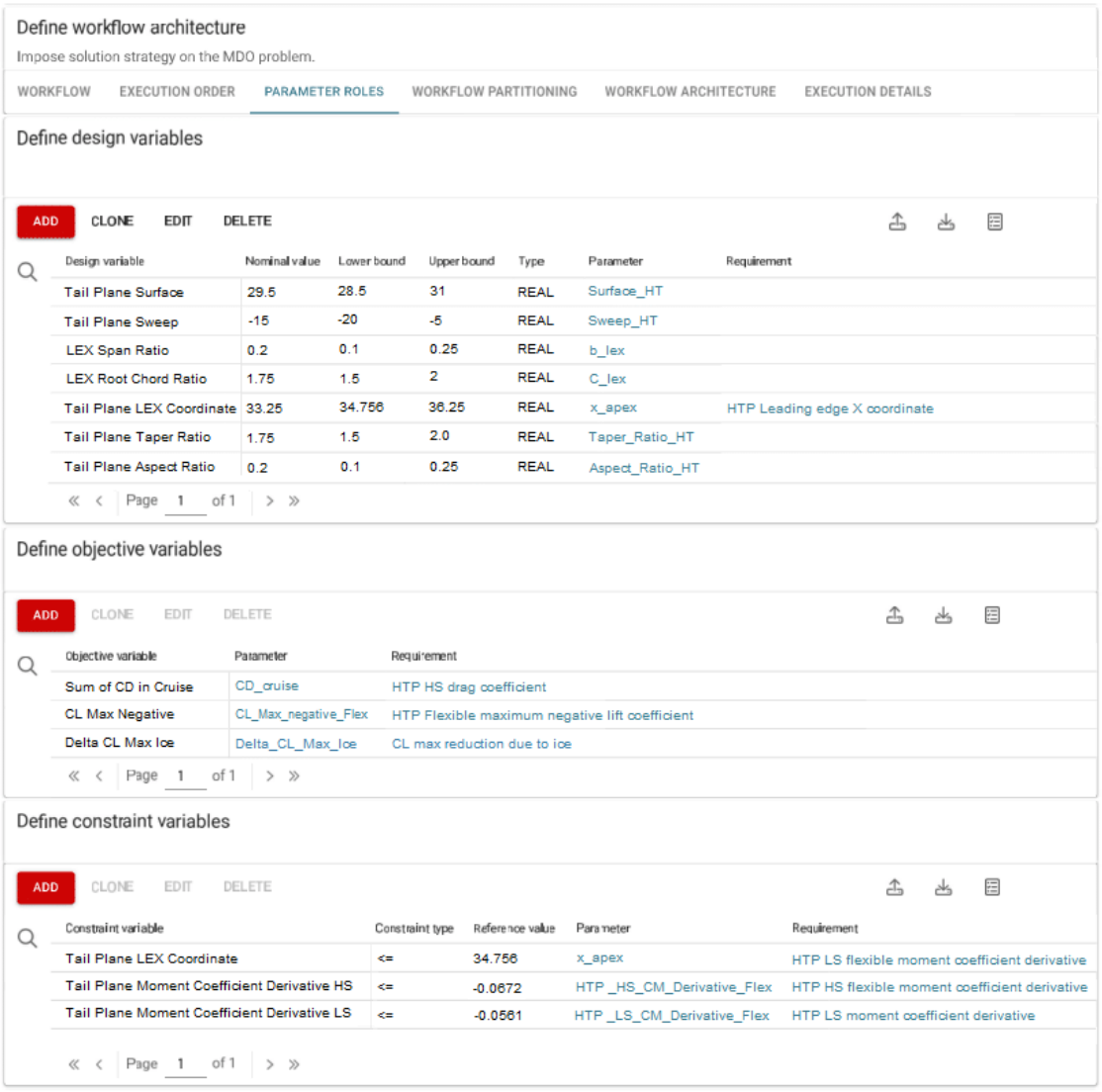

Figure 5.37: Parameters formalization executed in KE-Chain for Aerostructural ice optimization Test Case. Poor image quality due to acquisition from OCE.

Each parameter can be designated as a design variable, objective variable, or constraint by being inserted into a specific table. In the figure, the depicted parameters correspond to those outlined in Table 5.18. As shown in the diagram, each parameter representing an objective variable or a constraint is connected to a requirement that needs to be validated in the test case. Furthermore, as detailed in Sections 5.2.5 and 5.2.6, each parameter is also linked to a discipline and a specific variable in the CPACS file.

Finally, once the various optimization variables have been generated by KE-Chain, the MDAO workflow can be formulated. Figure 5.38 represents the XDSM generated through KADMOS and VISTOMS for the aerostructural ice optimization test case. In this case, the specified objective, variables, and constraints are not

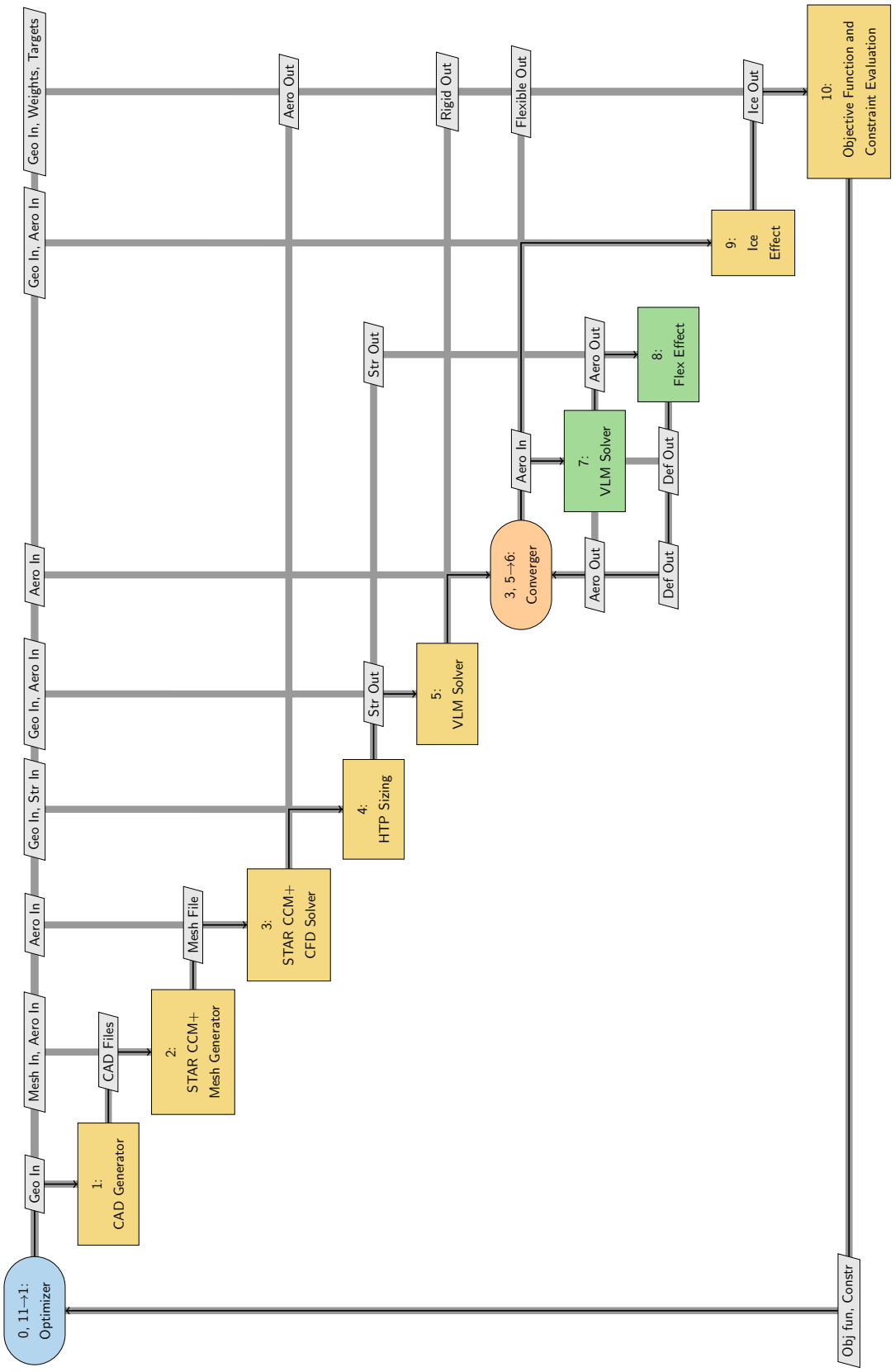

Figure 5.38: XDSM representing the MDAO workflow generated from the Aerostructural Ice Optimization test case.

highlighted in the diagram due to space limitations. The workflow closely resembles the one outlined in Section 5.4.1. It involves a high-fidelity method for calculating pure aerodynamic data. The data is then refined using results obtained from a low-fidelity approach specifically designed for FSI computations. Following this, the aerodynamic impact caused by ice accumulation is determined. A final block is used to calculate the objective function and constraints for the optimization.

5.5.2 Response Surface for Ice Effect on Aerodynamic

The workflow depicted in Figure 5.38 includes several high-fidelity CFD analyses, which are computationally intensive. In such a situation, the number of iterations required to compute an optimization can become prohibitive. For this reason, an additional RSM has been developed, distinct from those presented in the previous sections, to provide the possibility of solving the optimization problem within a reasonable amount of time. To achieve this, RSMs based on high-fidelity ice accretion results have been generated.

In-flight ice accretion analysis was conducted using Ansys FENSAP-ICE on different horizontal stabilizers with negative sweep, simulating the tail attached to a full-scale aircraft during a 45-minute holding pattern. Aerodynamic analyses of the iced tails were conducted using Ansys Fluent Aero, covering angles of attack ranging from 0° to -15°. The turbulence model used was the original version of the Spalart-Allmaras model, which includes the sand-grain roughness extension. A uniform roughness of 0.5 mm was applied to the iced surfaces during the RANS calculations. The flight conditions for this study involved a 45-minute holding pattern for a twin-engine jet airliner at an altitude of $16000ft$, with a V_{CAS} of $220knots$ ($TAS = 145m/s$), and a static temperature of $-12°C$. These data, along with the cloud conditions, LWC, and droplet Mean Volumetric Diameter (MVD), were chosen in accordance with FAR 25 Appendix C, which specifies $0.38g/m^3$ and 20 microns, respectively. The droplet size range was determined using a 7-bin Langmuir-D distribution. The aircraft was assumed to be in a configuration with retracted flaps and slats at an angle of attack of 4 degrees. Following the calculation of ICE accretion, Fluent was used to compute lift versus angle of attack curves for both clean and iced tails. For these calculations, the main wing was excluded in favor of a full fuselage and HTP configuration. The Navier-Stokes solver utilized node-based gradients and integrated all equations with a second-order spatial scheme. It employed a pseudo-time steady-state time integration with a time-stepping factor of 0.01. A maximum of 1000 time steps were set as the iteration limit for each

case. However, lower angles of attack reached convergence criteria much earlier. Additional information about the analysis can be found in reference [219].

Figure 5.39 illustrates a comparison of lift coefficient versus angle of attack plots for both clean and iced wings at three different sweep angles. In all three cases, there is a noticeable decrease in lifting performance under icing conditions, attributed to early separation.

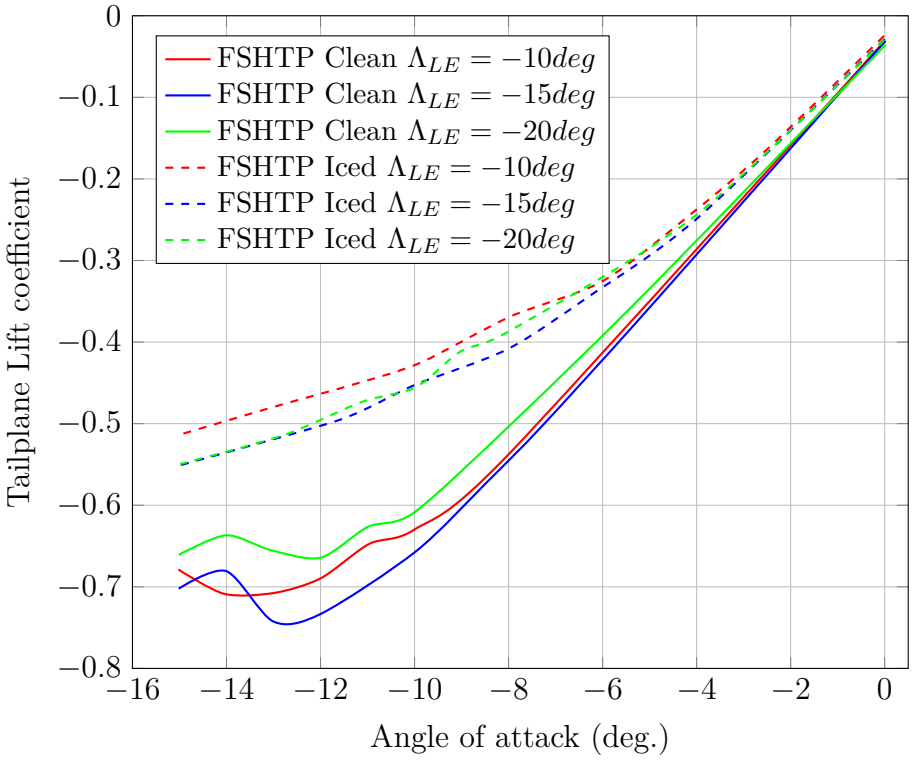

Figure 5.39: Lift curves for clean and iced HTP configurations with three different values of sweep angle. Adapted from [219].

The figure illustrates that increasing sweep angles reduces the early separation tendency along the span, resulting in an overall reduction of icing-related lift degradation at higher sweep angles. The results for clean wings show the expected linear relationship between lift coefficient and angle of attack, extending up to approximately -8° to -10°. Beyond this range, the gradient gradually diminishes until reaching the maximum lift coefficient. In contrast, the iced wings exhibit relatively smaller linear regions with gradients that are lower than those for clean wings. This effect diminishes further as the angle of attack becomes more negative. For aerodynamically efficient wings, the highest curve slope and maximum absolute lift coefficient are observed at intermediate sweep angles, while the lowest values of these properties are found at high sweep angles. After ice accretion, the lowest absolute lift coefficients are observed at low sweep angles, and the lift coefficients at

intermediate sweep angles appear to have decreased more than those for high sweep angles. The plots reveal a clear trend showing a reduced lift coefficient penalty at high sweep angles for all angles of attack, except those close to zero.

5.5.3 Aerostructural Optimization including Ice Effect Results

Utilizing the previously introduced RSM prediction models, a variety of optimization challenges can be formulated and executed through the specialized optimization workflow illustrated in Figure 5.40. The goal of this workflow is to simplify the modeling and resolution of optimization problems that involve the outcomes produced by the previously mentioned RSM. The response surface inputs are used as design variables for the problem. Five response surfaces have been incorporated into this workflow. The first two relate to high-fidelity predictions of aerodynamic parameters, one for high-speed conditions and another for low-speed conditions. The same applies to the other two aero-structural response surfaces. The final response surface is capable of predicting the aerodynamic penalty caused by icing effects in low-speed conditions. The primary goal of this toolchain is to optimize the aerodynamic and stability characteristics of the ARE concept, including the effects of icing, by modeling its geometry and accounting for the influence of tailplane flexibility. The aero-structural optimization workflow, including ice effects, has been developed, integrated, and implemented within the RCE environment. This approach has been implemented to effectively handle the input and output of each tool and to conveniently formulate various optimization problems. The RCE-embedded Dakota genetic algorithm has been used to conduct the optimization process.

Table 5.19 presents the geometric characteristics of the solution obtained from the optimization problem described in Table 5.18. A visual representation of this solution is depicted in Figure 5.41. In this instance, the optimal sweep angle is significantly lower compared to the previous aerodynamic optimization solution. This modification is necessary because the ice penalty is mainly influenced by the sweep angle of the final configuration. Furthermore, a significant reduction in the tailplane surface area has been achieved, resulting in a 4% decrease compared to the conventional HTP case. Additionally, the aspect ratio and taper ratio values have been increased compared to the previous optimization solution. The aerodynamic parameters of the rigid and flexible solutions are listed in Table 5.20. In this scenario, a significant increase in the maximum negative lift coefficient of the tailplane is achieved. The benefit becomes more apparent when considering the lift and moment

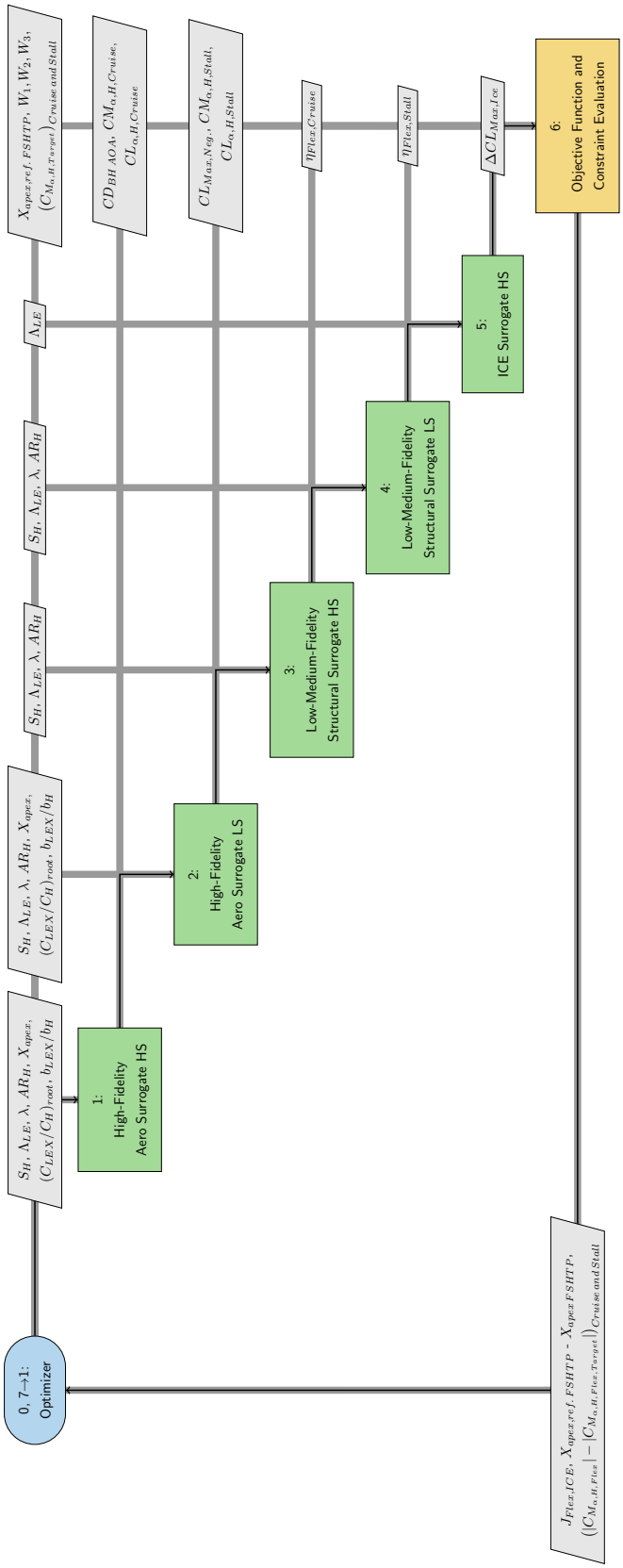

Figure 5.40: XDSM representing the Aerostructural Optimization executable workflow including ice effect. The workflow is integrated in RCE enviroment.

coefficient derivatives in both rigid and flexible solutions, which leads to improved performance. The body-horizontal drag coefficient is reduced for two out of four angles of attack. In the remaining cases, the reduction can be attributed to the formation of shock waves at high angles of incidence. Table 5.20 also provides information on the total weight of the optimized and conventional solutions. As can be observed, a reduction of approximately 10% can be achieved by utilizing the forward-swept solution and by reducing the dimensions of the tailplane.

Table 5.19: Comparison of the geometric characteristics of the flexible Optimization solution with respect to reference HTP and FSHTP.

Parameter	Ref. HTP	Flex. OPT
$\mathbf{AR_H}$	5.76	5.93 (+2.92%)
$(\mathbf{C_{LEX}/C_H})_{\mathbf{root}}$		1.933
$\mathbf{b_{LEX}/b_H}$		0.139
$\mathbf{S_H}$	31.36 m^2	30.12 m^2 (-3.95%)
$\mathbf{\Lambda_{LE}}$	32.00 *deg*	-19.55 *deg*
λ	0.336	0.405 (+21%)
$\mathbf{X_{Apex}}$	31.585 m	34.756 m (+10%)

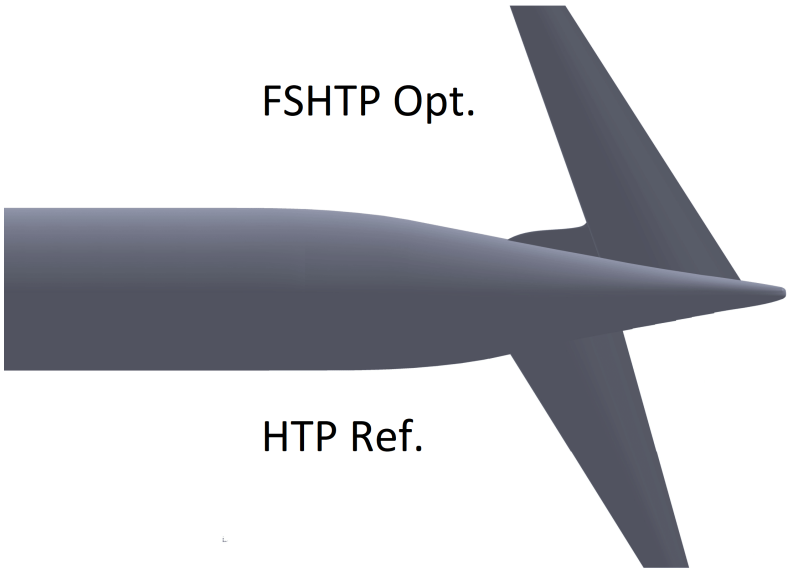

Figure 5.41: Comparison of the top views of the geometries of the flexible optimization problem including ice effect and the reference conventional rear-end.

In Table 5.21, a summary of the primary geometric and aerodynamic parameters from the previously presented optimization solutions is provided. Additionally, data for the conventional HTP reference is included. Figure 5.42 illustrates the geometry of the configurations achieved through the optimization of the FSHTP

Table 5.20: Aerodynamics of flexible optimization solution with ice effect vs. reference HTP. Data are referred to body-horizontal configuration. Aerodynamic conditions are described in Table 5.3.

Parameter	Ref. $\mathbf{HTP}_{Flex.}$	$\mathbf{OPT}_{Flex.,ice}$	$\Delta(\%)$
$\mathbf{CL_{max,H}}$ **negative**	-0.152	-0.171	**+12.70 %**
$\mathbf{CL_{max,H}}$ **negative flex.**	-0.149	-0.172	**+15.70 %**
$\mathbf{CD_{BH\,AOA=0deg}}$	0.0086	0.0085	**-0.95 %**
$\mathbf{CD_{BH\,AOA=2deg}}$	0.0085	0.0086	**+0.97 %**
$\mathbf{CD_{BH\,AOA=4deg}}$	0.0100	0.0110	**+9.63 %**
$\mathbf{CD_{BH\,AOA=-4deg}}$	0.0129	0.0141	**+9.30 %**
$\mathbf{CM_{\alpha,H}}$ **cruise**	-0.0707	-0.0736	**+4.10 %**
$\mathbf{CM_{\alpha,H}}$ **cruise flex.**	-0.0672	-0.0752	**+11.92 %**
$\mathbf{CM_{\alpha,H}}$ **low speed**	-0.0572	-0.0607	**+6.18 %**
$\mathbf{CM_{\alpha,H}}$ **low speed flex.**	-0.0561	-0.0611	**+9.04 %**
$\mathbf{CL_{\alpha,H}}$ **cruise**	0.0171	0.0187	**+9.16 %**
$\mathbf{CL_{\alpha,H}}$ **cruise flex.**	0.0162	0.0191	**+17.37 %**
$\mathbf{CL_{\alpha,H}}$ **low speed**	0.0145	0.0155	**+6.69 %**
$\mathbf{CL_{\alpha,H}}$ **low speed flex.**	0.0142	0.0156	**+9.56 %**
$\eta_{\mathbf{Flex}}$ **low speed**	0.9800	1.0064	**+2.69 %**
$\eta_{\mathbf{Flex}}$ **high speed**	0.9500	1.0214	**+7.52 %**
$\mathbf{W_{HTP}}$ **[Kg]**	555	502	**-9.55 %**
$\mathbf{\Delta CL_{Max,H,ICE}}$		-0.1226	

solution and the reference HTP. Regarding the geometry of the solutions, certain variables, such as the root chord ratio, show similar values, suggesting optimal performance for all introduced optimization functions. The surface area consistently decreases compared to the conventional tailplane, resulting in a reduction of more than $1\,m^2$. This reduction is a key factor contributing to the decrease in the body-horizontal drag coefficient at low angles of incidence. However, at higher angles of incidence, the presence of LEX leads to an increased tailplane drag coefficient due to the generation of shock waves. The negative sweep angle is approximately $-7.5\,deg$ for both the aerodynamic and aerostructural solutions. In the scenario considering icing effects, this value decreases to approximately $-20.0\,deg$ due to the beneficial impact of sweep on the aerodynamic penalty caused by icing accretion. Conversely, a greater sweep angle results in a reduced tailplane stall lift coefficient. Nevertheless, this coefficient still improves compared to the conventional HPT because of the presence of LEX. Parameters related to tailplane moment and lift coefficients consistently show improvement, especially in the flexible solution, as evidenced by the η_{flex} parameters. The optimized solution results in a reduced total weight, achieved by utilizing the forward-swept configuration and reducing

Table 5.21: Optimization solutions versus reference HTP. Data are referred to body-horizontal configuration. Aerodynamic conditions are described in Table 5.3.

Parameter	Ref. $\mathbf{HTP}_{Flex.}$	$\mathbf{OPT}_{Rigid}$	$\mathbf{OPT}_{Flex.}$	$\mathbf{OPT}_{Flex.,ice}$
$\mathbf{AR_H}$	5.76	5.07	4.83	5.93
$(\mathbf{C_{LEX}/C_H})_{\mathbf{root}}$		1.969	1.985	1.933
$\mathbf{b_{LEX}/b_H}$		0.107	0.119	0.139
$\mathbf{S_H}$ (m^2)	31.36	30.24	30.11	30.12
$\mathbf{\Lambda_{LE}}$ (deg)	32.00	-7.82	-7.45	-19.55
λ	0.336	0.400	0.335	0.405
$\mathbf{X_{Apex}}$ (m)	31.585	34.756	34.756	34.756
$\mathbf{CL_{max,H}}$ **negative**	-0.152	-0.179	-0.181	-0.171
$\mathbf{CL_{max,H}}$ **negative flex.**	-0.149		-0.181	-0.172
$\mathbf{CD_{BH\,AOA=0deg}}$	0.0086	0.0084	0.0084	0.0085
$\mathbf{CD_{BH\,AOA=2deg}}$	0.0085	0.0086	0.0085	0.0086
$\mathbf{CD_{BH\,AOA=4deg}}$	0.0100	0.0109	0.0107	0.0110
$\mathbf{CD_{BH\,AOA=-4deg}}$	0.0129	0.0132	0.0131	0.0141
$\mathbf{CM_{\alpha,H}}$ **cruise**	-0.0707	-0.0746	-0.0692	-0.0736
$\mathbf{CM_{\alpha,H}}$ **cruise flex.**	-0.0672		-0.0697	-0.0752
$\mathbf{CM_{\alpha,H}}$ **low speed**	-0.0572	-0.0617	-0.0579	-0.0607
$\mathbf{CM_{\alpha,H}}$ **low speed flex.**	-0.0561		-0.0580	-0.0611
$\mathbf{CL_{\alpha,H}}$ **cruise**	0.0171	0.0178	0.0169	0.0187
$\mathbf{CL_{\alpha,H}}$ **cruise flex.**	0.0162		0.0170	0.0191
$\mathbf{CL_{\alpha,H}}$ **low speed**	0.0145	0.0149	0.0143	0.0155
$\mathbf{CL_{\alpha,H}}$ **low speed flex.**	0.0142		0.0143	0.0156
$\eta_{\mathbf{Flex}}$ **low speed**	0.9800		1.0023	1.0064
$\eta_{\mathbf{Flex}}$ **high speed**	0.9500		1.0077	1.0214
$\mathbf{W_{HTP}}$ **[Kg]**	555	489	467	502
$\mathbf{\Delta CL_{Max,H,ICE}}$				-0.1226

the dimensions of the tailplane. As observed from the table, the sweep angle, taper ratio, and aspect ratio are the variables that most significantly influence the total weight of the horizontal tailplane. This occurs because an increase in the values of these variables leads to higher loads on the tailplane structure.

It is essential to emphasize that the three optimization solutions originate from different test cases defined within the OCE. Table 5.21 clearly shows that certain output parameters are missing for specific solutions. This result is achieved by associating each test case with specific requirements, and only computing parameters linked to these requirements. Consequently, each solution excels in different parameters, showcasing the diverse optimizations achieved for the specified test cases.

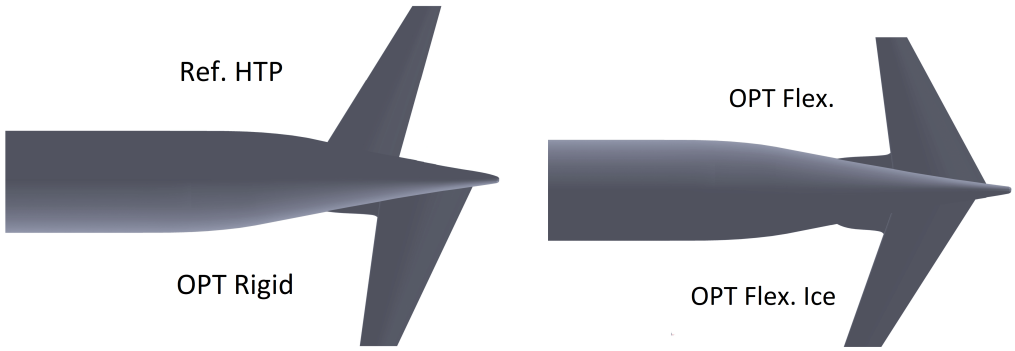

(a) Reference HTP Vs Pure Aerodynamic Opt. solution.

(b) Aerostructural Opt. Vs Aerostructural Opt. including ice effect solutions.

Figure 5.42: Comparison between optimization solutions and reference HTP.

5.5.4 Multi-Objective Optimization: Requirements' Effect

The impact of specific requirements on the final solution is now being investigated, as presented in section 5.4.4. The entire process outlined in this chapter has been executed once again, excluding the same requirements highlighted in section 5.4.4. After this modification, the optimization problem described in Table 5.18 has undergone minor adjustments. The optimization objectives and weights remain unchanged as they were applied to the original optimization problem. The only difference lies in the exclusion of constraints on the tailplane moment coefficient derivative, which were derived from the excluded requirements. Additionally, a multi-objective optimization has been conducted to tackle the optimization problem. The main distinction is in decomposing the optimization function J_{Flex} into three separate functions: the sum of the tailplane drag coefficients at various angles of attack, the inverse function of the maximum flexible lift coefficient of the tailplane, and the aerodynamic penalty resulting from an ice accretion scenario. The JPAD Optimizer was used as the optimization tool. Three different algorithms (GDE3, CellDE, and SMPSO) were utilized, leading to the Pareto front depicted in Figure 5.43.The blue points represent the analyses required to conduct the optimization and define the design space of interest. Multiple Pareto fronts were generated from this set using the optimization algorithms mentioned above. Figure 5.43 depicts the results obtained from three distinct algorithms. Notably, the results are quite similar, confirming the consistency of the final results. The main difference compared to the previous optimization is that when the sum of drag coefficients equals 0.039, the Pareto front is divided into two distinct frontiers. This division arises from the inclusion of a third objective function in the problem. The Pareto front with the lowest value of the negative maximum lift coefficient contains solutions that are similar to

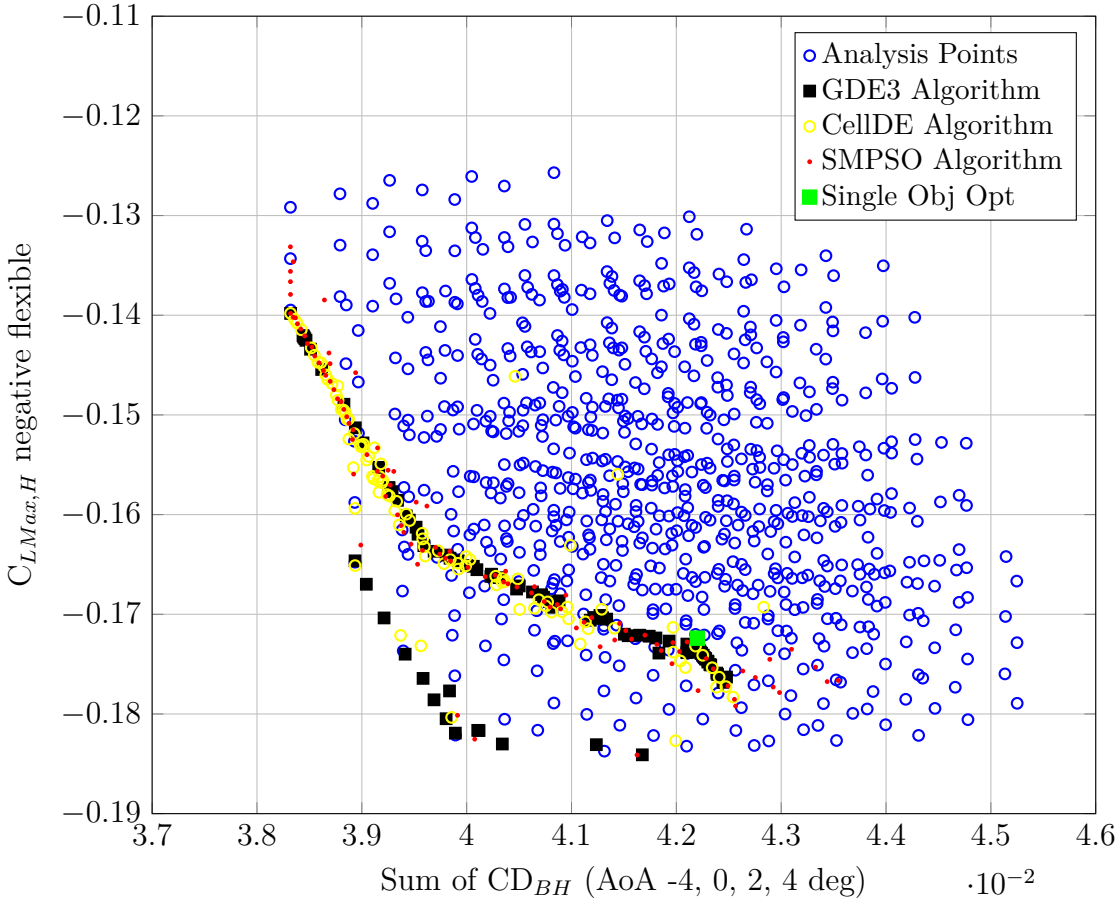

Figure 5.43: Flexible Optimization including ice effect results. Comparison between single-objective solution and multi-objective pareto front results. Data are referred to body-horizontal configuration. Aerodynamic conditions are described in Table 5.3.

the ones obtained in the previous optimization. The other branch of the Pareto frontier represents the optimal point considering the ice penalization conditions. The green dot represents the results of the single-objective optimization as shown in Table 5.17. This result was achieved by using specific weights for the three optimization objectives, and the solution is located near the Pareto frontier. This implies that by using different weights, all the points that make up the frontier can be attained as potential solutions for the optimization problem outlined in Table 5.18.

Furthermore, to better illustrate the impact of the excluded requirement, the multi-objective optimization was conducted by including the previously excluded requirement. Consequently, constraints were added to the derivatives of the moment coefficient. The results are displayed in Figure 5.44. As can be observed, the Pareto frontier is shifted towards a higher value of the drag coefficient in cruise conditions. This implies that in order to meet the constraint on the moment coefficient, a higher drag value during cruise must be accepted. As a result, all the analysis points

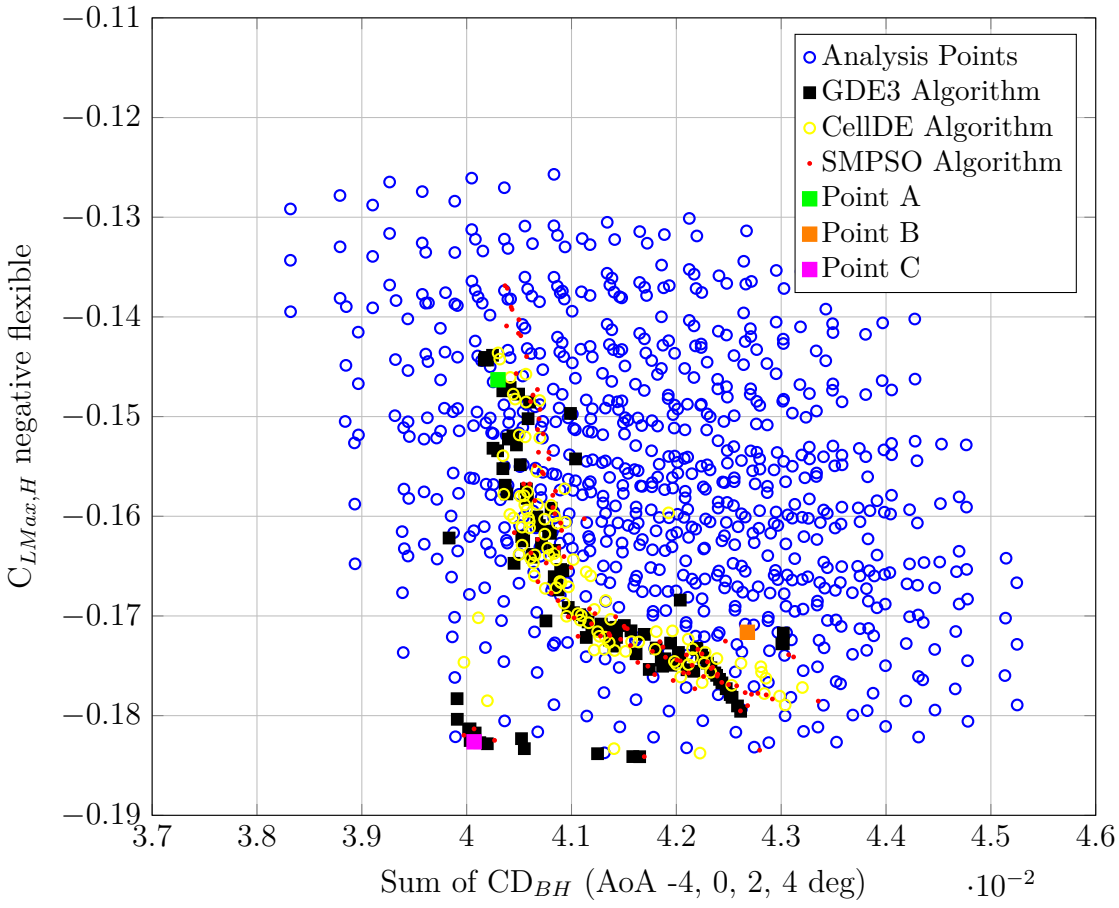

Figure 5.44: Constrained Flexible Optimization including ice effect results. Comparison between single-objective solution and multi-objective Pareto front results. Data refer to body-horizontal configuration. Aerodynamic conditions are described in Table 5.3. Points A, B, and C are detailed in Table 5.22.

Table 5.22: Characteristics of Points A, B, and C illustrated in Figure 5.44.

Parameter	Point A	Point B	Point C
$\mathbf{AR_H}$	5.12	5.73	4.13
$\mathbf{(C_{LEX}/C_H)_{root}}$	1.989	1.993	1.978
$\mathbf{b_{LEX}/b_H}$	0.109	0.114	0.112
$\mathbf{S_H}$ (m^2)	28.67	31.03	30.96
$\mathbf{\Lambda_{LE}}$ (deg)	-15.40	-19.84	-5.12
λ	0.331	0.336	0.338
$\mathbf{X_{Apex}}$ (m)	34.756	34.756	34.756
$\mathbf{CL_{max,H}}$ **negative flex.**	-0.146	-0.172	-0.183
Sum of $\mathbf{CD_{BH\,AOA=-4,0,2,4deg}}$	0.0403	0.0427	0.0401
$\mathbf{\Delta CL_{Max,H,ICE}}$	-0.148	-0.119	-0.201

located to the left of the Pareto frontier can be considered for exclusion due to the constraint on the moment coefficient. In addition, Figure 5.44 contains three points taken from the depicted Pareto front. The purpose of this representation is to provide an example of a potential optimal solution achieved through multi-objective optimization. More detailed characteristics of these solutions can be found in Table 5.22. As previously explained, Point B belongs to the section of the Pareto front with a lower value of aerodynamic penalty caused by ice accretion. Points A and C represent solutions with a lower drag coefficient value during cruise. The first option has a favorable icing aerodynamic penalty, while the second option has a higher maximum lift coefficient.

5.6 Aerostructural adjoint optimization: MDAO Workflow and results

5.6.1 Aerostructural adjoint optimization: Problem Formulation

Upon generating the "Aerostructural adjoint optimization" test case with associated design competences, parameters, and requirements, the initial rigid optimization problems were formulated and executed using a specialized optimization workflow integrated into the RCE environment. The aerostructural optimization problem is described in Table 5.23.

Table 5.23: Adjoint based Aerostructural optimization problem. Optimization function, variables, weights and constraints.

	Function/Variable
Minimize	$J = \beta_1 C_{D,H} + W_{HTP}$
With respect to	Λ_{LE}, $\mathbf{u}^*$, t
Subject to	$\mathbf{g}_j^{IDF} = \mathbf{u}^* - \mathbf{u} = 0$
	$-20deg \leq \Lambda_{LE} \leq -10deg$
	$3mm \leq t \leq 10mm$
Where	$\beta_1 = 10^4$

The optimization problem is similar to the generic one presented in Equation 4.21c. β_1 is an arbitrary weight, which is set to 10^4. This decision is made to

express the drag coefficient and, more importantly, to keep it at a comparable order of magnitude with the structural weight. The spar thickness, t, has been included as a design variable representing the thickness of all three spars modeled in the wingbox use case. It is assumed to be constant across the wingspan and initially set to 5 mm. The reduction in weight is achieved by decreasing the spar thickness, but this results in increased flexibility and, consequently, structural stresses. Typically, imposing a constraint on the maximum stress would address this issue. However, it has been observed that the maximum Von-Mises stress across the wingbox does not exceed the yield strength of aluminum within the specified boundaries of the design variables. For this optimization test case, the sweep angle ranges from -20 to -10 degrees, while the optimal spar thickness is sought within 3 and 7 mm.

Once the MDO problem is defined, along with its parameters, their roles are formalized within the OCE environment using KE-Chain, as illustrated in Figure 5.45. Each parameter can be designated as a design variable, objective variable, or constraint by being inserted into a specific table. In the figure, the depicted parameters correspond to those outlined in Table 5.23. As shown in the diagram, each parameter representing an objective variable or a constraint is connected to a requirement that needs to be validated in the test case. In this scenario, the constraint is not associated with a specific requirement because its role is not to fulfill a particular requirement. The consistency constraint has been incorporated to steer the adjoint optimizer toward a solution with physical significance. A similar rationale is applied to the structural surrogate variables; they are included to enforce the consistency constraint. This design variable is represented by a vector containing both rotational and translational variables. Consequently, no boundaries are established in the OCE for this variable. Furthermore, as detailed in Sections 5.2.5 and 5.2.6, each parameter is also linked to a discipline and a specific variable in the CPACS file.

Finally, once the various optimization variables have been generated by KE-Chain, the MDAO workflow can be formulated. Figure 5.46 represents the XDSM generated through KADMOS and VISTOMS for the aerostructural adjoint optimization test case. A multidisciplinary workflow has been employed to solve the aerostructural problem just presented. The design process is guided by a gradient-based algorithm, and three high-fidelity disciplines are carried out simultaneously. A synthesis function is used to compute the objective function and all the gradients necessary for the optimizer. As depicted in the diagram, only the CFD solver receives surrogate structural displacements as input, while the FEA solver does not require surrogate loads, owing to its internal DLM aerodynamics.

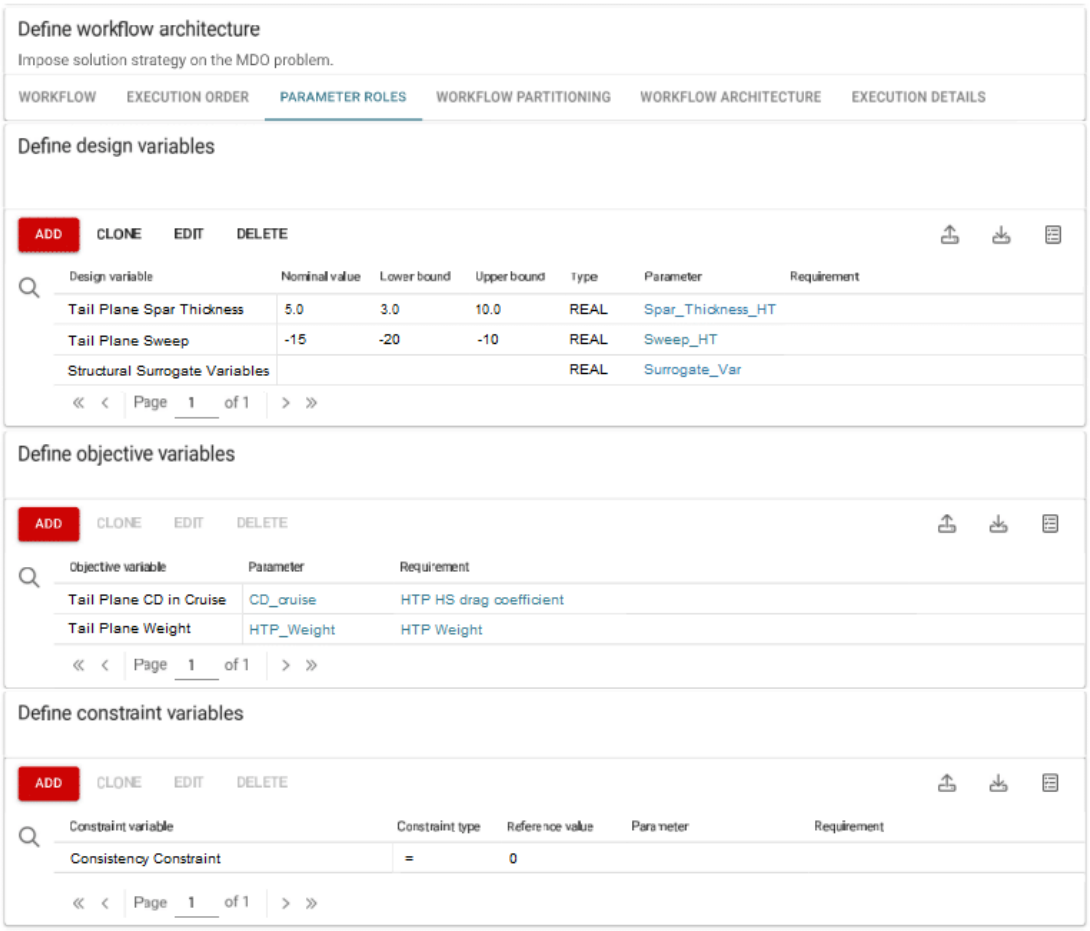

Figure 5.45: Parameters formalization executed in KE-Chain for Aerostructural adjoint optimization Test Case. Poor image quality due to acquisition from OCE.

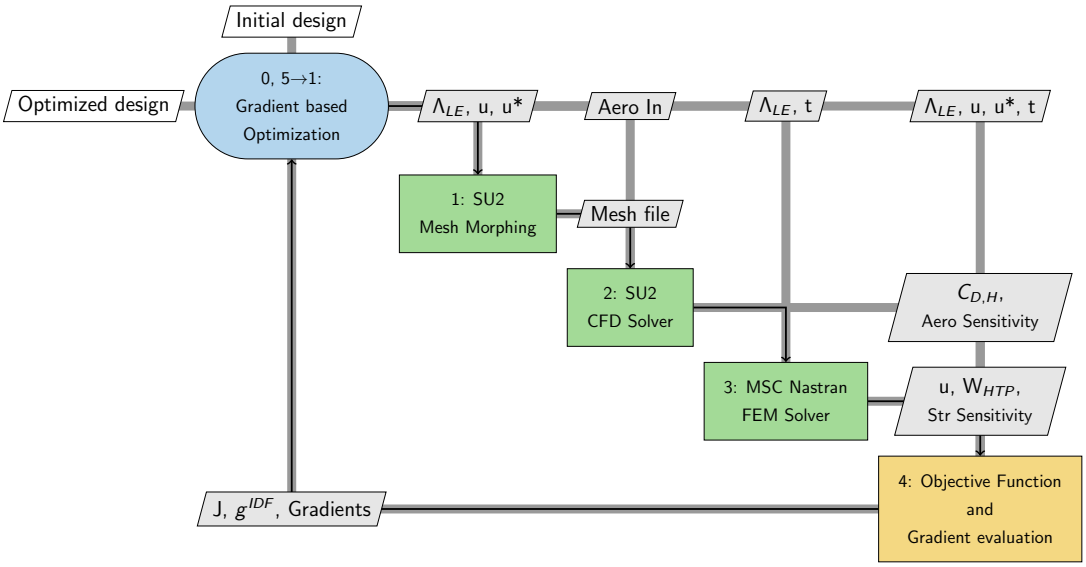

Figure 5.46: XDSM representing the MDAO workflow generated from the Adjoint based Aerostructural optimization test case.

5.6.2 Aerostructural adjoint optimization Results

Figure 5.47 displays both the CFD mesh and the FEM generated for the geometry presented in Section 5.1. The analyses presented in this section will be conducted using these two models. As previously mentioned, the isolated FSHTP has been considered for the evaluations. The CFD mesh is an Eulerian mesh consisting of approximately 1,000,000 cells. The FEM of the wingbox, which is designed with three spars and no ribs, includes shell elements to represent the skins and the spars, while beam elements are utilized to simulate stringers and spar caps. The first spar is located at approximately 15% of the wing chord to meet certification requirements for bird strike protection, while the rear spar is positioned at 55% of the chord due to manufacturing constraints associated with the sizing of the control surfaces and their actuators, which are not included in this model. The visible FEM is underpinned by the structural line, which is introduced to support the definition of structural surrogates in the IDF approach. The external wingbox grid points are interconnected using RBE2 elements in MSC Nastran software, which define a rigid body connection.

Firstly, the results of the derivative of the tailplane drag coefficient with respect to the sweep angle are presented. These calculations are performed based on Equation 4.23, which depends on the evaluation of the surface sensitivity using the discrete adjoint solver provided in the SU2 software. The optimizer requires these gradients to guide the design towards minimizing the objective function while satisfying all constraints. Figure 5.48 illustrates the distribution of the surface sensitivity of the drag and lift coefficients, respectively, in comparison with the distribution of the pressure coefficient. These results were obtained using the numerical setup outlined in Table 5.3, under Eulerian conditions. The distribution of C_p from the CFD solver indicates the presence of a shock wave, extending over nearly two-thirds of the wingspan. The flow structure is reflected in the distribution of the drag surface sensitivity, which is significantly higher in the vicinity of areas with a large pressure gradient. This indicates that in these areas, the drag coefficient will be highly responsive to a perturbation of the geometry.

Following this, gradients are computed with respect to surrogate design variables that represent the vertical displacements and axial rotations of the structural line. These gradients are derived from projecting the surface sensitivity onto the geometry perturbation and have been compared to the results obtained from an FD scheme, in which the mesh is warped by displacing a single node of the structural line at a time. Figures 5.49a and 5.49b illustrate the gradients of the vertical displacements and axial rotations of the nodes along the structural line, respectively. The nodes are

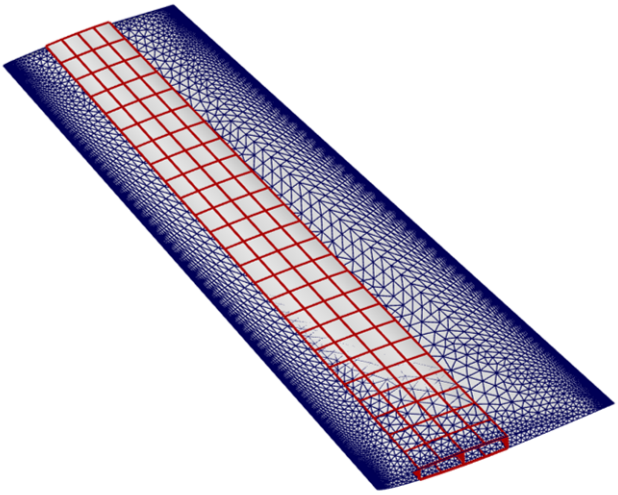

Figure 5.47: CFD mesh and FEM of the horizontal tailplane.

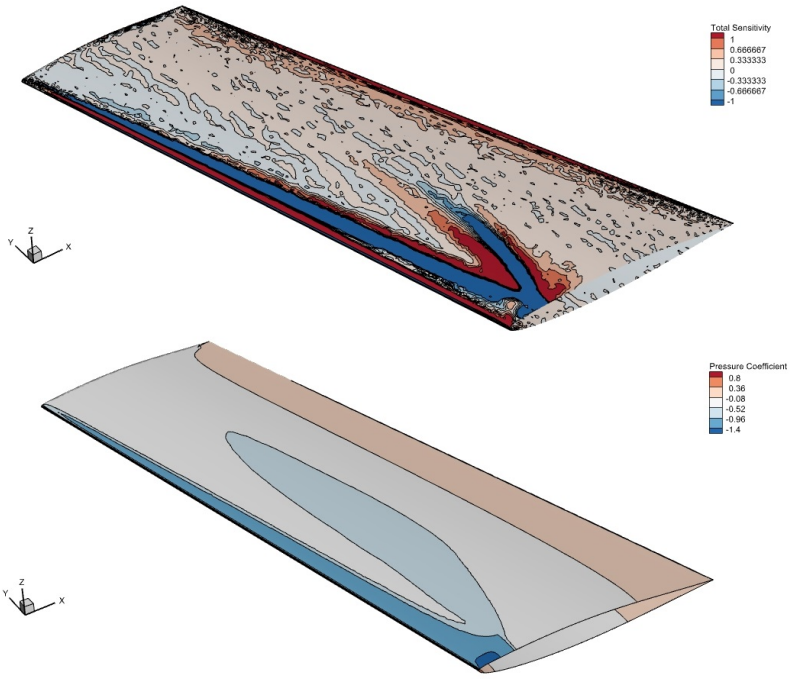

Figure 5.48: Surface sensitivity of C_D on the upper figure, and C_p distribution on the lower figure. Flow conditions summarized in Table 5.9.

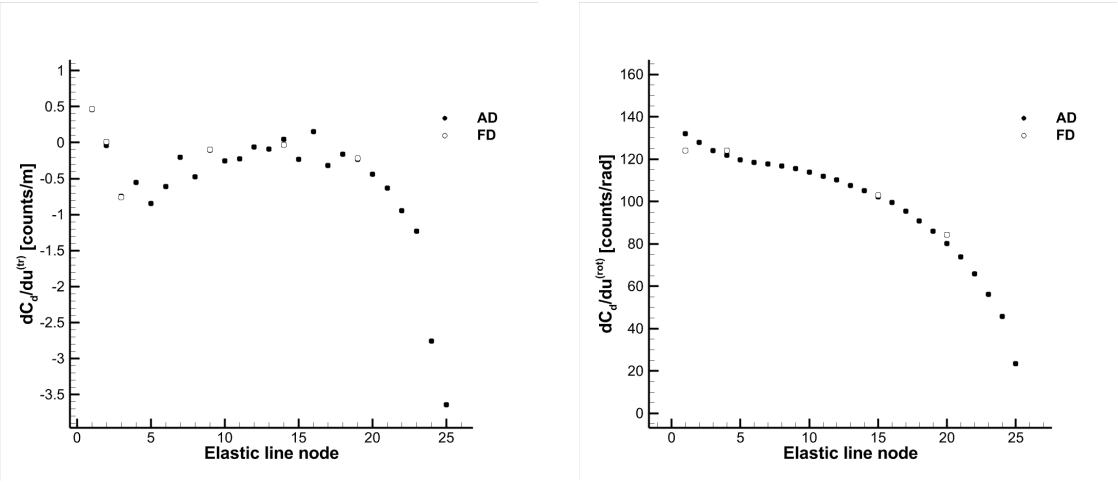

(a) Vertical translations. **(b)** Axial rotations.

Figure 5.49: Drag coefficient derivative with respect to structural degrees of freedom. Flow conditions summarized in Table 5.9.

located at 25 equally spaced positions across the wingspan, and they are numbered in plots according to their increasing span-wise position. Both trends are in good agreement with the benchmark FD results. Furthermore, especially with regard to the impact of axial rotation, the decreasing trend towards the wingtip seems plausible as it follows an almost elliptical distribution of pressure.

In relation to the consistency constraint, the derivative of the structural degrees of freedom of interest with respect to the sweep angle is computed. As explained in Section 4.3.1, this is accomplished using a traditional FD scheme. The static aeroelastic response is evaluated using MSC Nastran software for a sweep angle incremented by a chosen, relatively small step size, and then compared to the response for the current design. Finally, the derivatives of the structural weight are computed using an FD scheme. For more details about the derivative results and their validations, refer to [92].

Optimization results are summarized in Figures 5.50 and 5.51, which present the convergence history of the percentage variation of the objective function and the consistency constraint, respectively. These plots reveal a local minimum at a sweep angle of -20 degrees, confirming the beneficial effect of further sweeping the wing forward on drag reduction. Conversely, weight reduction is achieved by reducing the spar thickness to 3 millimeters from the initial 5 millimeters. The convergence history also shows the presence of another local minimum that was found during the second iteration. However, as shown in Figure 5.51, the consistency constraint is not satisfied at that iteration, indicating a physically infeasible design. Fulfillment of the constraint is achieved in the final design, as indicated in Figure 5.52, with a perfect

match between the output from MSC Nastran software and the final surrogates. A more comprehensive depiction of the final design is provided in Table 5.24. The minimization of the objective function, as shown in Table 5.23, is primarily influenced by a decrease in weight, which results in an increase in drag coefficient. Finally, Figure 5.53 illustrates the distribution of Von Mises stresses in the final design. A well-optimized structural design aimed at reducing weight should not exceed certain stress levels, typically the yield strength ($s_y = 240$ MPa for aluminum), in similar applications. In this particular case, the final design meets this requirement, with a maximum Von Mises stress well below the material yield strength.

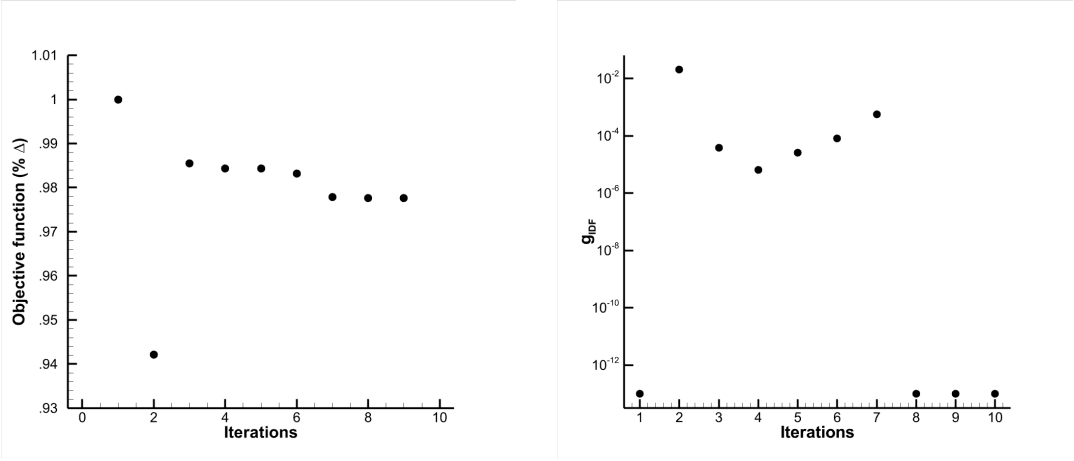

(a) Objective function. **(b)** Consistency constraint.

Figure 5.50: Convergence history of the optimisation problem. Flow conditions summarized in Table 5.9.

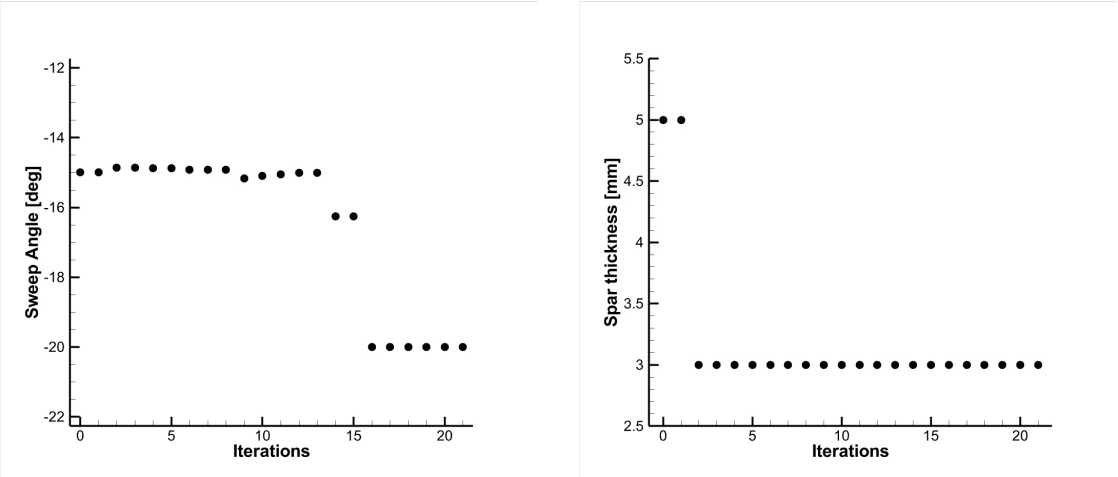

(a) Sweep Angle. **(b)** Spar thickness.

Figure 5.51: Convergence history of the optimisation variables. Flow conditions summarized in Table 5.9.

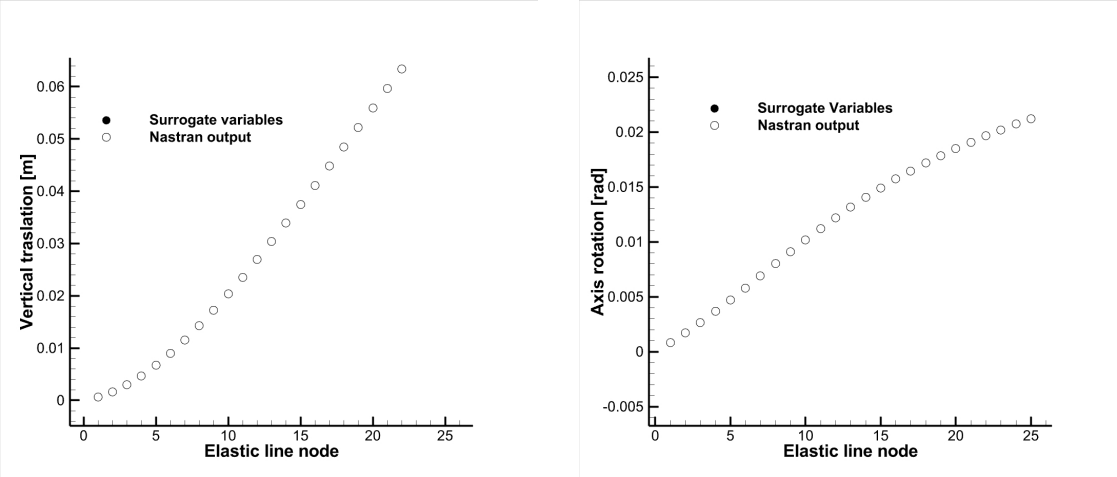

(a) Vertical translations. **(b)** Axial rotations.

Figure 5.52: Structural surrogates vs MSC Nastran output at convergence. Flow conditions summarized in Table 5.9.

	Initial Design [Sweep angle = -15 deg]	**Final Design** [Sweep angle = -19.15 deg]	$\mathbf{\Delta}(\%)$
$\mathbf{C_{D,H}}$ **[counts]**	82.0	95.0	+15.8
$\mathbf{W_{HTP}}$ **[Kg]**	555	482.46	-13.1

Table 5.24: Comparison between initial and final design. Flow conditions summarized in Table 5.9.

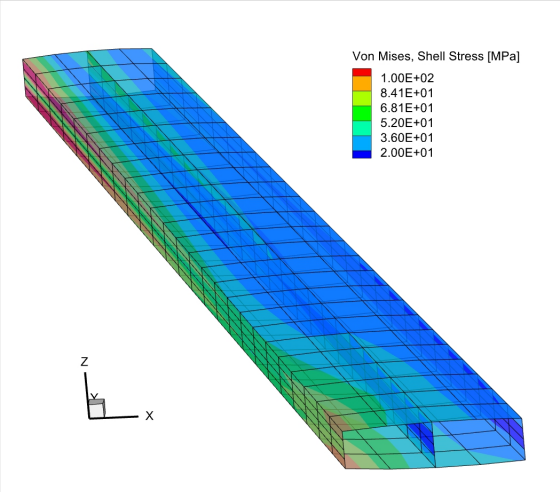

Figure 5.53: Von Mises stresses on final design.

5.7 Requirement Verification

The final activity conducted in the current study involves verifying the requirements. Starting from the requirements already specified in the OCE, several MDO workflows have been defined to validate the requirements using the workflow results. As previously mentioned, the requirements have been linked to specific design variables utilized by the tools and defined in the CPACS file. Several test cases have been defined, along with their purpose and the tools involved. Next, the parameters of the MDO problem are formalized. Each requirement related to a disciplinary tool has been associated with a specific role. In this manner, each parameter is traced back to the requirement and linked to the specific CPACS variable. Once the MDAO workflows have been executed and the promising solutions are identified, it is important to verify whether the solution meets the requirements and is thus valid. This examination is made possible by the results obtained from the implementation of the workflows/optimization presented in the previous sections. In KE-Chain, the CPACS files obtained after the workflow execution can be linked to its workflow, and the associated requirements can be verified using the RVF. Through the RVF, it is possible to automatically check if requirements are met or not. In Figure 5.54, an excerpt of the RVF obtained for the pure aerodynamic optimization test case results is presented. For each requirement, the compliance value and its relative margin with reference to the target value are indicated. The RVF automatically calculates this difference and informs the user whether the requirement is verified or not. It is possible to observe that meeting requirements related to flight conditions or system geometry is achieved by treating these elements as input parameters for the tool. Consequently, the value assigned to the items will be exactly equal to the required one, and the margin of compliance will be zero. The other requirements include the computation and output of workflow. In this case, they all pertain to aerodynamic and stability parameters. The only requirement that has not been satisfied is the drag cruise, as previously explained in the preceding sections. It is evident that the requirements related to structural or ice constraints are not validated in this use case. Figure 5.55 displays a section of the RVF obtained for the aerostructural optimization test case results. In this case, a higher number of requirements are satisfied. The workflow indeed concerns both aerodynamic and structural requirements. A requirement concerning pure aerodynamic parameters is not validated here. The reason for this consists of the change in the optimization objective. The flexible moment coefficient represents a constraint for the described test case. Consequently, the optimizer will drive the solution to satisfy its related constraint, and not anymore the rigid moment coefficient requirements, which is more

demanding. In Figure 5.56, all the presented requirements are validated. It shows an excerpt of the RVF obtained for the aerostructural ice optimization test case results achieved. In this case, only the drag coefficient requirement is not satisfied.

Execution run overview

Please manually download the executable CMDOWS file and run the RCE workflow.

EXPORT RESULTS

EDIT DELETE

Executable workflow	CMDOWS file	Status	Result report
Workflow	cmdows_mdax_Workflow_Initial_workflow.xml	Ready for execution	OPT3_result_VYxKt10.xml

Page 1 of 1 Displaying 1 - 1 of 1

Requirements verification framework

Verification file Workflow

Requirement	ID	Text	Type	Validation	Compliance value	Compliance margin (%)
HTP Dihedral Angle	R-0032	The HTP shall possess a dihedral angle equal to 0 degree	Design constraint	Valid	0	100
HTP HS lift coefficient derivative	R-0025	The HTP shall match at least reference Aircraft lift coefficient derivative for condition: high speed cruise condition	Performance	Valid	0.0178	4.19
HTP Leading edge X coordinate	R-0005	The HTP shall not be placed backwards with respect to reference Aircraft	Design constraint	Valid	34.756	0
Cruise Mach	R-0045	The Aircraft shall fly at MLR equal to 0.78 Mach for condition: cruise condition 39000 ft	Performance	Valid	0.78	0
HTP HS drag coefficient	R-0024	The HTP shall match at least reference Aircraft drag coefficient for condition: high speed cruise condition	Performance	Invalid	0.0103	-3
HTP HS moment coefficient derivative	R-0027	The HTP shall match at least reference Aircraft moment coefficient derivative for condition: high speed cruise condition	Performance	Valid	-0.0746	-5.47
HTP maximum negative lift coefficient	R-0018	The HTP shall achieve at least reference Aircraft maximum negative lift coefficient for condition: pushover maneuver	Performance	Valid	-0.179	-18
HTP stall angle of attack	R-0003	The HTP shall achieve at least reference Aircraft negative stall angle of attack for condition: pushover maneuver	Performance	Valid	-11.4338	-14.34
HTP Weight	R-0034	The HTP shall achieve at least reference Aircraft weight	Design constraint	Not started		
HTP HS Flexible lift coefficient derivative	R-0011	The HTP shall achieve at least reference Aircraft flexible lift derivative for condition: high speed cruise condition	Performance	Not started		
ARE HS Elastic efficiency	R-0040	The ARE shall increase its elastic efficiency by 5% with respect to reference Aircraft for condition: high speed cruise condition	Performance	Not started		
HTP Flexible maximum negative lift coefficient	R-0012	The HTP shall achieve at least reference Aircraft flexible maximum negative lift coefficient for condition: pushover maneuver	Performance	Not started		
CL max reduction due to ice	R-0004	The HTP shall achieve at least reference The HTP shall not exceed a reduction of CL max due to ice equal to 0.2 for condition: pushover	Performance	Not started		

Figure 5.54: Excerpt of Requirements verification done through the RVF. Results concern pure aerodynamic optimization test case. Poor image quality due to acquisition from OCE.

Execution run overview

Please manually download the executable CMDOWS file and run the RCE workflow.

EXPORT RESULTS

EDIT DELETE

Executable workflow	CMDOWS file	Status	Result report
Workflow	cmdows_mdax_Workflow_Initial_workflow.xml	Ready for execution	OPT3_Flex_result_VYxKt10.xml

Page 1 of 1 Displaying 1 - 1 of 1

Requirements verification framework

Verification file Workflow

Requirement	ID	Text	Type	Validation	Compliance value	Compliance margin (%)
HTP Dihedral Angle	R-0032	The HTP shall possess a dihedral angle equal to 0 degree	Design constraint	Valid	0	100
HTP Weight	R-0034	The HTP shall achieve at least reference Aircraft weight	Design constraint	Valid	467.0	16
HTP HS Flexible lift coefficient derivative	R-0011	The HTP shall achieve at least reference Aircraft flexible lift derivative for condition: high speed cruise condition	Performance	Valid	0.017	4.68
HTP HS moment coefficient derivative	R-0027	The HTP shall match at least reference Aircraft moment coefficient derivative for condition: high speed cruise condition	Performance	Valid	-0.0692	2.18
ARE HS Elastic efficiency	R-0040	The ARE shall increase its elastic efficiency by 5% with respect to reference Aircraft for condition: high speed cruise condition	Performance	Valid	1.0077	0.77
HTP Leading edge X coordinate	R-0005	The HTP shall not be placed backwards with respect to reference Aircraft	Design constraint	Valid	34.756	0
Cruise Mach	R-0045	The Aircraft shall fly at MLR equal to 0.78 Mach for condition: cruise condition 39000 ft	Performance	Valid	0.78	0
HTP HS lift coefficient derivative	R-0025	The HTP shall match at least reference Aircraft lift coefficient derivative for condition: high speed cruise condition	Performance	Invalid	0.0169	-1.32
HTP HS drag coefficient	R-0024	The HTP shall match at least reference Aircraft drag coefficient for condition: high speed cruise condition	Performance	Invalid	0.0102	-2
HTP stall angle of attack	R-0003	The HTP shall achieve at least reference Aircraft negative stall angle of attack for condition: pushover maneuver	Performance	Valid	-11.2863	-12.86
HTP maximum negative lift coefficient	R-0018	The HTP shall achieve at least reference Aircraft maximum negative lift coefficient for condition: pushover maneuver	Performance	Valid	-0.181	-19
HTP Flexible maximum negative lift coefficient	R-0012	The HTP shall achieve at least reference Aircraft flexible maximum negative lift coefficient for condition: pushover maneuver The HTP shall achieve at least reference	Performance	Valid	-0.181	-22
CL max reduction due to ice	R-0004	The HTP shall not exceed a reduction of CL max due to ice equal to 0.2 for condition: pushover	Performance	Not started		

Figure 5.55: Excerpt of Requirements verification done through the RVF. Results concern aerostructural optimization test case. Poor image quality due to acquisition from OCE.

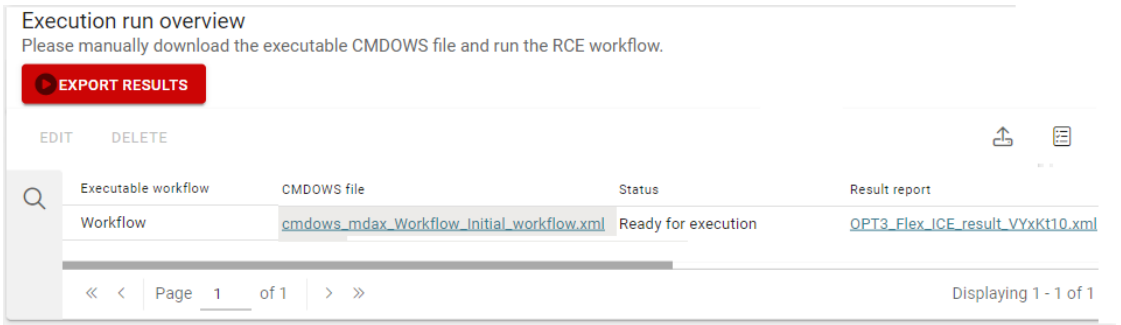

Requirements verification framework

Verification file Workflow

Requirement	ID	Text	Type	Validation	Compliance value	Compliance margin (%)
HTP Dihedral Angle	R-0032	The HTP shall possess a dihedral angle equal to 0 degree	Design constraint	Valid	0	100
HTP HS Flexible lift coefficient derivative	R-0011	The HTP shall achieve at least reference Aircraft flexible lift derivative for condition: high speed cruise condition	Performance	Valid	0.0191	17.4
HTP Weight	R-0034	The HTP shall achieve at least reference Aircraft weight	Design constraint	Valid	502	9.55
HTP HS lift coefficient derivative	R-0025	The HTP shall match at least reference Aircraft lift coefficient derivative for condition: high speed cruise condition	Performance	Valid	0.0187	9.16
ARE HS Elastic efficiency	R-0040	The ARE shall increase its elastic efficiency by 5% with respect to reference Aircraft for condition: high speed cruise condition	Performance	Valid	1.0214	2.14
HTP Leading edge X coordinate	R-0005	The HTP shall not be placed backwards with respect to reference Aircraft	Design constraint	Valid	34.756	0
Cruise Mach	R-0045	The Aircraft shall fly at MLR equal to 0.78 Mach for condition: cruise condition 39000 ft	Performance	Valid	0.78	0
HTP HS moment coefficient derivative	R-0027	The HTP shall match at least reference Aircraft moment coefficient derivative for condition: high speed cruise condition	Performance	Valid	-0.0736	-4.1
HTP HS drag coefficient	R-0024	The HTP shall match at least reference Aircraft drag coefficient for condition: high speed cruise condition	Performance	Invalid	0.0107	-7
HTP HS Flexible moment coefficient derivative	R-0009	The HTP shall achieve at least reference Aircraft flexible pitching moment derivative for condition: high speed cruise condition	Performance	Valid	-0.0752	-11.92
HTP maximum negative lift coefficient	R-0018	The HTP shall achieve at least reference Aircraft maximum negative lift coefficient for condition: pushover maneuver	Performance	Valid	-0.171	-12.7
HTP Flexible maximum negative lift coefficient	R-0012	The HTP shall achieve at least reference Aircraft flexible maximum negative lift coefficient for condition: pushover maneuver	Performance	Valid	-0.172	-15.7
HTP stall angle of attack	R-0003	The HTP shall achieve at least reference Aircraft negative stall angle of attack for condition: pushover maneuver	Performance	Valid	-12.5707	-25.71
CL max reduction due to ice	R-0004	The HTP shall not exceed a reduction of CL max due to ice equal to 0.2 for condition: pushover	Performance	Valid	-0.1226	-38.7

Figure 5.56: Excerpt of Requirements verification done through the RVF. Results concern aerostructural ice optimization test case. Poor image quality due to acquisition from OCE.

5.8 Impact of Advanced Rear End at Aircraft Level

The impact of integrating the Advanced Rear-End solutions investigated in this chapter at the aircraft level is explored in this section. The reference aircraft selected for this analysis is a large passenger aircraft similar to the A320neo, with a designed mission profile covering 3,400 nautical miles and a seating capacity of 180. Table 5.2 presents some of the essential overall aircraft data. The analysis at the aircraft level was conducted using the multidisciplinary analysis software JPAD [2], which allows the assessment of the potential effects of decreasing tailplane area and weight on the aircraft's maximum takeoff weight and fuel consumption. As outlined in Section 5.3.1, a fair comparison between conventional and advanced rear-end designs was achieved by positioning the forward-swept tailplane to maintain a constant tail-level arm. This was achieved by keeping the tail aerodynamic center of the tail in the same position as the conventional tailplane arrangement. The key findings of the multidisciplinary analysis are presented in Table 5.25.

Table 5.25: Impact of the ARE configuration and conventional HTP at aircraft level.

	HTP	**OPT**$_{Rigid}$	**OPT**$_{Flex.}$	**OPT**$_{Flex.,ice}$
$\mathbf{W_{MTO}}$**[Kg]**	73,900	73,535 (-0.5%)	73,397 (-0.7%)	73,450 (-0.6%)
$\mathbf{W_{BlockFuel}}$ **[Kg]**	15,400	15,298 (-0.7%)	15,299 (-0.7%)	15,308 (-0.6%)
$\mathbf{W_{HTP}}$ **[Kg]**	555	489 (-12%)	467 (-16%)	502 (-10%)
$\mathbf{W_{Wing}}$ **[Kg]**	7,760	7,753 (-0.1%)	7,750 (-0.1%)	7,755 (-0.1%)
$\mathbf{W_{Fuselage}}$ **[Kg]**	7,120	7,117 (-0.04%)	7,117 (-0.04%)	7,116 (-0.06%)
TOFL [m]	2,190	2,173 (-0.8%)	2,164 (-1.2%)	2,168 (-1.0%)
LFL [m]	1,440	1,422 (-1.2%)	1,421 (-1.3%)	1,421 (-1.3%)
$\mathbf{AR_H}$	5.76	5.07 (-12%)	4.83 (-16%)	5.93 (+2.92%)
$\mathbf{S_H}$ (m^2)	31.36	30.24 (-3.6%)	30.11 (-4.0%)	30.12 -(3.95%)
$\mathbf{\Lambda_{LE}}$ (deg)	32.00	-7.82	-7.45	-19.55
λ	0.336	0.400 (+19%)	0.335 (-0.3%)	0.405 (+20%)

It is estimated that a potential reduction in take-off weight of approximately 0.6% results in a block fuel saving of about 0.7% of the total fuel required for the design mission of 3,400 nm while maintaining similar overall performance. The introduction of the innovative designed ARE configurations slightly reduces both the Takeoff Field Length (TOFL) and the Landing Field Length (LFL). The weight

[2]JPAD software's home page: `https://www.smartup-engineering.com/jpad` [retrieved March 11, 2024]

reduction achievement is attributed to a decrease of up to 4% in tailplane surface area and a reduction of up to 16% in tailplane weight, as shown in Table 5.21.

It is crucial to note that the increased elastic efficiency of the forward-swept tail is just one of the innovative features of the proposed Advanced Rear End. The key aspect of this concept is its ability to eliminate the fuselage cut-out, removing the need for local reinforcements to withstand the bending and torsional loads introduced by the horizontal and vertical tail. The elimination of the fuselage cut-out not only streamlines the aircraft's structural integrity but also reduces the need for local reinforcements. This innovative approach tackles the challenges presented by bending and torsional loads, which have traditionally been addressed with metal frames, by harnessing the strength and flexibility of composite materials. The primary weight advantages of the FSHTP stem from the fuselage, resulting from the elimination of the cut-out for the empennage, as mentioned earlier.

Table 5.26 presents the performance results of the aircraft, considering the introduction of ARE configurations and the resulting reduction in fuselage weight. Assuming that advanced rear-end technology could reduce the weight of the fuselage by 10% (a conservative estimate compared to the reported -20% in Clean Sky 2 reports [3]), the potential savings could be up to 2.3% of the maximum take-off weight, resulting in a fuel saving of approximately 2% (based on a design range of 3,400 nm) compared to a traditional single-aisle aircraft.

Results shown in Table 5.26 demonstrate a significant advantage achievable through the implementation of the ARE solution in a new aircraft configuration. Indeed, due to the objective function and constraints applied in the optimizations, the innovative tailplane achieves improved performance regarding stall behavior, stability, controllability, and ice accretion, while also enabling a reduction in the overall aircraft fuel consumption and related air emissions by over 2% per flight. These aspects could persuade an OEM to redesign a new aircraft with such a configuration. Furthermore, a designer can choose a solution with a slightly lower level of performance compared to the one presented in Table 5.26, but with improved fuel emission characteristics, or vice versa, as illustrated in Figure 5.44. The results presented in Table 5.26 can be considered reliable, as the reduction in fuel consumption is primarily driven by decreases in weight and drag. Both quantities are affected by an error of less than 1%, as outlined in Sections 5.3.2 and 5.4.2, as well as in [192].

[3]Clean Sky's Advanced Rear End Demo shapes up website: `https://clean-aviation.eu/clean-skys-advanced-rear-end-demo-shapes-up` [retrieved March 11, 2024]

Table 5.26: Impact of the ARE configuration and conventional HTP at aircraft level. A weight fuselage reduction of 10% is considered.

	HTP	**OPT**$_{Rigid}$	**OPT**$_{Flex.}$	**OPT**$_{Flex.,ice}$
$\mathbf{W_{MTO}}$**[Kg]**	73,900	72,170 (-2.3%)	72,229 (-2.2%)	72,309 (-2.15%)
$\mathbf{W_{BlockFuel}}$ **[Kg]**	15,400	15,099 (-2.0%)	15,100 (-2.0%)	15,106 (-1.9%)
$\mathbf{W_{HTP}}$ **[Kg]**	555	489 (-12%)	467 (-16%)	502 (-10%)
$\mathbf{W_{Wing}}$ **[Kg]**	7,760	7,66 (-1.2%)	7,665 (-1.2%)	7,666 (-1.2%)
$\mathbf{W_{Fuselage}}$ **[Kg]**	7,120	6,405 (-10%)	6,405 (-10%)	6,405 (-10%)
TOFL [m]	2,190	2,085 (-4.8%)	2,094 (-4.4%)	2,094 (-4.4%)
LFL [m]	1,440	1,407 (-2.3%)	1,409 (-2.2%)	1,410 (-2.1%)
$\mathbf{AR_H}$	5.76	5.07 (-12%)	4.83 (-16%)	5.93 (+2.92%)
$\mathbf{S_H}$ (m^2)	31.36	30.24 (-3.6%)	30.11 (-4.0%)	30.12 -(3.95%)
$\mathbf{\Lambda_{LE}}$ (deg)	32.00	-7.82	-7.45	-19.55
λ	0.336	0.400 (+19%)	0.335 (-0.3%)	0.405 (+20%)

Author contribution

The author of this thesis was the primary and sole contributor to the activities outlined in this chapter. The scientific activities presented were made possible by the knowledge and experience gained through the AGILE, AGILE 4.0, and IMPACT projects, collaboration with the DAF group, and insights provided by Airbus company. The author has created an environment that combines MBSE with collaborative technologies for MDAO, with a specific focus on ARE configurations. The analysis considered all potential stakeholder needs, which were then translated into requirements, forming the basis for modeling the systems under examination. Surrogate modeling techniques were integrated using design of experiments applied to response surface modeling. These models were validated and used to integrate disciplines at a high-fidelity level in complex workflows. The framework's adaptability and flexibility are demonstrated by generating four distinct optimization problems, each solved using different techniques and architectures. Notably, the framework can be easily restructured to meet the designer's specific requirements through an automated process that can adapt to changes in information within the models.

List of related publications

Journal papers

- (Under Review) S. Corcione, **M. Mandorino** and V. Cusati. Beyond Conventional: An Integrated Aerostructural Optimization Approach for Innovative Tailplane Configurations. *Aerospace Science and Technology*

  This paper presents a comprehensive study focused on optimizing

innovative tailplane configurations for transport jet aircraft. The study aims to improve the aerodynamics of the aircraft's rear end by introducing a new tail arrangement. The ultimate goal is to decrease the size of the horizontal tail assembly, which will have a positive effect on aircraft fuel efficiency. To achieve its objectives, this work employs a systematic approach that integrates advanced methodologies such as Design of Experiments and Response Surface Models for both aerodynamics and structural disciplines.

Conference papers

- C. Conti , **M. Mandorino**, A. Da Ronch and A. Elham. High-fidelity Aero-Structural Optimisation using Individual Discipline Feasible Strategy. In *2023 AIAA Aviation and Aeronautics Forum and Exposition*, 12-16 June 2023, San Diego, California. DOI: https://doi.org/10.2514/6.2023-3317.

  This paper presents an application of the IDF strategy to adjoint-driven high-fidelity aero-structural optimization of an innovative concept for tailplane design. Optimized solutions for drag and weight, achievable in a few iterations, are presented. Additionally, results regarding the gradients of the objective functions and constraints with respect to structural and geometrical macroparameters are presented.

Conclusions

Multidisciplinary frameworks are essential for designing and analyzing modern aircraft, as they are needed to address the increasing number of variables and requirements, enabling consistent and effective studies of both evolutionary and revolutionary aircraft concepts. The exploration of these solutions is motivated by the need for improved performance and the ambitious targets set by environmental agendas, which aim to reduce emissions. In the exploration of novel aircraft configurations and innovative concepts, researchers have identified the potential advantages of developing the Advanced Rear End solution. This solution could make a significant contribution to the necessary improvements in terms of weight reduction, emissions, and performance. The development of such a novel and complex system involves multidisciplinary processes that impose requirements on system components, technologies, and interactions. The interconnected data encompasses various aspects of product development, generating vast amounts of information. To address the challenges of navigating a complex design space, early aircraft designers can benefit from an innovative framework that combines Model-Based Systems Engineering and Multidisciplinary Design and Optimization approaches.

These observations lead to the formulation of the following research question:

How can model-based systems engineering methodologies be utilized to develop multidisciplinary analysis and optimization workflows for designing an innovative rear-end for large passenger commercial jet aircraft?

This thesis aims to propose a practical solution that fulfills the need for a framework possessing the mentioned characteristics, thereby facilitating the design of advanced rear-end configurations.

The author's experience in several European research projects has equipped him with the knowledge and capabilities required to establish an environment that combines Model-Based Systems Engineering with collaborative technologies for Multidisciplinary Design and Optimization. The author's research goes beyond the classical design approach by developing and applying unique design and optimization methods to innovative rear-end configurations. The proposed methodology facilitated the development of the rear-end of a large passenger commercial jet aircraft, incorporating features such as a negatively-swept horizontal tail, a leading-edge extension, and a bottleneck-shaped fuselage. The analysis outlined all stakeholder needs and translated them into requirements, forming the foundation for modeling

the systems under examination. Multiple workflows were subsequently created to analyze the systems, leading to a solution designed to meet all identified requirements. The framework also verifies the consistency of both workflows and optimized solutions with respect to the defined requirements. The entire process is capable of encompassing various aspects that extend beyond design considerations, resulting in final designs guided by certification and regulatory requirements. Surrogate modeling techniques have been used to integrate disciplines at a high-fidelity level, such as aeroelasticity and in-flight ice formation. Various optimization techniques and architectures have been incorporated into the framework.

The proposed framework, in conjunction with the development system, effectively utilizes modeling methods and technologies to enhance the agility required during the definition phases of complex systems. Various automated processes are integrated to streamline, enhance, and expedite the development of such systems. The most significant advantage lies in the coherence among all the data and information generated and managed during the design process. Traceability is improved through the use of a model-based approach. Another crucial benefit is the comprehensive addressing of all stakeholder needs, which is a key factor for the success of a product. The proposed architectural framework clarifies the expectations of each stakeholder for the system and how these expectations are translated into system requirements. Moreover, stakeholder needs can be easily validated through model-based scenarios, enabling automatic verification of the correctness of the entire information. In this way, the development process has been optimized for time and efficiency, with various development activities expedited. Furthermore, a higher level of comprehensiveness is achieved because more activities from a typical Systems Engineering approach can now be seamlessly integrated into the development process.

A process that has the capability to significantly reduce time in setting up and resolving Multidisciplinary Design and Optimization problems from an execution perspective has been developed. This is primarily due to the reduced time in the formulation and integration phases. Any problem formulation can be quickly translated into an executable workflow, allowing more time to be devoted to exploring the design space for the proposed configuration. Furthermore, a decrease in time-to-convergence has been achieved by using surrogate models, design of experiments, and advanced optimization algorithms. The integration of surrogate models has been crucial in harnessing high-fidelity analysis within integrated workflows. The framework's adaptability to meet specific requirements and its flexibility in addressing various types of optimization problems are demonstrated through the generation of four distinct optimization problems, each featuring different problem architectures.

The results indicate potential benefits in adopting an advanced rear-end solution. This demonstrates a reduction in tail area by approximately 4% and a mass decrease of up to 16%, while maintaining drag capabilities similar to the conventional configuration. Additionally, there has been an improvement in lift and aeroelastic performance. The multidisciplinary optimization study emphasizes the potential for utilizing a forward-swept tailplane to reduce the dimensions of the horizontal empennage when paired with a leading-edge extension device. Moreover, all optimization tasks highlight the vital role of the leading-edge extension in improving the maximum negative lift coefficient of the tail, even when facing difficult constraints. The Pareto Front results from multi-objective optimization demonstrate how designers can select from several optimal solutions based on specific needs. In conclusion, the evaluation of the innovative rear-end configuration at the aircraft level indicates a potential 0.7% reduction in block fuel for a mission profile comparable to that of the Airbus A320-neo (design range of 3200 nautical miles with 180 passengers). This reduction could potentially reach 2.0%, assuming that advanced rear-end technology could reduce the weight of the fuselage by 10%. These results demonstrate a significant advantage achievable through the implementation of the ARE solution in a new aircraft configuration. Indeed, the innovative tailplane achieves improved performance regarding stall behavior, stability, controllability, and ice accretion, while also enabling a reduction in the overall aircraft fuel consumption and related air emissions.

Future developments could aim at expanding the design and optimization framework to encompass full aircraft analysis. Specifically, such an application could yield significant results if integrated with IDF architecture optimization methodologies. IDF has indeed marked a substantial advancement in the state-of-the-art by introducing an optimization framework based on adjoint methods concerning macro-parameters of geometric and structural solutions. This approach could be extended to encompass the entire aircraft. Furthermore, methodologies pertaining to the effects of implementing the new ARE configuration on aircraft performance could be assimilated into the optimization framework to address them within the process itself. By incorporating objective functions and constraints associated with the performance of the entire aircraft during its flight mission, these methodologies could bolster the overall optimization process.

Bibliography

[1] Aircraft Technology Roadmap to 2050, Tech. rep., Geneva: International Air Transport Association IATA (2019).

[2] L. Boggero, P. Ciampa, B. Nagel, An MBSE architectural framework for the agile definition of system stakeholders, needs and requirements, in: AIAA Aviation 2021 Forum, 2021, p. 3076. doi:https://doi.org/10.2514/6.2022-3720.

[3] Defense acquisitions: Assessments of selected weapon programs, Tech. rep., Government Accountability Office. Washington DC (US) (2011).
URL https://apps.dtic.mil/sti/citations/ADA558843

[4] W. J. Fabrycky, B. S. Blanchard, Life-cycle cost and economic analysis, Vol. 135383234, Prentice Hall Englewood Cliffs, NJ, 1991.

[5] P. D. Ciampa, G. La Rocca, B. Nagel, A mbse approach to mdao systems for the development of complex products, in: AIAA Aviation 2020 Forum, 2020, p. 3150. doi:https://doi.org/10.2514/6.2020-3150.

[6] I. Mayk, A. M. Madni, The role of ontology in system-of-systems acquisition, in: Proceedings of the 2006 Command and Control Research and Technology Symposium, San Diego, CA, 2006.

[7] A. Bruggeman, B. van Manen, T. van der Laan, T. van den Berg, G. La Rocca, An MBSE-Based Requirement Verification Framework to support the MDAO Process, in: AIAA AVIATION 2022 Forum, 2022, p. 3722. doi:https://doi.org/10.2514/6.2022-3722.

[8] A. Smith, Requirements management: A core competency for project and program success, Tech. rep., Project Management Institute (2014).
URL https://www.pmi.org/learning/thought-leadership/pulse/core-competency-project-program-success

[9] N. Tabesh, A. K. Jeyaraj, A. Tamayo, S. Liscouet-Hanke, Integration of the Functional Hazard Assessment within a Model-based System Engineering Framework, in: AIAA SCITECH 2023 Forum, 2023, p. 1116. doi:https://doi.org/10.2514/6.2023-1116.

[10] L. Boggero, M. Fioriti, G. Donelli, P. D. Ciampa, Model-Based Mission Assurance/Model-Based Reliability, Availability, Maintainability, and Safety (RAMS), in: Handbook of Model-Based Systems Engineering, Springer, 2022, pp. 1–39. doi:https://doi.org/10.1007/978-3-030-27486-3_34-1.

[11] S. Friedenthal, A. Moore, R. Steiner, A practical guide to SysML: the systems modeling language, Morgan Kaufmann, 2014. doi:https://doi.org/10.1016/C2013-0-14457-1.

[12] Model-based systems engineering: An emerging approach for modern systems, author=Ramos, Ana Luísa and Ferreira, José Vasconcelos and Barceló, Jaume, IEEE Transactions on Systems, Man, and Cybernetics, Part C (Applications and Reviews) 42 (1) (2011) 101–111. doi:https://doi.org/10.1109/TSMCC.2011.2106495.

[13] F. Bruno, M. Fioriti, G. Donelli, L. Boggero, P. D. Ciampa, B. Nagel, A model-based RAMS estimation methodology for innovative aircraft on-board systems supporting MDO applications, in: AIAA Aviation 2020 Forum, 2020, p. 3151. doi:https://doi.org/10.2514/6.2020-3151.

[14] A. Joshi, M. P. Heimdahl, Model-based safety analysis of simulink models using SCADE design verifier, in: Computer Safety, Reliability, and Security: 24th International Conference, SAFECOMP 2005, Fredrikstad, Norway, September 28-30, 2005. Proceedings 24, Springer, 2005, pp. 122–135. doi:https://doi.org/10.1007/11563228_10.

[15] P. Ciampa, B. Nagel, Accelerating the Development of Complex Systems in Aeronautics via MBSE and MDAO: a Roadmap to Agility, in: AIAA AVIATION 2021 FORUM, 2021, p. 3056. doi:https://doi.org/10.2514/6.2021-3056.

[16] Systems engineering vision 2020, Tech. rep., INCOSE-TP-2004-004-02 (2007).

[17] "ISO/IEC 15288 – Systems and software engineering–system life cycle processes, Tech. rep., International Organization for Standardization (2002).

[18] L. Boggero, P. D. Ciampa, B. Nagel, The application of the AGILE 4.0 MBSE Architectural Framework for the modeling of system stakeholders, needs and requirements, in: ICAS Conference, 2021. doi:https://zenodo.org/doi/10.5281/zenodo.5735416.

[19] T. van der Laan, T. van den Berg, An open source part cost estimation tool for MDO purposes, in: AIAA AVIATION 2021 FORUM, 2021, p. 3058. doi:https://doi.org/10.2514/6.2023-1116.

[20] L. Boggero, T. Lefebvre, J. Vankan, B. Beijer, V. Saluzzi, B. Nagel, The AGILE 4.0 MBSE-MDAO development framework: overview and assessment (2022).
URL https://elib.dlr.de/188837/

[21] J. Holt, S. Perry, SysML for systems engineering, Vol. 7, IET, 2008.

[22] A. K. Jeyaraj, N. Tabesh, S. Liscouet-Hanke, Connecting Model-based Systems Engineering and Multidisciplinary Design Analysis and Optimization for Aircraft Systems Architecting, in: AIAA AVIATION 2021 FORUM. doi:https://doi.org/10.2514/6.2021-3077.vid.

[23] A. K. Jeyaraj, S. Liscouët-Hanke, A Safety-Focused System Architecting Framework for the Conceptual Design of Aircraft Systems, Aerospace 9.12 (2022). doi:https://doi.org/10.3390/aerospace9120791.

[24] B. Grossman, R. T. Haftka, P.-J. Kao, D. Polen, M. Rais-Rohani, J. Sobieszczanski-Sobieski, Integrated aerodynamic-structural design of a transport wing, Journal of Aircraft 27 (12) (1990) 1050–1056. doi:https://doi.org/10.2514/3.45980.

[25] K. Maalawi, H. Negm, M. El Sheikh, Aerodynamic/structural optimization of a training aircraft wing, in: International Conference on Aerospace Sciences and Aviation Technology, Vol. 13, The Military Technical College, 2009, pp. 1–16. doi:https://doi.org/10.21608/asat.2009.23446.

[26] J. R. Martins, A. B. Lambe, Multidisciplinary design optimization: a survey of architectures, AIAA journal 51 (9) (2013) 2049–2075. doi:https://doi.org/10.2514/1.J051895.

[27] Strategic Research and Innovation Agenda (SRIA) Vol. 1, Delivering Europe's Vision for Aviation, Tech. rep., ACARE (2017).
URL https://open4aviation.at/resources/pdf/ACARE-Strategic-Research-Innovation-Volume-1.pdf

[28] J. Giesing, J.-F. Barthelemy, A summary of industry MDO applications and needs, in: 7th AIAA/USAF/NASA/ISSMO Symposium on Multidisciplinary Analysis and Optimization, 1998, p. 4737. doi:https://doi.org/10.2514/6.1998-4737.

[29] J. Sobieszczanski-Sobieski, A. Morris, M. Van Tooren, Multidisciplinary design optimization supported by knowledge based engineering, John Wiley & Sons, 2015. doi:10.1002/9781118897072.

[30] K. Bowcutt, A perspective on the future of aerospace vehicle design, in: 12th AIAA International Space Planes and Hypersonic Systems and Technologies, 2003, p. 6957. doi:https://doi.org/10.2514/6.2003-6957.

[31] R. M. Arnaldo Valdes, S. Burmaoglu, V. Tucci, L. M. Braga da Costa Campos, L. Mattera, V. F. Gomez Comendador, Flight path 2050 and ACARE goals for maintaining and extending industrial leadership in aviation: a map of the aviation technology space, Sustainability 11 (7) (2019) 2065. doi:https://doi.org/10.3390/su11072065.

[32] E. Livne, T. A. Weisshaar, Aeroelasticity of nonconventional airplane configurations-past and future, Journal of aircraft 40 (6) (2003) 1047–1065. doi:https://doi.org/10.2514/2.7217.

[33] D. Kaslow, G. Soremekun, H. Kim, S. Spangelo, Integrated model-based systems engineering (MBSE) applied to the Simulation of a CubeSat mission, in: 2014 IEEE Aerospace Conference, IEEE, 2014, pp. 1–14. doi:10.1109/AERO.2014.6836317.

[34] M.-H. Bleu-Laine, M. V. Bendarkar, J. Xie, S. I. Briceno, D. N. Mavris, A model-based system engineering approach to normal category airplane airworthiness certification, in: AIAA Aviation 2019 Forum, 2019, p. 3344. doi:https://doi.org/10.2514/6.2019-3344.

[35] A. Maheshwari, Industrial adoption of model-based systems engineering: Challenges and strategies, Ph.D. thesis, Purdue University (2015).

[36] O. Lisagor, T. Kelly, R. Niu, Model-based safety assessment: Review of the discipline and its challenges, in: The Proceedings of 2011 9th International Conference on Reliability, Maintainability and Safety, IEEE, 2011, pp. 625–632. doi:https://doi.org/10.1109/ICRMS.2011.5979344.

[37] G. Girard, I. Baeriswyl, J. J. Hendriks, R. Scherwey, C. Müller, P. Hönig, R. Lunde, Model based safety analysis using SysML with automatic generation of FTA and FMEA artifacts, in: Proceedings of the 30th European Safety and Reliability Conference and the 15th Probabilistic Safety Assessment and Management Conference (Esrel 2020 PSAM 15), 1-5 November 2020, Venice, Italy, no. CONFERENCE, 2020. doi:http://dx.doi.org/10.3850/978-981-14-8593-0_4941-cd.

[38] A. A. Abdellatif, F. Holzapfel, Model Based Safety Analysis (MBSA) Tool for Avionics Systems Evaluation, in: 2020 AIAA/IEEE 39th Digital Avionics Systems Conference (DASC), IEEE, 2020, pp. 1–5. doi:https://doi.org/10.1109/DASC50938.2020.9256578.

[39] T. Prosvirnova, M. Batteux, P.-A. Brameret, A. Cherfi, T. Friedlhuber, J.-M. Roussel, A. Rauzy, The AltaRica 3.0 project for model-based safety assessment, IFAC proceedings volumes 46 (22) (2013) 127–132. doi:https://doi.org/10.3182/20130904-3-UK-4041.00028.

[40] S. Gradel, B. Aigner, E. Stumpf, Model-based safety assessment for conceptual aircraft systems design, CEAS Aeronautical Journal (2022) 1–14doi:https://doi.org/10.1007/s13272-021-00562-2.

[41] A. Landi, M. Nicholson, ARP4754A/ED-79A-guidelines for development of civil aircraft and systems-enhancements, novelties and key topics (2011). URL https://www.sae.org/standards/content/arp4754a/

[42] N. A. Tepper, Exploring the use of Model-Based Systems Engineering (MBSE) to develop systems architectures in naval ship design, Ph.D. thesis, Massachusetts Institute of Technology (2010).

[43] A. K. Jeyaraj, A model-based systems engineering approach for efficient system architecture representation in conceptual design: A case study for flight control systems, Ph.D. thesis, Concordia University, Gina Cody School of Engineering and Computer Science (2019).

[44] M. Chami, P. Oggier, O. Naas, M. Heinz, Real world application of MBSE at Bombardier Transportation, The Swiss Systems Engineering Day (SWISSED 2015), Kongresshaus Zurich, 8th September (2015).

[45] T. J. Bayer, S. Chung, B. Cole, B. Cooke, F. Dekens, C. Delp, I. Gontijo, K. Lewis, M. Moshir, R. Rasmussen, D. Wagner, Model Based Systems Engineering on the Europa mission concept study, in: 2012 IEEE Aerospace Conference, 2012, pp. 1–18. doi:https://doi.org/10.1109/AERO.2012.6187337.

[46] T. Bayer, S. Chung, B. Cole, B. Cooke, F. Dekens, C. Delp, I. Gontijo, K. Lewis, M. Moshir, R. Rasmussen, D. Wagner, Early Formulation Model-Centric Engineering on NASA's Europa Mission Concept Study, in: INCOSE International Symposium, Vol. 22, 2012, pp. 1695–1710. doi:https://doi.org/10.1002/j.2334-5837.2012.tb01431.x.

[47] B. A. Mousavi, R. Azzouz, C. Heavey, H. Ehm, A survey of model-based system engineering methods to analyse complex supply chains: A case study in semiconductor supply chain, IFAC-PapersOnLine 52 (13) (2019) 1254–1259. doi:https://doi.org/10.1016/j.ifacol.2019.11.370.

[48] P. George Mathew, S. Liscouet-Hanke, Y. Le Masson, Model-Based Systems Engineering Methodology for Implementing Networked Aircraft Control System on Integrated Modular Avionics – Environmental Control System Case Study (2011). doi:https://doi.org/10.4271/2018-01-1943.

[49] S. Liscouët-Hanke, H. Jahanara, J.-L. Bauduin, A Model-Based Systems Engineering Approach for the Efficient Specification of Test Rig Architectures for Flight Control Computers, IEEE Systems Journal 14 (4) (2020) 5441–5450. doi:https://doi.org/10.1109/JSYST.2020.2970545.

[50] R. Malone, B. Friedland, J. Herrold, D. Fogarty, Insights from Large Scale Model Based Systems Engineering at Boeing, INCOSE International Symposium 26 (1) (2016) 542–555. doi:https://doi.org/10.1002/j.2334-5837.2016.00177.x.

[51] M. Cencetti, P. Maggiore, System Modeling Framework and MDO Tool Integration: MBSE Methodologies Applied to Design and Analysis of Space System, in: AIAA Modeling and Simulation Technologies (MST) Conference. doi:https://doi.org/10.2514/6.2013-4590.

[52] P. Leserf, P. de Saqui-Sannes, J. Hugues, K. Chaaban, SysML modeling for embedded systems design optimization: A case study, in: 2015 3rd International Conference on Model-Driven Engineering and Software Development (MODELSWARD), 2015, pp. 449–457.

[53] T. F. Beernaert, L. F. P. Etman, Multi-level Decomposed Systems Design: Converting a Requirement Specification into an Optimization Problem, Proceedings of the Design Society: International Conference on Engineering Design 1 (1) (2019) 3691–3700. doi:https://doi.org/10.1017/dsi.2019.376.

[54] J. M. Génova, Gonzalo amd Fuentes, J. Llorens, O. Hurtado, V. Moreno, A framework to measure and improve the quality of textual requirements, Requirements Engineering 18 (2013). doi:https://doi.org/10.1007/s00766-011-0134-z.

[55] J. B. Dabney, T. L. Harman, Mastering simulink, Upper Saddle River: Pearson/Prentice Hall, 2004.

[56] A. Joshi, M. P. E. Heimdahl, Model-Based Safety Analysis of Simulink Models Using SCADE Design Verifier, in: Computer Safety, Reliability, and Security, Springer Berlin Heidelberg, 2005, pp. 122–135. doi:https://doi.org/10.1007/11563228_10.

[57] M. W. Joshi, Anjali, M. Heimdahl, Model-Based Safety Analysis Final Report, Tech. rep., NASA Techreport (2005).
URL https://shemesh.larc.nasa.gov/people/cam/publications/Model-BasedSafetyAnalysis.pdf

[58] M. van Tooren, G. La Rocca, Systems engineering and multi-disciplinary design optimization, in: Collaborative Product and Service Life Cycle Management for a Sustainable World: Proceedings of the 15th ISPE International Conference on Concurrent Engineering (CE2008), Springer, 2008, pp. 401–415. doi:https://doi.org/10.1007/978-1-84800-972-1_38.

[59] L. Boggero, P. Ciampa, B. Nagel, An MBSE architectural framework for the agile definition of complex system architectures, in: AIAA Aviation 2022 Forum, 2022, p. 3720. doi:https://doi.org/10.2514/6.2022-3720.

[60] P. D. Ciampa, P. S. Prakasha, F. Torrigiani, J.-N. Walther, T. Lefebvre, N. Bartoli, H. Timmermans, P. Della Vecchia, L. Stingo, D. Rajpal, et al., Streamlining cross-organizational aircraft development: results from the AGILE project, in: AIAA Aviation 2019 Forum, 2019, p. 3454. doi:https://doi.org/10.2514/6.2019-3454.

[61] A. K. Jeyaraj, N. Tabesh, S. Liscouet-Hanke, Connecting Model-based Systems Engineering and Multidisciplinary Design Analysis and Optimization for Aircraft Systems Architecting, in: AIAA AVIATION 2021 FORUM, 2021, p. 3077. doi:https://doi.org/10.2514/6.2021-3077.

[62] J. Bussemaker, L. Boggero, P. D. Ciampa, From system architecting to system design and optimization: A link between mbse and mdao, in: INCOSE International Symposium, Vol. 32, 2022, pp. 343–359. doi:https://doi.org/10.1002/iis2.12935.

[63] J. H. Bussemaker, P. D. Ciampa, B. Nagel, System architecture design space exploration: An approach to modeling and optimization, in: AIAA Aviation 2020 Forum, 2020, p. 3172. doi:https://doi.org/10.2514/6.2020-3172.

[64] J. Bussemaker, P. D. Ciampa, MBSE in architecture design space exploration (2022) 1–41doi:https://doi.org/10.1007/978-3-030-27486-3_36-1.

[65] Regional jet retrofitting design from stakeholders need and system requirements to MDAO workflow formulation. doi:https://doi.org/10.5281/zenodo.7071016.

[66] F. Torrigiani, S. Deinert, M. Fioriti, F. Di Fede, A. Jungo, L. Pisu, F. Sanchez, S. Liscouet-Hanke, P. D. Ciampa, B. Nagel, An MBSE certification-driven design of a UAV MALE configuration in the AGILE 4.0 design environment, in: AIAA Aviation 2021 Forum, 2021, p. 3080. doi:https://doi.org/10.2514/6.2021-3080.

[67] C. Cabaleiro, M. Fioriti, L. Boggero, Methodology for the Automated Preliminary Certification of On-Board Systems Architectures through Requirements Analysis, in: Proceedings of the 33rd Congress of the International Council of the Aeronautical Sciences, Stockholm, Sweden, 2022, pp. 4–9.
URL https://elib.dlr.de/188476/

[68] M. Fioriti, C. Cabaleiro De La Hoz, T. Lefebvre, P. Della Vecchia, M. Mandorino, S. Liscouet-Hanke, A. K. Jeyaraj, G. Donelli, A. Jungo, Multidisciplinary design of a more electric regional aircraft including certification constraints, in: AIAA AVIATION 2022 Forum, 2022, p. 3932. doi:https://doi.org/10.2514/6.2022-3932.

[69] L. M. Nicolai, G. E. Carichner, Fundamentals of aircraft and airship design: Volume I–aircraft design, American Institute of Aeronautics and Astronautics, Inc., 2010. doi:https://doi.org/10.2514/5.9781600867538.0000.0000.

[70] L. A. Schmit, Structural synthesis-its genesis and development, AIAA Journal 19 (10) (1981) 1249–1263. doi:https://doi.org/10.2514/3.7859.

[71] R. T. Haftka, Optimization of flexible wing structures subject to strength and induced drag constraints, Aiaa Journal 15 (8) (1977) 1101–1106. doi:https://doi.org/10.2514/3.7400.

[72] H. Ashley, On making things the best-aeronautical uses of optimization, Journal of Aircraft 19 (1) (1982) 5–28. doi:https://doi.org/10.2514/3.57350.

[73] J. A. Green, Aeroelastic tailoring of aft-swept high-aspect-ratio composite wings, Journal of Aircraft 24 (11) (1987) 812–819. doi:https://doi.org/10.2514/3.45525.

[74] I. Kroo, S. Altus, R. Braun, P. Gage, I. Sobieski, Multidisciplinary optimization methods for aircraft preliminary design, in: 5th symposium on multidisciplinary analysis and optimization, 1994, p. 4325. doi:https://doi.org/10.2514/6.1994-4325.

[75] Y. Takekoshi, T. Kawamura, H. Yamaguchi, M. Maeda, N. Ishii, K. Kimura, T. Taketani, A. Fujii, Study on the design of propeller blade sections using the optimization algorithm, Journal of marine science and technology 10 (2005) 70–81. doi:https://doi.org/10.1007/s00773-005-0197-y.

[76] R. Ganguli, A survey of recent developments in rotorcraft design optimization, Journal of Aircraft 41 (3) (2004) 493–510. doi:https://doi.org/10.2514/1.58.

[77] P. Fuglsang, H. A. Madsen, Optimization method for wind turbine rotors, Journal of wind engineering and industrial aerodynamics 80 (1-2) (1999) 191–206. doi:https://doi.org/10.1016/S0167-6105(98)00191-3.

[78] J. Agte, O. De Weck, J. Sobieszczanski-Sobieski, P. Arendsen, A. Morris, M. Spieck, MDO: assessment and direction for advancement—an opinion of one international group, Structural and Multidisciplinary Optimization 40 (2010) 17–33. doi:https://doi.org/10.1007/s00158-009-0381-5.

[79] O. de Weck, J. Agte, J. Sobieszczanski-Sobieski, P. Arendsen, A. Morris, M. Spieck, State-of-the-art and future trends in multidisciplinary design optimization, in: 48th Aiaa/Asme/Asce/Ahs/Asc Structures, Structural

Dynamics, and Materials Conference, 2007, p. 1905. doi:https://doi.org/10.2514/6.2007-1905.

[80] J. R. Martins, J. T. Hwang, Review and unification of methods for computing derivatives of multidisciplinary computational models, AIAA journal 51 (11) (2013) 2582–2599. doi:https://doi.org/10.2514/1.J052184.

[81] M. Abu-Zurayk, C. Ilic, A. Merle, A. Stück, A. Rempke, S. Keye, T. Klimmek, M. Schulze, R. Liepelt, A. Schuster, et al., Status of Gradient-based Airframe MDO at DLR;"The VicToria Project", 2017.
URL https://elib.dlr.de/115557/

[82] J. R. Martins, G. J. Kennedy, Enabling large-scale multidisciplinary design optimization through adjoint sensitivity analysis, Structural and Multidisciplinary Optimization (2019) 1–16doi:https://doi.org/10.2514/6.2019-1702.

[83] J. S. Gray, J. T. Hwang, J. R. Martins, K. T. Moore, B. A. Naylor, OpenMDAO: An open-source framework for multidisciplinary design, analysis, and optimization, Structural and Multidisciplinary Optimization 59 (2019) 1075–1104. doi:https://doi.org/10.1007/s00158-019-02211-z.

[84] B. Boden, J. Flink, R. Mischke, K. Schaffert, A. Weinert, A. Wohlan, C. Ilic, T. Wunderlich, C. M. Liersch, S. Goertz, et al., Distributed multidisciplinary optimization and collaborative process development using RCE, in: AIAA aviation 2019 forum, 2019, p. 2989. doi:https://doi.org/10.2514/6.2019-2989.

[85] J. R. Martins, J. J. Alonso, J. J. Reuther, A coupled-adjoint sensitivity analysis method for high-fidelity aero-structural design, Optimization and Engineering 6 (2005) 33–62. doi:https://doi.org/10.1023/B:OPTE.0000048536.47956.62.

[86] G. K. Kenway, G. J. Kennedy, J. R. Martins, Scalable parallel approach for high-fidelity steady-state aeroelastic analysis and adjoint derivative computations, AIAA journal 52 (5) (2014) 935–951. doi:https://doi.org/10.2514/1.J052255.

[87] A. Jameson, Automatic design of transonic airfoils to reduce the shock induced pressure drag, in: Proceedings of the 31st Israel annual conference on aviation and aeronautics, Tel Aviv, 1990, pp. 5–17.

[88] A. Elham, M. J. van Tooren, Coupled adjoint aerostructural wing optimization using quasi-three-dimensional aerodynamic analysis, Structural and Multidisciplinary Optimization 54 (2016) 889–906. doi:https://doi.org/10.1007/s00158-016-1447-9.

[89] Y. Ma, M. Abouhamzeh, A. Elham, Geometrically Nonlinear Coupled Adjoint Aerostructural Optimization of Natural-Laminar-Flow Strut-Braced Wing, Journal of Aircraft 60 (3) (2023) 935–954. doi:https://doi.org/10.2514/1.C036988.

[90] J. E. Hoogervorst, A. Elham, Wing aerostructural optimization using the individual discipline feasible architecture, Aerospace Science and Technology 65 (2017) 90–99. doi:https://doi.org/10.1016/j.ast.2017.02.012.

[91] A. Elham, M. J. Van Tooren, Toward Wing Aerostructural Optimization Using Simultaneous Analysis and Design Strategy, in: 58th AIAA/ASCE/AHS/ASC Structures, Structural Dynamics, and Materials Conference, 2017, p. 0802. doi:https://doi.org/10.2514/6.2017-0802.

[92] C. Conti, M. Mandorino, A. Da Ronch, A. Elham, High-fidelity Aero-Structural Optimisation using Individual Discipline Feasible Strategy, in: AIAA AVIATION 2023 Forum. doi:https://doi.org/10.2514/6.2023-3317.vid.

[93] H. C. Patel, D. J. Neiferd, J. J. Alonso, J. D. Deaton, J. Akkala, J. W. Gallman, Aeroelastic Wing Design Sensitivity Analysis with SU2-Nastran Coupling in OpenMDAO, in: AIAA SCITECH 2022 Forum, 2022, p. 2241. doi:https://doi.org/10.2514/6.2022-2241.

[94] J. P. Jasa, J. T. Hwang, J. R. Martins, Open-source coupled aerostructural optimization using Python, Structural and Multidisciplinary Optimization 57 (2018) 1815–1827. doi:https://doi.org/10.1007/s00158-018-1912-8.

[95] Low-fidelity aerostructural optimization of aircraft wings with a simplified wingbox model using OpenAeroStruct, author=Chauhan, Shamsheer S and Martins, Joaquim RRA, in: EngOpt 2018 Proceedings of the 6th International Conference on Engineering Optimization, Springer, 2019, pp. 418–431. doi:https://doi.org/10.1007/978-3-319-97773-7_38.

[96] T. R. Brooks, G. K. Kenway, J. R. Martins, Undeflected common research model (uCRM): an aerostructural model for the study of high aspect ratio transport aircraft wings, in: 35th AIAA Applied Aerodynamics Conference, 2017, p. 4456. doi:https://doi.org/10.2514/6.2017-4456.

[97] C. Xie, C. An, Y. Liu, C. Yang, Static aeroelastic analysis including geometric nonlinearities based on reduced order model, Chinese Journal of Aeronautics 30 (2) (2017) 638–650. doi:https://doi.org/10.1016/j.cja.2016.12.031.

[98] M. Drela, Development of the D8 transport configuration, in: 29th AIAA Applied Aerodynamics Conference, 2011, p. 3970. doi:https://doi.org/10.2514/6.2011-3970.

[99] S. Kilimtzidis, V. Kostopoulos, Static aeroelastic optimization of high-aspect-ratio composite aircraft wings via surrogate modeling, Aerospace 10 (3) (2023). doi:https://doi.org/10.3390/aerospace10030251.
URL https://www.mdpi.com/2226-4310/10/3/251

[100] K. Sommerwerk, B. Michels, K. Lindhorst, M. Haupt, P. Horst, Application of efficient surrogate modeling to aeroelastic analyses of an aircraft wing, Aerospace Science and Technology 55 (2016) 314–323. doi:https://doi.org/10.1016/j.ast.2016.06.011.
URL https://www.sciencedirect.com/science/article/pii/S1270963816302206

[101] S. Goertz, C. Ilic, J. Jepsen, M. Leitner, M. Schulze, A. Schuster, J. Scherer, R. Becker, S. Zur, M. Petsch, Multi-level MDO of a long-range transport aircraft using a distributed analysis framework, in: 18th AIAA/ISSMO multidisciplinary analysis and optimization conference, 2017, p. 4326. doi:https://doi.org/10.2514/6.2017-4326.

[102] B. Boden, J. Flink, N. Först, R. Mischke, K. Schaffert, A. Weinert, A. Wohlan, A. Schreiber, RCE: an integration environment for engineering and science, SoftwareX 15 (2021) 100759. doi:https://doi.org/10.1016/j.softx.2021.100759.

[103] P. D. Ciampa, B. Nagel, AGILE Paradigm: The next generation collaborative MDO for the development of aeronautical systems, Progress in Aerospace Sciences 119 (2020) 100643. doi:https://doi.org/10.1016/j.paerosci.2020.100643.

[104] I. Van Gent, B. Aigner, B. Beijer, J. Jepsen, G. La Rocca, Knowledge architecture supporting the next generation of MDO in the AGILE paradigm, Progress in Aerospace Sciences 119 (2020) 100642. doi:https://doi.org/10.1016/j.paerosci.2020.100642.

[105] P. Prakasha, P. Ciampa, P. Della Vecchia, D. Ciliberti, M. Voskuijl, D. Charbonnier, A. Jungo, M. Fioriti, K. Anisimov, A. Mirzoyan, Multidisciplinary design analysis of blended wing body through collaborative design approach: Agile eu project, in: 31st Congress of th Interantional Council of the Aeronautical Sciences, 2018. doi:http://dx.doi.org/10.13140/RG.2.2.30859.54561.

[106] P. S. Prakasha, P. Della Vecchia, P. Ciampa, D. Ciliberti, D. Charbonnier, A. Jungo, M. Fioriti, L. Boggero, A. Mirzoyan, K. Anisimov, et al., Model based collaborative design & optimization of blended wing body aircraft configuration: Agile eu project, in: 2018 Aviation Technology, Integration, and Operations Conference, 2018, p. 4006. doi:https://doi.org/10.2514/6.2018-4006.

[107] A. Morris, P. Arendsen, G. LaRocca, M. Laban, R. Voss, H. Hönlinger, Mob-a european project on multidisciplinary design optimisation, in: 24th ICAS Congress, ICAS Yokohama, Japan, 2004.
URL https://elib.dlr.de/14464/

[108] F. Torrigiani, J. Bussemaker, P. D. Ciampa, M. Fioriti, F. Tomasella, B. Aigner, D. Rajpal, H. Timmermans, A. Savelyev, D. Charbonnier, Design of the Strut Braced Wing Aircraft in the AGILE collaborative MDO framework, in: 31st Congress of th Interantional Council of the Aeronautical Sciences, ICAS, 2018.

[109] D. Rajpal, R. De Breuker, H. Timmermans, W. Lammen, F. Torrigiani, Including aeroelastic tailoring in the conceptual design process of a composite strut-braced wing, in: 31st Congress of the International Council of the Aeronautical Sciences, ICAS, 2018, pp. 1–12.

[110] P. Della Vecchia, L. Stingo, F. Nicolosi, A. De Marco, G. Cerino, P. D. Ciampa, P. S. Prakasha, M. Fioriti, M. Zhang, A. Mirzoyan, et al., Advanced turboprop multidisciplinary design and optimization within AGILE project, in: 2018 Aviation Technology, Integration, and Operations Conference, 2018, p. 3205. doi:https://doi.org/10.2514/6.2018-3205.

[111] L. Stingo, P. Della Vecchia, G. Cerino, F. Nicolosi, A. De Marco, MDO applications to conventional and novel turboprop aircraft within agile European project (2018).

[112] M. Fioriti, L. Boggero, A. Mirzoyan, A. Isyanov, Studies on propulsion and on-board systems matching in agile project distributed collaborative MDO environment applying for advanced regional and medium haul jet, in: 31st Congress of the International Council of the Aeronautical Sciences, 2018.

[113] R. Maierl, A. Gastaldi, J.-N. Walther, A. Jungo, Aero-structural optimization of a male configuration in the agile mdo framework, in: Flexible Engineering Toward Green Aircraft: CAE Tools for Sustainable Mobility, Springer, 2020, pp. 169–187. doi:https://doi.org/10.1007/978-3-030-36514-1_10.

[114] J.-N. Walther, A.-A. Gastaldi, R. Maierl, A. Jungo, M. Zhang, Integration aspects of the collaborative aero-structural design of an unmanned aerial vehicle, CEAS Aeronautical Journal 11 (1) (2020) 217–227. doi:https://doi.org/10.1007/s13272-019-00412-2.

[115] E. Guinaldo, Clean sky 2 advanced rear end demonstrator, in: AIAA SCITECH 2024 Forum, 2024, p. 1302. doi:10.2514/6.2024-1302.

[116] N. Krone, Jr, Forward swept wing flight demonstrator, in: Aircraft Systems Meeting, 1980, p. 1882. doi:https://doi.org/10.2514/6.1980-1882.

[117] T. A. Weisshaar, Aeroelastic stability and performance characteristics of aircraft with advanced composite sweptforward wing structures, Tech. rep., Virginia Polytechnic Inst And State Univ Blacksburg Dept Of Aerospace And Ocean Engineering (1978).

[118] T. A. Weisshaar, Aeroelastic tailoring of forward swept composite wings, Journal of Aircraft 18 (8) (1981) 669–676. doi:https://doi.org/10.2514/3.57542.

[119] T. Hertz, M. Shirk, R. Ricketts, T. Weisshaar, Aeroelastic tailoring with composites applied to forward swept wings, Tech. rep., Air Force Wright Aeronautical Labs Wright-Patterson AFB OH (1981).

[120] N. Krone, Jr, Divergence elimination with advanced composites, in: Aircraft Systems and Technology Meeting, 1975, p. 1009. doi:https://doi.org/10.2514/6.1975-1009.

[121] T. Weisshaar, Divergence of forward swept composite wings, in: 20th Structures, Structural Dynamics, and Materials Conference, 1979, p. 722. doi:https://doi.org/10.2514/6.1979-722.

[122] M. H. Shirk, T. J. Hertz, T. A. Weisshaar, Aeroelastic tailoring-theory, practice, and promise, Journal of Aircraft 23 (1) (1986) 6–18. doi:https://doi.org/10.2514/3.45260.

[123] T. Wunderlich, L. Reimer, Integrated process chain for aerostructural wing optimization and application to an NLF forward swept composite wing, in: AeroStruct: Enable and Learn How to Integrate Flexibility in Design, Springer, 2018, pp. 3–33. doi:https://doi.org/10.1007/978-3-319-72020-3_1.

[124] G. Redeker, G. Wichmann, Forward sweep-A favorable concept for a laminar flow wing, Journal of aircraft 28 (2) (1991) 97–103. doi:https://doi.org/10.2514/3.45997.

[125] A. Seitz, M. Kruse, T. Wunderlich, J. Bold, L. Heinrich, The DLR project LamAiR: design of a NLF forward swept wing for short and medium range transport application, in: 29th AIAA applied aerodynamics conference, 2011, p. 3526. doi:https://doi.org/10.2514/6.2011-3526.

[126] T. A. Weisshaar, Forward swept wing static aeroelasticity, Virginia Polytechnic Inst And State Univ Blacksburg Dept Of Aerospace And Ocean Engineering, 1979.
URL https://apps.dtic.mil/sti/citations/ADB042815

[127] M. Kruse, T. Wunderlich, L. Heinrich, A conceptual study of a transonic NLF transport aircraft with forward swept wings, in: 30th AIAA Applied Aerodynamics Conference, 2012, p. 3208. doi:https://doi.org/10.2514/6.2012-3208.

[128] A. Seitz, A. Hübner, K. Risse, The DLR TuLam project: design of a short and medium range transport aircraft with forward swept NLF wing, CEAS Aeronautical Journal 11 (2020) 449–459. doi:https://doi.org/10.1007/s13272-019-00421-1.

[129] F. T. Lynch, A. Khodadoust, Effects of ice accretions on aircraft aerodynamics, Progress in Aerospace Sciences 37 (8) (2001) 669–767. doi:https://doi.org/10.1016/S0376-0421(01)00018-5.

[130] A. P. Broeren, M. P. Bragg, Effect of residual and intercycle ice accretions on airfoil performance, US Federal Aviation Administration, Office of Aviation Research, 2002.

[131] J. Reichhold, M. Bragg, Residual Ice Characteristics and the Resulting Aerodynamic Performance Penalties, Tech. rep., NASA AGATE WP4 (1998).

[132] M. B. Bragg, A. P. Broeren, L. A. Blumenthal, Iced-airfoil aerodynamics, Progress in Aerospace Sciences 41 (5) (2005) 323–362. doi:https://doi.org/10.1016/j.paerosci.2005.07.001.

[133] S. Lee, M. B. Bragg, Experimental investigation of simulated large-droplet ice shapes on airfoil aerodynamics, Journal of Aircraft 36 (5) (1999) 844–850. doi:https://doi.org/10.2514/2.2518.

[134] R. K. Calay, A. E. Holdø, P. Mayman, I. Lun, Experimental simulation of runback ice, Journal of aircraft 34 (2) (1997) 206–212. doi:https://doi.org/10.2514/2.2173.

[135] H. Kim, B. Michael B., Effects of leading-edge ice accretion geometry on airfoil performance, in: 17th Applied Aerodynamics Conference, University of Illinois at Urbana-Champaign, 2004. doi:https://doi.org/10.2514/6.1999-3150.

[136] S. Hoerner, H. Borst, Fluid dynamic lift, Hoerner fluid dynamics, Brick Town, NJ, 1975.

[137] M. Ingelman-Sundberg, O. Trunov, A. Ivaniko, Methods for prediction of the influence of ice on aircraft flying characteristics, Tech. rep., Swedish-Soviet Working Group on Scientific-Technical Cooperation in the Field of Flight Safety (1977).

[138] S. Lee, T. Dunn, H. Gurbacki, M. Bragg, E. Loth, An experimental and computational investigation of spanwise-step-ice shapes on airfoil aerodynamics, in: 36th AIAA Aerospace Sciences Meeting and Exhibit, 1998, p. 490. doi:https://doi.org/10.2514/6.1998-490.

[139] Effects of ice geometry on airfoil performance using neural networks prediction, author=Cao, Yihua and Yuan, Kungang and Li, Guozhi, Aircraft Engineering and Aerospace Technology 83 (5) (2011) 266–274. doi:https://doi.org/10.1108/00022661111159870.

[140] P. Ciampa, B. Nagel, AGILE the next generation of collaborative MDO: achievements and open challenges, in: 2018 Multidisciplinary Analysis and Optimization Conference, 2018, p. 3249. doi:https://doi.org/10.2514/6.2018-3249.

[141] E. Baalbergen, E. Moerland, W. Lammen, P. Ciampa, Methods supporting the efficient collaborative design of future aircraft, in: Aerospace Europe 6th CEAS Conference, Netherlands Aerospace Centre NLR, 2017.
URL https://hdl.handle.net/10921/1531

[142] L. Stingo, 3rd generation of collaborative MDO for more efficient aircraft preliminary design. The turboprop case within the AGILE project, Ph.D. thesis, University of Naples Federico II (2020).

[143] M. Mandorino, Automatic Aero-Structural Analysis and Aerodynamic Optimization for Collaborative Aircraft Design Process, Master's thesis, University of Naples Federico II (2020).

[144] P. Ciampa, L. Boggero, J. Vankan, T. Lefebvre, B. Beijer, A. Bruggeman, T. van der Laan, M. Fioriti, P. della Vecchia, J. Vos, MBSE-MDAO agility in Aircraft Development: Achievements and Open Challenges from the AGILE4.0 Project, in: AIAA Aviation 2022 Forum, 2022.

[145] M. Mandorino, P. Della Vecchia, S. Corcione, F. Nicolosi, V. Trifari, G. Cerino, M. Fioriti, C. Cabaleiro De La Hoz, T. Lefebvre, D. Charbonnier, et al., Multidisciplinary Design and Optimization of Regional Jet Retrofitting Activity, in: AIAA AVIATION 2022 Forum, 2022, p. 3933. doi:https://doi.org/10.2514/6.2022-3933.

[146] P. Della Vecchia, M. Mandorino, V. Cusati, F. Nicolosi, Retrofitting Cost Modeling in Aircraft Design, Aerospace 9 (7) (2022) 349. doi:https://doi.org/10.3390/aerospace9070349.

[147] M. Mandorino, P. Della Vecchia, F. Nicolosi, G. Cerino, Regional jet retrofitting through multidisciplinary aircraft design, in: IOP Conference Series: Materials Science and Engineering, Vol. 1226, IOP Publishing, 2022, p. 012047. doi:10.1088/1757-899X/1226/1/012047.

[148] J. H. Bussemaker, P. D. Ciampa, J. Singh, M. Fioriti, C. Cabaleiro De La Hoz, Z. Wang, D. Peeters, P. Hansmann, P. Della Vecchia, M. Mandorino, Collaborative Design of a Business Jet Family Using the AGILE 4.0 MBSE Environment, in: AIAA Aviation 2022 Forum, 2022, p. 3934. doi:https://doi.org/10.2514/6.2022-3934.

[149] E. Baalbergen, J. Vankan, L. Boggero, J. H. Bussemaker, T. Lefèbvre, B. Beijer, A.-L. Bruggeman, M. Mandorino, Advancing cross-organizational collaboration in aircraft development, in: AIAA AVIATION 2022 Forum, 2022, p. 4052. doi:https://doi.org/10.2514/6.2022-4052.

[150] J. Bussemaker, L. Boggero, B. Nagel, The AGILE 4.0 Project: MBSE to Support Cyber-Physical Collaborative Aircraft Development, in: INCOSE International Symposium, Vol. 33, Wiley Online Library, 2023, pp. 163–182. doi:https://doi.org/10.1002/iis2.13015.

[151] ISO/IEC 29148 FDIS Systems and software engineering—Life cycle processes—Requirements engineering, Tech. rep., International Organization for Standardization (2011).

[152] Guide for Writing Requirements, Tech. rep., INCOSE-TP-2010-006-01 (2012).

[153] S. J. Kapurch, NASA systems engineering handbook, Diane Publishing, 2010.

[154] R. S. Carson, Implementing structured requirements to improve requirements quality, in: INCOSE International Symposium, Vol. 25, Wiley Online Library, 2015, pp. 54–67. doi:https://doi.org/10.1002/j.2334-5837.2015.00048.x.

[155] P. Roques, Systems architecture modeling with the Arcadia method: a practical guide to Capella, Elsevier, 2017.

[156] J.-L. Voirin, Model-based system and architecture engineering with the arcadia method, Elsevier, 2017.

[157] P. Roques, MBSE with the ARCADIA Method and the Capella Tool, in: 8th European Congress on Embedded Real Time Software and Systems (ERTS 2016), 2016.

[158] ISO/IEC/IEEE 42010 FDIS Systems and software engineering - Architecture description, Tech. rep., International Organization for Standardization (2011).

[159] E. Crawley, B. Cameron, D. Selva, System architecture: strategy and product development for complex systems, Prentice Hall Press, 2015.

[160] I. van Gent, G. La Rocca, M. F. Hoogreef, CMDOWS: a proposed new standard to store and exchange MDO systems, CEAS Aeronautical Journal 9 (2018) 607–627. doi:https://doi.org/10.1007/s13272-018-0307-2.

[161] A. B. Lambe, J. R. Martins, Extensions to the design structure matrix for the description of multidisciplinary design, analysis, and optimization processes, Structural and Multidisciplinary Optimization 46 (2012) 273–284. doi:https://doi.org/10.1007/s00158-012-0763-y.

[162] D. V. Steward, The design structure system: A method for managing the design of complex systems, IEEE transactions on Engineering Management (3) (1981) 71–74. doi:http://dx.doi.org/10.1109/TEM.1981.6448589.

[163] I. van Gent, G. La Rocca, Formulation and integration of mdao systems for collaborative design: A graph-based methodological approach, Aerospace Science and Technology 90 (2019) 410–433. doi:https://doi.org/10.1016/j.ast.2019.04.039.

[164] A. Page Risueño, J. Bussemaker, P. D. Ciampa, B. Nagel, Mdax: Agile generation of collaborative mdao workflows for complex systems, in: AIAA Aviation 2020 Forum, 2020, p. 3133. doi:https://doi.org/10.2514/6.2020-3133.

[165] B. Nagel, D. Böhnke, V. Gollnick, P. Schmollgruber, A. Rizzi, G. La Rocca, J. J. Alonso, Communication in aircraft design: Can we establish a common language, in: 28th International Congress of the Aeronautical Sciences, Vol. 201, 2012.

[166] M. Alder, E. Moerland, J. Jepsen, B. Nagel, Recent advances in establishing a common language for aircraft design with cpacs (2020).

[167] M. Siggel, J. Kleinert, T. Stollenwerk, R. Maierl, Tigl: an open source computational geometry library for parametric aircraft design, Mathematics in Computer Science 13 (3) (2019) 367–389. doi:https://doi.org/10.1007/s11786-019-00401-y.

[168] L. P. Swiler, G. D. Wyss, A user's guide to Sandia's latin hypercube sampling software: LHS UNIX library/standalone version., Tech. rep., Sandia National Laboratories (SNL), Albuquerque, NM, and Livermore, CA ... (2004).

[169] B. Tang, Orthogonal array-based Latin hypercubes, Journal of the American statistical association 88 (424) (1993) 1392–1397. doi:https://doi.org/10.1080/01621459.1993.10476423.

[170] A. B. Owen, Orthogonal Arrays for Computer Experiments, Integration and Visualization, Statistica Sinica 2 (2) (1992) 439–452.
URL http://www.jstor.org/stable/24304869

[171] K. Q. Ye, Orthogonal column Latin hypercubes and their application in computer experiments, Journal of the American Statistical Association 93 (444) (1998) 1430–1439. doi:https://doi.org/10.1080/01621459.1998.10473803.

[172] H. Wendland, Scattered data approximation, Vol. 17, Cambridge university press, 2004.

[173] C. S. K. Dash, A. K. Behera, S. Dehuri, S.-B. Cho, Radial basis function neural networks: a topical state-of-the-art survey, Open Computer Science 6 (1) (2016) 33–63. doi:https://doi.org/10.1515/comp-2016-0005.

[174] C.-C. Lee, P.-C. Chung, J.-R. Tsai, C.-I. Chang, Robust radial basis function neural networks, IEEE Transactions on Systems, Man, and Cybernetics, Part B (Cybernetics) 29 (6) (1999) 674–685. doi:10.1109/3477.809023.

[175] D. O. Tools, D. U. Manual, Vanderplaats Research & Development, Tech. rep., Inc., Colorado Springs, CO (1999).

[176] J. D. Griffin, T. G. Kolda, Nonlinearly-constrained optimization using asynchronous parallel generating set search., Tech. rep., Sandia National Laboratories (SNL), Albuquerque, NM, and Livermore, CA ... (2007).

[177] J. Dennis, V. Torczon, Derivative-free pattern search methods for multidisciplinary design problems, in: 5th Symposium on Multidisciplinary Analysis and Optimization, 1994, p. 4349. doi:https://doi.org/10.2514/6.1994-4349.

[178] F. Nicolosi, A. De Marco, L. Attanasio, P. D. Vecchia, Development of a Java-based framework for aircraft preliminary design and optimization, Journal of Aerospace Information Systems 13 (6) (2016) 234–242. doi:https://doi.org/10.2514/1.I010404.

[179] V. Trifari, M. Ruocco, V. Cusati, F. Nicolosi, A. De Marco, Java framework for parametric aircraft design–ground performance, Aircraft Engineering and Aerospace Technology 89 (4) (2017) 599–608. doi:http://dx.doi.org/10.1108/AEAT-11-2016-0209.

[180] S. Kukkonen, J. Lampinen, GDE3: The third evolution step of generalized differential evolution, in: 2005 IEEE congress on evolutionary computation, Vol. 1, IEEE, 2005, pp. 443–450. doi:https://doi.org/10.1109/CEC.2005.1554717.

[181] J. J. Durillo, A. J. Nebro, F. Luna, E. Alba, Solving three-objective optimization problems using a new hybrid cellular genetic algorithm, in: Parallel Problem Solving from Nature–PPSN X: 10th International Conference, Dortmund, Germany, September 13-17, 2008. Proceedings 10, Springer, 2008, pp. 661–670. doi:https://doi.org/10.1007/978-3-540-87700-4_66.

[182] A. J. Nebro, A new PSO-based metaheuristic for multi-objective optimization, in: Proceedings of IEEE Symposium on Computational Intelligence in Miulti-Criteria Decision-Making, 2009, 2009, pp. 66–73. doi:https://doi.org/10.1109/MCDM.2009.4938830.

[183] A. De Marco, V. Cusati, V. Trifari, M. Ruocco, F. Nicolosi, P. Della Vecchia, A java toolchain of programs for aircraft design, in: Proceedings of the Aerospace Europe 6th CEAS Conference, Bucharest, Romania, 2017, pp. 16–20.

[184] F. Nicolosi, P. Della Vecchia, V. Trifari, M. Di Stasio, F. Marulo, A. De Marco, V. Marciello, V. Cusati, Noise, Emissions and Costs trade factors for regional jet platforms using a new software for aircraft preliminary design, in: AIAA Aviation 2020 Forum, 2020, p. 2638. doi:https://doi.org/10.2514/6.2020-2638.

[185] M. Di Stasio, V. Trifari, F. Nicolosi, A. De Marco, S. Fuhrmann, R. Schaber, Multidisciplinary Optimization of a Regional Jet Including Advanced Airframe and Engine Technologies, in: AIAA Aviation 2021 Forum, 2021, p. 2424. doi:https://doi.org/10.2514/6.2021-2424.

[186] M. Di Stasio, V. Trifari, F. Nicolosi, A. De Marco, R. Schaber, Bypass Ratio Parametric Analyses on a Narrow-Body Aircraft Using a New Tool for Turbofan Rubberization, in: AIAA AVIATION 2022 Forum, 2022, p. 3289. doi:https://doi.org/10.2514/6.2022-3289.

[187] A. De Marco, M. Di Stasio, P. Della Vecchia, V. Trifari, F. Nicolosi, Automatic modeling of aircraft external geometries for preliminary design workflows, Aerospace Science and Technology 98 (2020) 105667. doi:https://doi.org/10.1016/j.ast.2019.105667.

[188] V. Trifari, A. De Marco, M. Di Stasio, M. Ruocco, F. Nicolosi, G. Grazioso, V. Ahuja, R. Hartfield, An aircraft design workflow using the automatic knowledge-based modelling tool JPAD Modeller, in: AIAA AVIATION 2022 Forum, 2022, p. 3737. doi:https://doi.org/10.2514/6.2022-3737.

[189] F. Lindner, M. Mehl, B. Uekermann, Radial Basis Function Interpolation for Black-Box Multi-Physics Simulations, 2017.

[190] G. Yang, A. D. Ronch, D. Kharlamov, J. Drofelnik, Wing twist optimisation using aerodynamic solvers of different fidelity, in: International Council of the Aeronautical Sciences, 2018.
URL https://eprints.soton.ac.uk/423722/

[191] P. Albuquerque, F. Cunha, L. Reis, Evaluation of structural loads, in: 3rd Aircraft Structural Design Conference. Royal Aeronautical Society, Delft University, NL, 2012, pp. 1–13. doi:http://dx.doi.org/10.13140/2.1.4615.3288.

[192] S. Corcione, V. Cusati, V. Memmolo, F. Nicolosi, R. Llamas Sandin, Impact at aircraft level of elastic efficiency of a forward-swept tailplane, Aerospace Science and Technology 140 (2023) 108461. doi:https://doi.org/10.1016/j.ast.2023.108461.
URL https://www.sciencedirect.com/science/article/pii/S1270963823003589

[193] D. Scholz, Empennage sizing with the tail volume complemented with a method for dorsal fin layout, INCAS bulletin 13 (3) (2021) 149–164. doi:https://doi.org/10.13111/2066-8201.2021.13.3.13.

[194] J. Roskam, Methods for estimating stability and control derivatives of conventional subsonic airplanes, 1971.

[195] W. F. Phillips, Mechanics of flight, John Wiley & Sons, 2004.

[196] D. P. Raymer, Aircraft design: a conceptual approach, American Institute of Aeronautics and Astronautics, 1999.

[197] M. Calcara, Elementi di dinamica del velivolo, Università degli studi, Facoltà di ingegneria, Istituto di progetti velivoli., 1988.

[198] T. H. G. Megson, Aircraft structures for engineering students, Butterworth-Heinemann, 2016.

[199] O. Schrenk, A simple approximation method for obtaining the spanwise lift distribution, The Aeronautical Journal 45 (370) (1941) 331–336.

[200] Readers Forum, Journal of the Aeronautical Sciences 16 (8) (1949) 505–511. doi:https://doi.org/10.2514/8.11841.

[201] E. Torenbeek, Synthesis of subsonic airplane design: an introduction to the preliminary design of subsonic general aviation and transport aircraft, with emphasis on layout, aerodynamic design, propulsion and performance, Springer Science & Business Media, 2013.

[202] E. Roux, Modèle de Masse Voilure Avions de transport civil pour une approche analytique de la Dynamique du Vol, Intitut Supérieur de l'Aéronautique et de l'Espace-Supaero & ONERA (2006).

[203] T. Economon, F. Palacios, S. Copeland, T. Lukaczyk, J. Alonso, SU2: An Open-Source Suite for Multiphysics Simulation and Design, AIAA Journal 54 (2015) 1–19. doi:https://doi.org/10.2514/1.J053813.

[204] T. Albring, M. Sagebaum, N. Gauger, Development of a Consistent Discrete Adjoint Solver in an Evolving Aerodynamic Design Framework, 2015. doi:10.2514/6.2015-3240.

[205] S. F. Walter, L. Lehmann, Algorithmic differentiation in Python with AlgoPy, Journal of Computational Science 4 (5) (2013) 334 – 344. doi:http://dx.doi.org/10.1016/j.jocs.2011.10.007.

[206] D. Masters, N. Taylor, T. Rendall, C. Allen, D. Poole, Review of Aerofoil Parameterisation Methods for Aerodynamic Shape Optimisation, 2015. doi:https://doi.org/10.2514/6.2015-0761.

[207] P. Della Vecchia, F. Nicolosi, M. Ruocco, L. Stingo, A. De Marco, An improved high-lift aerodynamic prediction method for transport aircraft, CEAS Aeronautical Journal 10 (2019) 795–804. doi:https://doi.org/10.1007/s13272-018-0349-5.

[208] J. A. Blackwell, A finite-step method for calculation of theoretical load distributions for arbitrary lifting-surface arrangements at subsonic speeds, Tech. rep., NASA, National Aeronautics and Space Administration (1969).
URL https://ntrs.nasa.gov/citations/19690021959

[209] P. E. Purser, M. L. Spearman, Wind-tunnel tests at low speed of swept and yawed wings having various plan forms, Tech. rep., NASA, National Aeronautics and Space Administration (1947).
URL https://ntrs.nasa.gov/citations/19930083063

[210] D. Holt, Introduction To transonic aerodynamics of aerofoils and wings, ESDU data item 90008 (1990).
URL https://www.esdu.com/cgi-bin/ps.pl?sess=unlicensed_1220304093323cgp&t=doc&p=esdu_90008#

[211] J. Mariens, A. Elham, M. J. L. van Tooren, Quasi-Three-Dimensional Aerodynamic Solver for Multidisciplinary Design Optimization of Lifting Surfaces, Journal of Aircraft 51 (2) (2014) 547–558. doi:https://doi.org/10.2514/1.C032261.

[212] E. Obert, Aerodynamic design of transport aircraft, IOS press, 2009.

[213] I. Desktop Aeronautics, Oblique Flying Wings : An Introduction and White Paper, 2005.
URL https://api.semanticscholar.org/CorpusID:15170582

[214] M. Drela, Astronautics, Simultaneous Optimization of the Airframe , Powerplant , and Operation of Transport Aircraft, 2010.
URL https://api.semanticscholar.org/CorpusID:14354512

[215] J. D. Anderson, Fundamentals of aerodynamics, McGraw (2009).

[216] Z. Boutanios, Y. Bourgault, W. Habashi, G. Issac, S. Cober, 3D droplets impingement analysis around an aircraft's nose and cockpit using FENSAP-ICE, in: 36th AIAA Aerospace Sciences Meeting and Exhibit, 1998, p. 200. doi:https://doi.org/10.2514/6.1998-200.

[217] F. Morency, H. Beaugendre, G. Baruzzi, W. Habashi, FENSAP-ICE-A comprehensive 3D simulation system for in-flight icing, in: 15th AIAA computational fluid dynamics conference, 2001, p. 2566. doi:https://doi.org/10.2514/6.2001-2566.

[218] I. Ozcer, D. Switchenko, G. S. Baruzzi, J. Chen, Multi-shot icing simulations with automatic re-meshing, in: International Conference on Icing of Aircraft, Engines, and Structures, 2019. doi:https://doi.org/10.4271/2019-01-1956.

[219] J. Page, I. Ozcer, A. Zanon, M. De Gennaro, IMPACT: Numerical Study of Aerodynamics of an Iced Forward-Swept Tail with Leading Edge Extension, in: International Conference on Icing of Aircraft, Engines, and Structures, 2023. doi:https://doi.org/10.4271/2023-01-1371.

[220] de Saint-Venant, Mémoire sur la flexion des prismes, sur les glissements transversaux et longitudinaux qui l'accompagnent lorsqu'elle ne s'opère pas uniformément ou en arc de cercle, et sur la forme courbe affectée alors par leurs sections transversales primitivement planes., Journal de Mathématiques Pures et Appliquées (1856) 89–189.
URL http://eudml.org/doc/234512

[221] T. L. Lomax, Structural loads analysis for commercial transport aircraft: theory and practice, American Institute of Aeronautics and Astronautics, 1996.

[222] R. C. Llamas Sandin, M. Luque Buzo, Aircraft horizontal stabilizer surface.
URL https://patents.google.com/patent/US20100148000A1/

[223] Certification Specifications and Acceptable Means of Compliance for Large Aeroplanes CS-25, European Aviation Safety Agency, 2020.

Acknowledgements

The candidate's participation in international research projects significantly contributed to the development of this thesis. My acknowledgments go to the IMPACT and AGILE 4.0 research projects.

The IMPACT project received funding from the Clean Sky 2 Joint Undertaking (JU) under grant agreement No 885052. The JU is supported by the European Union's Horizon 2020 research and innovation programme, along with the Clean Sky 2 JU members other than the Union. I express my gratitude to the partners of the IMPACT consortium for their valuable feedback. The content of this thesis reflects solely the author's view, and neither the European Commission nor the Clean Sky 2 Joint Undertaking is responsible for any use that may be made of the information it contains.

The AGILE 4.0 project received funding from the European Union Horizon 2020 Programme under grant agreement No 815122. I am thankful to the partners of the AGILE 4.0 consortium for their invaluable feedback. The content of this thesis represents only the author's perspective, and the European Commission is not accountable for any use that may be made of the information it contains.